Movement Artefact Rejection in Impedance Pneumography

Niranjan D. Khambete

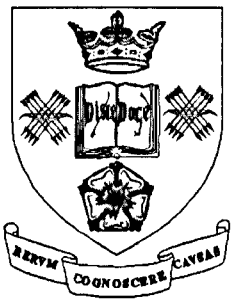

A thesis submitted for the degree of Doctor of Philosophy.
Department of Medical Physics and Clinical Engineering,
University of Sheffield

May 2000

Movement Artefact Rejection in Impedance Pneumography

Niranjan D. Khambete

Summary

Impedance pneumography is a non-invasive and a very convenient technique for monitoring breathing. However, a major drawback of this technique is that it is impossible to monitor breathing due to large artefacts introduced by the body movements. The aim of this project was to develop a technique for reducing these 'movement artefacts'.

In the first stage of the project, experimental and theoretical studies were carried out to identify an 'optimum' electrode placement that would maximise the 'sensitivity' of measured thoracic impedance to lung resistivity changes. This maximum sensitivity was obtained when the drive and the receive electrode pairs were placed in two different horizontal planes. This sensitivity was also found to increase with increase in electrode spacing.

In the second stage, the optimum electrode placement was used to record thoracic impedance during movements. Movement artefacts occurred only when the electrodes moved from their initial location along with the skin, during movements. Taking into consideration these observations, a strategy was decided for placing 4 electrodes in one plane so that movement artefacts could be reduced by combining the two independent measurements. Further studies showed that movement artefacts could be reduced using a strategic 6-electrode placement in three dimensions. It was also possible to detect obstructive apnoea, as the amplitude of the breathing signal was higher than that due to obstructive apnoea and this difference was statistically significant.

In these studies, the main cause of movement artefacts was identified as the movement of electrodes with the skin. A significant reduction in movement artefacts was obtained using the 6-electrode placement. This advantage of the 6-electrode placement proposed in this project, can be of great use in clinical applications such as apnoea monitoring in neonates. Further studies can be carried out to determine an optimum frequency of injected current to achieve reduction in residual movement artefacts.

Acknowledgements

I would particularly like to thank my supervisor Prof. B. H. Brown and co-supervisor Prof. R. H. Smallwood for providing me with an opportunity to work on this thesis. I am extremely grateful to my supervisor Prof. B. H. Brown for giving me the confidence to complete this work, and for his help, guidance and valuable contribution, as well as for his constant encouragement and support throughout the completion of this thesis. I would also like to thank my co-supervisor Prof. R. H. Smallwood for his encouragement, support and help. I was greatly benefited by his valuable suggestions and timely comments and I am thankful for the support he provided me in the successful completion of my Research Training Program in the first year. I would also like to take this opportunity to thank my colleague Dr. Peter Metherall who generously provided me with his experimental data which helped me in initiating this work. In the final stages, he patiently and critically read through the thesis and provided his valuable comments and suggestions. Dr. Andrew Leathard was always available to help me with the problems I had regarding computing. I am thankful to him for that. My friend Alan Waterworth was always ready to undergo the torture of applying and removing of the electrodes during numerous trial and error experiments that I carried out throughout this work. I am extremely thankful to him for his patience. I also wish to thank Dr. R. Hose for making me understand the fundamentals of finite element methods and Dr. A. Wilson for giving me his entire collection of journal papers on impedance pneumography. Dr. N. D. Harris suggested the thermistor method for monitoring breathing and provided me with the circuit for it. I am thankful to him for his help. I would also like to thank all the staff members of the instrumentation laboratory from the department and Lisa from the administrative staff for promptly typing letters for me as and when I needed them urgently. I would also like to thank all the volunteers who spared time to participate in the experimental studies carried out for this work.

I would like to express my sincere gratitude to Prof. Mohandas, Director of Sree Chitra Tirunal Institute for Medical Sciences and Technology for forwarding my application for the Commonwealth Scholarship, and also for recommending my

leave sanction and extension to the governing body of the Institute. Dr. R. Sivakumar provided his unfailing support throughout the tenure of my leave. He went out of his way to get my leave sanctioned without which, it would have been impossible for me to pursue my higher studies. I am extremely grateful to him for his support. Dr. G. S. Bhuvaneshwar also supported my final leave extension which helped in the satisfactory and stress free completion of the final write up of this thesis. I am grateful to him for his support. I could not have thought of taking this opportunity of doing my Ph.D., but for the strong encouragement, support and guidance of my friend and colleague Nagesh. I am grateful to him for his advice and help. I would also like to thank my colleagues Dr. C. P. Sharma and Dr. H. K. Varma for encouraging me to take this opportunity, as well as Dr. Uttarwar for being kind enough to sign the surety bond. I would like to thank Mr Edwin for taking care of all the administrative formalities regarding my leave sanction. I would also like to thank my professor, Dr. Pandey from the Indian Institute of Technology, Mumbai for giving me reference for my scholarship as well as for my admission. I am also grateful to my friends Dr. Archana Desurkar and Dr. Vinayak Desurkar for their timely financial support during my extended stay in the UK.

My wife Aarti, provided her unfailing support, encouragement and help throughout the completion of this thesis. I would like to thank her for her help, appreciation and understanding. I would also like to thank my mother and all the other family members for their support and encouragement. Finally, I am grateful to the Commonwealth Scholarship Commission for providing me with the Commonwealth scholarship to complete my Ph.D. I would also like to thank all the staff members of the British Council for looking after my and my family's general welfare and making my stay in the UK comfortable, enjoyable and an unforgettable experience.

Niranjan D. Khambete

Table of Contents

Chapter 1. Introduction

1.1. Background to the project

It has been known for many years that the electrical properties of the tissues of a human body undergo changes during physiological activity. A typical example is that of the lung tissue. The resistivity of the lung tissue is a function of the ratio of air volume to fluid volume and thus, undergoes a change during breathing. The technique of 'Impedance pneumography' involves measuring these changes in lung tissue resistivity for monitoring the physiological activity of breathing.

Impedance pneumography has several advantages. It is a non-invasive technique and thus, safe for long term monitoring applications. It does not involve placing any device within the airway that may cause an obstruction to the flow of air. As a result, it is well tolerated by patients. These advantages have led to its widespread use for monitoring apnoea (absence of breathing) in children and for monitoring breathing in inaccessible environments such as a manned space capsule, where other techniques are difficult to use.

A major disadvantage of impedance pneumography is its inability to function satisfactorily in the presence of body movements such as arm movements and changes in posture. These body movements introduce large artefacts in the impedance signal. Under such circumstances, it is impossible to measure parameters such as breathing rate or to detect apnoea, using the impedance signal. Therefore, it is important to reduce these 'movement artefacts'.

Electrical Impedance Tomography (EIT) is an imaging modality, developed to a considerable extent in recent years. It involves generating an image, which shows the internal resistivity distribution of a body segment. An EIT image of the thoracic cavity displays two distinct lung regions undergoing a change in resistivity during breathing. Thus, it is possible to independently monitor ventilation in a particular lung or in a specific region of a lung. The technique of EIT Spectroscopy (EITS) involves recording impedance data at more than one frequency of injected current. The results of EITS have suggested that there

exists a characteristic relationship between breathing related changes in lung resistivity and the frequency of injected current. However, a major limitation of EIT is that it requires using a large number of electrodes which become inconvenient to use in a clinical environment. In addition, movement artefacts are also a problem in EIT.

1.2. Aim of the project

Keeping this background in mind, the main aim of this project is,

- To increase the reliability of impedance pneumography by developing a method for reducing movement artefacts.

The other aims are,

- To make use of multi-frequency measurements to distinguish between breathing related impedance changes and movement artefacts.
- To obtain reduction in movement artefacts by using a minimum number of electrodes.

The following sections outline some basic concepts regarding impedance based monitoring of physiological events. The two-electrode and the four-electrode impedance measurement configurations are explained. This is followed by a discussion on the fundamentals of electrical properties of biological tissues. The safety implications of injecting a current into the human body are also discussed. Finally, applications of electrical impedance techniques in physiology and medicine are described.

1.3. Two-electrode and four-electrode configurations

The impedance of a segment of a human body is measured by injecting a current into the body via a pair of surface electrodes and by measuring the resulting voltage. The location of the electrodes depends on the physiological activity

being monitored. For example, to monitor breathing, electrodes are usually placed on the surface of the thoracic cavity. In a 'two-electrode' or 'bipolar' configuration, the current injection and the voltage measurement is achieved using the same pair of electrodes as shown in Figure 1.1. This is the most simple configuration and requires only two electrical connections to the body. However, the impedance of the electrode-skin interface is an integral part of the measured impedance. This may cause problems in monitoring the physiological activity. For example, in impedance pneumography, mechanical disturbances occurring at the electrode-skin interface due to body movements, can cause the electrode-skin contact impedance to change unpredictably and thus, introduce artefacts.

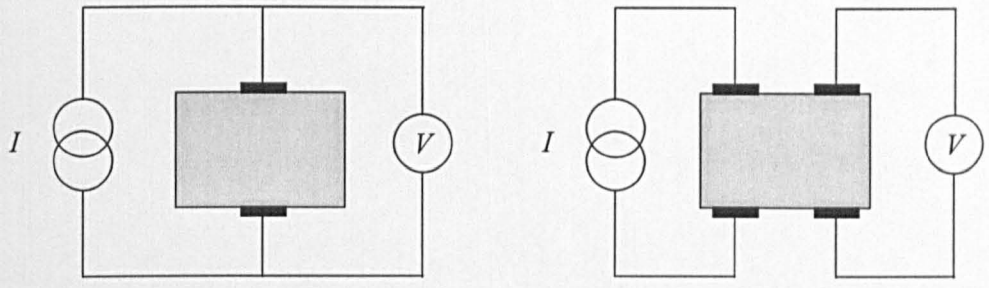

Two-electrode configuration Four-electrode configuration

Figure 1.1 Electrode configurations used for impedance measurements on a human body

This problem can be overcome by using a 'four-electrode' or 'tetrapolar' configuration, also shown in Figure 1.1. In this configuration, a different pair of electrodes is used to measure the voltage. If the input impedance of the voltage measuring circuit is high compared to that of the electrode-skin interface, then a very small current flows through the electrode-skin contact impedance and hence, its effect is negligible on the measured impedance. In order to eliminate the effect of the electrode-skin contact impedance on the amplitude of the injected current, a constant current circuit is normally used to inject the current. Thus, a four-electrode configuration is better than a two-electrode configuration. However, the disadvantage of a four-electrode configuration is that it requires more electrical connections to the body and this may create an inconvenience in clinical use.

1.4. Electrical properties of biological tissues

In order to understand the interaction between the injected current and the body tissues, it is necessary to study the electrical properties of biological tissues. It has also been considered important to study the effects of electrical properties of the intervening tissues on the amplitude and waveform shape of bioelectric events, recorded from the surface of the body (Geddes and Baker, 1967). Therefore, many studies have been carried out by the researchers to investigate the electrical properties of biological tissues as reviewed by Geddes and Baker (1967), Gabriel *et al* (1996), Pethig (1987), Duck (1990), McAdams and Jossinet (1995), Rigaud *et al* (1996) and Faes *et al*, (1999). This section briefly outlines the basic concepts regarding the electrical properties of biological tissues.

The electrical properties of biological tissues can be expressed in terms of conductivity (σ) or resistivity ($\rho = 1/\sigma$) and relative permittivity (ε). A flow of electric current is always accompanied by a magnetic field. However, the magnetic permeability of biological tissues is close to that of free space. Therefore, it is not necessary to consider the magnetic properties of tissues in the context of impedance based monitoring of physiological events (Pethig, 1987).

The electrical properties of tissues depend on their structure and composition. The ions dissolved in the tissue fluid are the charge carriers while the polar molecules of the tissue water, and the protein and lipid structure of the cell membranes, are responsible for the dielectric relaxation phenomenon (Rigaud *et al*, 1996). The equation proposed by Cole in 1940 has been considered suitable for mathematically describing the experimentally observed electrical behaviour of tissues (Duck, 1990; Rigaud *et al*, 1996). According to this equation, relative permittivity can be written as

$$\varepsilon = \varepsilon_{\infty} + \frac{\varepsilon_s - \varepsilon_{\infty}}{1 + (j\omega\tau)^{(1-m)}} - j\frac{\sigma_s}{\omega\varepsilon_0} \qquad 1.1$$

where,
ε_∞ = relative permittivity at a very high frequency
ε_0 = permittivity of free space
ε_s = relative permittivity at a very low frequency
σ_s = conductivity at a very low frequency
ω = frequency of injected current in radians s^{-1}
τ = relaxation time constant
m = relaxation coefficient

Alternatively, the conductivity can be expressed using an equivalent Cole equation as (Duck, 1990),

$$\sigma = \sigma_\infty + \frac{\sigma_s - \sigma_\infty}{1 + (-j\omega\tau)^{(1-m)}} + j\omega\varepsilon_\infty\varepsilon_0 \qquad 1.2$$

where,
σ_∞ = conductivity at a very high frequency

The empirical parameter m represents the distribution of relaxation times associated with the complex tissue structure and composition. The value of τ in equations 1.1 and 1.2 is the mean value of these relaxation times. If m is equal to 0, then there exists only one relaxation, and as the value of m approaches 1, it represents a wider Gaussian distribution of relaxation times (Rigaud *et al*, 1996).

The relative permittivity of biological tissues decreases with increasing frequency in three major steps denoted as α- β- and γ-dispersions. Figure 1.2 shows a schematic plot of relative permittivity and conductivity, versus frequency. The three dispersions characterise a type of relaxation that occurs in the three specific frequency ranges, and is typical for all types of biological tissues although the magnitude and the frequency ranges may vary (Rigaud *et al*, 1996).

The variation in electrical properties of tissues with frequency can be understood by taking into consideration their internal structure. The biological tissues are made up of cells, and each cell is surrounded by a 'cell membrane'. This cell membrane separates the intracellular components from the extracellular environment. The bilayer lipid structure of the cell membrane acts as a barrier to

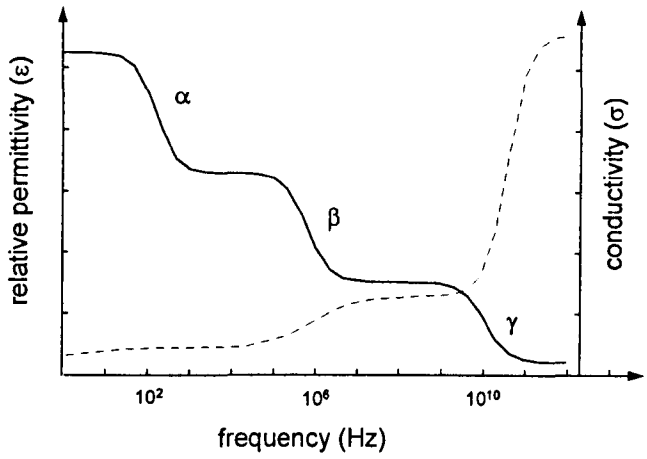

Figure 1.2 *A schematic plot of relative permittivity (continuous line) and conductivity (dashed line) of a typical biological tissue versus frequency showing α-, β-, and γ-dispersions; not to scale (adapted from Rigaud et al, 1996).*

the flow of charge carrying ions. The protein macromolecules embedded into the membrane enable only a selective passage of ions across the membrane. Thus, a cell can be considered as a capacitor having the intracellular and the extracellular fluids as the two conducting plates, separated by the membrane dielectric.

At a very low frequency (less than 100 Hz), the charging and the discharging of cell membranes can take place within one cycle of the injected sinusoidal current and thus, tissue permittivity is very high at these frequencies. At these frequencies, the flow of current occurs only through the extracellular spaces and the measured conductivity is only that of the extracellular fluid. The α-dispersion is believed to occur due to accumulation of charges at the membrane-electrolyte interface, thus forming an electrochemical double layer and also due to the ionic movement at the outer surface of the cell membrane (Duck, 1990; Rigaud *et al*, 1996).

The β-dispersion occurs at a frequency typically about 500 kHz. The cell membrane cannot charge and discharge completely within one time period of the sine wave at this frequency and therefore, the tissue permittivity decreases. The cell membrane capacitive reactance starts to decrease at this frequency allowing

the current to flow through the intracellular compartment. As a result, the tissue conductivity increases. Finally, γ-dispersion occurs at very high frequencies (in GHz range) due to relaxation of the polar molecules of the tissue water. At these very high frequencies, the cell membrane capacitive reactance is very low and therefore, the tissue appears to be a homogeneous medium in electrical terms.

Thus, it can be seen that by measuring the impedance of biological tissues at different frequencies, it is possible to probe into their structure at the microscopic level and to some extent identify the changes occurring in it. The techniques based on this approach are being developed to detect pre-malignant changes in the cervical (Brown *et al*, 2000) and oesophageal tissue (Gonzalez-Correa *et al*, 1999), and to detect tumours in the breast (Pethig, 1987).

At the macroscopic level, the structure and composition of different tissues, and hence, their electrical properties vary to a great extent. A list of resistivity values of some tissues is given in Table 1.1. All the values are at body temperature and in low-frequency region, i.e. below 1 MHz (Geddes and Baker, 1989). On the one hand, body fluids such as blood, digestive juices, urine, cerebrospinal fluid and lymph, have a high conductivity as they are rich in dissolved salts (Geddes and Baker, 1967). On the other, tissues such as bone and fat have a low conductivity due to low water content. The lung tissue also has a low conductivity due to presence of air inside the lungs. Some tissues such as skeletal muscles exhibit anisotropy. The conductivity of these tissues is higher in the direction of the fibres compared to that in the direction perpendicular to the fibres. In addition, this anisotropy depends on frequency of the injected current and reduces with increasing frequency (Epstein and Foster, 1983).

Table 1.1 *Resistivity values of biological tissues (adapted from Geddes and Baker, 1989)*

Tissue type	Resistivity (Ω cm)	Species
Blood	150	Human
Plasma	50-60	Mammal
Cerebrospinal fluid	65	Human
Bile	60	Cow, pig
Urine	30	Cow, pig
Cardiac muscle	400	Dog
Skeletal muscle (transverse)	1600	Dog
Skeletal muscle (longitudinal)	300	Dog
Lung	1500	Mammal
Kidney	370	Mammal
Liver	820	Dog
Spleen	885	Dog
Brain	580	Mammal
Fat	2500	Mammal

The impedance measurements carried out at a single frequency also provide useful information regarding the tissue composition and the associated physiological activity. For instance, the conductivity of lung tissue is a function of the ratio of air volume to fluid volume and hence, changes during breathing.

When impedance measurements are carried out on a particular segment of the body, these measurements reflect the changes in electrical properties of tissues within that body segment. These changes in electrical properties of tissues are due to the associated physiological activity. Thus, it is possible to monitor physiological activities occurring in different parts of the body by measuring impedance. Many applications of this technique such as Impedance cardiography, Impedance plethysmography and Impedance pneumography have been developed. These applications are described in some detail, in the latter part of this chapter.

The electrical properties of biological tissues also depend on temperature. The tissues have a positive temperature coefficient of conductivity (Geddes and Baker, 1967). At low frequencies, the conductivity changes by 1% to 3% for a 1°C change in temperature (Duck, 1990).

In order to understand the safety implications of injecting current into a human body, it is necessary to understand in what way this current might affect the body tissues, especially the electrically excitable tissues. This will be discussed in the following section.

1.5. Safety considerations

In order to monitor physiological activities using impedance, it is necessary to inject current into the body. It is important that this current should neither interfere with the functioning of the body nor cause any harm to it. The injected current flows through different types of tissues including the electrically excitable tissues such as skeletal muscles, cardiac muscles and nerve fibres. These tissues should not get stimulated by the passage of the current. When impedance measurements are carried out on the thoracic cavity, it is particularly important to make sure that the myocardium does not get stimulated because it may lead to potentially lethal consequences such as ventricular fibrillation.

The parameters of electrical stimulation of the excitable tissues can be obtained from their strength-duration curves. A typical strength-duration curve is shown in Figure 1.3. This curve shows the amplitude and the duration of a current pulse that would stimulate the particular tissue. The 'rheobase', denoted by 'b' in Figure 1.3, is defined as that amplitude of current required for stimulation with a pulse of infinitely long duration. This value depends on the size of the electrodes and their location with respect to the excitable tissue (Geddes and Baker, 1989). The time duration corresponding to a point on the curve having current amplitude equal to two times the rheobase is called 'chronaxie', as denoted by 'c' in Figure 1.3. The excitable tissues are characterised by their value of chronaxie. Typical values of chronaxie are 0.05 ms to 0.1 ms for the myocardium, 0.2 ms for the nerve fibres and 100 ms for the smooth muscles (Geddes *et al*, 1962). To avoid stimulation of

any tissue, the stimulus pulse width should be many times smaller than the chronaxie. The sinusoidal current can be considered as a train of pulses. Thus, taking into consideration the lowest value of chronaxie (0.05 ms), the frequency of injected sinusoidal current should be in excess of 20 kHz. In practice, a few millamperes (maximum 5 mA peak-to-peak), used in the frequency range of 10 kHz to 1 MHz, are considered safe.

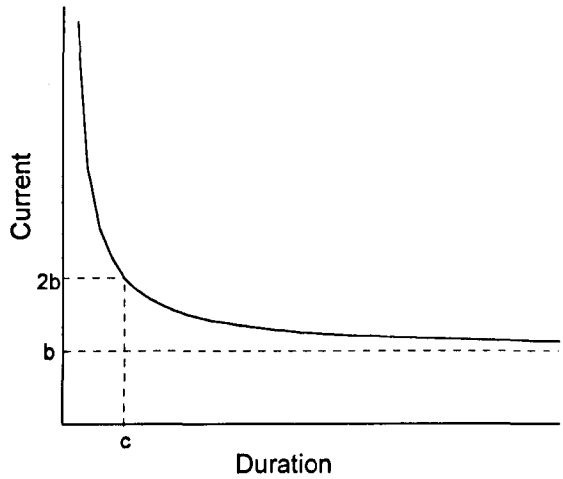

Figure 1.3 *A typical strength-duration curve for an excitable tissue (adapted from Geddes and Baker, 1989)*

The low amplitude of current used in impedance based physiological monitoring does not cause any significant heating of the tissues. It has been also shown that in human subjects, frequencies in kHz range do not cause stimulation of the sensory fibres located immediately underneath the electrodes (Geddes *et al*, 1962).

1.6. Applications of impedance techniques in physiology and medicine

A review of research in the field of impedance based monitoring of physiological events shows that this technique has many applications. Valentinuzzi *et al* (1996) have listed these applications as seen in Figure 1.4. Following is a brief description of some of these applications.

Impedance cardiography

- left ventricular ejection time
- systolic time interval
- pre-ejection period
- stroke index
- cardiac index
- preload
- peripheral vascular resistance
- left ventricular contractility

- stroke volume
- ventricular volume
- systolic ejection volume
- cardiac output
- blood flow (pulmonary artery and veins)
- ejection fraction

Intracardiac impedance
- ventricular volume

Myocardial impedance (in beating and transplanted heart)

Thoracic impedance (fibrillation, defibrillation)

Systemic lysis of a coronary thrombosis

Impedance pneumography

- apnoea, respiration and ventilation monitoring

- pulmonary perfusion, oedema effusion, congestion
- haemorrhage into the chest

Other applications

Skin impedance
- cutaneous impedance
- skin hydration
- endocrine activity

Cerebral and hydrocephalic blood flow

Intraventricular haemorrhage

Brain tissue impedance (with computed tomography guided stereotaxic biopsies)

Cerebrospinal impedance (early detection of epileptic seizures)

Neonatal cerebral circulation

Oviductal and uterine activity

Uterine contractions

Gait analysis (electrodes on the calf)

Muscular contractions

Muscular tissue bubbles after decompression schedule

Body fluids (pregnancy, hemodylasis)

Extra cellular and intracellular fluid volume

Eye movements

Nervous activity

Seasonal variations

Urine accumulation

Bladder volume

Stomach emptying

Cross sectional area in the gastrointestinal tract

Pulse transmission velocity from the aorta to the leg

Limb plethysmography (blood volume, deep venous thrombosis)

Figure 1.4 Physiological events recorded using impedance techniques (adapted from Valentinuzzi et al, 1996)

1.6.1. Impedance Cardiography

The resistivity of blood is lower than the resistivity of soft tissues. Therefore, the impedance of any body segment undergoes pulsatile changes during the cardiac cycle due to pulsatile changes in the blood volume. Impedance cardiography is an impedance based technique for monitoring the blood volume changes within the thoracic cavity. The impedance of the thoracic cavity is measured by placing band electrodes around the neck and the chest as shown in Figure 1.5. A typical record of impedance during breath hold is also shown along with the corresponding ECG waveform for time reference.

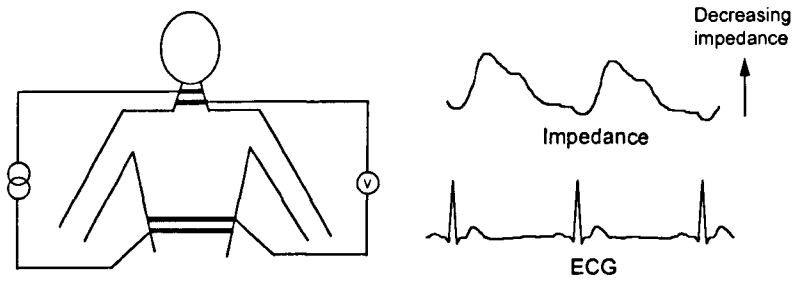

Figure 1.5 *Electrode placements, impedance and ECG plots in Impedance cardiography (adapted from Geddes and Baker, 1989)*

As reported by Geddes and Baker (1989), this impedance signal was mathematically related to stroke volume by Nyboer in 1959 and his expression was later modified by Kubicek and colleagues in 1966. However, this method has not been considered suitable for measuring stroke volume or cardiac output in quantitative terms due to a lack of understanding of the physiological origins of the observed impedance signal. On the other hand, this technique is considered suitable for monitoring changes in stroke volume from one physiological state to another in one individual. For example, this technique is used for studying changes in stroke volume from resting state to exercise state. Impedance cardiography is being currently investigated by many researchers as it is an inexpensive as well as a non-invasive technique for monitoring cardiac haemodynamics.

1.6.2. Impedance plethysmography of extremities

Impedance plethysmography is the technique for measuring blood flow and blood volume changes in an extremity such as a finger or a limb. In this technique, impedance of the extremity is measured by placing band electrodes as shown in Figure 1.6.

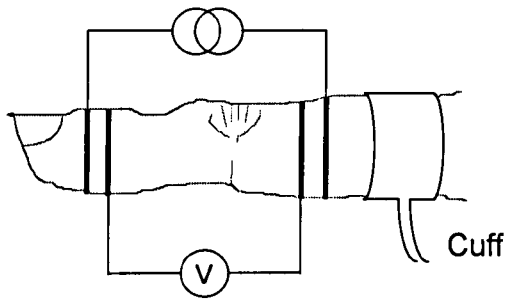

Figure 1.6 *Electrodes and cuff placement for Impedance plethysmography of a finger (adapted from Baker, 1979)*

The distance between the voltage sensing electrodes is required to be higher than 1.5 times the mean radius of the extremity. A cuff is placed proximal to the electrodes so that the venous return from the extremity can be blocked by pressurising this cuff. During the measurements, the cuff pressure is suddenly stepped up to about 50 mm of Hg. This pressure is sufficient to block the venous return, but is lower than the diastolic pressure so that the arterial flow is not affected. As a result, the blood volume in the extremity starts increasing. This causes the impedance to decrease, initially linearly and then logarithmically. The rate at which the impedance starts to decrease is calibrated in terms of blood flow. Once the cuff pressure is reduced to normal, the accumulated blood starts flowing out of the extremity. As a result, the impedance starts to increase to its initial value. The time taken by the impedance to reach its initial high value depends on the condition of the venous system. Thus, this technique is used to detect deep vein thrombosis.

1.6.3. Estimation of body composition using impedance

A knowledge of body composition is useful for determining the nutritional status of a patient. The conventional methods of measuring body composition are

relatively invasive and expensive. Thus, impedance techniques are a non-invasive and relatively inexpensive alternative to these methods. The body can be considered as made up of two components, the lean body mass and the fat body mass. The lean tissues are largely composed of water (73%) and the lean body mass is closely correlated with the total body water (Valentinuzzi *et al*, 1996). Thus, the lean tissues are relatively good conductors of current. On the other hand, the fat body mass consists of fat and bone tissue, which are a poor conductors of current. Therefore, the body impedance gives an estimate of the lean body mass provided differences in body shape can be taken into account. This body impedance is measured by placing electrodes on hand and foot. At low frequencies, the currents flows only through the extracellular compartment of the lean body mass because at these frequencies, the capacitive reactance of the cell membranes is too high. At high frequencies, the capacitive reactance of the cell membranes reduces, thus allowing the current to flow through the intracellular compartment as well. Thus, at these frequencies, the body impedance may be a measure of total lean body mass. Many studies have been carried out using this technique and active research still continues in this area.

1.6.4. Impedance pneumography

The conductivity of lung tissue is a function of the ratio of the air volume to fluid volume in the lungs and hence, undergoes a change during breathing. These changes in lung conductivity combined with the changes in thoracic geometry cause the impedance of the thoracic cavity to change during breathing. Impedance pneumography is the technique of monitoring breathing by measuring these changes in thoracic impedance. A typical arrangement of electrodes and the measured impedance trace are shown in Figure 1.7.

The outer electrodes are the 'drive' electrodes and a constant amplitude alternating current is injected into the thoracic cavity via these electrodes. The inner electrodes are the 'receive' electrodes and the voltage between these electrodes is measured. The thoracic impedance increases during inspiration and decreases during expiration. There is a high correlation between the impedance change and the volume of respired air and the relationship between these two

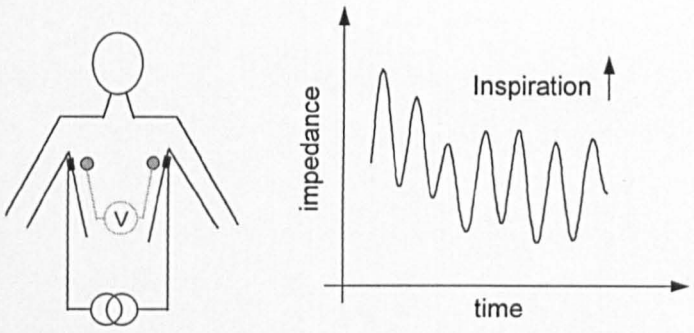

Figure 1.7 *Electrode placement and impedance waveform in Impedance pneumography*

variables is approximately linear. However, impedance pneumography is not considered suitable for measuring changes in lung air volume in quantitative terms because the relationship varies with the shape and size of the thoracic cavity and is also affected by the changes in posture and body movements. The important aspects of impedance pneumography are discussed in detail in the following chapter.

1.7. Outline of the thesis

The following chapter (Chapter 2) begins with a historical overview of impedance pneumography. This is followed by a review of the work carried out by investigators to understand various aspects of impedance pneumography such as physiological origins of breathing related impedance changes and choice of electrode placement. The chapter ends by stating the strategy adopted in this project.

The study of the relationship between electrode placement and breathing related impedance measurements is described in Chapters 3 and 4. This relationship has been studied experimentally by analysing the data recorded from human subjects and is described in Chapter 3. The same relationship has also been studied theoretically using the 'sensitivity method' and is described in Chapter 4.

Chapter 5 begins with a discussion of the problem of movement artefacts and reviews different techniques suggested in the literature for reduction of

movement artefacts. This is followed by a description of the work based on impedance imaging and aimed at developing a technique for detecting breathing in the presence of gross body movements. Chapter 6 describes the work involving a strategic placement of electrodes for the reduction of movement artefacts and also describes the experiments carried out to study the effect of frequency of injected current on movement artefacts.

Chapter 7 summarises the work carried out in this project, draws conclusions from the results and gives some suggestions for future work. The scientific papers published in journals during this work are appended in Appendix A.

Chapter 2. Impedance pneumography and electrode placement

2.1. Introduction

The technique of impedance pneumography has been investigated to a considerable extent for many years. This chapter begins with a look at the history of impedance pneumography. This is followed by a review of the work aimed at investigating the physiological origins of breathing related changes in thoracic impedance. It is also important to understand the effect of electrode placement on the measured value of thoracic impedance. Therefore, a review of the literature has been carried out to study this aspect of impedance pneumography. This chapter ends by stating the approach adopted in the present project.

2.2. Historical background of impedance pneumography

The early developments in the field of impedance pneumography have been reviewed by Pacela (1966) and Baker (1979). According to Baker (1979), Atzler and Lehmann were the first to observe and report breathing related impedance changes in 1932-1935. Their technique involved measuring capacitance changes associated with cardiac activity in human subjects. However, large changes in capacitance were observed in association with breathing as well. Fenning and Bonar (1936-37) recorded maternal respiration, intrauterine foetal respiration and uterine contractions in rats using a similar capacitance method. Pacela (1966) has reported that Nyboer in 1940, had observed breathing related impedance changes while studying cardiac activity and had verified their source by simultaneously recording the respired air volume using a spirometer. It appears from the account of Baker (1979) that Schaefer and his colleagues were the first to monitor breathing by placing electrodes directly in contact with the body. In an experimental study carried out by them in 1949, they used Wheatstone bridge to measure impedance between two subcutaneous electrodes attached to the thoracic cavity in animals as well as in human subjects.

The first systematic study of monitoring breathing by measuring impedance in human subjects was carried out by Goldensohn and Zablow (1959). They measured impedance by placing two electrodes on either wrists to inject current at a frequency of 10 kHz. The voltage was measured by placing two more electrodes higher up on each arm. They also attempted to quantify the relationship between impedance changes and the volume of respired air.

The research on impedance based monitoring of breathing in humans gathered pace in 1960 and thereafter, when the American government was planning to carry out manned space flights (Valentinuzzi, 1996). An essential requirement of this project was to develop techniques for monitoring vital physiological activities of the space crew such as cardiac activity and breathing. It was obviously not possible to monitor breathing using a spirometer inside the manned capsule of the shuttle as there was very limited room in it, and the space crew was not to be distracted from their tasks. Under such circumstances, impedance pneumography appeared to be the most suitable technique of monitoring breathing. According to Valentinuzzi (1996), the research group at Baylor University, Houston, TX, USA, undertook the task of developing an impedance based breathing monitor for use in space.

Geddes and his colleagues from Baylor University seem to be the first to come up with the term 'Impedance pneumograph' and also to discuss in detail various issues involved in this technique (Geddes *et al*, 1962). They discussed the safety requirements of an impedance based breathing monitor and laid out the basis for selecting the frequency of injected current. They observed that, for a given change in the volume of respired air, the magnitude of change in thoracic impedance was affected by the electrode placement. They reported that there was a good correlation between impedance changes and the volume of respired air. They also suggested that if the impedance pneumograph was calibrated using a spirometer, then it could be used to measure lung ventilation.

Thus, the aim of many subsequent studies was to investigate the impedance-air volume relationship in quantitative terms (Allison *et al*, 1964; Kubicek *et al* 1964; Hamilton *et al*, 1965; Baker *et al*, 1965,1966). In spite of many such studies and

even though it was easy to calibrate the impedance pneumograph using a spirometer, there was a reluctance to use it for quantitative studies. This was due to a limited understanding of the physiological origins of breathing related impedance changes of the thoracic cavity (Baker, 1979). Initially it was believed that, changes in lung resistivity due to changes in lung air volume, were solely responsible for the changes in thoracic impedance. However, it was later reported that, in addition to changes in lung resistivity, the changes in circumference of the thoracic cavity and the downward movement of the diaphragm were also responsible for changes in thoracic impedance (Baker *et al*, 1966). It was also reported that, the impedance-air volume relationship was dependant on the physical build of the subject (Baker *et al*, 1965; Valentinuzzi *et al*, 1971), and also on the posture and electrode placement (Hamilton *et al*, 1965; Logic *et al*, 1967). Furthermore, Albisser and Carmichael (1974) concluded from their model studies that geometrical changes of the thoracic cavity had a greater influence on the changes in thoracic impedance. Thus, impedance pneumography was considered suitable only to monitor qualitative parameters such as breathing rate and absence of breathing, i.e. apnoea, than for any quantitative studies.

Steinschneider (1972) was the first to propose a hypothesis that there was a link between prolonged apnoea and Sudden Infant Death Syndrome (SIDS). He suggested that if breathing could be monitored in children at risk of SIDS and an alarm could be raised on the occurrence of apnoea, then it would prevent death. In spite of the doubts expressed by some doctors regarding this hypothesis, many others started recommending use of such apnoea monitors at home (BBC, 1999). Impedance pneumography again appeared to be a suitable technique for monitoring breathing in these apnoea monitors because of its many advantages. According to a report by the National Institute of Health, USA (1987), impedance pneumography was used in a majority of the commercially available apnoea monitors by 1987, in the USA. These impedance based monitors had an advantage of not requiring a device to be placed within the airway. They also created very little obstruction to the body movements. Hence, they were well tolerated by children. They were also very easy to use at home (Baker, 1979).

Furthermore, it was possible to monitor cardiac activity using the same electrodes (Geddes *et al*, 1962). However, there were some major drawbacks of these impedance based apnoea monitors. The apnoea could not be detected in the presence of gross body movements such as arm movements and changes in posture because large artefacts appeared in the impedance signal during such movements. In some cases, the cardiac related impedance changes were misclassified as breathing and thus, apnoea went undetected (Southall *et al*, 1980). They were also reported to fail in detecting obstructive apnoea (Warburton *et al*, 1977). Thus, many researchers carried out studies to develop methods of overcoming these drawbacks (Wilson *et al*, 1982, Shaikain *et al*, 1985). These studies continue to be carried out in recent years (Mayotte *et al*, 1994; Mayotte *et al*, 1996; Rosell and Webster, 1995a; Rosell *et al*, 1995b).

Another important development in recent years is that of Electrical Impedance Tomography (EIT). In EIT, a cross-sectional image displaying an internal resistivity distribution of a body segment is produced. These EIT images have a resolution of the order of 10% of the dimension of the body segment (Dijkstra *et al*, 1993). This resolution is considerably lower than that of the anatomical images obtained from CAT scan or MRI. However, it is sufficient to separate the two lungs in an image of the thoracic cavity. In addition, the EIT images contain useful functional information as the resistivity of the lungs appears to change during breathing. The changes in lung resistivity as obtained by EIT were observed to correlate well with the volume of inspired air ($r > 0.95$), and the volumetric accuracy was within ±10% of the spirometric measurements. Thus, EIT can be used to monitor lung ventilation (Harris *et al*, 1988). Further developments in EIT Spectroscopy have created a possibility of being able to identify lung pathology (Brown *et al*, 1995). However, there are two major drawbacks of EIT. Firstly, EIT requires attaching a large number of electrodes to the body and this is inconvenient in a clinical environment (Boone *et al*, 1997). Secondly, the EIT measurements are also affected by movement artefacts (Hampshire *et al*, 1995).

From this historical account, it can be seen that under many circumstances, impedance pneumography has been considered a very suitable technique to monitor breathing. However, the problem of movement artefacts appears to be a major limitation of this technique. In order to decide a strategy to overcome this limitation, it seems necessary to first understand the physiological origins of the breathing related impedance changes of the thorax. The following sections review the experimental and theoretical studies aimed at identifying the physiological origins of these thoracic impedance changes. As a first step, the subsequent section describes the physiology of breathing.

2.3. Physiology of breathing

All the living cells of a human body need oxygen (O_2) to carry out their metabolic processes and they generate carbon dioxide (CO_2) as a waste product of the metabolic processes. The respiratory system along with the cardiovascular system is responsible to supply O_2 and to remove CO_2 from the cells. The exchange of gases between the cells, the blood and the atmosphere is called 'respiration' (Tortora and Grabowski, 1993). This process of respiration involves three basic processes. The 'pulmonary ventilation' or 'breathing' is the process of in-flow (inspiration) and out-flow (expiration) of air in and out of the lungs, respectively. The 'external respiration' involves gas exchange between the lungs and the blood, and the 'internal respiration' is the process of gas exchange between the blood and the cells. The technique of impedance pneumography is concerned with breathing and therefore, this process is further explained below.

The direction of the flow of air in and out of the lungs, depends upon the direction of the pressure gradient established between the lungs and the atmosphere. Just before the start of inspiration, the pressure inside the lungs is equal to the atmospheric pressure. For the air to flow into the lungs, the lung pressure needs to drop below the atmospheric pressure. This occurs due to a sequence of events as explained below.

During inspiration the thoracic cavity expands due to contraction of the principle inspiratory muscles, which are the diaphragm and the external intercostal

muscles. The diaphragm is a dome shaped skeletal muscle forming the lower floor of the thoracic cavity and is innervated by the phrenic nerve fibres. The contraction of the diaphragm causes it to flatten and move downward, thus increasing the vertical dimension of the thoracic cavity. The diaphragm moves through a distance of about 1 cm to 1.5 cm during quiet tidal breathing and can move up to 7 cm to 13 cm during deep breathing (Wade, 1954). At the same time, the external intercostal muscles also contract, causing the ribs to lift and the sternum to move forward. This results in an increase in the circumference of the thoracic cavity by about 1.2 cm during quiet tidal breathing (Wade, 1954). The lungs are covered by a two layer serous membrane, the 'pleural membrane'. The outer 'parietal' layer is attached to the thoracic cavity and is pulled outward due to the expansion of the thoracic cavity. The inner 'visceral' layer is also pulled outward along with the parietal layer because both these layers strongly adhere to each other. This is due to the surface tension of the moist adjoining surfaces and also due to the fact that the pressure between the two layers is below the atmospheric pressure. This leads to an expansion of the lungs causing the pressure inside the lungs to drop below the atmospheric pressure. As a result the air flows into the lungs. The diaphragm movement is responsible for about 75% of the total air movement during breathing, while the remaining 25% occurs due to an increase in the circumference of the thoracic cavity (Wade, 1954).

During quiet tidal breathing, the process of expiration is a passive process unlike the inspiration. When the diaphragm relaxes, it moves upwards and returns to its initial dome shape due to elasticity. The external intercostal muscles also relax causing the rib cage to move downwards and the sternum to move backwards. This reduces the size of the thoracic cavity. In addition, an inward pull is exerted due to elasticity of the alveolar membrane, alveolar ducts and bronchioles. The surface tension of the alveolar fluid also exerts further inward pull. As a result, the lung volume reduces causing the lung pressure to increase above the atmospheric pressure, thus forcing the air out of the lungs.

During forced inspiration, the accessory muscles such as sternocleidomastoid and pectoralis minor also participate in causing a further increase in the size of

the thoracic cavity. Similarly, during forced expiration, the abdominal muscles and internal intercostal muscles contract to force the air out of the lungs.

After considering the various events that occur during breathing, it is now important to understand the way in which these events affect the impedance measurements of the thoracic cavity.

2.4. Origins of breathing related changes in thoracic impedance

Let us first consider the general problem of monitoring physiological events by measuring impedance. The impedance of a body segment is measured by injecting a current into the body segment via a pair of 'drive' electrodes placed on the surface. The voltage is measured from the same pair of electrodes as in a 'two-electrode' or 'bipolar' configuration, or from a different pair of 'receive' electrodes placed at an appropriate location as in a 'four-electrode' or 'tetrapolar' configuration. The injected current establishes a potential distribution inside and on the surface of the body. This potential distribution is a function of three factors, namely the geometry of the body, the electrical properties of the tissues and the location of the drive electrodes. Therefore, the measured voltage is also a function of these three factors. However, in addition to these three factors, the measured voltage also depends on the location of the receive electrodes. The physiological activity being monitored may affect all or some these factors, thus causing a change in the measured impedance.

In order to monitor breathing, the electrodes are normally placed on the surface of the thoracic cavity. Therefore, for a given electrode placement, the measured impedance will depend on the electrical properties of the tissues within the thoracic cavity and also on the geometry of the thoracic cavity. The resistivity of the lung tissue is a function of its air content and undergoes a change during breathing. As lungs occupy a majority of the thoracic cavity volume, these changes in lung resistivity will significantly affect the thoracic impedance during breathing. In addition, the circumference of the thoracic cavity also changes and the diaphragm moves vertically during breathing, and these two factors will also

have some effect on the thoracic impedance. Thus, the physiological activity of breathing appears to affect the thoracic impedance through these three factors.

In the following sub-section, an attempt is made to understand the relationship between the lung resistivity and the lung air content by reviewing the literature. This is followed by a review of the studies aimed at investigating the effect of the other two factors on the thoracic impedance. Finally, a review of the literature is carried out to know the relative contribution of each of these three factors to the thoracic impedance.

2.4.1. Structure of the lung tissue

In order to understand the relationship between the electrical properties of lung tissue and its air content, it is necessary to first know its structure. The lungs are a complex network of air ducts and blood vessels of varying sizes, which are held together by connective and muscular tissues. Each of the two lungs is connected to the trachea via a 'primary bronchus'. The primary bronchus divides and re-divides into air ducts which progressively become smaller in size, the smallest being the 'respiratory bronchiole'. The respiratory bronchiole further branches into 'alveolar ducts' and these alveolar ducts terminate into 'alveolar sacs'. An alveolar sac is formed by two or more 'alveoli' sharing a common opening. An 'alveolus' is a cup-shaped cavity lined by two types of epithelial cells from inside and supported by a basement membrane. The type II epithelial cells of the inner lining secrete a fluid that forms an interface between the air and the alveolar cells. This fluid has a very low surface tension and thus, does not cause alveoli to collapse. The blood vessels of the lungs also have a similar branched pattern, the smallest blood vessel being the 'blood capillary'. These blood capillaries form a network on the outside of the alveolar walls and the gas exchange takes place across the alveolar and the capillary walls.

2.4.2. Electrical properties of the lung tissue

Taking into consideration the structure of the lung tissue, in electrical terms, it can be considered as a composite material having two components, the

biological tissues and air. The biological tissues have a relatively low resistivity and therefore, can conduct current. On the other hand, the air is an almost perfect insulator. The resistivity of lung tissue is a function of the relative volumes of these two components. About 80% of the lung volume is occupied by air (Severinghaus *et al*, 1972). Therefore, the resistivity of lung tissue is higher compared to the resistivity of other soft tissues. This can be seen in Table 1.1 of the previous chapter. In addition, the lung air volume undergoes a change during breathing and thus, the resistivity varies during breathing.

Geddes and Baker (1967) have listed the values of lung resistivity, obtained by reviewing the work of many researchers. The average value of lung resistivity according to Geddes and Baker (1967) is equal to 1275 Ω cm at frequencies below 100 kHz. The ratio of the resistivity at maximum inspiration to maximum expiration has been observed to lie between 1.23 and 3.41.

An experimental study was carried out by Witsoe and Kinnen (1967) to establish a quantitative relationship between the lung resistivity and air content. The resistivity of lung tissue was measured *in-vivo* on the surface of a canine lung at a frequency of 100 kHz. The average value of lung resistivity obtained from 7 dogs was found to increase linearly with increasing lung air content. The lung resistivity was between 1500 Ω cm and 2000 Ω cm at the level of normal expiration and increased at the rate of 200 Ω cm per 100 cm^3 of inspired air.

A linear relationship between lung resistivity and air content was also obtained experimentally by Harris *et al* (1988). They obtained EIT images from the thoracic cavity of normal human subjects between the 3rd and 4th intercostal space. The volume of inspired air was measured using a spirometer. The resistivity values within a region-of-interest defined over the lungs were obtained for different volumes of inspired air. The relationship between the lung resistivity and the lung air volume was found to be linear and the volumetric accuracy was within ±10% of the spirometric measurements.

There have also been some studies based on an electrical model of the lung tissue. A simple electrical model of the lung tissue was suggested by Pasaquali

(1967) and Olsson *et al* (1970). In this model, the lung tissue was assumed to be a suspension of small particles, representing the air compartments, in a homogeneous medium, representing the biological tissues in a simplified way. The air is known to have a very high resistivity. Therefore, a simplified Maxwell's equation was used to write an equation for the lung resistivity (ρ_l) as,

$$\rho_l = \frac{\left(1+\frac{V_r}{x}\right)}{(1-V_r)} \cdot \rho_t \qquad 2.1$$

where,
ρ_t = lumped value of resistivity of different types of tissues constituting a lung
V_r = ratio of the volume of air to the total volume of the lung

The ratio V_r can be written as,

$$V_r = \frac{V_a}{V_a + V_t} \qquad 2.2$$

where,
V_a = volume of air
V_t = volume of biological tissues

The value of factor x in equation 2.1 depends on the shape of the suspended particles. In the case of spherical particles x is equal to 2, in the case of cylindrical particles arranged with their axes perpendicular to the direction of current flow, x is equal to 1, and in the case of cylindrical particles arranged with their axes parallel to the direction of current flow, x is equal to ∞ (Olsson *et al*, 1970). As described earlier, the lungs consist of air ducts having a cylindrical shape and oriented in many possible directions and also the alveolar sacs, having an approximately spherical shape. Therefore, it is difficult to assign a single value to x. Olsson *et al* (1970) suggested that on examining the structure of the lung tissue, it appeared that the direction of the current flow was parallel to the cylindrical air ducts in the majority of the lung regions. Therefore, it was considered reasonable to assume a very high value for x. Thus, by further

simplifying equation 2.1, the following equation could be written for lung resistivity.

$$\rho_l = \left(1 + \frac{V_a}{V_t}\right) \cdot \rho_t \qquad 2.3$$

If no change occurs in the tissue volume (V_t) during breathing, then it can be seen from equation 2.3 that lung resistivity increases linearly with air volume.

An experimental and a theoretical study were carried out by Nopp *et al* (1993) to investigate the variation of lung electrical properties with the air content, and to explain the underlying physical phenomenon by developing a model based on the actual structure of the lung tissue. *In-vitro* measurements were carried out on the lung tissue samples, excised from calves, in the frequency range of 5 kHz to 100 kHz. In this study, the dielectric properties were expressed in terms of conductivity instead of resistivity and relative permittivity, and the lung air content was expressed in terms of a 'filling factor' (F). This filling factor was defined as the ratio of air volume to tissue volume. The results at the frequency of 50 kHz indicated that conductivity as well as relative permitivity decreased with increasing lung air volume. The plot of conductivity versus F had a large scatter of points and therefore, a definite mathematical relationship could not be established. This large scatter was attributed to the destruction of some tissue samples due to accidental hyperventilation that seemed to have occurred while carrying out some testing before taking the actual measurements.

A model of lung tissue was developed to investigate the underlying causes of the observed variation in the lung dielectric properties with air volume. This model was based on the actual structure of the lung parenchyma. The alveoli were assumed to have a cube shape and their walls were assumed to be made up of 85% blood-filled capillaries, 12% epithelial cells and 3% intracellular fluid. The results obtained from this model suggested that the observed variation in the lung dielectric properties with air content was due to a change in the thickness of

the alveolar walls, and also due to deformation of blood capillaries and epithelial cells.

Further studies have been carried out by researchers to investigate the relationship between lung electrical properties and frequency of injected current. Brown *et al* (1994) measured the real part of lung impedance using a four-electrode system as well as a multi-frequency EIT system, in the frequency range of 9.6 kHz and 614 kHz. The base value of the lung impedance (Z_l) reduced to about 60-70% of its low frequency value, at the frequency of 614 kHz. There was not much variation with frequency in the value of change in lung impedance during breathing (ΔZ_l). The fractional change in impedance ($\Delta Z_l/Z_l$) was found to increase to 150% of its low frequency value, at the frequency of 614 kHz. These changes were satisfactorily modelled using a Cole-Cole equation. A model, based on the actual structure of the lung tissue, was also developed. However, there was only a limited agreement between the experimental results and the model results. Therefore, a need was expressed to develop a better model to explain the multi-frequency electrical properties of the lung tissue.

Nopp *et al* (1997) modified their model of the lung tissue (Nopp *et al*, 1993; described earlier) to include the effect of frequency of injected current. They first obtained experimental data by measuring lung impedance from EIT images at different frequencies (9.6 kHz to 1.2 MHz) and at different values of the filling factor (F, defined earlier). The lung resistivity linearly increased with F and the slope of the line describing this relationship increased with frequency. As expected for any biological tissue, the base value of lung resistivity was found to decrease with frequency. These variations in lung resistivity with frequency were hypothesised to be originating from the dispersion of the extra-capillary blood vessels. Therefore, the walls of the cube-shaped alveoli were modelled as a suspension of blood filled spheres having a diameter of 70 μm. The variation of lung resistivity with F obtained from the model was similar to that obtained experimentally. However, the multi-frequency electrical behaviour of the lung tissue as obtained from this model, seemed to agree with the experimental data

only to a limited extent. It was suggested that the lung tissue had four dispersions, those caused by the extra-capillary blood vessels, the epithelial cells, the blood and the blood capillaries.

The studies reviewed above suggest one important result that the lung resistivity is a linear function of the air content. The latter studies also suggest that the electrical properties of the lung tissue have a characteristic variation with the frequency of injected current.

Thus, it can be seen that the changes in lung resistivity are one of the physiological factors responsible for a change in the thoracic impedance during breathing. As mentioned earlier, the geometrical changes of the thoracic cavity will also affect the thoracic impedance. There have been studies to investigate the effect of these factors on the thoracic impedance. These studies are reviewed in the following sub-section.

2.4.3. Effects of breathing related changes in thoracic geometry on thoracic impedance

It was stated in section 2.3 while describing the physiology of breathing that the circumference of the thoracic cavity changes and the diaphragm moves vertically during breathing. These factors will also have some effect on the thoracic impedance. This aspect has been studied by many investigators as seen in the following review.

Baker *et al* (1966) measured thoracic impedance in anaesthetised dogs by placing two electrodes bilaterally on the midaxillary line at the xiphoid level. The impedance was measured at a frequency of 50 kHz. The thoracic circumference was measured at the same level using a bellows-type pneumograph and the intra-tracheal pressure was measured using a strain gauge pressure transducer. The volume of air was either measured using a spirometer during spontaneous breathing or was controlled using an adjustable stroke respirator. In order to cause tetanus of the diaphragm, the phrenic nerves were sectioned at the level of the neck and were stimulated distally by placing bipolar electrodes. During the tetanus, the diaphragm remained motionless and thus, it was possible to

eliminate the contribution of the diaphragm movement to the changes in the thoracic impedance. In this way, the effects of the two factors, the change in thoracic circumference and the diaphragm movement, could be studied independently. On the other hand, when the diaphragm was not stimulated, it could move normally during artificial ventilation. The thoracic impedance was measured during spontaneous breathing and also during artificial ventilation, under different conditions such as before and after sectioning of the phrenic nerves, and in the presence and the absence of the diaphragmatic tetanus. However, only the results obtained during constant volume positive pressure ventilation are discussed here as they seem to provide useful information regarding the effect of the diaphragm movement. These results showed that the change in impedance per unit volume of the respired air was lower when the diaphragm was tetanised, than when it was not tetanised. This indicated that the diaphragm movement added an extra component to the changes in thoracic impedance. A possible explanation for this result could be that as the diaphragm moves, the low resistivity abdominal organs move into and out of the measurement field causing a change in the measured thoracic impedance.

In a second study carried out by the same research group and reviewed by Baker (1979), the effect of change in thoracic circumference was studied independently using the same experimental set-up. The dogs were made to carry out spontaneous breathing after sectioning the phrenic nerves. As a result, the diaphragm could not move during this period and the breathing occurred only due to the activity of the intercostal muscles. After some time, the air inlet to the lungs was closed. As a consequence, the magnitude of the breathing related impedance changes dropped to a low value. However, small excursions in the impedance signal continued to occur. They were attributed to the changes in thoracic circumference, which was due to continued efforts of the dogs to breath against the closed air inlet. The tetanus of the diaphragm caused a small and sustained increase in the impedance. The small excursions due to the changes in thoracic circumference were superimposed on this sustained increase in impedance. This indicated that the changes in thoracic circumference also added a component to the overall changes in thoracic impedance during breathing. The

fact that the magnitude of the impedance change was low when the air inlet was closed, suggested that the changes in lung resistivity had a greater influence on the thoracic impedance.

An experimental study was carried out by Kawakami *et al* (1964), with an aim of identifying the components of the breathing related changes in thoracic impedance. The impedance was measured on anaesthetised dogs by injecting a current of 1 mA peak-to-peak at 50 kHz via two electrodes placed bilaterally on the midaxillary line. These measurements were obtained from three different levels, corresponding to the 4^{th}, 6^{th} and 8^{th} intercostal spaces. The thoracic diameter was also measured at these three levels by placing two coils on the midaxillary line, one on either side. The change in mutual inductance between these two coils was a measure of change in the thoracic diameter. The intra-tracheal pressure was also measured using a low pressure strain gauge transducer. There was a high correlation between the impedance and the thoracic diameter at the level of the 4th intercostal space during artificial ventilation. However, at the same level, the impedance decreased whereas the thoracic diameter increased after a bolus of hypertonic saline solution was injected in the inferior vena cava or in the right heart. This indicated that the changes in lung resistivity dominated the measured thoracic impedance at this level.

Further experiments were carried out to investigate the effect of the diaphragm movement on the thoracic impedance. The impedance and the thoracic diameter were measured at the level of the 6^{th} and the 8^{th} intercostal space during artificial ventilation. The changes in impedance and thoracic diameter were in the same direction at both these levels during artificial ventilation. These measurements were also obtained after injecting 1 ml of ether gas along with 5 ml of physiological saline solution into the inferior vena cava during breath hold at expiratory level. At the level of the 6^{th} intercostal space, the impedance as well as the thoracic diameter increased after the injection. However, at the level of the 8^{th} intercostal space, the thoracic diameter increased but the impedance remained unaffected after the injection. This indicated that the increase in lung resistivity

due to ether was not sensed at the level of the 8th intercostal space. Therefore, it was suggested that the changes in impedance observed at this level were mainly due to the diaphragm movement. It was thought that, at end expiration, the region in the vicinity of the electrodes was occupied by the low resistivity abdominal organs such as liver and spleen. These organs moved downward along with the diaphragm during inspiration and were replaced by the high resistivity lung tissue. Thus, it was suggested that breathing related impedance changes measured at the level of the 8th intercostal space were due to the diaphragm movement and not due to the changes in lung resistivity.

The results of these two studies indicate that apart from the changes in lung resistivity, the geometrical changes of the thoracic cavity also contribute to the breathing related changes of the thoracic impedance. It appears from these results that the changes in lung resistivity dominate the measured thoracic impedance. However, this second conclusion has been questioned by some other researchers. These researchers carried out experimental as well as theoretical studies to demonstrate that the geometrical factors dominated the thoracic impedance. The following is the review of some such studies.

In a study carried out by Baker and Geddes in 1966 and reviewed by Baker (1979), the current pathways within the thoracic cavity were obtained in dead dogs. The current injecting electrodes were placed bilaterally on the midaxillary line at the xiphoid level. It was observed that 4.7% of the total injected current passed through the lungs, 5.6% passed through the anterior thoracic pathway, 79.9% passed through the posterior thoracic pathway and 9.8% passed through the liver and the diaphragm. Baker (1970) suggested that on the basis of these values a simple model could be developed. This model consisted of four resistors having appropriate values to represent the four current pathways, and a shunt capacitance. According to the results obtained from this model, the change in lung resistivity required to cause the observed change in the thoracic impedance, was much higher than the change in lung resistivity normally observed during breathing. It is important to note that it is necessary to treat these results with

caution because anatomy of the thoracic cavity of a dog is very different from that of a human.

Albisser and Carmichael (1974) carried out a theoretical study with an aim of investigating the relative contribution of various physiological factors. They modelled the thoracic cavity as two concentric cylinders. The inner cylinder was assumed to represent the lungs while the annular space between the two cylinders was assumed to be the thoracic wall. They used a two-electrode configuration with electrodes placed at diametrically opposite locations on the surface of the outer cylinder. This model was analysed to study the effect of thoracic circumference and electrode size on the thoracic impedance. The effect of the diaphragm movement was studied by measuring impedance across the diameter of a saline filled cylindrical tank. The movement of the diaphragm was simulated by holding an insulating disk within the tank at different vertical distances from the electrodes. The impedance data was also recorded from two human subjects during diaphragmatic breathing and costal breathing. The results of the model studies showed that the changes in thoracic circumference were 5 times more important than the changes in lung resistivity and the electrode size was 40 times more important for the two-electrode configuration used, than the lung resistivity. The results obtained from the tank experiment suggested that the diaphragm movement was not as significant as the thoracic circumference or the electrode size. However, it was still more important than the changes in lung resistivity. The impedance data obtained from human subjects indicated that the magnitude of change in impedance during the costal breathing was about 1.7 to 1.8 times the impedance changes during the diaphragmatic breathing. From these results, the researchers concluded that the geometrical changes of the thoracic cavity and other factors such as electrode size had much more influence on the thoracic impedance than the lung resistivity. Therefore, they suggested that impedance pneumography could not be considered suitable as a quantitative technique for monitoring the changes in lung air volume. Instead, they suggested that it should only be used to monitor qualitative parameters such as breathing rate and to detect apnoea.

It can be seen that the findings of the above two studies contradict with those of the studies described before. A more systematic study might be needed for deciding which factors actually have a greater influence on the thoracic impedance. However, in this context, it is important to take a note of some other studies, which seem to suggest that the electrode placement may have an important role in deciding the relative contribution of the three factors mentioned above. The following is a review of such studies.

Kawakami *et al* (1973) measured thoracic impedance in dogs using a four-electrode configuration. The drive as well as the receive electrodes were placed on the same side of the thoracic cavity. A balloon catheter was placed in the bronchus associated with the lobe of a lung in the vicinity of the electrodes, so that it could be blocked. The impedance was measured during artificial ventilation, before and after blocking the particular airway. It was observed that the magnitude of the change in impedance reduced when the bronchus was blocked. This indicated that for the electrode placement used, the changes in thoracic impedance were mainly due to changes in lung resistivity.

Another example that can be considered in this context is that of EIT. In EIT, an electrode placement very different from the midaxillary placement is used to record impedance data from the thoracic cavity. An EIT image displays two distinct lung regions, undergoing a change in resistivity during breathing. By measuring the resistivity changes within a region-of-interest defined specifically over the lungs, it is possible to reduce the influence of resistivity changes of tissues other than lungs. Thus, it appears that, if an appropriate electrode placement is used, then it is possible to maximise the contribution of the changes in lung resistivity to the thoracic impedance.

Let us now understand why it is necessary to maximise the contribution of the changes in lung resistivity for increasing the reliability of impedance pneumography. If we consider the sequence of physiological events taking place during breathing, we can identify a distinct cause-effect relationship between those events. The geometrical changes of the thoracic cavity, due to contraction of the principle inspiratory muscles, act as 'causative' factors to the changes in

lung air volume whereas the changes in lung resistivity are an 'effect' of these changes in lung air volume. However, in some situations such as obstructive apnoea and during gross body movements, the geometrical changes do not necessarily cause a change in the lung air volume. During obstructive apnoea, the patient continues to carry out breathing efforts using the respiratory muscles even though the upper airway has been blocked. Therefore, even though the breathing related geometrical changes of the thoracic cavity are present, there is no movement of air in or out of the lungs. During body movements such as arm movements and changes in posture, the geometrical changes due to these movements are also not related to air movement. Thus, in these two situations, if the geometrical factors have a greater influence than the lung resistivity on the thoracic impedance, then it will not reflect faithfully the movement of air in and out of the lungs, and thus, will lead to an unreliable monitoring of breathing. On the other hand, any change in the lung air volume will always cause a change in the lung resistivity. Therefore, if the thoracic impedance is more influenced by the lung resistivity, then impedance pneumography will be a more reliable technique for monitoring breathing.

Thus, in order to increase the reliability of impedance pneumography, it would be necessary to increase the 'specificity' of the impedance measurements to lung resistivity changes, and this can be achieved by using an appropriate electrode placement. Many different electrode placements have been suggested by the researchers in the past. The following section reviews these electrode placements.

2.5. Electrode placements in impedance pneumography

The first systematic attempt at monitoring breathing using impedance was made by Goldensohn and Zablow (1959). They placed two electrodes on either wrist to inject current and placed two more electrodes higher up on each arm to measure the voltage. They did not state the criteria for using these electrode placements. However, they clearly stated that they used a four-electrode configuration instead of a two-electrode configuration, to reduce the artefacts due to the electrode-skin

contact impedance. The impedance measurements obtained from this electrode placement during breathing correlated well with the volume of the respired air. However, there were large changes in impedance due to cardiac activity and the movement of the arms had to be restricted to obtain a reliable breathing signal.

The studies carried out in the early 1960s were aimed at developing a breathing monitor suitable for use in space. The choice of electrode placement had to be such that it would not restrict any normal movements of the arms of the space crew, as they had to carry out their tasks while the monitoring took place. Therefore, a two-electrode configuration with electrodes placed bilaterally along the midaxillary line at the same rib level was used for this application. Geddes *et al* (1962) showed that for a given volume of respired air, the impedance change was maximum when the two electrodes were placed at the level of the 6th rib and the impedance change reduced when the electrodes were placed on either side of this rib level. Many other researchers experimented with different electrode placements, but found that the midaxillary electrode placement was more suitable because it had certain advantages as explained below.

Kubicek *et al* (1964) preferred the midaxillary placement with two electrodes placed at the level of the 7^{th} intercostal space because it produced large impedance changes due to breathing, compared to the small changes produced due to cardiac activity. Pallett and Scopes (1965) carried out some preliminary experiments to find a suitable electrode placement for monitoring breathing in babies. They considered an electrode placement suitable if it produced a linear impedance-air volume relationship and was least affected by movement artefacts. They measured impedance using two different electrode placements, called by them as 'sternum-to-spine' and 'electrodes placed at the extremities of the thoracic spine'. The results showed that both these electrode placements were susceptible to movement artefacts. In addition, the sternum-to-spine placement had large artefacts due to cardiac related impedance changes. The placement of electrodes at the extremities of the thoracic spine had a low signal due to breathing. Finally, it appeared that the midaxillary placement, with

electrodes at the level of the 6th rib, was better than the other two electrode placements, and hence, was used for monitoring breathing in babies.

Hamilton *et al* (1967) also carried out similar preliminary studies to choose an electrode placement for their study of impedance-air volume relationship. They described the electrode placements being evaluated as 'anterior-posterior', 'scapular-midclavicular' and 'right-left midclavicular'. They observed that the midaxillary placement, with electrodes placed at higher rib levels, produced consistently reliable results. They used a special type of 'ridged' electrode having a size of 6.25 cm × 1.25 cm and a ridge in the centre, along the length of the electrode. These electrodes were placed vertically on the midaxillary line with the top edge of the electrodes 1″ below the axilla and the central ridge pressed into the skin. The electrodes were taped to the skin using a moisture resistant adhesive tape and an elastic band was placed over the electrodes and around the thoracic cavity, not tightly but firmly, to avoid any skin movements. The impedance-air volume relationship obtained from this placement was linear except during forced expiration. It was also observed that movement artefacts due to moderate body movements such as quiet walking were considerably low for this electrode arrangement. However, the movement artefacts were large during vigorous body movements such as arm movements.

Farman and Juett (1967) also found the midaxillary placement very convenient, as it was possible to place the electrodes very quickly along the midaxillary line without disturbing the patient. This placement also allowed sufficient freedom of movement to the patient. Once the electrodes were in place, the patients were not particularly aware of the electrodes.

Logic *et al* (1965) carried out studies to investigate the effect of rib level of the electrodes on the impedance-air volume relationship, for the midaxillary placement. They observed that impedance measurements obtained from electrodes placed along the midaxillary line and at the level of the 5th intercostal space had a linear relationship with the lung air volume. The relationship was observed to become non-linear at the level of the 7th intercostal space. They also measured impedance at the level of the 7th intercostal space after placing a rigid

plaster cast around the lower part of the thoracic cavity. This cast prevented any shape changes at this level during breathing. The results showed that the linearity in the impedance-air volume relationship improved when the cast was in place. These results suggested that when the electrodes were placed at the lower level, the shape changes of the lower thorax and possibly the abdomen, affected the impedance measurements. Therefore, they suggested that it was necessary to place electrodes higher up on the midaxillary line to increase the influence of the lung resistivity changes on the thoracic impedance.

It can be seen from the above studies that the midaxillary placement appears to be the most suitable electrode placement for impedance pneumography, as it was found to be very convenient to use in any environment. It can also be seen that researchers attempted to find a rib level along the midaxillary line, at which the impedance-air volume relationship was linear. A linear relationship was desired because the aim of many of the researchers was to develop a quantitative method for monitoring lung ventilation using impedance based techniques. A linear relationship was the most simple relationship for calibrating the impedance pneumograph for quantitative measurements. However, it was shown by other researchers that a linear impedance-air volume relationship could also be obtained from other electrode placements as explained below.

Allison *et al* (1964) used some definite criteria for selecting the electrode placement for their study which aimed at establishing the impedance-air volume relationship. According to these criteria, the electrode placement was expected to be least affected by the movement of the thoracic wall during breathing so that the distance between the voltage measuring electrodes remained constant throughout the breathing cycle. The electrodes were to be placed in such a way that the maximum fraction of the injected current passed through the lungs. Finally, the impedance measurements were expected to reflect the changes in the lung air volume over the entire vital capacity range, including the extremes. The investigators carried out some preliminary experiments to evaluate five different electrode placements. All the electrode placements were based on a four-electrode configuration. These electrode placements were described by

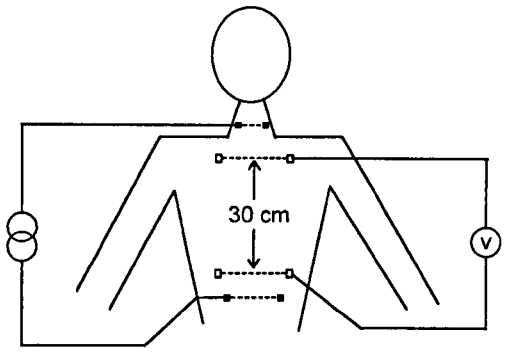

Figure 2.1 Best electrode placement suggested by Allison et al (1964)

them as wrist-wrist, deltoid-deltoid, torso, posterior thorax and lumbar region, and posterior thorax. They observed that the electrode placement termed as posterior thorax and shown in Figure 2.1, was the most suitable of all. The impedance-air volume relationship was also found to be linear for this electrode placement.

It was also reported by Baker *et al* (1965) that the impedance-air volume relationship obtained from the midaxillary placement was a function of the physical build of the subject. Therefore, Khalafalla *et al* (1970) carried out experimental studies on 37 normal human subjects to determine an electrode placement least affected by the anatomical variations in different subjects. They used 14 different electrode placements to measure impedance during breathing. The majority of the electrodes were placed on the thorax, but some were also placed on the arms and the legs. The results indicated that for the electrode placement shown in Figure 2.2a, the impedance-air volume relationship had less variability among the subjects. Another, electrode placement shown in Figure 2.2b had maximum sensitivity in all the subjects. The impedance-air volume relationship obtained from these electrode placements was not affected by factors such as weight, height, age and chest-to-back dimension of the subjects.

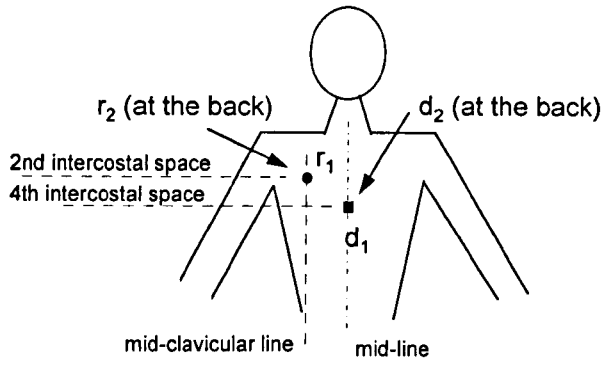

Anterior view

Figure 2.2 a

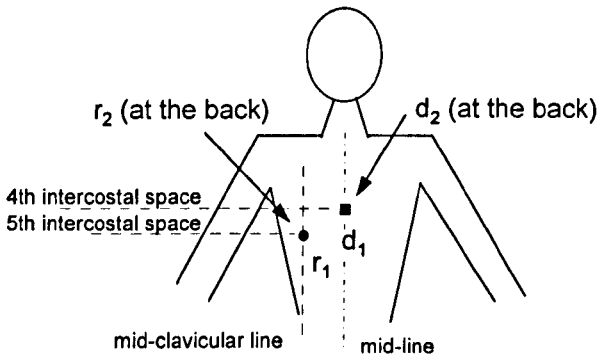

Anterior view

Figure 2.2 b

Figure 2.2 Best electrode positions suggested by Khalafalla et al (1970)

Thus, from the electrode placements described above, it is difficult to identify any one electrode placement that may satisfy the requirement of increased specificity to lung resistivity changes. Though the midaxillary placement is the most widely used electrode placement, there is no indication that it is more specific to lung resistivity changes. In fact, some researchers have argued that for this electrode placement, the geometrical factors such as changes in thoracic circumference and diaphragm movement dominate the thoracic impedance. This has been mentioned while reviewing the work of Albisser and Carmichael (1974) in the previous section. It can also be seen that in the majority of these studies, an electrode placement is considered suitable when the impedance-air volume relationship is linear. It has been stated earlier that the lung resistivity is a linear

function of the air volume. Thus, in the first instance, it may appear that this linear relationship is indicative of the greater influence of the lung resistivity changes on the thoracic impedance. However, this assumption may not be necessarily valid because other factors such as geometrical factors might also result in a linear change in thoracic impedance with air volume. Thus, to increase the specificity, some researchers have suggested electrode systems involving special types of electrodes such as guard ring electrodes. The following is the review of these studies.

2.5.1. Guard electrode technique

A guarded electrode configuration consists of 3 electrodes as shown in Figure 2.3a. The central sensing electrode is a disk surrounded by an annular guard ring electrode. The third electrode is another disk electrode, having a diameter equal to the outer diameter of the guard ring electrode and is placed on the opposite side. The voltage of the guard ring electrode is maintained at the same level as that of the sensing electrode. In a constant voltage impedance measuring system, a voltage is applied to the sensing electrode and the current through this sensing electrode is measured. A simple two-electrode configuration is shown in Figure 2.3b.

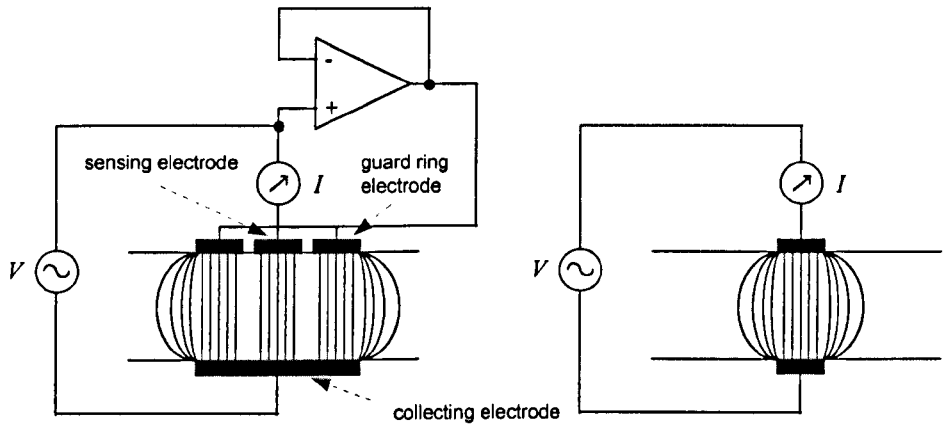

Figure 2.3 a Guarded Configuration *Figure 2.3 b Unguarded Configuration*

$$Z = \frac{V}{I}$$

Figure 2.3 Unguarded (two-electrode) and guarded electrode configurations

In this two-electrode configuration, when the electrodes are small compared to the medium of which the impedance is being measured, the current spreads beyond the electrodes. However, when a guard ring electrode is used, the spreading current is supplied by this guard ring electrode while the current being measured remains confined to the central cylindrical region and has a uniform current density as shown in Figure 2.3a. Thus, it is possible to specifically measure impedance of the central cylindrical region.

Graham (1965) was the first to use the guarded electrode configuration for impedance pneumography. One disk electrode was placed anteriorly on the right side, just below the level of the nipples. A second disk electrode was placed posteriorly, also on the right side and in the same horizontal plane. A guard ring electrode was placed around the posterior electrode. The impedance was measured by applying a voltage of 10 mV at 50 kHz to the sensing electrode. The base value of the impedance was 400 Ω and it changed by 1% during breathing. The impedance was also measured by applying 200 mV at 50 kHz to the sensing electrode and the guard ring electrode connected to the posterior electrode. In this case, the base value of the impedance was 8000 Ω and it changed by 10% under the same breathing conditions. Thus, the sensitivity of impedance measurements to breathing related impedance changes appeared to increase when a guard ring electrode was used. It was also suggested that this electrode arrangement could be used to measure resistivity changes in specific regions of the thoracic cavity.

Cooley and Longini (1968) used the guard ring electrode and an auto-balancing impedance bridge to develop a highly sensitive breathing monitor. They proposed a hypothesis that in an unguarded electrode configuration, most of the injected current passed through the low resistivity tissues of the thoracic wall rather than passing through the high resistivity lungs. They called this as a 'fringing current'. As a result, the fractional change in the thoracic impedance was normally less than the fractional change observed in the lung resistivity. A simplified electrical model of the thoracic cavity was developed to study the effect of guard ring electrode on the impedance measurements. It was observed that if

a guard ring electrode, having a width equal to or greater than the thickness of the thoracic wall was used, then the measurements were more sensitive to lung resistivity changes because the fringing current was supplied by this guard ring electrode.

They also carried out experiments on 6 human subjects. The sensing and the guard ring electrode were placed along the midaxillary line at the level of the 6^{th} intercostal space on one side of the thoracic cavity while the collecting electrode was placed on the opposite side of the thorax. The sensing electrode had a diameter of 3.5 cm and guard ring electrodes of two different sizes were used in the study. The width of one guard ring electrode was equal to 1″, which was assumed to be equal to the thickness of the thoracic wall, and the outer diameter of this electrode was equal to 8.9 cm. The second guard ring electrode had a width of 2″ (2 × thoracic wall thickness) and an outer diameter equal to 13.3 cm. The collecting electrode was also large in size. The results of this study indicated that, under the same breathing conditions, the impedance change without guarding was 4% while that with guarding was about 35% irrespective of the size of the guard ring electrode. They also observed that, due to guarding, movement artefacts were reduced to 15% from 100% of the maximum amplitude of the breathing signal.

Severinghaus *et al* (1972) also used the guarding technique to specifically measure the resistivity changes in the lung tissue for detecting pulmonary oedema. The sensing electrode and the guard ring electrode were placed on the midaxillary line, on one side of the thorax, while the collecting electrode was placed on the opposite side of the thoracic cavity. The guard ring was segmented into four quadrants. In between each quadrant and the sensing electrode there was an intermediate arc shaped electrode. Instead of driving the guard ring electrode at the same potential as the sensing electrode, the potential on the guarding electrode was adjusted such that the potential gradient between the sensing electrode and the intermediate electrode was minimised. Thus, it was possible to prevent the flow of current in the lateral direction. One more electrode was used to sense the potential at the sternum and this potential was used to

balance the bridge. Thus, it was possible to specifically measure the resistivity of the lung near to the sensing electrode. As the aim of this study was to investigate the resistivity changes associated with the pulmonary oedema, comparison was not made between the guarded and unguarded electrode configurations. However, it was reported that large changes in impedance occurred during breathing.

It may appear from the above studies that the technique of using a guard ring electrode is effective in increasing the specificity of impedance measurements to lung resistivity. However, Plonsey and Collin (1977) suggested that the guarded electrode configuration did not have any significant advantage when used on an non-homogeneous volume conductor such as the thoracic cavity. They carried out a study based on the field theory to compare the performance of the guarded and unguarded electrode configurations. The results of this study showed that the technique of electrode guarding could not be used effectively when the internal resistivity distribution was not known exactly. They concluded that as it was very difficult to exactly obtain the resistivity distribution of the thoracic cavity, the technique of electrode guarding would not be useful to improve the performance in impedance pneumography. Baker (1979) also reported that the technique of electrode guarding was not sensitive enough to detect resistivity changes taking place within the deeper regions of a saline filled cylindrical tank. Thus, it appears from these studies, that guarding may not necessarily increase the specificity to lung resistivity changes. Moreover, this technique requires a special type of guard ring electrode that is large in size, and this would prove to be inconvenient in a clinical environment.

Recently, researchers have suggested some other electrode configurations using the standard ECG type 'spot' electrodes to direct the current into the lungs and hence, increase the specificity. Bhat (1990) suggested two multiple-electrode systems as shown in Figure 2.4. He observed that there was a considerable reduction in the impedance excursions during obstructive apnoea when these electrode placements were used.

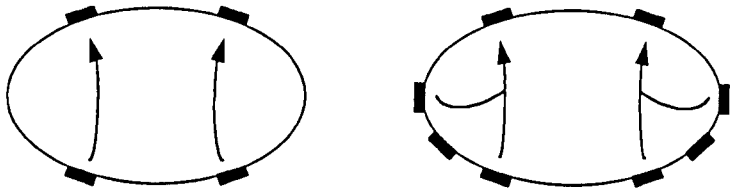

4-electrode placement 8-electrode placement

Figure 2.4 *A 4-electrode and 8-electrode placement suggested by Bhat (1990)*

A 6 electrode configuration was developed by Rabbani *et al* (1999). They called their technique as 'Focused impedance measurement' and it involved two pairs of drive electrodes (*a* and *b*, *c* and *d*), placed at right angles, and one pair of receive electrodes (*p* and *q*), placed at diagonal locations as shown in Figure 2.5. Two electrically isolated current injection circuits were used to inject current of the same frequency, amplitude and phase into the two drive pairs.

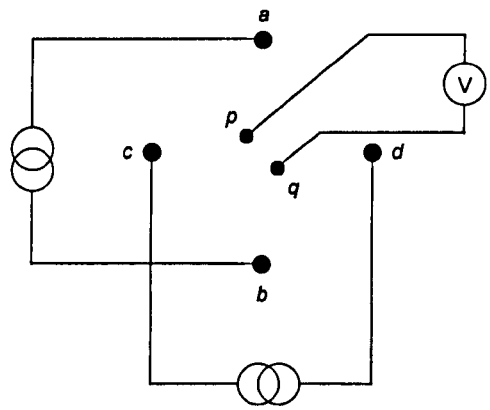

Figure 2.5 *Electrode placement of Focused impedance measurement system of Rabbani et al (1999)*

It was observed that the sensitivity within an approximately circular region between the two receive electrode was very high and positive while the sensitivity in the other regions was significantly low, and either positive or negative. Thus, it was possible to measure impedance changes within a specific region with minimum interference from the surrounding regions. This electrode arrangement was successfully used to detect gastric emptying. It was also suggested that this

electrode system could be used to detect the breathing related changes within a specific part of a lung.

The impedance imaging based techniques of monitoring physiological events such as 'Impedance Camera' developed by Henderson and Webster (1978) and EIT also provide a possibility of measuring impedance changes within a specific region of the body. However, as stated in Chapter 1, these techniques require a large number of electrodes and are therefore inconvenient to use in a clinical environment.

2.6. Discussion

This chapter has examined several important aspects of impedance pneumography. An overview of the history of this technique suggests that it has many advantages which makes it a very suitable technique for monitoring breathing under different circumstances, where other techniques are difficult to use. However, a major drawback of this technique is its inability to faithfully monitor breathing when body movements, such as arm movements and changes in posture, are present. There are three physiological factors responsible for breathing related changes in thoracic impedance. These are, changes in lung resistivity, changes in thoracic circumference, and vertical movement of the diaphragm. The resistivity of lung tissue is a function of the lung air volume and thus, undergoes a change during breathing. The breathing related changes in the thoracic circumference and the vertical movement of the diaphragm also independently contribute to the breathing related changes in the thoracic impedance. This contribution would vary with the vertical level at which the thoracic impedance is measured. However, at a given vertical level, it is not yet clear which of the three factors dominate the measurements.

It may be argued that, if a reliable technique for monitoring breathing is needed, then it is necessary to increase the specificity of the impedance measurements to the changes in lung resistivity and reduce the influence of all the other factors. Some studies suggest that an appropriate choice of electrode placement may help in increasing this specificity. Many different electrode placements have been

used in the past. However, it is difficult to identify one single electrode placement that has the optimum specificity. The midaxillary placement has been found to be the most convenient and has been widely used. However, there is no clear evidence that it has the required specificity. On the contrary, it has been shown that for this electrode placement, geometrical factors dominate the measured impedance. The guarded electrode configurations may have the ability to measure the resistivity changes within a specific region. However, this is based on the assumption that the medium is homogeneous. These electrode configurations do not seem to have any significant advantage when the measurements are carried out on the thoracic cavity, which has a non-uniform resistivity distribution. Moreover, they need special type of electrodes that are not normally used in clinical practice. These guard ring electrodes are also large in size and thus, may cause inconvenience in clinical use. Some special electrode systems such as the 6-electrode 'focused impedance measurement' system may have an increased specificity. The impedance imaging techniques have an ability to provide regional resistivity measurements, but require a large number of electrodes, which is again inconvenient in clinical practice.

2.7. Strategy adopted in the present project

The aim of the present project was to develop a technique for reducing movement artefacts. We may consider this problem to be solved in two steps. As a first step, it would be necessary to maximise the contribution of lung resistivity changes to the thoracic impedance. The review of the literature carried out in this chapter suggests that it would be necessary to choose an appropriate electrode placement for maximising the contribution of lung resistivity changes. Many different electrode placements have been used for impedance pneumography in the past. However, it is difficult to identify a single electrode placement that may maximise the contribution of lung resistivity changes to the thoracic impedance. Therefore, the first objective was defined as:

- To experimentally identify an electrode placement that will maximise the contribution of lung resistivity changes to the thoracic impedance.

Once this first step is achieved, the second step would be to minimise movement artefacts. The amplitude of movement artefacts may also depend on electrode placement. Therefore, the second objective was:

- To identify an electrode placement that will minimise movement artefacts.

The literature concerned with techniques of reducing movement artefacts suggests that it may be possible to use multi-frequency measurements for reducing movement artefacts. A review of this literature has been presented in Chapter 5 in the thesis. Therefore, the third objective was:

- To investigate whether it is possible to reduce movement artefacts using multi-frequency measurements.

Chapter 3. Electrode placement and impedance measurements of the thoracic cavity: experimental studies

3.1. Introduction

It has been stated in the previous chapter that in order to increase the reliability of impedance pneumography, it is necessary to maximise the contribution of lung resistivity changes to thoracic impedance and reduce the effect of any other factors. It has been also argued that this 'specificity' to lung resistivity changes can be achieved by selecting an appropriate electrode placement. This chapter begins with a mathematical analysis to define the criteria for selecting such an 'optimum' electrode placement. This is followed by a description of the experimental studies carried out to identify the optimum electrode placement.

3.2. Criteria for selection of an electrode placement

Let us consider a general case of measuring transfer impedance of a volume conductor as shown in Figure 3.1. Let us assume that this volume conductor has a uniform internal conductivity distribution and is surrounded by an insulating medium.

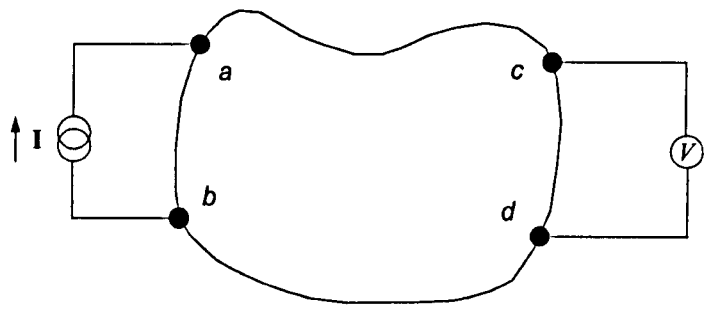

Figure 3.1 Transfer impedance measurement on a volume conductor

If a unit current ($\mathbf{I}$ = 1) is injected into the volume conductor via electrodes *a* and *b*, then the voltage (V) measured between electrodes *c* and *d* is equal to the 'transfer impedance' (Z). This impedance can be mathematically expressed on the basis of a forward mapping relationship described by Avis (1993) as in the equation below. A detailed derivation of this relationship is given in the following chapter.

$$Z = \int_{volume} \sigma \nabla\phi \cdot \nabla\psi dv \qquad 3.1$$

where,
σ = conductivity of the volume conductor
∇ = gradient operator
ϕ = potential distribution within and on the surface of the volume conductor when a unit current is injected between electrodes *a* and *b*
ψ = potential distribution within and on the surface of the volume conductor when a unit current is injected between electrodes *c* and *d*

Equation 3.1 can be further modified by taking into consideration a general form of Ohm's law for a continuous medium as follows (Lorrain and Corson, 1962).

$$\mathbf{J} = -\sigma\nabla\phi \qquad 3.2$$

where,
$\mathbf{J}$ = current density vector

Now, if we consider that σ = 1, then we get,

$$\mathbf{J} = -\nabla\phi_u \qquad 3.3$$

where,
ϕ_u = potential distribution for injected current $\mathbf{I}$ and σ = 1.

The current density ($\mathbf{J}$), on the surface, is equal to the unit current $\mathbf{I}$ under the current injecting electrodes *a* and *b* and zero elsewhere. This is because we have assumed that the volume conductor is surrounded by an insulating medium. By combining equations 3.2 and 3.3 we can write an expression for $\nabla\phi$, for any value of conductivity σ, in terms of $\nabla\phi_u$, when the same current is injected in both the cases.

$$\nabla\phi = \frac{1}{\sigma}\nabla\phi_u \qquad 3.4$$

By substituting appropriate values of $\nabla\phi$ and $\nabla\psi$ in 3.1 we get,

$$Z = \int_{volume} \sigma(\frac{1}{\sigma}\nabla\phi_u)\cdot(\frac{1}{\sigma}\nabla\psi_u)dv \qquad 3.5$$

We have assumed a uniform internal conductivity distribution for the volume conductor. Therefore, equation 3.5 can be further simplified as,

$$Z = \frac{1}{\sigma}\int_{volume} \nabla\phi_u \cdot \nabla\psi_u dv \qquad 3.6$$

Equation 3.6 can also be written as,

$$Z = k\cdot\rho \qquad 3.7$$

where,

$$k = \int_{volume} \nabla\phi_u \cdot \nabla\psi_u dv \qquad 3.8$$

and,

ρ = resistivity of the volume conductor (= $1/\sigma$)

Factor k is a function of the shape of the volume conductor and location of the electrodes as the potential distributions ϕ_u and ψ_u are functions of these two factors.

Now, let the resistivity of the volume conductor change to ρ' without causing any change in its shape. Therefore, the value of k will be the same and an equation for the changed value of transfer impedance (Z') can be written as,

$$Z' = k\cdot\rho' \qquad 3.9$$

Thus, a change in the transfer impedance (ΔZ) can be written as,

$$\Delta Z = Z' - Z = k \cdot (\rho' - \rho) = k \cdot \Delta\rho \qquad 3.10$$

where,
$\Delta\rho$ = change in resistivity of the volume conductor

If we consider the ratio $\Delta Z/Z$, then it is possible to eliminate factor k, i.e. the effect of shape and location of electrodes on the measured transfer impedance. The fractional change in transfer impedance is equal to the fractional change in resistivity as in the following equation.

$$\frac{\Delta Z}{Z} = \frac{\Delta\rho}{\rho} \qquad 3.11$$

Let us imagine a situation in which it is possible to place electrodes directly on the surface of a lung to measure its impedance. For the sake of this argument, let us also assume that it has a uniform internal resistivity distribution and is surrounded by an insulating medium. This situation is similar to the case of transfer impedance measurement on a volume conductor as considered above. In this situation, the measured fractional change in lung impedance during breathing will be free from the effects of factors other than the fractional change in lung resistivity as above. However, in practice, electrodes can only be placed on the surface of the body. Therefore, it would be necessary to develop an equation for the fractional change in measured impedance of the body during breathing, to see whether it leads to an equation similar to equation 3.11.

A human body is a volume conductor having a non-uniform internal resistivity distribution and surrounded by air, which is an insulating medium. Let a unit current ($\mathbf{I} = 1$) be injected into the body using a pair of electrodes *a* and *b* and let the voltage be measured using another pair of electrodes *c* and *d* as shown in Figure 3.2. The transfer impedance of the body (Z_b) can be mathematically expressed on the basis of the forward mapping relationship given by Avis (1993) as,

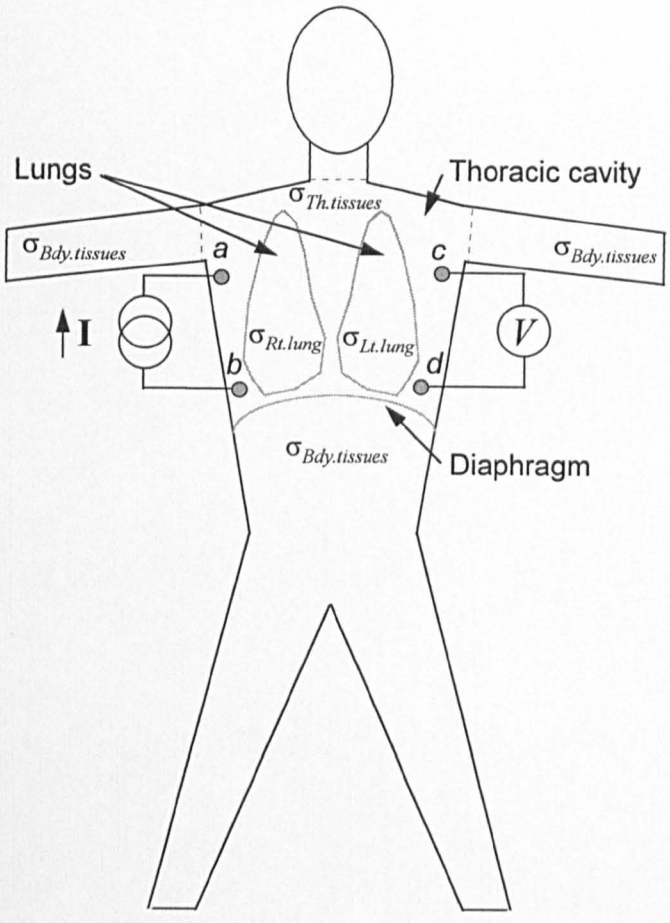

Figure 3.2 Impedance measurements on a human body

$$Z_b = \int_{\substack{body \\ volume}} \sigma_b \nabla\phi \cdot \nabla\psi dv \qquad 3.12$$

where,

σ_b = lumped representation of conductivity values of all the tissues in the body

∇ = gradient operator

ϕ = potential distribution within and on the surface of the body when a unit current is injected between electrodes *a* and *b*

ψ = potential distribution within and on the surface of the body when a unit current is injected between electrodes *c* and *d*

It can be seen that, apart from conductivity values of different tissues (ρ_b), Z_b is also a function of the shape of the body and electrode placement. In addition to

being a function of these two factors, the potential distributions (ϕ and ψ), are also functions of the non-uniform internal resistivity distribution of the body. Therefore, further simplification of equation 3.12 is not possible, on the lines carried out in the earlier case. However, Z_b can be further written in terms of its individual components as,

$$Z_b = \int_{\substack{Rt.lung \\ volume}} \sigma_{Rt.lung} \nabla\phi \cdot \nabla\psi dv + \int_{\substack{Lt.lung \\ volume}} \sigma_{Lt.lung} \nabla\phi \cdot \nabla\psi dv + \int_{\substack{thoracic-tissues' \\ volume}} \sigma_{Th.tissues} \nabla\phi \cdot \nabla\psi dv + \int_{\substack{body-tissues' \\ volume}} \sigma_{Bdy.tissues} \nabla\phi \cdot \nabla\psi dv \qquad 3.13$$

where, as shown in Figure 3.2,
$\sigma_{Rt.lung}$ = conductivity of right lung
$\sigma_{Lt.lung}$ = conductivity of left lung
$\sigma_{Th.tissues}$ = conductivity of tissues within the thoracic cavity other than lungs
$\sigma_{Bdy.tissues}$ = conductivity of tissues of the remaining parts of the body

The first and the second term in equation 3.13 is the impedance of the right and the left lung, respectively, and can be represented using one term, $Z_{lung(R\&L)}$, for simplicity. The third term is the impedance of the tissues within the thoracic cavity other than lungs ($Z_{Th.tissues}$), and the last term is the impedance of the tissues of body parts other than the thoracic cavity ($Z_{Bdy.tissues}$). It may be noted that the conductivity values $\sigma_{Th.tissues}$ and $\sigma_{Bdy.tissues}$ are bulk representations of the conductivity values of different tissues within the respective regions. Thus, Z_b can be written as,

$$Z_b = Z_{lung(R\&L)} + Z_{Th.tissues} + Z_{Bdy.tissues} \qquad 3.14$$

Z_b will undergo a change during breathing (ΔZ_b) due to change in conductivity of both the lungs and can be expressed using the sensitivity relationship of Geselowitz (1971) as,

$$\Delta Z_b = \int_{\substack{Rt.lung \\ volume}} \Delta\sigma_{Rt.lung} \nabla(\phi + \Delta\phi) \cdot \nabla\psi dv + \int_{\substack{Lt.lung \\ volume}} \Delta\sigma_{Lt.lung} \nabla(\phi + \Delta\phi) \cdot \nabla\psi dv \qquad 3.15$$

where,

$\Delta\sigma_{Rt.lung}$ = change in conductivity of the right lung during breathing
$\Delta\sigma_{Lt.lung}$ = change in conductivity of the left lung during breathing
$\Delta\phi$ = change in potential distribution within and on the surface of the body due to change in lung resistivity

It may be noted that the sensitivity relationship is not valid if the geometry of the volume under consideration also undergoes a change along with the conductivity of any internal region (Lehr, 1972). However, for simplicity, it is assumed that there is no significant change in the geometry of the thoracic cavity during breathing so that the sensitivity relationship can be used. An equation for ΔZ_b can be written as,

$$\Delta Z_b = \Delta Z_{lung(R\&L)} \qquad 3.16$$

Now, let us take the ratio $\Delta Z_b/Z_b$, as in the earlier case of the volume conductor.

$$\frac{\Delta Z_b}{Z_b} = \frac{\Delta Z_{lung(R\&L)}}{Z_{lung(R\&L)} + Z_{Th.tissues} + Z_{Bdy.tissues}} \qquad 3.17$$

It is not obvious as in the earlier case whether by taking the above ratio, the effect of body shape and electrode placement has been reduced or eliminated. Pallett and Scopes (1965) experimentally observed that for a given change in the volume of the inspired air, this ratio was less affected by the changes in posture than the absolute change in impedance (ΔZ_b). This indicates that it might be possible to obtain some reduction in the effect of shape on impedance by

measuring the fractional change in impedance ($\Delta Z_b/Z_b$) instead of the absolute change in impedance (ΔZ_b), for monitoring breathing.

It can be seen from equation 3.17 that, in order to increase the specificity of the measured impedance to changes in the lung impedance ($\Delta Z_{lung(R\&L)}/Z_{lung(R\&L)}$), it would be necessary to reduce the additional two components of the denominator Z_b ($Z_{Th.tissues}$ and $Z_{Bdy.tissues}$). If the drive and the receive electrodes are placed on the surface of the thoracic cavity as shown in Figure 3.2, then the current density will be high within the thoracic cavity and low in other parts of the body. Therefore, for this electrode placement, $Z_{Bdy.tissues}$ will be low and can be ignored. The ratio, $\Delta Z_b/Z_b$ can be simplified into a ratio of thoracic cavity impedance ($\Delta Z_{Th}/Z_{Th}$) as,

$$\frac{\Delta Z_{Th}}{Z_{Th}} = \frac{\Delta Z_{lung(R\&L)}}{Z_{lung(R\&L)} + Z_{Th\,tissues}} \qquad 3.18$$

The denominator in equation 3.18 still has the additional component $Z_{Th\,tissues}$ and there seems no direct way of reducing it. An indirect way of reducing this component would be to maximise the ratio $\Delta Z_{Th}/Z_{Th}$. For a given change in the lung resistivity and the shape of the thoracic cavity, $\Delta Z_{Th}/Z_{Th}$ will be a function of the electrode placement. Thus, in order to increase the specificity to lung resistivity changes it would be necessary to find an electrode placement that maximises the ratio $\Delta Z_{Th}/Z_{Th}$.

The experimental results obtained by Brown *et al* (1994) seem to support this argument. They measured fractional changes in impedance during breathing using a four-electrode linear array as well as from the EIT images of the thoracic cavity. They observed that this fractional change in impedance during breathing was about 14 times larger when obtained from the EIT images than when obtained using the four-electrode measurements. They explained this difference by stating two possible reasons. Firstly, the volume of the inspired air during each experiment was not measured and it was possible that it had varied between experiments. However, it seems unlikely that the volume of the inspired air might have varied by 14 times between experiments. Secondly, the

measurements obtained from the EIT images using the region-of-interest analysis, were specific to the lungs whereas the four-electrode measurements included the impedance of the peripheral tissues such as fat and muscle. Thus, by using region-of-interest analysis, it was possible to specifically measure the fractional change in lung impedance ($\Delta Z_{lung(R\&L)}/Z_{lung(R\&L)}$) of equation 3.18, and minimise the impedance component $Z_{Th.tissues}$. On the other hand, the four-electrode measurements included the impedance component $Z_{Th.tissues}$ and hence, caused the fractional change $\Delta Z_{Th}/Z_{Th}$ to reduce. From these results it appears that a high value of fractional change in measured impedance ($\Delta Z_{Th}/Z_{Th}$) is an indicator of the increased specificity of impedance measurements to the lung resistivity changes. Therefore, the first criterion for selection of an optimum electrode placement is that it should maximise $\Delta Z_{Th}/Z_{Th}$ or the 'sensitivity'.

There is one more criterion to be considered for selecting an electrode placement. In practice, it would be necessary to take into account the effect of noise in the instrumentation, which will be independent of the electrode placement. In order to reliably monitor breathing, the Signal-to-Noise Ratio (SNR) should be sufficiently high. SNR is a function of absolute value of change in thoracic impedance (ΔZ_{Th}) and can be mathematically expressed as,

$$SNR = 20 \cdot \lg\left(\frac{\Delta Z_{Th}}{Z_n}\right) \qquad 3.19$$

where,
Z_n = noise in the instrumentation

In order to maximise SNR, it would be necessary to find an electrode placement that maximises ΔZ_{Th}. An electrode placement that maximises $\Delta Z_{Th}/Z_{Th}$ will not necessarily maximise ΔZ_{Th} because even if we get a high $\Delta Z_{Th}/Z_{Th}$, the absolute values of ΔZ_{Th} and Z_{Th} can be low. Thus, the second criterion for selecting an optimum electrode placement is that it should maximise SNR or ΔZ_{Th}.

Thus, in order to achieve the first objective of the project, it was necessary to identify one or more electrode placements that would satisfy both the criteria mentioned above. Let us now consider the parameters that define an electrode placement. In practice, it is possible to place electrodes anywhere on the thoracic cavity. In order to constrain this situation, it was decided that the required optimum electrode placement would be identified from the electrode placements used in two dimensional and three dimensional EIT. These electrode placements can be expressed in terms of the following three parameters as illustrated in Figure 3.3. These are,

- centre-to-centre distance between the drive and the receive electrode pairs (Figure 3.3a).
- distance between the two horizontal planes containing the drive and the receive electrode pairs, when placed on a three dimensional object (Figure 3.3b).
- distance separating the two electrodes forming a drive or a receive electrode pair, i.e. electrode spacing (Figure 3.3c).

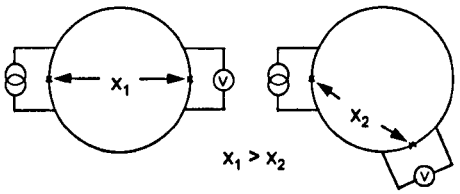

Figure 3.3a

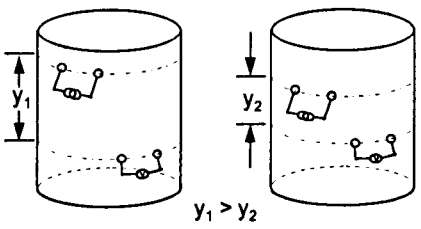

Figure 3.3b

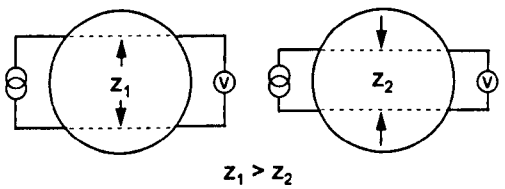

Figure 3.3c

Figure 3.3 Parameters specifying an electrode placement

The first part of this chapter describes the experimental work carried out to study the relationship between impedance measurements and centre-to-centre distance between the drive and the receive electrode pairs. The analysis was carried out on the data collected by placing electrodes on the thorax in one horizontal plane as well as in more than one horizontal planes. The electrode spacing was kept constant for this analysis. The effect of electrode spacing on the impedance measurements was also studied in this project and is described later in this chapter. The ratio $\Delta Z_{Th}/Z_{Th}$, will be referred to as $\Delta Z/Z$ henceforth in the thesis for clarity.

3.3. Analysis of co-planar EIT data

The data used in this analysis was recorded by placing an array of electrodes around the thoracic cavity in one horizontal plane. This data will be denoted as 'co-planar data' henceforth in the thesis. The purpose of this data analysis was to get a preliminary idea of the relationship between the impedance measurements and the electrode placement. A similar analysis was also carried out on the data recorded by placing electrode arrays in more than one horizontal plane. This analysis is described in the subsequent section.

3.3.1. Data collection

The impedance measurements were carried out on 2 normal male volunteers (age, 25 & 29). A Sheffield Mark 2 Real-time EIT system was used for this purpose (Smith *et al*, 1995). An array of 16 equally spaced electrodes was placed around the thoracic cavity at the level of the nipples. The system injected a current of 5 mA peak-to-peak at a frequency of 20 kHz. Each frame of data was recorded according to the adjacent drive - adjacent receive protocol used in EIT (Brown and Seagar, 1987). This involved injecting current between a pair of adjacent 'drive' electrodes and measuring voltage between all the pairs of adjacent 'receive' electrodes, and repeating this step for all the pairs of drive electrodes. For each drive pair, the voltage measurements obtained from that drive pair and the two adjacent receive pairs, having one electrode in common with the drive pair, were discarded as they were expected to be affected by the unpredictable changes in the electrode-skin contact impedance. Thus, this data collection strategy produced 208 measurements (13 receive pairs × 16 drive pairs), out of which only half the measurements were independent due to reciprocity (Geselowitz, 1971). Thus, each frame of the data consisted of 104 measurements, obtained from 104 different electrode placements. The subjects were asked to perform tidal breathing in an upright sitting position and 1500 frames were recorded over 60 s at a frame rate of 25 frames s^{-1}.

3.3.2. Data analysis

The data analysis was carried out to calculate the values of $\Delta Z/Z$ for each of the 104 impedance measurements. The software MATLAB® (version 4.2, The Mathworks Inc., USA) was used for this analysis.

A first step in the data analysis was to identify the frames corresponding to the instants of maximum inspiration and maximum expiration. A mean of 104 values, for each of the 1500 frames, was obtained to derive an impedance signal similar to that shown in Figure 3.4. This mean impedance signal was digitally low pass filtered (filter type: Butterworth; order: 10; cut-off frequency: 0.6 Hz), to reject the cardiac related impedance changes. This signal was further processed using a peak detection routine to detect the frames corresponding to instants of maximum inspiration and expiration, marked by 'circles' and 'crosses', respectively, in Figure 3.4. The value of ΔZ for each measurement was equal to the difference between Zi and Ze, where Zi and Ze were the mean of impedance values at all the instants of maximum inspiration (Zi_1, Zi_2,... Zi_n) and maximum expiration (Ze_1, Ze_2,... Ze_m), respectively (Figure 3.4). The value of Z was calculated by taking a mean of impedance values for all the 1500 frames.

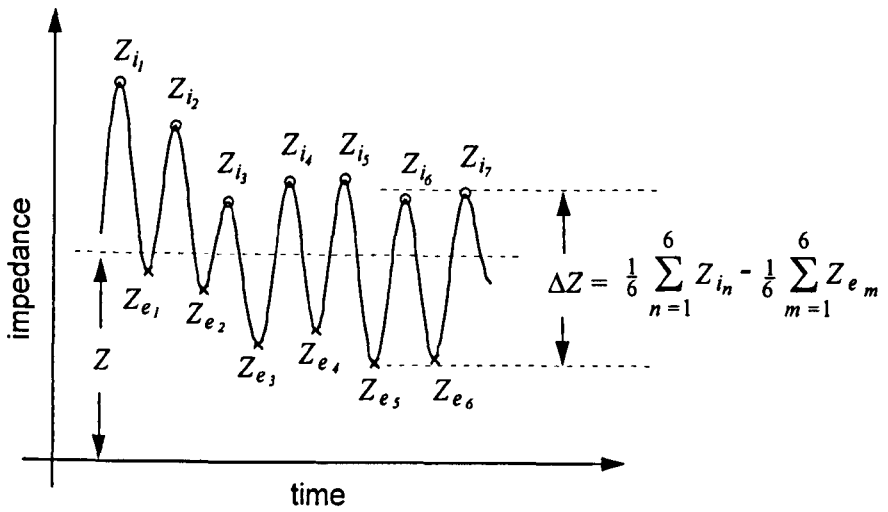

Figure 3.4 Calculation of Z and Δ Z

3.3.3. Calculation of centre-to-centre distance

In order to calculate the centre-to-centre distance between the drive and the receive electrode pairs, it was necessary to know the locations of the electrodes on the surface of the thoracic cavity. The dimensions of the thoracic cavity could be measured on the subjects, but it seemed difficult to define the shape of the thoracic cavity at the level of electrodes and hence, it was also difficult to define the electrode locations. Therefore, an alternative method was used to calculate the distance between the drive and the receive electrode pairs by assuming an elliptical model for the thoracic cavity.

The cross-section of the thoracic cavity was modelled as an ellipse having a major to minor axis ratio of 1.7 as suggested by Kiber (1991). Figure 3.5 shows such an ellipse with 16 equally spaced electrodes, E_1 to E_{16}, marked by 'stars'. The centre points of the 16 electrode pairs are marked by 'circles' and are labelled as C_1 to C_{16}. In order to calculate the distance between the centre points, it was first necessary to obtain the co-ordinates of these points and they were obtained in the following way.

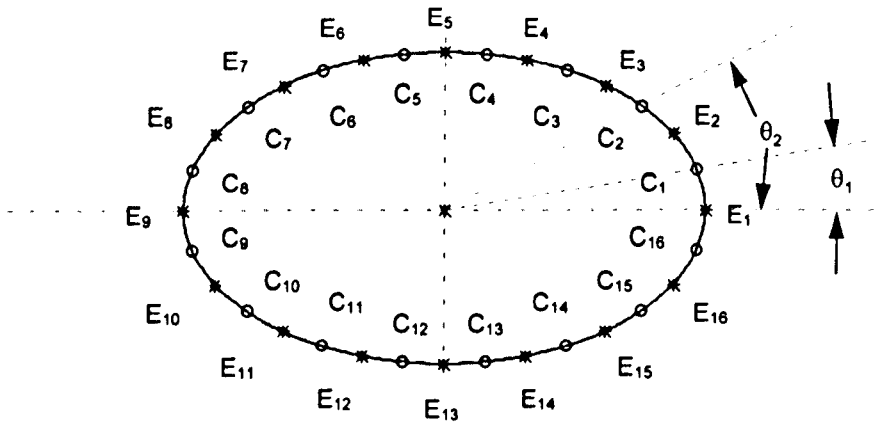

Figure 3.5 *Ellipse showing the electrodes E_1 to E_{16} and centre points C_1 to C_{16}*

The perimeter length of the ellipse (P) was first calculated by numerically evaluating the integral in equation 3.20, between the limits 0 and 2π, using Simpson's Rule (Stroud, 1985).

$$P = \int_{\theta_1}^{\theta_2} \{a^2 + b^2 - (a^2 + b^2)\cos 2\theta\}^{1/2} d\theta \qquad 3.20$$

where,
P = perimeter of the ellipse
a = semi-major axis of the ellipse
b = semi-minor axis of ellipse

The co-ordinates of point C_1 were first determined in the following way. The angle corresponding to E_1 was equal to 0 and was assumed to be the lower limit (θ_1). The angle corresponding to C_1 was assumed to be the upper limit (θ_2). The distance between E_1 and C_1, along the boundary of the ellipse, was equal to the value of the integral (equation 3.20) within these limits. The value of θ_2 was determined recursively by either incrementing or decrementing it in progressively smaller steps so that the value of the integral approached the required distance equal to *P/32*. The angle corresponding to C_2 was then determined in the same way so that the distance between C_1, and C_2, was equal to *P/16*. The angles corresponding to other centre points (C_3 and C_4), in the first quadrant, were also determined in the same way, and the angles corresponding to the centre points in the remaining three quadrants were determined by symmetry. These polar co-ordinates were converted to Cartesian co-ordinates using the parametric equations of an ellipse as in equations 3.21 and 3.22.

$$x = a\cos\theta \qquad 3.21$$

$$y = b\sin\theta \qquad 3.22$$

where,
x, y = Cartesian co-ordinates of a point on the boundary of an ellipse

Finally, the straight line distance (X_i) between the two centre points C_d and C_r, corresponding to the drive and the receive electrode pairs, respectively, of an i^{th} electrode combination, was calculated using equation 3.23.

$$X_i = \{(x_d - x_r)^2 + (y_d - y_r)^2\}^{1/2} \qquad 3.23$$

where,
x_d, y_d = co-ordinates of centre point C_d, corresponding to the drive pair
x_r, y_r = co-ordinates of centre point C_r, corresponding to the receive pair

3.3.4. Results and discussion for the co-planar data

The plots of $\Delta Z/Z$ versus centre-to-centre distance, for the 2 subjects, are shown in Figure 3.6. The results of this study indicate that $\Delta Z/Z$ increases with distance ($p < 0.001$) for the co-planar electrode placement used.

It has been already argued while deciding the criteria for an optimum electrode placement that a larger value of $\Delta Z/Z$ is an indicator of the maximum contribution of the changes in lung resistivity to the measured thoracic impedance. Thus, these results suggest that, in order to maximise the contribution of lung resistivity to thoracic impedance, it would be necessary to place the drive and receive electrode pairs as far apart as possible.

These results agree with those obtained by Jossinet and Kardous (1987). They experimentally obtained the sensitivity distribution for the 16-electrode co-planar placement by measuring impedance changes on a cylindrical tank (diameter = 192 mm) filled with the tap water. A stainless steel sphere (diameter = 18 mm) was placed inside the tank, within different regions, to map the sensitivity distribution across the cross-section of the tank. An adjacent drive - adjacent receive strategy for data collection was used in these experiments, the same as that used in the above experiment. They observed that, when the drive and the receive electrode pairs were placed close to each other, the impedance measurements were dominated by the resistivity changes within the peripheral region close to the electrodes, i.e. there was less spread of sensitivity throughout the cross-section of the cylindrical tank. On the other hand, when the drive and the receive electrode pairs were placed as far apart as possible, i.e. placed diametrically opposite to each other in this case, the sensitivity to the resistivity changes in the deeper regions was comparable to the sensitivity within the peripheral regions. In other words, the sensitivity distribution was relatively uniformly spread throughout the cross-section of the cylindrical tank.

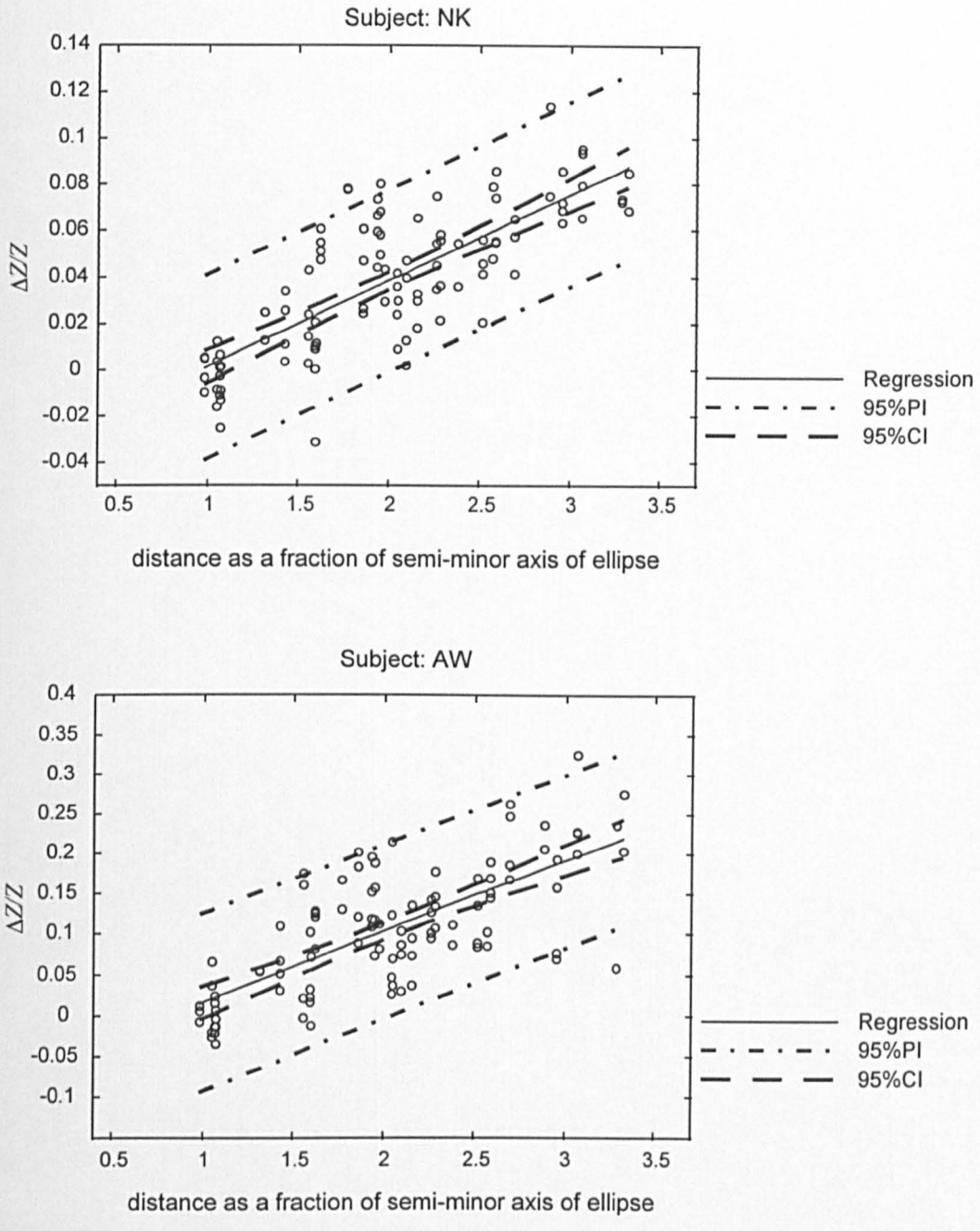

Figure 3.6 *Plot of ΔZ/Z versus distance for the co-planar data for the 2 subjects*

These results suggest that, in the case of thoracic impedance measurements, when the drive and the receive electrode pairs are placed close to each other, the measurements will be dominated by the resistivity of the peripheral tissues of the thoracic wall such as fat and muscles. However, when the electrode pairs are placed apart, the measured impedance will also have a contribution from the

resistivity of the deeper lung tissues and a relatively uniform spread of the sensitivity distribution throughout the cross-section of the thoracic cavity will also maximise the contribution from both the lungs.

For a three dimensional object such as the thoracic cavity, it is not necessary to restrict the electrode placement to one horizontal plane. In fact, the distance between the drive and the receive electrode pairs can be further increased by placing them in two different horizontal planes, as shown in Figure 3.3b. The following section describes an analysis of the impedance data obtained from the thoracic cavity by placing electrode arrays in four different horizontal planes. The purpose of this analysis was to find out whether it was possible to increase the value of $\Delta Z/Z$ beyond the maximum value obtained using the co-planar electrode placements, by placing electrodes in different horizontal planes.

3.4. Analysis of 3d EIT data

The thoracic cavity is three dimensional in shape and it is possible to place the drive and the receive electrode pairs in two different horizontal planes separated by a vertical distance. This section describes the experimental studies carried out to investigate the relationship between $\Delta Z/Z$ and distance between the drive and the receive electrode pairs for such 'non-planar' electrode placements. The data obtained from these electrode placements will denoted as '3d data' in the rest of the thesis.

3.4.1. Data collection

The impedance data was recorded from 8 normal male volunteers with a mean age of 27.9 years (range, 22-56) using a Sheffield Mark 3b EITS system[1] (Metherall, 1996). The system consisted of 32 drive and 32 receive electrode pairs separated in 4 horizontal planes. The anatomical location of the four planes is shown in Figure 3.7. Each plane had 16 equally spaced electrodes configured as 8 drive and 8 receive interleaved pairs. The vertical distance between any two horizontal electrode planes was equal to 0.08 times the circumference of the thoracic cavity of the subjects.

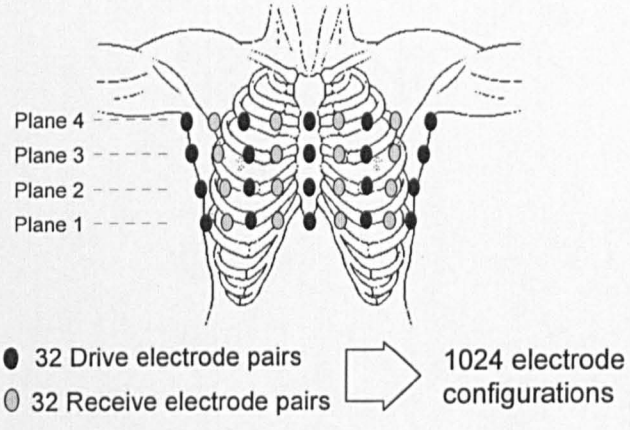

Figure 3.7 Electrode placement in 4 planes for collection of 3d data

[1] The data collection was actually carried out by Dr. P. Metherall as a part of his Ph.D. project. I am very thankful to Dr. P. Metherall for providing the data for analysis in this project.

A current of 2 mA peak-to-peak was injected between one pair of drive electrodes, and the voltage from all the 32 receive electrode pairs was recorded. This was repeated for all the 32 drive pairs resulting in a set of 1024 measurements acquired from 1024 different electrode placements. It would be important to note that out of 1024 measurements, only 784 (28^2) were independent measurements. The system injected current at 8 frequencies in the range of 9.6 kHz to 1.22 MHz in binary steps, but the data at a frequency of 76.8 kHz was chosen for the present analysis because this frequency was expected to be unaffected by the gain correction errors (Metherall, 1998). The data was recorded over 60 s during normal tidal breathing and in an upright sitting position, at a frame rate of 16.7 frames s^{-1}.

3.4.2. Data analysis

The analysis of 3d data was carried out in the same way as in the case of 2d data and is described in detail in section 3.3.2. The mean of 1024 measurements was low pass filtered to reject the cardiac related impedance changes. The frames corresponding to the instants of maximum inspiration and maximum expiration were identified using a peak detection routine. The value of ΔZ, for each of the 1024 measurements, was calculated by subtracting the mean impedance for expiration from the mean impedance for inspiration. The value of Z for each measurement was calculated by taking a mean of impedance values corresponding to all the frames.

3.4.3. Calculation of centre-to-centre distance

The centre-to-centre distance between the drive and receive pairs for each electrode combination was calculated geometrically using the same elliptical model of the thoracic cavity as described in section 3.3.3. The vertical distance between the two adjacent horizontal planes, was assumed to be equal to 0.08 times the perimeter length of the ellipse, which was measured during data collection from subjects.

3.4.4. Results of the analysis of 3d data

The relationship between $\Delta Z/Z$ and distance for the co-planar data analysed earlier indicated that $\Delta Z/Z$ increased with distance between the drive and the receive electrode pairs (Figure 3.6). The 3d experimental data consisted of the co-planar data, recorded from four different horizontal planes, as well as the non-planar data. Therefore, it was thought that a first step would be to see whether the same relationship was true for this 3d data.

A plot of $\Delta Z/Z$ versus distance for the 1024 measurements is shown in Figure 3.8. Each point represents $\Delta Z/Z$ for one out of 1024 drive-receive combinations and this value is calculated as the mean of 8 subjects for that particular drive-receive combination. The slope of the regression line of $\Delta Z/Z$ upon distance is positive (0.031) and statistically significant ($p < 0.001$). This slope of the regression line of $\Delta Z/Z$ upon distance was also found to be positive and statistically significant in all the 8 subjects as listed in Table 3.1.

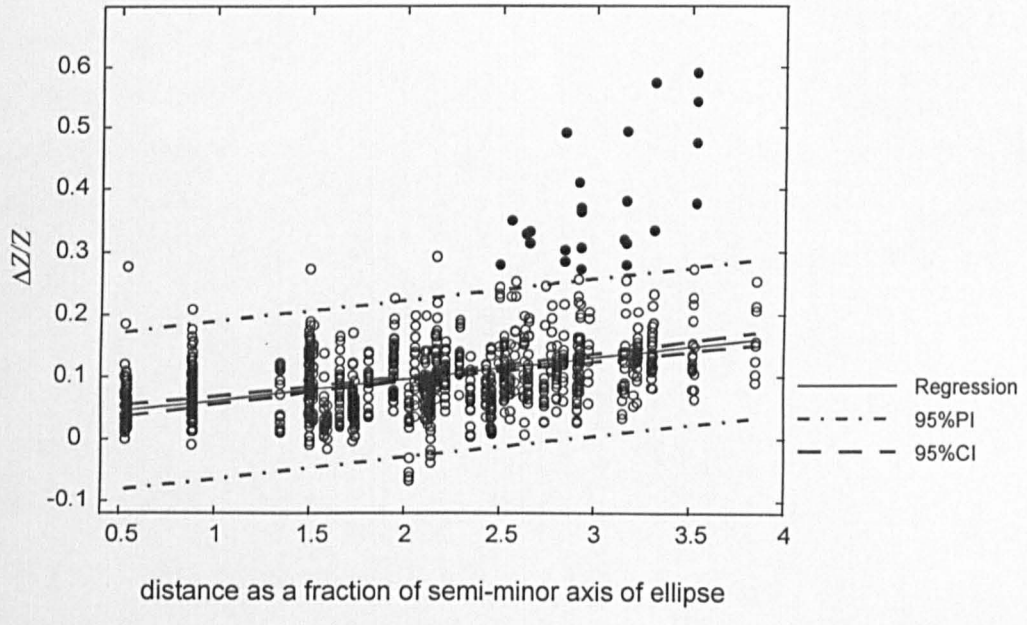

Figure 3.8 *Plot of $\Delta Z/Z$ versus distance for the measured data. The points marked as 'filled circles' correspond to values of $\Delta Z/Z$ much higher than the remaining values*

Table 3.1 *Slope of the regression line of $\Delta Z/Z$ upon distance for 8 subjects*

Subject	Slope of $\Delta Z/Z$ versus distance	p
AW	0.032	< 0.001
JW	0.020	< 0.001
HD	0.010	< 0.001
PM	0.015	< 0.001
NB	0.017	< 0.001
JN	0.031	< 0.001
JM	0.012	< 0.001
JS	0.011	< 0.001

A positive and statistically significant slope of the regression line of $\Delta Z/Z$ upon distance indicated that $\Delta Z/Z$ increased with increase in distance for the 3d data. However, there was a large scatter of points as seen in Figure 3.8. This large scatter of points suggested that there could be some other factors influencing the relationship between $\Delta Z/Z$ and distance between the drive and the receive electrode pairs.

In order to investigate the causes of this scatter, 64 measurements corresponding to 64 co-planar drive-receive combinations, for each of the 4 horizontal electrode planes, were extracted from the complete data set of 1024 measurements. Figure 3.9 shows plots of $\Delta Z/Z$ versus distance for the co-planar data corresponding to each of the 4 planes. The y-axis scale is the same as that in Figure 3.8 so that the plots from the two figures can be compared. It can be seen that these plots (Figure 3.9) have a relatively less scatter of points. As a result, the relationship between $\Delta Z/Z$ and distance seems to be better defined and agrees with the earlier result obtained for the co-planar data (Figure 3.6) and indicates that $\Delta Z/Z$ increases with distance. Furthermore, it also indicates that the

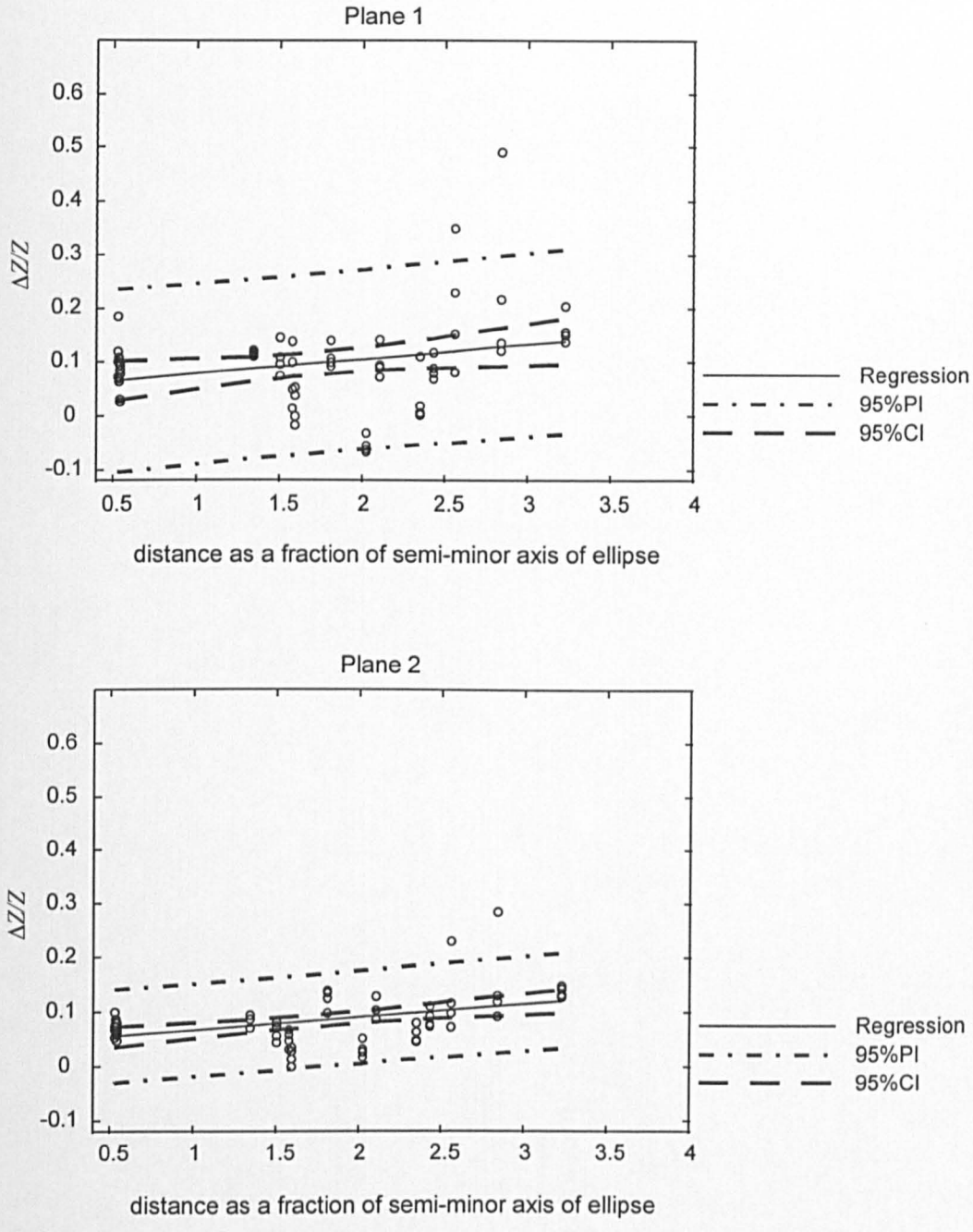

Figure 3.9a *Plot of ΔZ/Z versus distance for the co-planar data extracted from the 3d data (Plane 1 and Plane 2)*

large scatter in the plot of Figure 3.8 is mainly due to measurements obtained from the non-planar electrode placements.

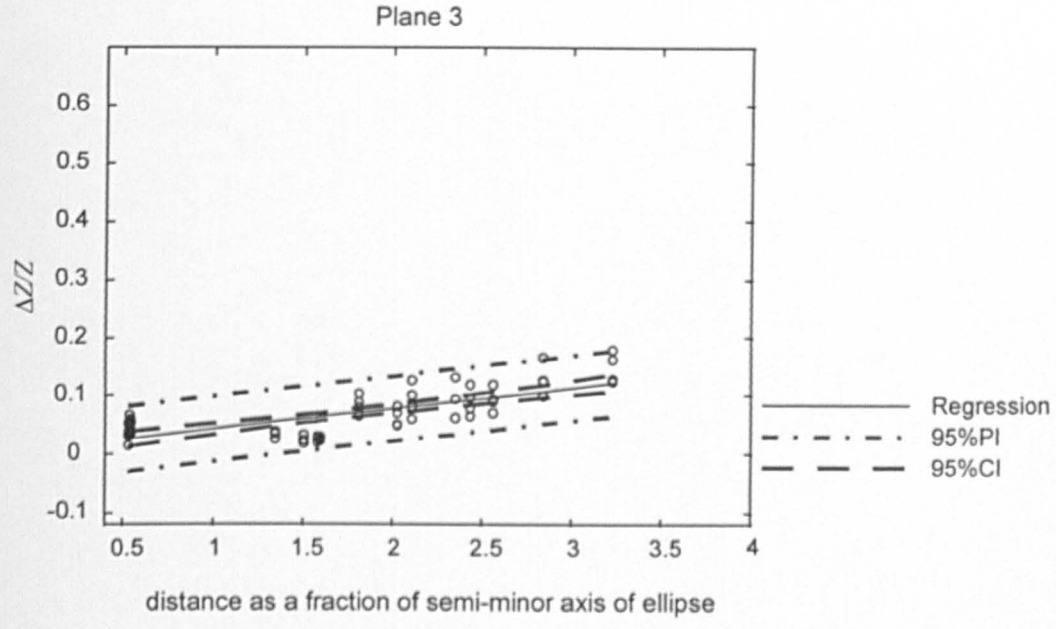

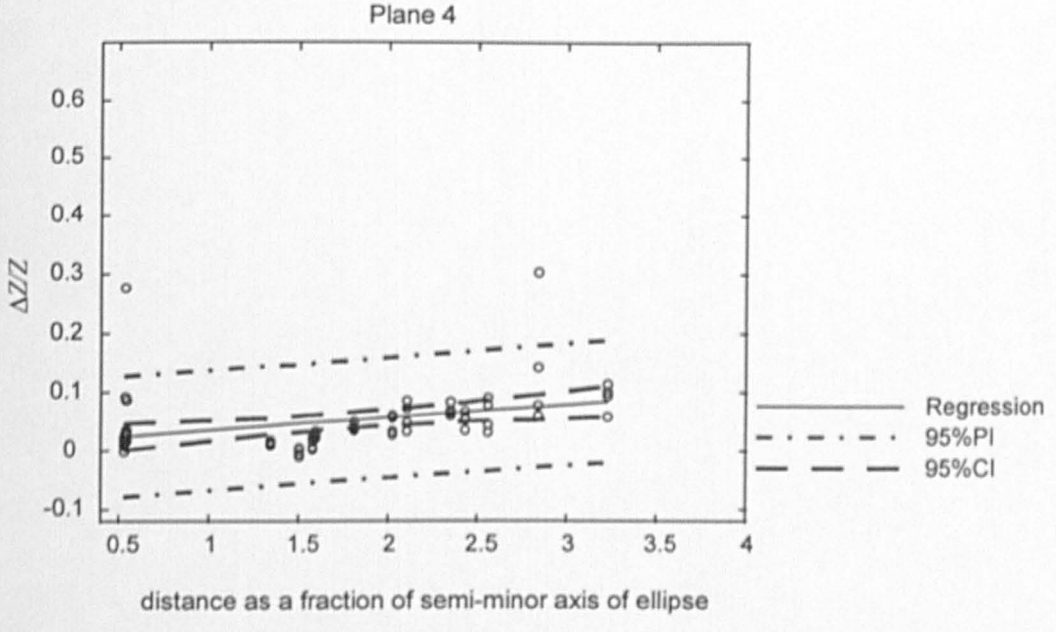

Figure 3.9b Plot of ΔZ/Z versus distance for the co-planar data extracted from the 3d data (Plane 3 and Plane 4)

The aim of this analysis on the 3d data was to invsetigate whether the sensitvity to lung resistivity changes could be further increased beyond that obtained using the co-planar placements, by placing electrodes in different horizontal planes. Therefore, further investigation into possible causes of the scatter were not

carried out. Instead, the data was examined to identify one or a few electrode placements that would have maximum sensitivity to lung resistivity changes. It was observed that there were some such electrode placements marked by 'filled circles' in Figure 3.8. A majority of these points belonged to the non-planar electrode placements as they did not appear in the plots of Figure 3.9. Thus, primarily it seemed that these non-planar electrode placements were more sensitive to lung resistivity changes than the co-planar electrode placements. However, it was important to note that these non-planar electrode placements also had a higher value of distance between the drive and the receive electrode pairs. At these higher distances, the absolute value of the signal would be expected to decrease and hence, *SNR* would be poor. An experimental study was carried out in this project to establish a relationship between *SNR* and distance, and is described in the subsequent section. Thus, even though some non-planar electrodes placements appeared to be more sensitive than the co-planar electrode placements, they could not be considered as optimum because they would not necessarily have a sufficiently high *SNR*, and hence would not be reliable.

In order to gain a better understanding as to which parameters were important in determining the relationship between impedance measurements and electrode placement, and to identify an optimum electrode placement, a theoretical study was carried out and is described in detail in the following chapter. This study was carried out on a volume conductor model of the thoracic cavity and was based on the sensitivity relationship of Geselowitz (1971). One advantage of this approach was thought to be that data generated from these theoretical studies would be free from measurement noise.

3.5. Effect of distance on Signal-to-Noise Ratio

An experimental study was carried out to investigate the relationship between distance and Signal-to-Noise Ratio (*SNR*). This study involved recording impedance data from a cylindrical tank having a diameter of 235 mm. The tank was filled with a salt solution having conductivity equal to 2.5 mS cm^{-1}, up to a

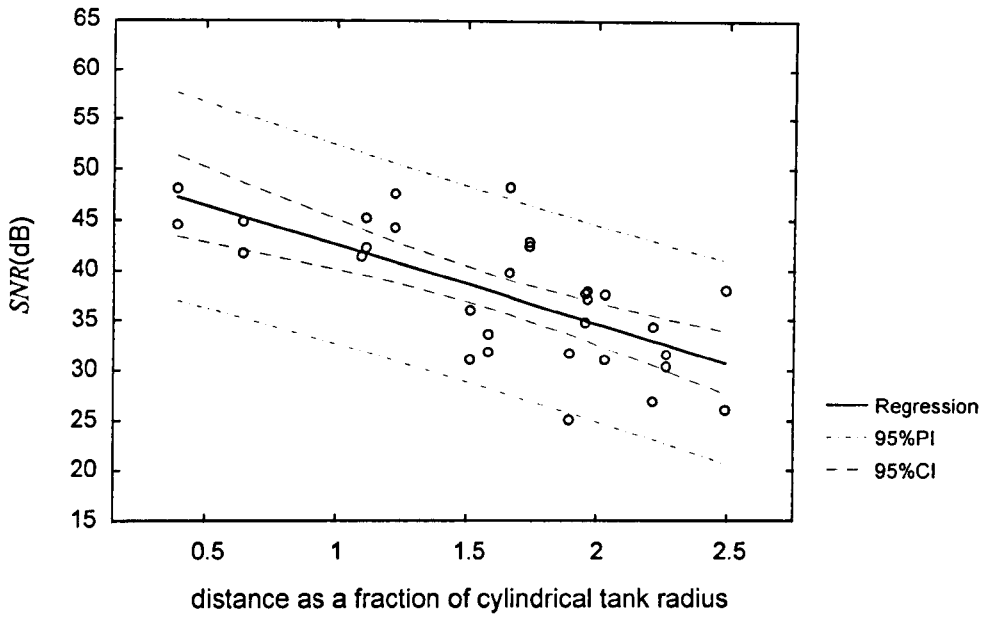

Figure 3.10 *Plot of SNR versus distance between the drive and the receive electrode pairs*

level of 420 mm from the bottom. The first electrode plane was located at a distance of 120 mm from the bottom of the tank and the distance between any two adjacent electrode planes was equal to 60 mm. The 32 drive and 32 receive electrodes were attached to this tank to record 1024 measurements, as recorded from the human subjects.

SNR was calculated using the following equation for each of the 1024 measurements.

$$SNR = 20 \cdot \lg\left(\frac{mean(Z)}{std.dev.(Z)}\right) \qquad 3.24$$

The distance between the drive and the receive electrode pairs was calculated on the basis of the dimensions of the cylindrical tank. Figure 3.10 shows a plot of *SNR* versus distance for 32 measurements corresponding to 1 drive electrode pair and 32 receive electrode pairs. This plot indicates that *SNR* reduces with distance ($p < 0.001$). A similar trend was observed in case of all the other measurements.

3.6. Effect of electrode spacing on impedance measurements

The spacing between the two electrodes forming a drive or a receive pair is one of the parameters that defines an electrode placement. Therefore, it was also important to study the effect of this parameter on the thoracic impedance measurements. An experimental study was carried out in this project to investigate the effect of electrode spacing on the impedance measurements and is described in this section.

3.6.1. Data collection and analysis

The impedance data used in this study was the same 'co-planar data', used in the earlier analysis described, in section 3.3. The data collection procedure has been described in detail in section 3.3.1 and is outlined here in brief.

The co-planar data was recorded from 2 normal human subjects during tidal breathing and in an upright sitting position, using a Sheffield Mark 2 REIT system (Smith *et al*, 1995). An array of 16 electrodes was placed around the thoracic cavity at the level of the nipples. The 1500 frames of data, each consisting of 104 independent measurements, were recorded over 60 s at a frame rate of 25 frames s^{-1}. Data was also recorded from a third subject by placing the 16 electrode array in an oblique plane. It was intuitively expected that when the electrodes were placed in an oblique plane, the impedance measurements would have more contribution from the lungs as this oblique plane spanned the lungs vertically.

The electrode spacing for all the 104 independent measurements for the 16-electrode adjacent data was the same and equal to 1/16 times the circumference of the thoracic cavity. However, for this study, it was necessary to obtain data from electrode placements having different values of electrode spacing. Therefore, the data corresponding to different values of electrode spacing was obtained from the 16-electrode data using the principle of superposition and reciprocity as explained below.

Let us consider a circular conductor with 16 equally spaced electrodes (e_1 to e_{16}) placed on its circumference as shown in Figure 3.11.

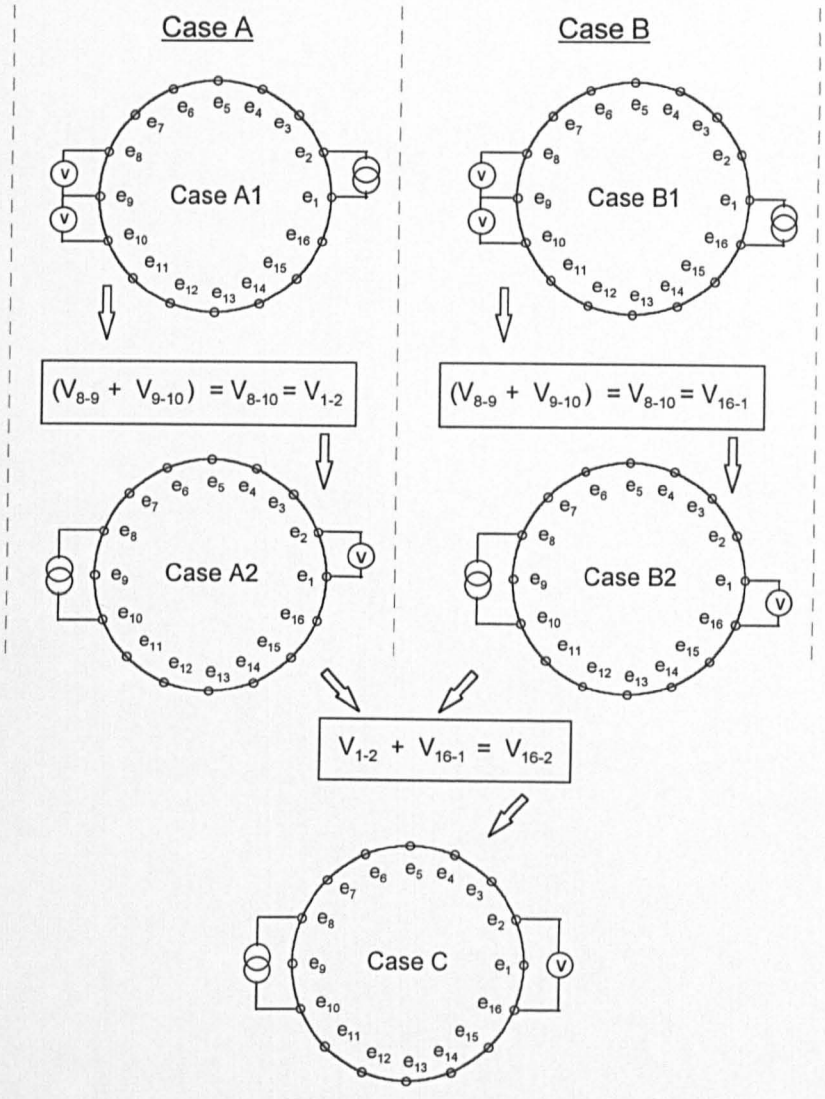

Figure 3.11 Deriving impedance measurements corresponding to a different electrode spacing using the principle of superposition and reciprocity

Let us first consider Case A1. The voltage between electrodes e_8 and e_{10} (V_{8-10}), for current injection between electrodes e_1 and e_2, can be obtained by adding the voltages between electrodes e_8 and e_9 (V_{8-9}), and electrodes e_9 and e_{10} (V_{9-10}). On the basis of reciprocity, it can be seen that the voltage between electrodes e_1 and e_2 (V_{1-2}), for current injection between electrodes e_8 and e_{10} (Case A2), is

equal to the voltage $V_{8\text{-}10}$ obtained in Case A1. In the same way, it can be shown that the voltage obtained in Case B2 is equal to that obtained in Case B1. Finally, by applying superposition and adding the voltages obtained in Case A and Case B, it is possible to determine the voltage between electrodes e_{16} and e_2, for current injection between electrodes e_8 and e_{10} (Case C). Thus, the voltage obtained in Case C corresponds to a different electrode spacing, i.e. 1/8 times the circumference of the circular conductor. In this way, it was possible to obtain impedance measurements for any electrode spacing in multiples of 1/16 times the circumference of the thoracic cavity from the 16-electrode data.

For the present study, the 16-electrode data was processed in two ways. It has been reported earlier in this chapter that for the co-planar data, $\Delta Z/Z$ increases with increase in distance between the drive and the receive electrode pairs. Therefore, an electrode placement having maximum distance between the drive and the receive electrode pairs was selected as shown in Figure 3.12a. The measurements corresponding to this and other values of electrode spacing as shown in Figure 3.12b and Figure 3.12c, were obtained using the method described above. The values of $\Delta Z/Z$ were obtained by processing these derived measurements as described earlier in section 3.3.2.

It has been mentioned before that for an adjacent drive - adjacent receive data collection protocol, a 16 electrode array produces 104 independent measurements. In the same way, an 8-electrode array will produce 20 independent measurements and a 4-electrode array will produce 2 independent measurements. Therefore, an alternative way of processing the 16-electrode data was to derive these independent measurements for the 8-electrode and 4-electrode, equally spaced electrode configurations shown in Figure 3.13a and Figure 3.13b, respectively. A mean of all the appropriate number of independent measurements, corresponding to the three equally spaced electrode configurations, was obtained and $\Delta Z/Z$ was calculated for these three mean impedance signals.

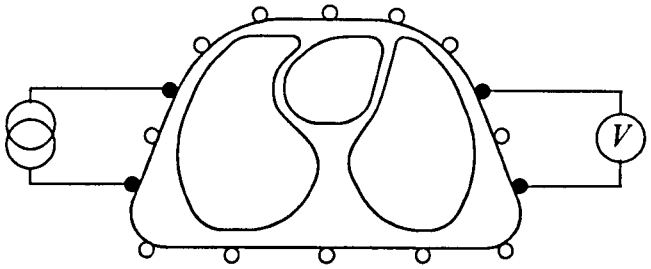

Figure 3.12a Electrode spacing: e-sp1

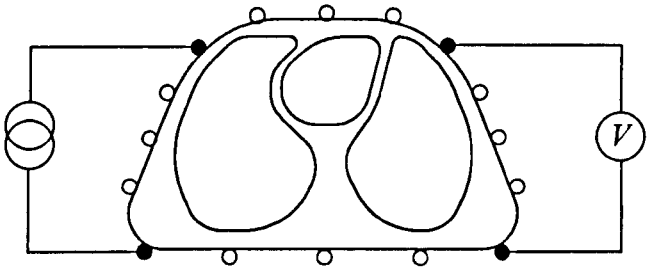

Figure 3.12b Electrode spacing: e-sp2

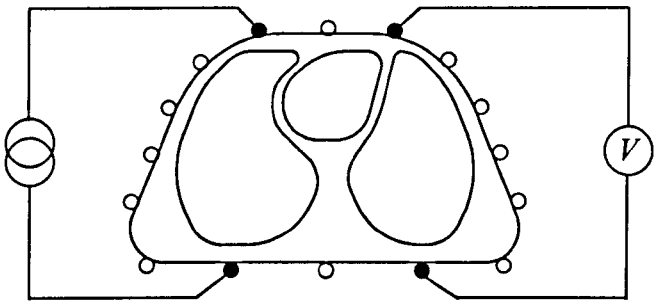

Figure 3.12c Electrode spacing: e-sp3

Figure 3.12 The 3 different values of electrode spacing, e-sp1, e-sp2 and e-sp3 used in the study

3.6.2. Results of the study

A plot of $\Delta Z/Z$ for different values of electrode spacing as in Figure 3.12, is shown in Figure 3.14. It can be seen that $\Delta Z/Z$ decreases as the electrode spacing increases. Figure 3.15 shows the three values of $\Delta Z/Z$ obtained by processing the mean of the independent measurements for the three electrode configurations. It can be seen that $\Delta Z/Z$ for this mean signal increases as the spacing for all the drive and the receive electrode pairs increases. These results

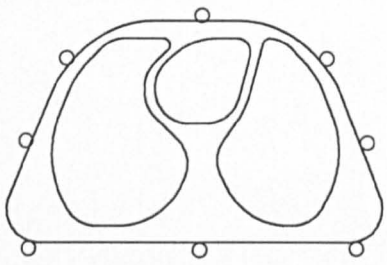

Figure 3.13a 8-electrode adjacent configuration

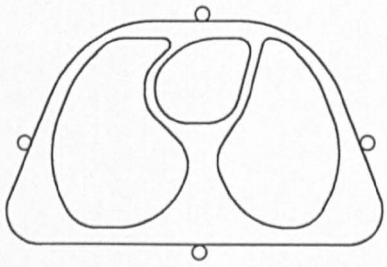

Figure 3.13b 4-electrode adjacent configuration

Figure 3.13 *Two different equally spaced electrode configurations used in the study*

are consistent in all the three subjects including Subject AN, which had the 16 electrodes placed in an oblique plane rather than in a horizontal plane.

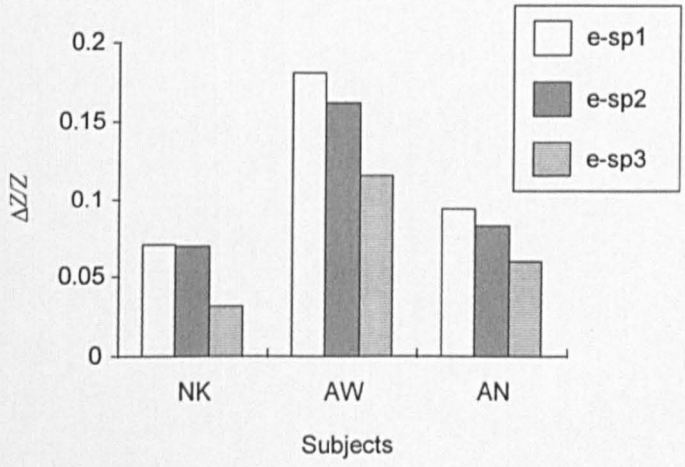

Figure 3.14 *Values of ΔZ/Z for different electrode spacing as shown in Figure 3.12 (e-sp1< e-sp2< e-sp3)*

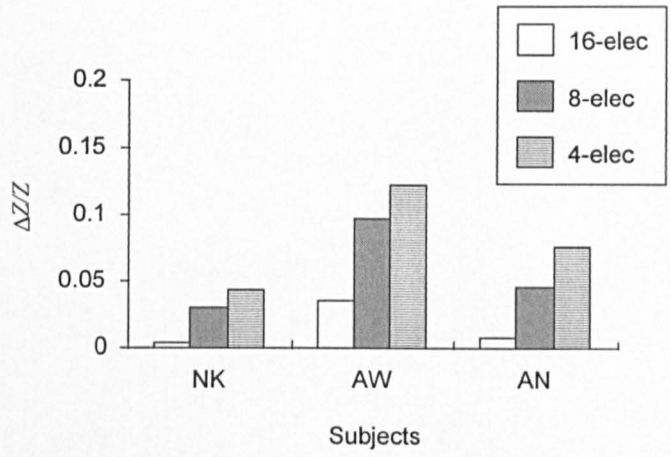

Figure 3.15 *Mean ΔZ/Z for three different adjacent electrode configurations (16-electrode, 8-electrode and 4-electrode). The later two configurations are shown in Figure 3.13*

3.7. Effect of electrode spacing on Signal-to-Noise Ratio

The effect of electrode spacing on SNR could be studied by taking measurements on a saline filled tank as in the earlier case. However, the measurements corresponding to different values of electrode spacing were derived by combining the individual measurements of the 16-electrode data. Thus, the random noise in the individual measurements would get averaged and reduced in this process. As a result, the synthesised value of SNR for a larger electrode spacing than that physically measured on the tank (1/16 in this case) would be higher. However, the SNR was directly proportional to the absolute value of ΔZ and the instrumentation noise (Z_n) was independent of the electrode placement (refer to equation 3.19). Therefore, in order to understand the effect of electrode spacing on SNR, its effect on ΔZ was studied. Figure 3.16 shows a plot of ΔZ versus electrode spacing and it indicates that ΔZ and hence, SNR increases with increase in electrode spacing.

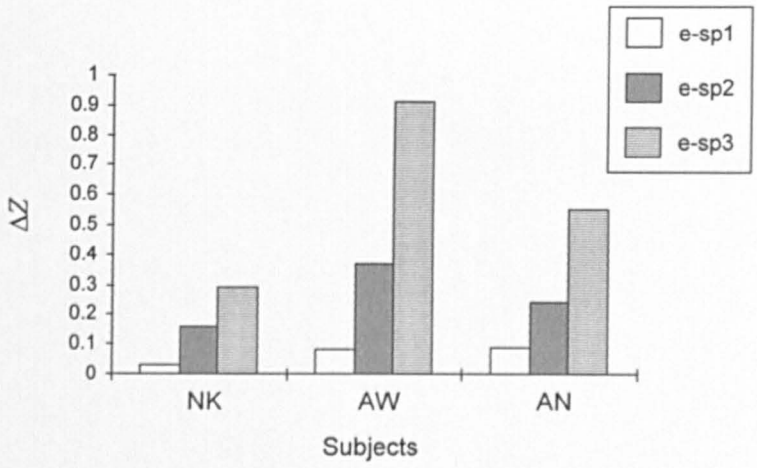

Figure 3.16 A plot of ΔZ for different values of electrode spacing as shown in Figure 3.12 (e-sp1< e-sp2< e-sp3)

3.8. Discussion

This chapter described experimental studies carried out to identify an electrode placement that would produce impedance measurements having a high specificity to lung resistivity changes. The theoretical analysis described in the first section of this chapter laid down two criteria for such an optimum electrode placement. Firstly, this optimum electrode placement should maximise the fractional changes in thoracic impedance ($\Delta Z/Z$). Secondly, it should also maximise SNR, which is the same as maximising the absolute value of impedance change ΔZ.

In practice, one may place electrodes at any locations on the thoracic cavity. In order to constrain this placement, only the electrode placements used in EIT were considered in this study. An electrode placement for EIT can be defined by three parameters namely, the distance between the drive and the receive electrode pairs, the vertical distance between the two horizontal planes containing the drive and the receive electrode pairs and the spacing between the two electrodes forming a drive or a receive pair.

The experimental study carried out using co-planar electrode placements showed that $\Delta Z/Z$ increased with increase in distance between the drive and the receive electrode pairs. The results of the experimental study involving electrode

placements in more than one horizontal planes also showed that $\Delta Z/Z$ increased with increase in distance. However, there was a large scatter of points in the plot of $\Delta Z/Z$ versus distance. This scatter of points appeared to be due to measurements obtained from the non-planar electrode placements.

The purpose of the experimental study involving the non-planar electrode placements was to find out whether $\Delta Z/Z$ could be increased beyond that obtained form the co-planar electrode placements. It was observed that some of the non-planar electrode placements had significantly higher values of $\Delta Z/Z$. However, the distance between the drive and the receive electrode pairs was also high for these electrode placements. An experimental study investigating the relationship between SNR and distance indicated that SNR decreased with increase in distance. Therefore, the non-planar electrode placements having higher values of $\Delta Z/Z$ could not be considered as optimum because they would have a low value of SNR.

It was observed that for a particular electrode placement, $\Delta Z/Z$ decreased with increase in electrode spacing. However, when a mean of all the independent measurements was used to calculate $\Delta Z/Z$, it increased with increase in electrode spacing. One possible explanation to this observation is as follows. It is known that Z increases with electrode spacing and hence, ΔZ would also increase with electrode spacing. However, for a given change in lung resistivity, ΔZ would also depend on the size of the lung region, resistivity changes of which contribute to ΔZ. This size may not increase significantly with increase in electrode spacing for a given electrode placement. As a result, for a single measurement, $\Delta Z/Z$ would decrease with increase in electrode spacing. However, when a mean of all the independent measurements is used to calculate $\Delta Z/Z$, it would include contribution from many different regions of the lungs. Furthermore, it seems possible that at larger electrode spacing, current would penetrate into deeper regions of the thoracic cavity causing an increase in the contribution from the deeper regions of the lungs. This would also cause $\Delta Z/Z$ to increase with an increase in electrode spacing. In order to understand the exact underlying

physical phenomenon behind these observations, a theoretical study was carried out and is described in the following chapter.

In general, these observations suggested that if an increase in the value of $\Delta Z/Z$ is required, then it would be necessary to increase the electrode spacing and make use of all the independent measurements obtained from such an electrode placement. This strategy has two advantages. Firstly, it would lead to requiring a fewer electrodes. In this project, it was decided that the aim of movement artefact reduction would be achieved using a minimum number of electrodes, and hence the reduction in number of electrodes was desirable. Secondly, it was also observed that the absolute value of the change in measured impedance (ΔZ) and hence SNR, increased with electrode spacing.

The theoretical studies were carried out in this project to investigate the relationship between electrode placement and impedance measurements of the thoracic cavity. These studies were based on the sensitivity method of Geselowitz (1971). One advantage of these studies was thought to be that it would be possible to eliminate the effect of instrumentation noise and thus, have a better understanding of the factors responsible for the observed relationship between the electrode placement and the measured thoracic impedance. The following chapter describes these theoretical studies.

Chapter 4. Electrode placement and impedance measurements of the thoracic cavity: theoretical studies

4.1. Introduction

The experimental studies carried out for identifying an optimum electrode placement for impedance pneumography were described in the previous chapter. It was observed that for co-planar electrode placements the fractional change in impedance ($\Delta Z/Z$) during breathing, increased with increase in distance between the drive and the receive electrode pairs. The experimental data showed a similar increasing trend when the impedance data recorded using the non-planar electrode placements and the co-planar electrode placements was analysed together. There were a few non-planar electrode placements having significantly higher values of $\Delta Z/Z$. However, these electrode placements also had a larger distance between the drive and the receive electrode pairs and hence, the measurements obtained from these electrode placements were expected to be greatly affected the instrumentation noise. As a result, it was difficult to identify one or a few optimum electrode placements from the experimental data.

In order to understand which factors determined the relationship between electrode placement and impedance measurements of the thoracic cavity, and to identify the optimum electrode placement, a theoretical study was carried out and is described in this chapter. It was also observed in the experimental studies that impedance measurements were affected by the electrode spacing. Therefore, this theoretical study was also aimed at understanding in what way the electrode spacing affected the impedance measurements.

Geselowitz (1971) suggested the 'sensitivity method' as a theoretical method for relating observed changes in transfer impedance of a volume conductor to changes in resistivity within a specific region of that volume conductor. A reference was made to this method in section 3.2 of the previous chapter (equation 3.15). The theoretical basis of this method is described in the following

section. This is followed by a description of a step by step approach adopted for implementing this method on a volume conductor model of the thoracic cavity using Finite Element Methods (FEM). The chapter ends by reporting the results of the study.

4.2. The sensitivity method

The relationship between the changes in conductivity distribution of a volume conductor and the changes in the transfer impedance measured on its surface, can be obtained using the sensitivity method. The following is the derivation of this sensitivity relationship. This derivation has been carried out on the lines suggested by Lehr (1972) because of the following reasons. Firstly, it is simple as it assumes that there are no internal current sources present. Secondly, it does not require the initial conductivity to be uniform, rather it can be a spatial function over the volume. Let us first consider the governing equations.

The general form of Ohm's law for conduction in a continuous volume conductor is given as (Lorrain and Corson, 1962),

$$\mathbf{J} = -\sigma \nabla \phi \qquad 4.1$$

where,
$\mathbf{J}$ = current density vector
σ = conductivity
ϕ = electric potential

If there are no current sources within the volume conductor, then

$$\nabla \cdot \mathbf{J} = 0 \qquad 4.2$$

where,
$\nabla\cdot$ = divergence operator

By combining equations 4.1 and 4.2 we get,

$$\nabla \cdot (\sigma \nabla \phi) = 0 \qquad 4.3$$

For a unique solution to exist, in the form of distribution of potential (ϕ), sufficient boundary conditions are required to be specified to equation 4.3. These may be either Dirichlet conditions in the form of potentials on the boundary, Neumann conditions in the form of current densities crossing the boundary or Cauchy conditions, which are a mixture of Dirichlet and Neumann conditions.

The solution to the above equation for a given conductivity distribution is generally called 'the forward problem'. The potential distribution is a function of the shape, the electrode positions and the conductivity distribution (Kiber, 1991). The solution to the forward problem can be obtained analytically only if the shape and the conductivity distribution is simple. Otherwise, numerical techniques such as Finite Element Methods (FEM) must be used to obtain the solution. FEM involves partitioning the volume conductor into a number of discrete elements, each having a uniform conductivity. The solution for each element is then obtained by imposing appropriate boundary conditions so that a continuity of voltage and current flow is maintained between adjacent elements. In order to find the sensitivity relationship for a given volume conductor, it is necessary to first solve the forward problem, and the technique of FEM has been used to solve it in this project.

In order to derive the sensitivity relationship we consider a continuous vector function $\mathbf{G}$, in an arbitrary closed region Ω bounded by a piecewise smooth orientable surface Γ (Figure 4.1a), the following equation is written using the divergence theorem (Kreyszig, 1993).

$$\int_{\Gamma} \mathbf{G} \cdot \mathbf{ds} = \int_{\Omega} \nabla \cdot \mathbf{G} dv \qquad 4.4$$

where,

$\mathbf{ds}$ = outward unit normal vector of Γ

Now, let the bounded region be a volume conductor. Let ϕ be some potential distribution, within and on the surface of this volume conductor. Let $\mathbf{J}_{\phi}$ be the current density associated with ϕ and let σ_{ϕ} be the conductivity distribution, when

ϕ and $\mathbf{J}_\phi$ exist. Similarly, let us also assume some other potential distribution ψ, within and on the surface of the volume conductor, and the associated current density $\mathbf{J}_\psi$. Let the conductivity distribution be σ_ψ, when ψ and $\mathbf{J}_\psi$ exist.

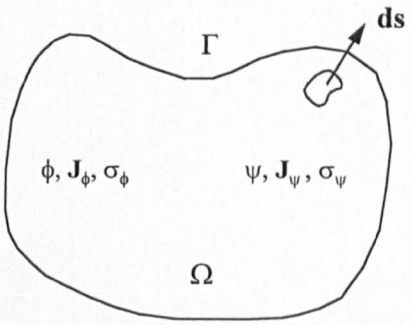

Figure 4.1a

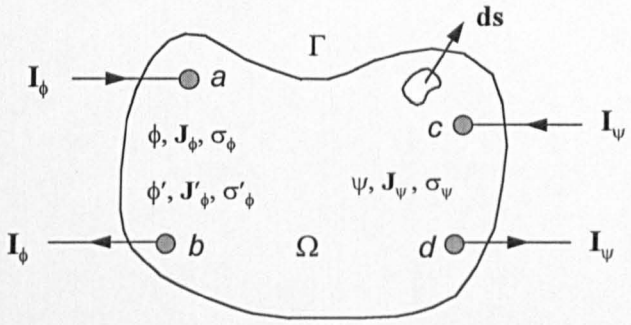

Figure 4.1b

Figure 4.1 *Volume conductor with drive electrodes a and b, and receive electrode c and d*

Substituting $\psi\mathbf{J}_\phi$ for $\mathbf{G}$ in equation 4.4 we get,

$$\int_\Gamma \psi\mathbf{J}_\phi \cdot \mathbf{ds} = \int_\Omega \nabla \cdot (\psi\mathbf{J}_\phi) dv \qquad 4.5$$

Expanding the divergence of a product on the RHS of equation 4.5 we get,

$$\int_\Gamma \psi\mathbf{J}_\phi \cdot \mathbf{ds} = \int_\Omega \psi(\nabla \cdot \mathbf{J}_\phi) dv + \int_\Omega \mathbf{J}_\phi \cdot \nabla\psi dv \qquad 4.6$$

If there are no current sources within the volume conductor, then $\nabla \cdot \mathbf{J}_\phi = 0$ and hence, the first term on the RHS is zero. Equation 4.6 reduces to,

$$\int_\Gamma \psi \mathbf{J}_\phi \cdot \mathbf{ds} = \int_\Omega \mathbf{J}_\phi \cdot \nabla \psi dv \qquad 4.7$$

Similarly, an equation for $\mathbf{J}_\psi$ and ϕ can be written as,

$$\int_\Gamma \phi \mathbf{J}_\psi \cdot \mathbf{ds} = \int_\Omega \mathbf{J}_\psi \cdot \nabla \phi dv \qquad 4.8$$

Subtracting equation 4.8 from 4.7 we get,

$$\int_\Gamma \psi \mathbf{J}_\phi \cdot \mathbf{ds} - \int_\Gamma \phi \mathbf{J}_\psi \cdot \mathbf{ds} = \int_\Omega \mathbf{J}_\phi \cdot \nabla \psi dv - \int_\Omega \mathbf{J}_\psi \cdot \nabla \phi dv \qquad 4.9$$

From the Ohm's law of equation 4.1, $-\sigma_\phi \nabla \phi$ is substituted for $\mathbf{J}_\phi$ and $-\sigma_\psi \nabla \psi$ is substituted for $\mathbf{J}_\psi$ in equation 4.9, and combining the integration on the RHS we get,

$$\int_\Gamma \psi \mathbf{J}_\phi \cdot \mathbf{ds} - \int_\Gamma \phi \mathbf{J}_\psi \cdot \mathbf{ds} = \int_\Omega (\sigma_\psi - \sigma_\phi)(\nabla \phi \cdot \nabla \psi) dv \qquad 4.10$$

If the two conductivity distributions are assumed to be equal, i.e. $\sigma_\phi = \sigma_\psi = \sigma$, then the volume integral on the RHS of equation 4.10 vanishes and we get,

$$\int_{\Gamma} \psi \mathbf{J}_{\phi} \cdot \mathbf{ds} = \int_{\Gamma} \phi \mathbf{J}_{\psi} \cdot \mathbf{ds} \qquad 4.11$$

Now, let the potential distribution ϕ be due to injection of current $\mathbf{I}_{\phi}$ between electrodes *a* and *b*, and the potential distribution ψ be due to injection of current injection $\mathbf{I}_{\psi}$ between electrodes *c* and *d*, as shown in Figure 4.1b. If the volume conductor is surrounded by a non-conducting medium, then the current density on the surface is zero everywhere except under the electrodes. Therefore, equation 4.11 becomes,

$$\mathbf{I}_{\phi}(\psi_a - \psi_b) \equiv \mathbf{I}_{\phi}\psi_{ab} = \mathbf{I}_{\psi}(\phi_c - \phi_d) \equiv \mathbf{I}_{\psi}\phi_{cd} \qquad 4.12$$

The transfer impedance *Z* is obtained by dividing both sides of equation 4.12 by a product $\mathbf{I}_{\phi} \cdot \mathbf{I}_{\psi}$ as below.

$$Z = \frac{\phi_{cd}}{\mathbf{I}_{\phi}} = \frac{\psi_{ab}}{\mathbf{I}_{\psi}} \qquad 4.13$$

This is the statement of the principle of reciprocity as given by Geselowitz (1971).

From equations 4.7, 4.11 and 4.12 and substituting $-\sigma\nabla\phi$ for $\mathbf{J}_{\phi}$ in equation 4.7, we get the relationship between transfer impedance *Z* and the conductivity distribution σ as,

$$Z = \int_{\Omega} \sigma \frac{\nabla\phi}{\mathbf{I}_{\phi}} \cdot \frac{\nabla\psi}{\mathbf{I}_{\psi}} dv \qquad 4.14$$

Let us now consider a third set of functions associated with electrodes *a* and *b*. Let the conductivity distribution be σ', the potential distribution be ϕ' and the current density be $\mathbf{J}_{\phi}'$, then from equation 4.10 we can write,

$$\int_{\Gamma} \psi \mathbf{J}_{\phi}' \cdot \mathbf{ds} - \int_{\Gamma} \phi' \mathbf{J}_{\psi} \cdot \mathbf{ds} = \int_{\Omega} (\sigma - \sigma')(\nabla \phi' \cdot \nabla \psi) dv \qquad 4.15$$

If the current injected in the primed case is the same as in the unprimed case, then we get,

$$\int_{\Gamma} \psi \mathbf{J}_{\phi}' \cdot \mathbf{ds} = \int_{\Gamma} \psi \mathbf{J}_{\phi} \cdot \mathbf{ds} \qquad 4.16$$

From equations 4.11 and 4.16 we get,

$$\int_{\Gamma} \psi \mathbf{J}_{\phi}' \cdot \mathbf{ds} = \int_{\Gamma} \phi \mathbf{J}_{\psi} \cdot \mathbf{ds} \qquad 4.17$$

Thus, from equation 4.17 and equation 4.15, and combining the integration on the LHS in equation 4.15 we get,

$$\int_{\Gamma} (\phi - \phi') \mathbf{J}_{\psi} \cdot \mathbf{ds} = \int_{\Omega} (\sigma - \sigma')(\nabla \phi' \cdot \nabla \psi) dv \qquad 4.18$$

Further simplifying equation 4.18 on the lines similar to those used to develop equation 4.14, an equation relating the changes in transfer impedance ΔZ and the changes in conductivity distribution $\Delta\sigma$ can be obtained as,

$$\Delta Z = \frac{\Delta\phi_{cd}}{\mathbf{I}_\phi} - = -\int_\Omega \Delta\sigma \frac{\nabla\phi'}{\mathbf{I}_\phi} \cdot \frac{\nabla\psi}{\mathbf{I}_\psi} dv \qquad 4.19$$

Equation 4.19 is the sensitivity relationship of Geselowitz (1971). It is important to note that the above relationship is non-linear because the potential distribution ϕ' is a function of difference in conductivity distributions $\Delta\sigma$. However, if $\Delta\sigma$ is small, then the potential distribution ϕ' will not be much different from the initial potential distribution ϕ, and equation 4.19 can be approximated as,

$$\Delta Z = -\int_\Omega \Delta\sigma \frac{\nabla\phi}{\mathbf{I}_\phi} \cdot \frac{\nabla\psi}{\mathbf{I}_\psi} dv \qquad 4.20$$

This is called the linearised sensitivity relationship as given by Avis (1993).

It can be seen that in order to solve the equation 4.20 for ΔZ, it would be necessary to determine the potential distributions ϕ and ψ, corresponding to the drive and the receive electrode pairs, respectively, for a given conductivity distribution σ. This is solving the forward problem. FEM was used in this project to solve the forward problem. A volume conductor model of the thoracic cavity was first developed. The forward problem was solved determining the potential distributions ϕ and ψ, for electrode placements and combinations, similar to those used in the experimental study described in the previous chapter. Finally, a sensitivity matrix was generated using MATLAB®(version 4.2, Mathworks Inc., USA), which related the 1024 boundary measurements to the conductivity changes occurring within each element of the volume conductor model. The following sections describe a step by step approach adopted for implementing the sensitivity method.

4.3. A volume conductor model of the thoracic cavity

A simplified volume conductor model of the thoracic cavity, having a cylindrical shape and a uniform internal conductivity distribution, was developed. This model was assumed to consist of two regions to represent the lungs as shown in Figure 4.2. The development of a three dimensional model having an exact shape and

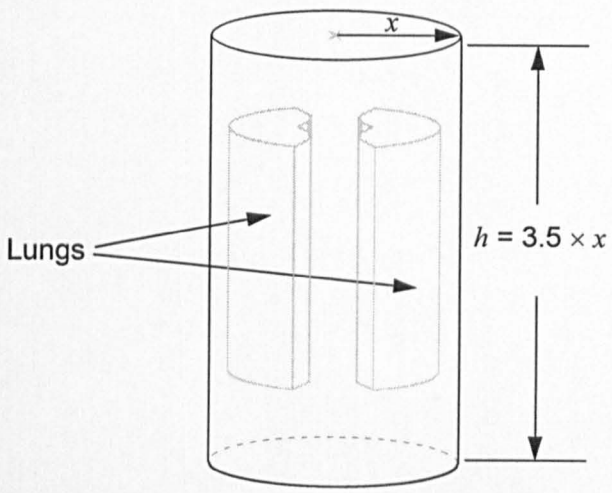

Figure 4.2 *A cylindrical volume conductor model of the thoracic cavity showing the two lungs (x is the radius of the cylinder)*

internal conductivity distribution of the thoracic cavity in all respects, seemed to be an ambitious task and was therefore considered beyond the scope of this project.

It would have been more appropriate to choose an elliptical cross-section for the model, as the human thorax is more elliptical in shape. However, a circular cross-section was chosen because by doing so it was possible to use a mesh having a cyclic symmetry with respect to the electrode placement. This cyclic symmetry in the meshing had the following advantages. Firstly, this type of mesh was expected to provide a significant reduction in the amount of computation required for solving the forward problem. Secondly, it would reduce the computation required for generating the sensitivity matrix (Metherall, 1998). It may be noted that one more advantage of having the cyclic symmetry is that it is easier to obtain an inverse of the corresponding sensitivity matrix for impedance imaging

(Metherall, 1998). However, this was not applicable in the present work. In general, a reduction in computation time was desirable because the complete three dimensional model was expected to have a large number of elements and 1024 different electrode combinations, and the software would take a very long time to run.

The second assumption of uniform conductivity distribution also did not agree with the actual conductivity distribution of the human thorax. However, the purpose of this study was to understand what factors were involved in determining the relationship between impedance measurements and electrode placement rather than modelling the exact conditions. Therefore, for simplicity, the model was assumed to have a uniform conductivity distribution.

It has been stated earlier that, when the shape and the conductivity distribution is simple, such as that of the model under consideration, it may be possible to derive an analytical solution to the forward problem. However, this was not thought to be a trivial task because it would have become necessary to write the software for this purpose. On the other hand, standard commercial FEM software was available, and therefore, FEM was used in this project. The following section describes a step by step development of the volume conductor model using FEM.

4.4. Development of a FEM model

The volume conductor model shown in Figure 4.2 was developed using commercial FEM software ANSYS® (version 5.3, Ansys Inc., USA) in the following steps. Firstly, a simple two dimensional model was developed with a cyclic symmetry in its mesh with respect to electrode placement. The forward problem was solved using this cyclic symmetry and a program was written to generate a sensitivity matrix for this model. Once a two dimensional model was successfully developed, the same procedure could be followed to develop a three dimensional model.

4.4.1. Development of a two dimensional FEM model

A two dimensional volume conductor model with 16 equally spaced electrodes is shown in Figure 4.3. The 8 drive (d_1 to d_8) and the 8 receive (r_1 to r_8) electrodes were configured as 8 interleaved electrode pairs, similar to those used in the experimental studies described in the previous chapter. Therefore, the mesh was required to have an 8-fold cyclic symmetry.

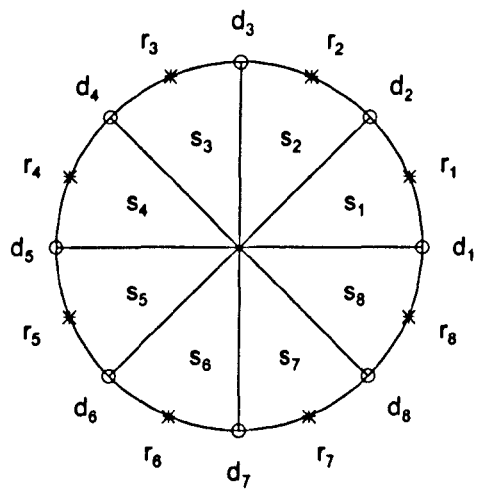

Figure 4.3 *A 2d volume conductor model with 8 drive electrodes, d_1 to d_8 ('circles') and 8 receive electrodes, r_1 to r_8 ('stars'). The circular shape is divided into 8 sectors s_1 to s_8*

A first step in the development of this two dimensional model of the thoracic cavity model was to define an internal geometry in such a way that the two lung regions could be defined. Therefore, the circular shape was divided into 8 sectors (s_1 to s_8) as shown in Figure 4.3. Each sector was further divided into 8 regions (1 to 8). The regions belonging to sector s_1 are shown in Figure 4.4a. The shapes of these regions were chosen in such a way that they could be combined into two regions, shown shaded in Figure 4.4b, to represent the lungs.

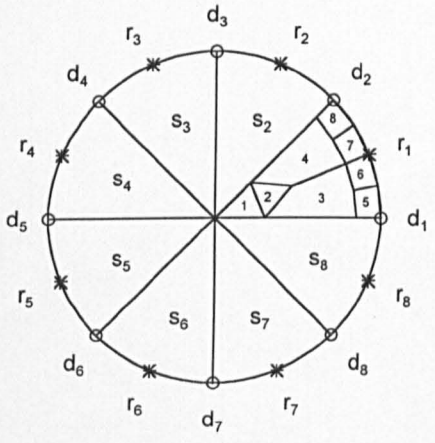

Figure 4.4a

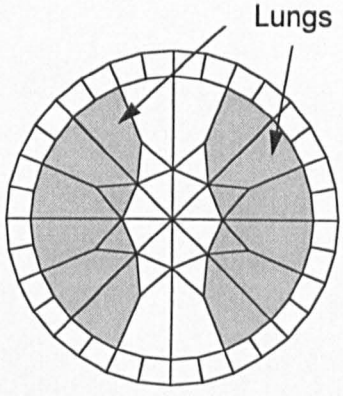

Figure 4.4b

Figure 4.4 *The 2d volume conductor with sector s_1 (Figure 4.4a) divided into 8 regions 1 to 8 and the same 2d volume conductor with two lung regions (Figure 4.4b).*

The next step was to carry out meshing of this model. It is known that the potential gradients are very high near the electrodes. Therefore, in order to achieve a reasonable accuracy, the density of the mesh close to the electrodes was required to be high. Thus, the regions close to the periphery were required to have a higher mesh density compared to the central regions. A command provided in the software could be used to define the mesh density within each region. As mentioned earlier, this mesh was also required to have an 8-fold cyclic symmetry with respect to electrode placement. This was achieved in the following way.

First, sector s_1 was meshed into elements of 4-node quadrilateral type. Then, this mesh was copied to other sectors in a cyclic order, i.e. from s_2 to s_8. This process

ensured that, in addition to an 8-fold cyclic symmetry in the mesh geometry, there was an 8-fold cyclic symmetry in the element numbering. This cyclic symmetry in the element numbering is explained with the help of an illustration in Figure 4.5. The 8 elements, one in each sector, having a cyclically symmetric numbering are shown shaded in Figure 4.5. If there were total of 'n' elements in each sector, then the location of a particular element in sector s_2, with respect to electrodes d_2 and d_3 and having a number equal to 'm+n', was the same as the location of the corresponding element in sector s_1 and having a number equal to 'm'.

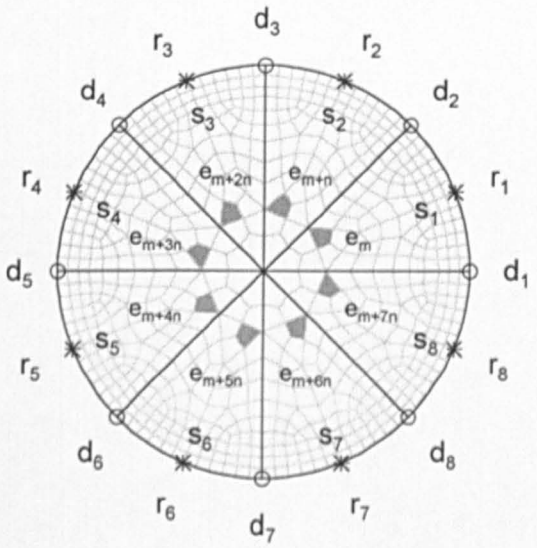

Figure 4.5 8-fold cyclic symmetry in element numbering

4.4.2. Determining potential distribution within the conductor

In order to generate a sensitivity matrix, it was necessary to determine the potential distribution within the volume conductor when a known current was injected between each drive and receive electrode pair. A sensitivity matrix expresses the relationship between conductivity changes occurring within each element and the boundary measurements, and is described in the subsequent sub-section.

Due to an 8-fold cyclic symmetry in the mesh, it was expected that it would be possible to determine the potential distribution for current injection between the 8

drive pairs, from the potential distribution for only 1 drive pair. Similarly, the potential distribution for the 8 receive pairs could be determined from the potential distribution for 1 receive pair. Therefore, the potential distribution, in the form of nodal voltages, for the first drive pair (d_1 and d_2), was determined by solving the FEM equations. The electrode d_1 was specified as the current injection electrode and the voltage on electrode d_2 was constrained to be equal to 0. The potential distribution for the adjacent drive pair (d_2 and d_3) was then obtained by solving the FEM equations and specifying appropriate boundary conditions on d_2 and d_3. However, this potential distribution could also be obtained using the cyclic symmetry in the mesh as explained below.

Let us consider element 'e_A' (shown shaded in Figure 4.6a), located within sector s_1, and at a particular position with respect to drive electrodes d_2 and d_3. Let us also consider element 'e_B' (shown shaded in Figure 4.6b), located within sector s_8 and at a position similar to e_A, but with respect to electrodes d_1 and d_2.

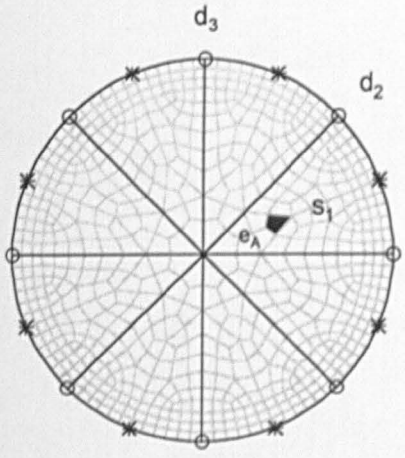

Figure 4.6a

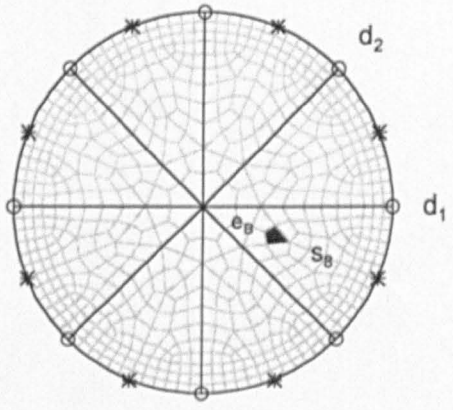

Figure 4.6b

Figure 4.6 *A schematic representation of the 8-fold cyclic symmetry in the voltage distribution*

It was observed that, the nodal voltages of element e_A, due to current injection between electrodes d_2 and d_3, were equal to the nodal voltages of element e_B, due to current injection between electrodes d_1 and d_2. Thus, the nodal voltages of any element due to current injection between electrodes d_2 and d_3, would be

equal to that of an element, due to current injection between electrodes d_1 and d_2, but shifted by an angle of 45° in the clockwise direction from the initial element. Due to an 8-fold cyclic symmetry in the element numbering, the difference between the element numbers for any such pair of elements was constant and equal to number of elements (n) in each sector. Thus, the potential distribution for d_2 and d_3 could be derived by appropriately re-indexing the array of nodal voltages for d_1 and d_2. In this way, the potential distribution for the remaining drive pairs could be determined from the potential distribution for the first drive pair, without solving the FEM equations. The same procedure could be used to determine the potential distribution corresponding to the 8 receive pairs. This reduced the required amount of computation by a factor of 8 as the potential distributions for the 16 electrode pairs could be determined only by solving the FEM equations twice.

4.4.3. Calculation of the sensitivity matrix

The linearised sensitivity relationship expressed in equation 4.20, for the descretised two dimensional conductor under consideration, can be represented as a set of linear equations in a matrix form as,

$$\Delta Z = \mathrm{S}\Delta\sigma \qquad 4.21$$

where,
ΔZ = array of change in boundary measurements
S = the Sensitivity Matrix
$\Delta\sigma$ = array of change in element conductivities

The matrix S is composed of sensitivity coefficients (S_{ij}), each corresponding to the j^{th} element and i^{th} drive-receive combination. It is given by a scalar product of the elemental voltage gradients $\nabla\phi_{id}$ and $\nabla\psi_{ir}$, when a unit current is injected between the drive and the receive pairs, respectively, of the i^{th} drive-receive combination. Therefore,

$$S_{ij} = -\int_{j^{th}\,element} \nabla\phi_{id} \cdot \nabla\psi_{ir}\, dv \qquad 4.22$$

where,
the integration is over the volume of the j^{th} element.

The elemental potential gradient $\nabla\phi_{id}$, associated with a drive pair of the i^{th} drive-receive combination, for the j^{th} element, was calculated from the array of nodal voltages (Φ_{jn}), for that element as,

$$\nabla\phi_{id} = \nabla\mathbf{N} \cdot \Phi_{jn} \qquad 4.23$$

where,
$\mathbf{N}$ = shape function of the quadrilateral elements with 4 nodes (Bruce and Sohrab, 1980)
∇ = gradient operator

The 8-fold cyclic symmetry in the mesh, was also useful in reducing the computation required to generate the complete sensitivity matrix as suggested by Metherall (1998). This is explained with the help of Figure 4.7. The sensitivity coefficient of element e_A (shaded) for the drive-receive combination shown in Figure 4.7a, was equal to that of element e_B (shaded) for the drive-receive combination shifted by an angle of 45° in the clockwise direction (Figure 4.7b). Thus, the sensitivity coefficients for 1 drive and 8 receive pairs were first calculated, and those for the remaining electrode combinations could be derived by appropriately re-indexing the previously calculated sensitivity coefficient arrays.

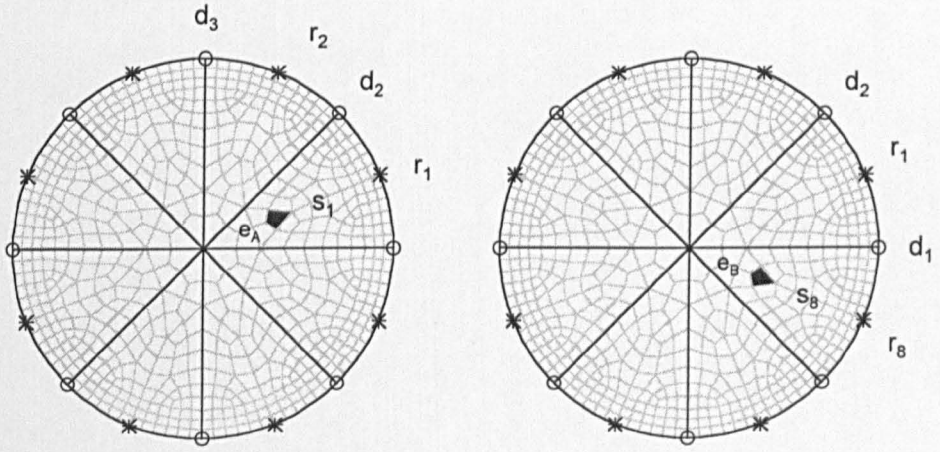

Figure 4.7a

Figure 4.7b

Figure 4.7 8-fold cyclic symmetry in the sensitivity coefficients

The base impedance (Z) for all the electrode placements, was calculated from the nodal voltages coinciding with the receive electrodes. The breathing related impedance changes were simulated by specifying a 10% change in the conductivity of elements belonging to the two lung regions as,

$$\Delta\sigma_{lungs} = 0.1 \qquad 4.24$$

$$\Delta\sigma_{other} = 0 \qquad 4.25$$

The value of ΔZ, was calculated using equation 4.21.

An alternative method of calculating ΔZ would have been to use the non-linear sensitivity relationship as expressed in equation 4.19 and repeated here for clarity.

$$\Delta Z = -\int_{\Omega} \Delta\sigma \cdot \frac{\nabla\phi'}{\mathbf{I}_{\phi}} \cdot \frac{\nabla\psi}{\mathbf{I}_{\psi}} dv \qquad 4.26$$

In this case, it was possible to determine the changed potential distribution ϕ', by assigning a changed value of the conductivity ($\sigma+\Delta\sigma$) to the elements belonging to the two lung regions in the model and then solving the FEM equations. The potential distribution ϕ' could then be used in equations 4.22 and 4.23 to determine the sensitivity coefficients. This method was more accurate, but required more computation. It was observed that the maximum error between the values of ΔZ, obtained by this method and the linearised sensitivity method was only 0.3%, when a 10% change in conductivity of the two lung regions was assumed. Therefore, it was decided that the linearised sensitivity method would be adopted for the following investigations.

4.5. Development of a 3d FEM model

A three dimensional FEM model was developed by following the steps similar to those described earlier in section 4.4 for a two dimensional model. A cylindrical volume, having the dimensions shown in Figure 4.2, was first defined. This volume was divided into 8 sectors, each of which was further divided into 8 regions. These regions could be appropriately combined to model the two lung regions as shown in Figure 4.2. The meshing of each sector was carried out, one by one in an anti-clockwise direction, to achieve the required cyclic symmetry with respect to electrode placement. The complete mesh was made up of 37,632 'brick' elements, each having 8 nodes. The vertical distance between the adjacent horizontal electrode planes was chosen to be equal to 0.5 times the radius of the cylindrical model. This distance was equal to 0.08 times the circumference of the model, which was the same as that used in the associated experimental studies on human subjects described in the previous chapter.

The potential distribution for one drive pair and one receive pair in each horizontal plane was first obtained by solving the FEM equations. These potential distributions were then used to derive the potential distributions for the remaining drive and the receive electrode pairs by making use of the cyclic symmetry in the mesh. Finally, a sensitivity matrix was developed, and values of $\Delta Z/Z$ for the 1024 electrode placements were obtained. The steps involved in computing the sensitivity matrix and $\Delta Z/Z$ were similar to those used for the two dimensional model as described in section 4.4. The centre-to-centre distance between the drive and receive electrode pairs was calculated geometrically from the electrode co-ordinates used in the model.

4.6. Validation of the 3d FEM model

The validation of the 3d FEM model was carried out in two ways. Firstly, the 1024 boundary measurements (Z) obtained using this FEM model were correlated with those measured on a tank having the same geometry.

The 1024 boundary measurements (Z) were measured using Sheffield Mark 3b EITS system on a cylindrical tank filled with a saline solution. The tank was 235 mm in diameter and the saline was filled up to a height of 420 mm from the bottom of the tank. Thus, the height to radius ratio of the conducting volume of the tank was 3.5, which was equal to that used in the FEM model as shown in Figure 4.2. The separation between any two horizontal electrode planes was 60 mm. i.e. 0.51 times the radius of the tank, and the lower most plane (plane 1)

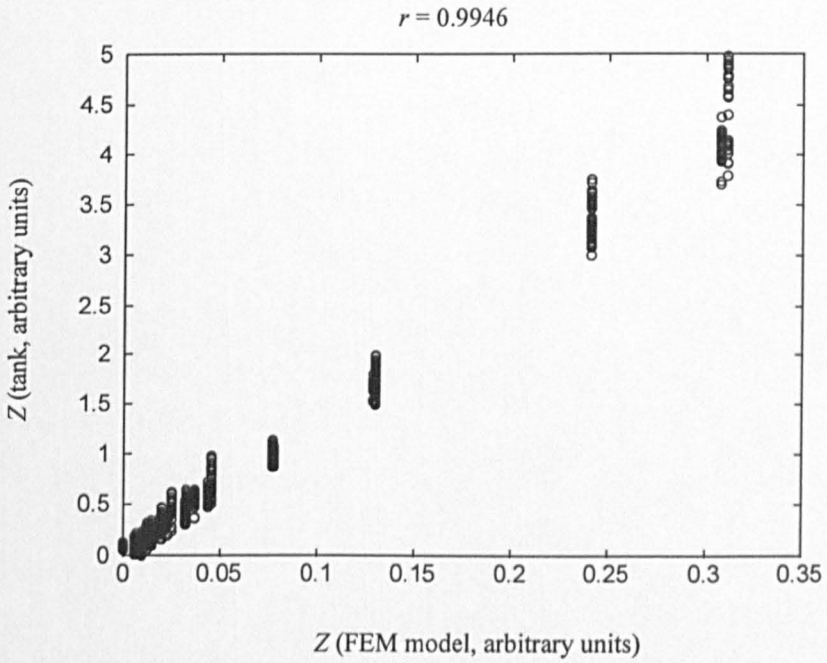

Figure 4.8 *A plot of boundary measurements measured on a tank versus those obtained from an identical volume conductor FEM model.*

was located at a height of 120 mm from the bottom of the tank. These locations also matched with those used in the FEM model. Therefore, the boundary measurements obtained from the FEM model were expected to correlate with those measured on the tank. Figure 4.8 shows a plot of Z (tank) versus Z (FEM model) and indicates that the two sets of boundary measurements correlate well (r = 0.9926). The small scatter of points is due to instrumentation noise in the tank data.

Secondly, the fractional change in impedance ($\Delta Z/Z$) in the 1024 measurements, due to a 10% change in conductivity of the two lung regions, was correlated with that obtained from a model developed by Metherall (1998). The later model was developed using an analytical '1/r method'. The internal geometry of the two lung regions in this '1/r model' was exactly the same as the internal geometry of the FEM model, and the 1/r model had been used successfully to reconstruct *in-vivo* images of the human thorax by Metherall (1998). Therefore, it was considered reasonable to use this 1/r model to validate the FEM model.

Figure 4.9 shows a plot of $\Delta Z/Z$ (FEM model) versus $\Delta Z/Z$ (1/r model). It can be seen that these two measurements also correlate well (r = 0.9236). It may be noted that there is some scatter of points in this plot. This scatter is due to the fact that the 1/r method assumes that the cylindrical volume conductor is a semi-infinite medium. On the other hand, the FEM method is a numerical method of obtaining the solution to the Laplace's equation, which takes into consideration the boundaries of the volume conductor. It has been shown by Metherall (1998) that there is a disparity between measurements obtained using the 1/r method and those obtained using the analytical solution to the Laplace's equation,

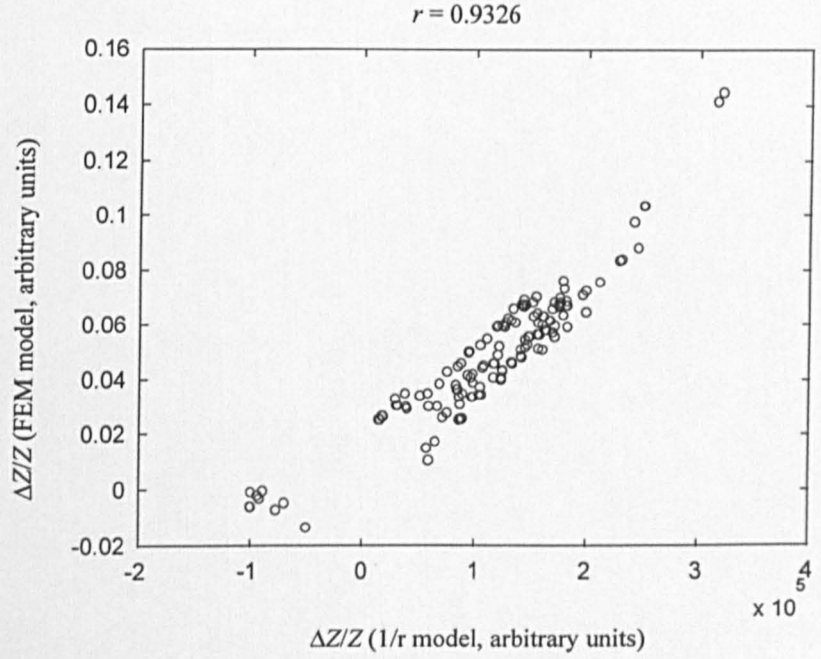

Figure 4.9 *Validation of the FEM model by plotting $\Delta Z/Z$ (FEM model) versus $\Delta Z/Z$ (1/r model). The 1/r model was developed by Metherall (1998).*

especially when the vertical distance between the drive and the receive electrode planes increases.

4.7. Results and discussion for theoretical data

The results of the associated experimental studies described in the previous chapter indicated that $\Delta Z/Z$ increased with increase in distance between the drive and the receive electrode pairs. Therefore, a first step in the analysis was to find out whether the same relationship was present in the theoretical data. A plot of $\Delta Z/Z$ versus centre-to-centre distance is shown in Figure 4.10. It was only necessary to plot 512 points instead of 1024 points because the first 512 measurements were equal to the last 512 measurements. This was due to the fact that the two lung regions were symmetrically located within the cylindrical volume and therefore, there was a 2-fold symmetry in the model.

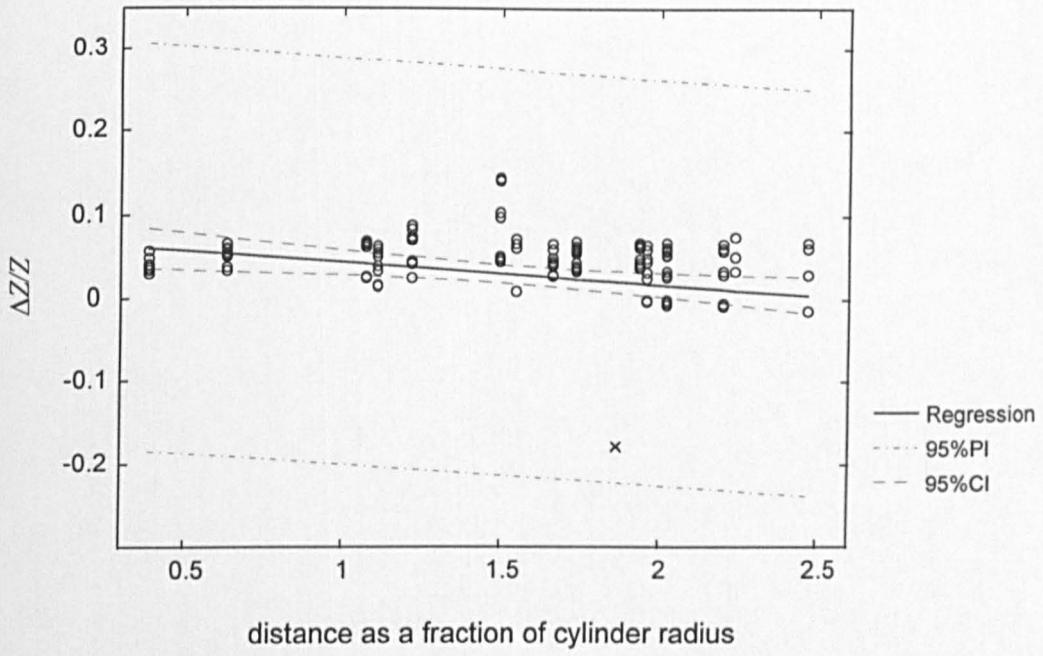

Figure 4.10 *A plot of $\Delta Z/Z$ versus distance for the data obtained from the volume conductor model by assuming a distance between the adjacent horizontal planes equal to 0.5 times the radius.*

It can be seen in Figure 4.10 that the slope of the regression line of $\Delta Z/Z$ upon distance is negative. This result was different from the result obtained for the

experimental data (Figure 3.8). It was thought that this difference between these two results was due to the following reasons.

Firstly, it was thought that the strategy adopted for choosing the distance between the adjacent horizontal electrode planes should have been based on the fact that the cross-section of thoracic cavity is better modelled by an ellipse having a major axis to minor axis ratio of 1.7 (Kiber, 1991). In the experimental studies, the distance between the two horizontal planes was equal to 0.08 times the circumference of the thoracic cavity. If we assume that the elliptical cross-section has a semi-minor axis equal to 1, then 0.08 times the perimeter length of this ellipse was found to be equal to 0.7. Therefore, the distance between the two horizontal planes was changed from 0.5 times the radius of the cylindrical model to 0.7 times the radius of the cylindrical model and analysis was repeated on the model.

A plot of $\Delta Z/Z$ versus distance for this data is shown in Figure 4.11. This plot shows that the slope of the regression line of $\Delta Z/Z$ upon distance has changed from that observed in Figure 4.10. However, the actual value of the slope was very low and equal to 5×10^{-4}, which indicated that $\Delta Z/Z$ did not depend on

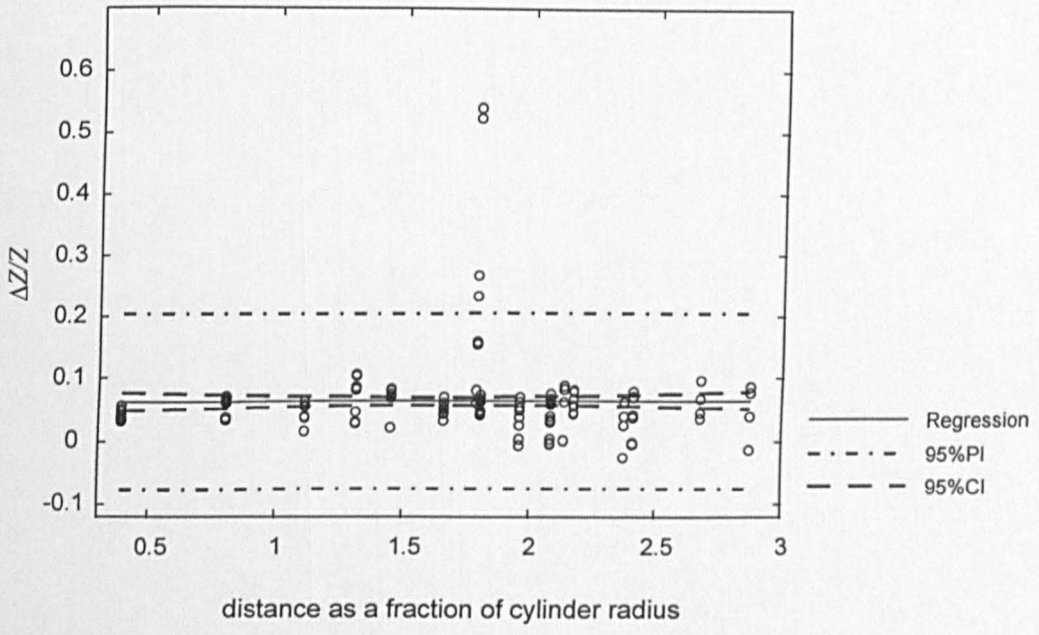

Figure 4.11 *A plot of $\Delta Z/Z$ versus distance for the data obtained from the volume conductor model by assuming a distance between the adjacent horizontal planes equal to 0.7 times the radius.*

distance. Thus, there was still a disagreement between the experimental and the theoretical results . However, it could be at least noted that the vertical distance between the electrode planes was one of the factors affecting the relationship between $\Delta Z/Z$ and distance between the drive and receive electrode pairs.

Secondly, it was noticed that the shape and the size of the two lung regions in the FEM model were assumed to be the same. A cross-sectional view of the model used in the study is shown in Figure 4.12 and shows the two lung regions having the same size.

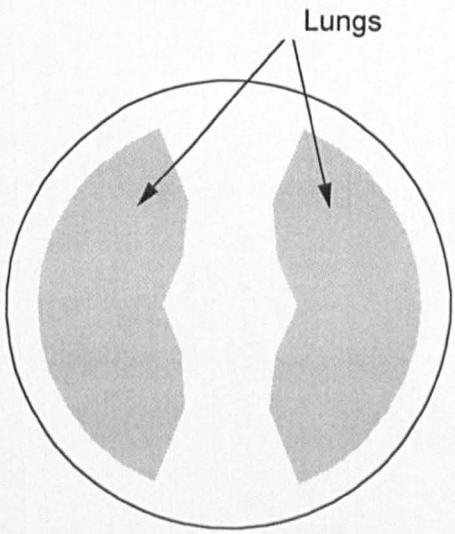

Figure 4.12 A cross-sectional view of the FEM model

In reality, the left lung is smaller than the right lung. This can be seen from a cross-sectional view of the thoracic cavity at the level of the 8th thoracic vertebra, shown in Figure 4.13. This level coincides with a horizontal plane, midway between electrode planes 2 and 3 shown in Figure 3.7. It was also noticed that the gap between the two lung regions for the FEM model (Figure 4.12) was almost equal to the width of the two lung regions. Furthermore, it was the same in the anterior as well as in the posterior. However, it can be seen from Figure 4.13 that this gap is much less compared to the width of the lungs, i.e. approximately only 30% of the width of the lungs. Moreover, it is not uniform from the anterior to the posterior, but is less in the posterior.

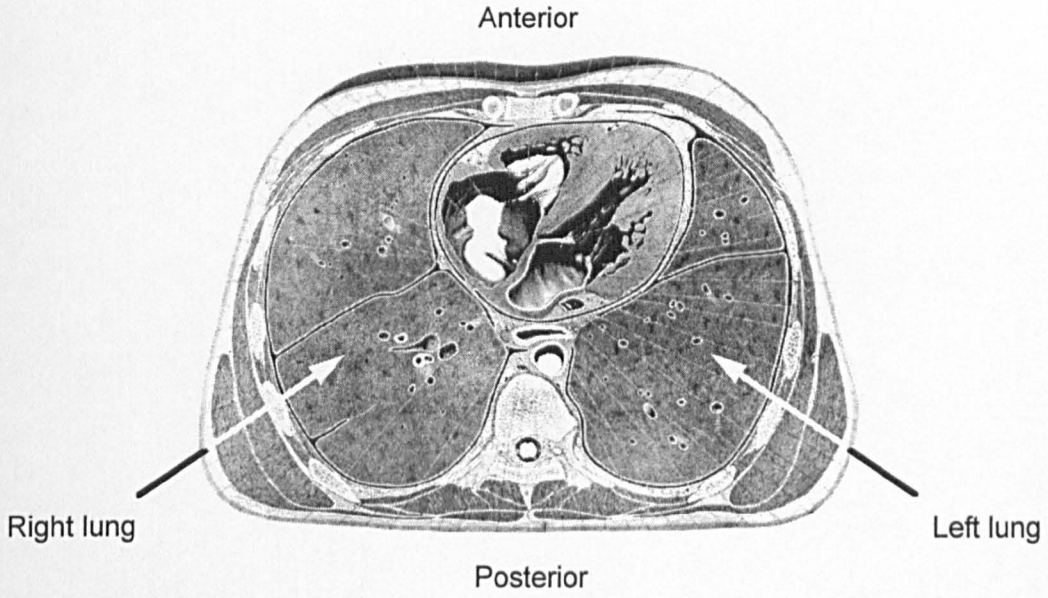

Figure 4.13 *A cross sectional view of the thoracic cavity at the level of the 8th thoracic vertebra*

Thus, taking into consideration these points, a modification was made in the internal geometry of the two lung regions of the FEM model so that it would approximately match with the internal anatomy of the thoracic cavity. Figure 4.14 shows a cross-sectional view of the FEM model after this modification. It can be seen that the right lung is larger in size than the left lung and the gap between the two lungs has also been reduced in the posterior. It may be important to note that in reality the cross-section of the lungs changes in the vertical direction as well. However, the geometry of the existing mesh of the FEM model was constant in the vertical direction, and due to this constraint, the cross-section of the two lung regions had to be assumed constant in the vertical direction. It may also be noted that the boundaries of the two lung regions are not smooth because they had to follow the boundaries of the elements of the existing mesh. Thus, the modifications were based only on some qualitative features of the thoracic anatomy because the purpose of these modifications was only to test whether the unrealistic size and shape of the two lung regions was responsible for the disagreement between the experimental and the theoretical results.

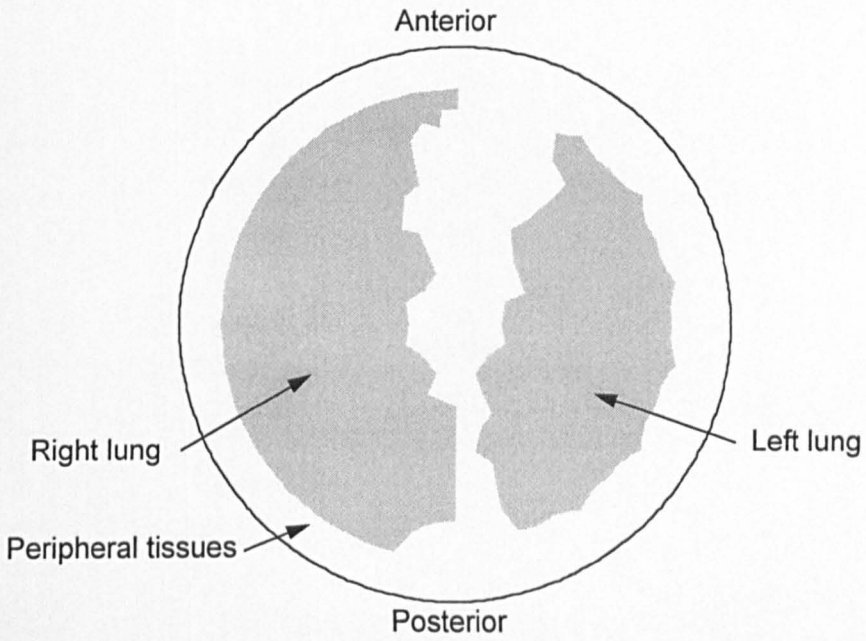

Figure 4.14 *The cross-sectional view of the FEM model having the modified internal geometry to match the internal anatomy of the thoracic cavity shown in Figure 4.13*

The analysis of this modified model was carried out to calculate the values of $\Delta Z/Z$. Figure 4.15 shows a plot of $\Delta Z/Z$ versus distance between the drive and the receive pairs for the modified model. It can be seen that after the modification, the slope of the regression line of $\Delta Z/Z$ upon distance has changed to a positive value (0.0096) and is significant ($p < 0.001$). Thus, this result seemed to agree with the experimental results and suggested that the choice of an inappropriate internal geometry of the earlier FEM model could have been one of the causes of the disagreement between the experimental and the theoretical results.

The purpose of this theoretical study was also to identify an optimum electrode placement for impedance pneumography, which should be characterised by maximum sensitivity to lung resistivity changes. In order to compare the theoretical data with the experimental data a correlation coefficient was obtained between the values of Z from the two data sets. A plot of the boundary measurements from the two data sets is shown in Figure 4.16. The correlation coefficient r was equal to 0.764 and statistically significant ($p < 0.001$) . However,

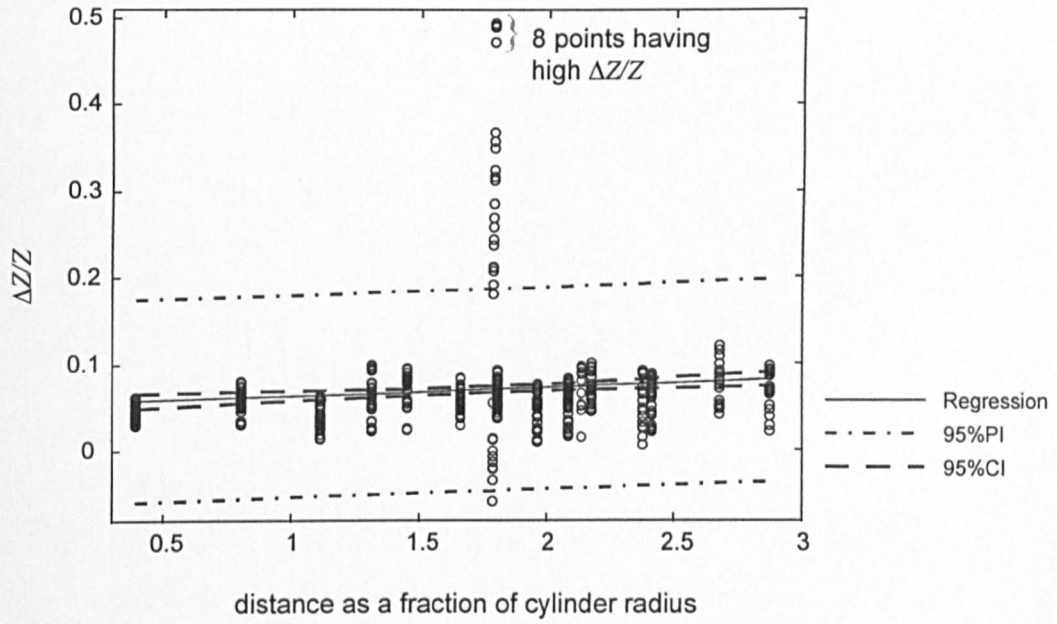

Figure 4.15 A plot of ΔZ/Z for the modified model shown in Figure 4.14. The 8 points having high ΔZ/Z are indicated on the plot.

it can be seen that there is a scatter of points in this plot. This was thought to be due to the following reasons.

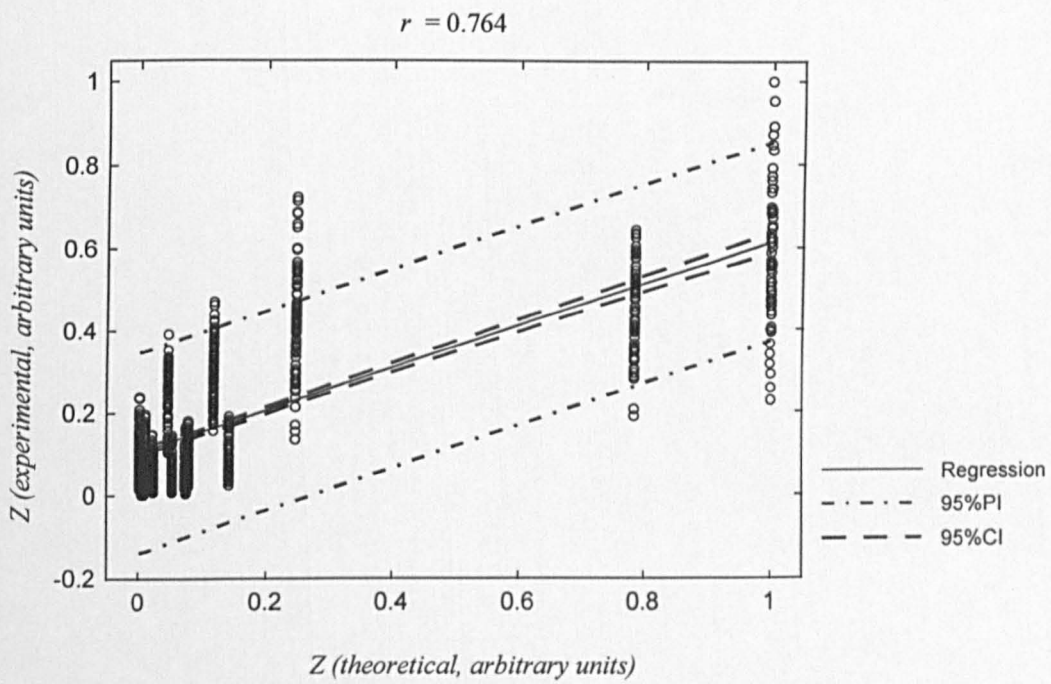

Figure 4.16 A plot of Z (experimental) versus and Z (theoretical)

Firstly, the theoretical boundary data was obtained from a model having a cylindrical shape whereas the shape of the thoracic cavity is more elliptical. Secondly, the model was assumed to have a homogeneous internal conductivity distribution while the thoracic cavity has a non-homogeneous internal conductivity distribution. Thirdly, the experimental data was expected to be affected by the instrumentation noise. The first two reasons were due to the simplifications assumed in the FEM model. Therefore, these two factors were the inherent limitations of the model. However, it seemed possible to reduce the effect of the instrumentation noise by examining the data and discarding the measurements affected by the noise.

In order to examine the effect of noise on the experimental data and to identify the measurements affected by the noise, a profile of measurements obtained by injecting current between electrodes d_1 and d_2 from all the 8 receive electrode pairs in the same horizontal plane as well as in the other three horizontal planes was plotted. The anatomical locations of the electrode planes was shown in Figure 3.7 and is shown again in Figure 4.17a. The interleaved placement of the drive and the receive electrodes is shown in Figure 4.17b along with the receive electrodes corresponding to each receive electrode pair number. The profiles of the boundary measurements are plotted in Figure 4.18. These measurements were normalised with their maximum value to aid viewing. It can be seen that when the receive electrodes were placed in the same horizontal plane as the drive electrode pair, the profile of the experimental data was comparable to that of the theoretical data. This profile also matched reasonably well when the receive electrodes were located in the horizontal plane nearest to that of the drive pair. However, as the vertical separation between the two horizontal planes further increased, the agreement between the two profiles decreased. This indicated that in spite of the differences between the model and the thoracic cavity regarding the shape and the internal conductivity distribution, the two profiles agreed reasonably well when the receive electrodes were located in the same plane as the drive pair or in the plane nearest to the plane containing the

drive pair. This also indicated that when the receive electrodes were placed in distant horizontal planes, the instrumentation noise dominated the measurements.

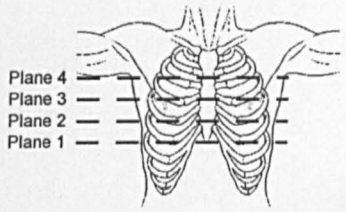

Figure 4.17a

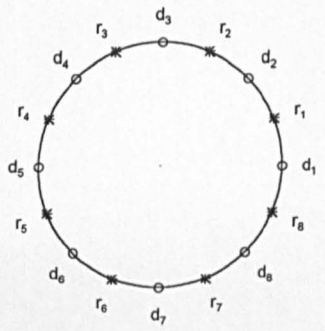

Receive electrode pair no.	Receive electrodes
1	r_1, r_2
2	r_2, r_3
3	r_3, r_4
4	r_4, r_5
5	r_5, r_6
6	r_6, r_7
7	r_7, r_8
8	r_8, r_1

Figure 4.17b

Figure 4.17 Anatomical locations of the four horizontal electrode planes and locations of the drive and receive electrodes in each plane. Electrode d_1 was placed centrally and anteriorly and the electrodes were numbered to the left.

Taking into consideration these observations, it was decided that the measurements associated only with the adjacent horizontal planes would be considered for further comparison between the two data sets. This comparison was made on the basis of the values of $\Delta Z/Z$. First, it was necessary to select the two adjacent horizontal planes. It was thought that the measurements obtained from the lower most plane (plane 1 in Figure 4.17), which was located at the level of the xiphoid process, would have a greater influence of the diaphragm movement than the changes in lung resistivity. It was also considered that the measurements obtained from the top most plane (plane 4 in Figure 4.17), located at the level of the axilla, would have less contribution from the changes in lung resistivity as the cross-section of the lungs decreases beyond the level of the axilla (Carter et al, 1977). Therefore, only the data corresponding to the two middle planes, plane 2 and plane 3, was used to compare the experimental and the theoretical data. In addition, it was observed from the tomographic images of the thoracic cavity that the cross-section of the lungs remained approximately constant between the two planes under consideration. Thus, this matched with the assumed constant cross-section of the two lung regions in the model.

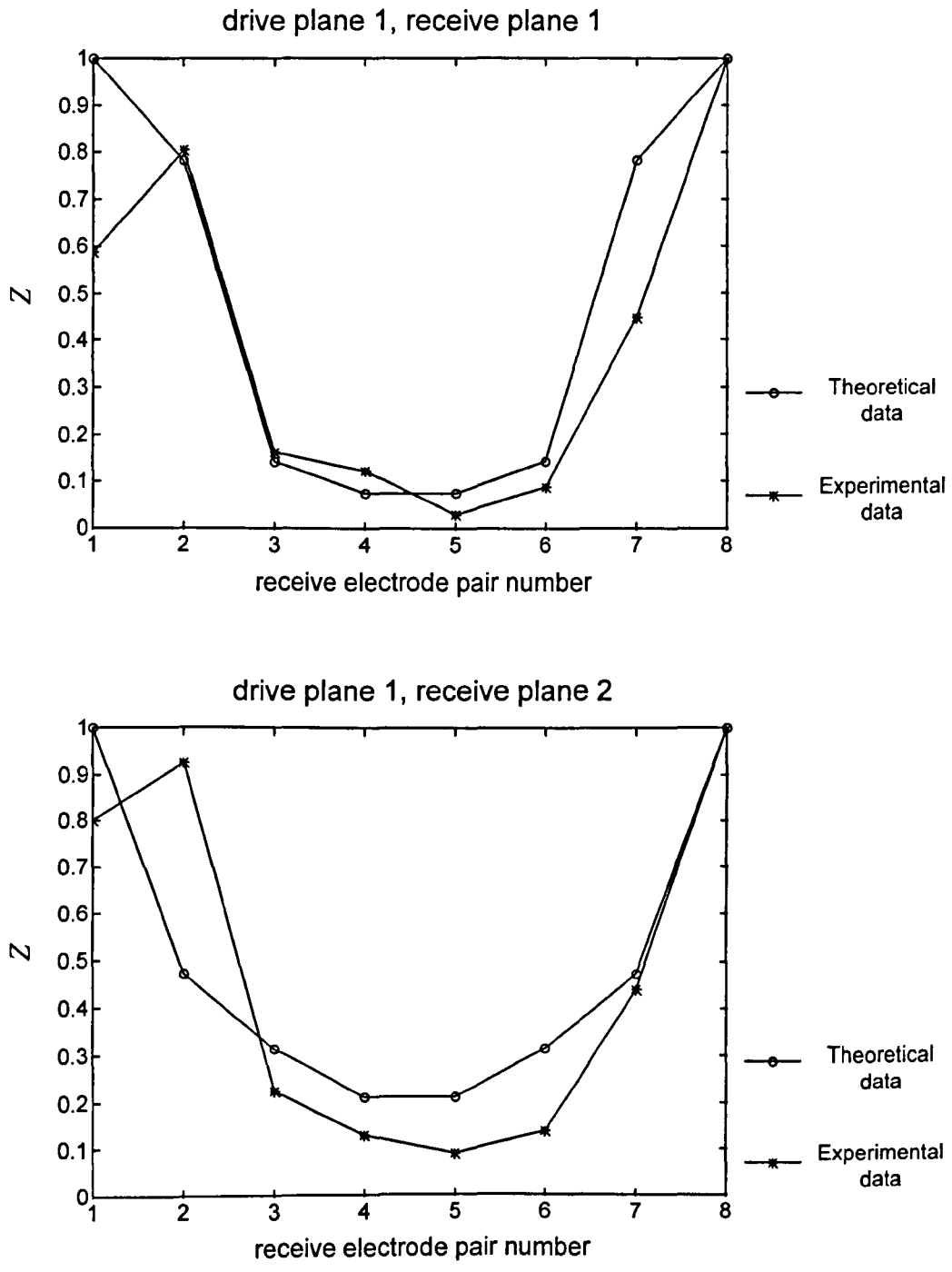

Figure 4.18a A plot of profile of Z for the experimental and the theoretical data for 1 drive pair and 8 receive pairs. The planes of the drive and the receive electrodes are marked on the plots and their anatomical locations are shown in Figure 4.17a. The locations of the receive electrode pairs with appropriate numbers are also shown in Figure 4.17b. Z is normalised with maximum value to aid comparison.

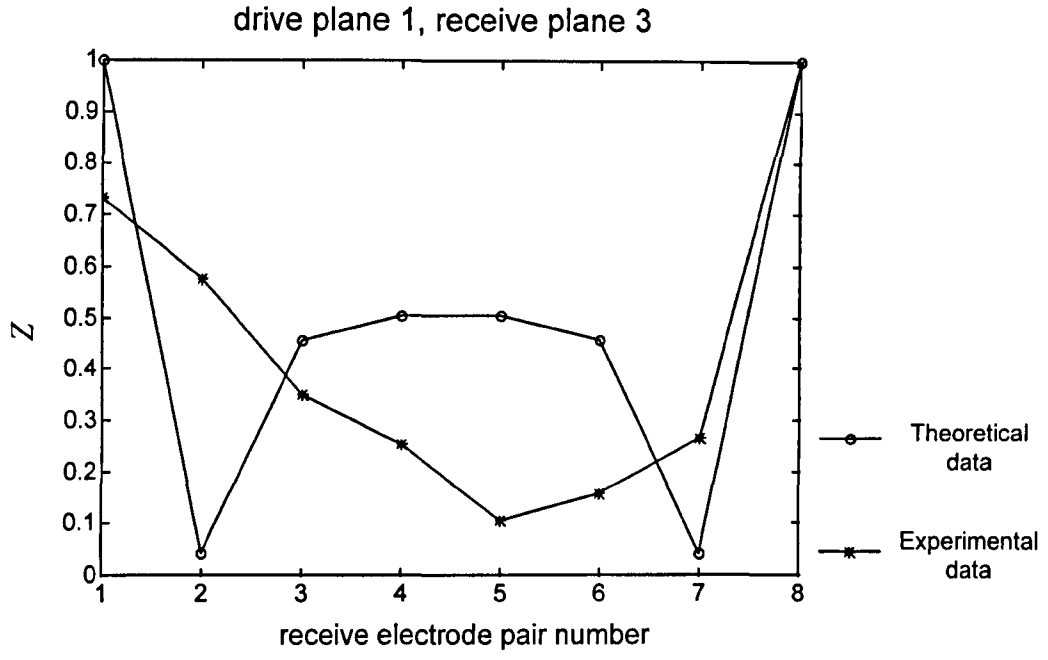

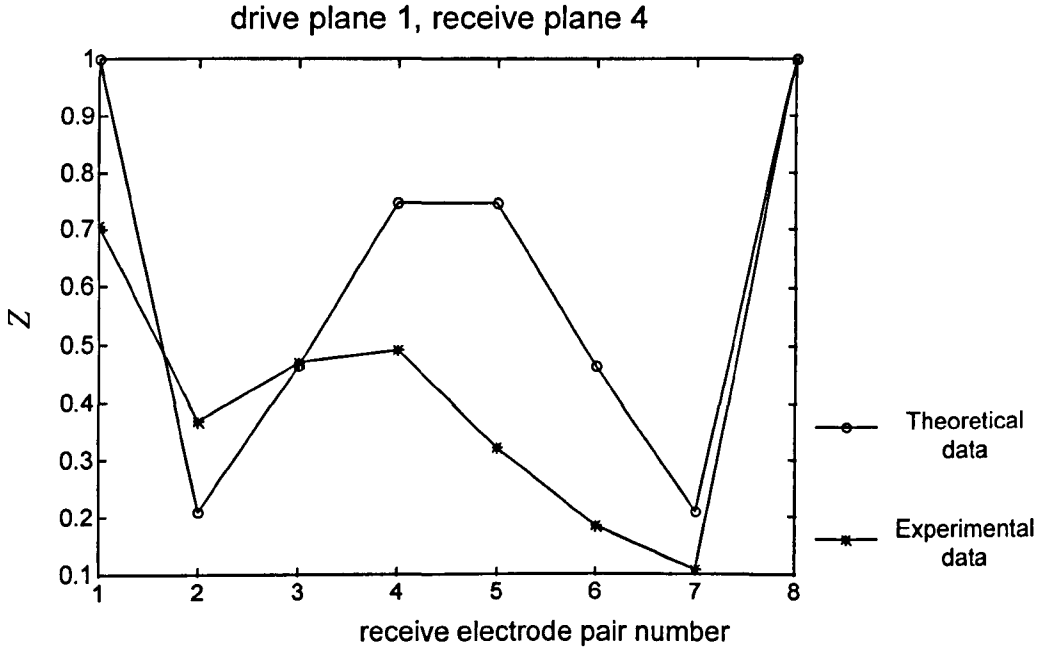

Figure 4.18b A plot of profile of Z for the experimental and the theoretical data for 1 drive pair and 8 receive pairs. The planes of the drive and the receive electrodes are marked on the plots and their anatomical locations are shown in Figure 4.17a. The locations of the receive electrode pairs with appropriate numbers are also shown in Figure 4.17b. Z is normalised with maximum value to aid comparison.

Figure 4.19 shows a plot of $\Delta Z/Z$ (experimental) versus $\Delta Z/Z$ (theoretical) for the measurements obtained in plane 2 and plane 3. The correlation coefficient between the two data sets was 0.534 and significant ($p < 0.001$). The correlation coefficient for the data obtained from plane 2 alone was 0.747 ($p < 0.001$) while that for data obtained from plane 3 alone was 0.529 ($p < 0.001$). This suggested that the two data sets were comparable within the limitations imposed by the disparity between the shape and the internal conductivity distribution, and by the instrumentation noise. Thus, some general conclusions regarding an optimum electrode placement could be drawn by examining the theoretical data.

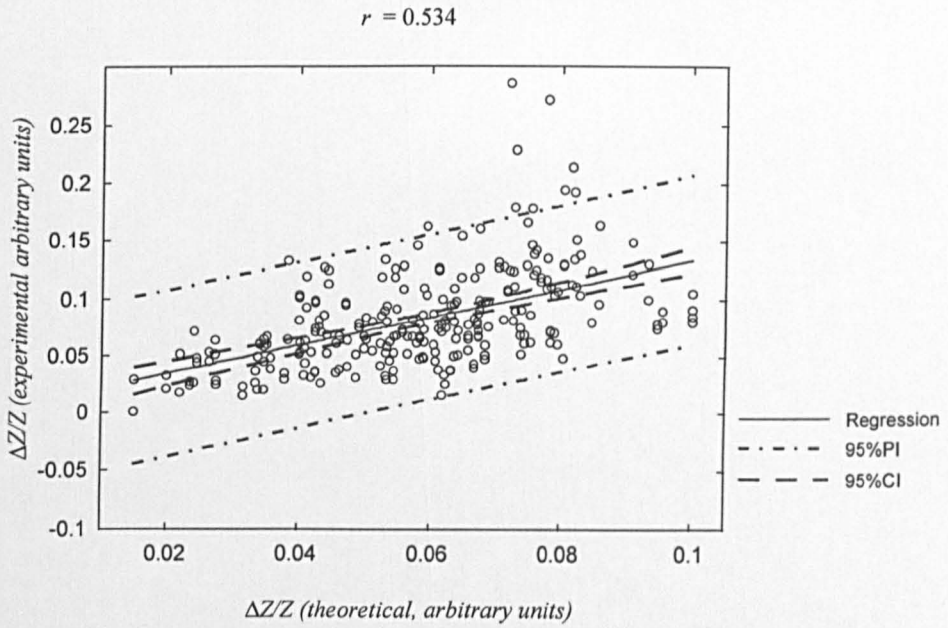

Figure 4.19 A plot of $\Delta Z/Z$ (experimental; measured on human subjects) versus $\Delta Z/Z$ (theoretical) for the measurements obtained from plane 2 and plane 3.

The theoretical data was examined to find one or a few electrode placements having a high value of $\Delta Z/Z$ which was indicative of high specificity to lung resistivity changes. It was observed that there were 8 electrode placements having much higher values of $\Delta Z/Z$. The 8 points corresponding to the measurements obtained from these 8 electrode placements are indicated in the plot of Figure 4.15. One such electrode placement is shown in Figure 4.20 and a top view of one more electrode placement is shown in Figure 4.21. The

remaining electrode placements were identical to these two electrode placements.

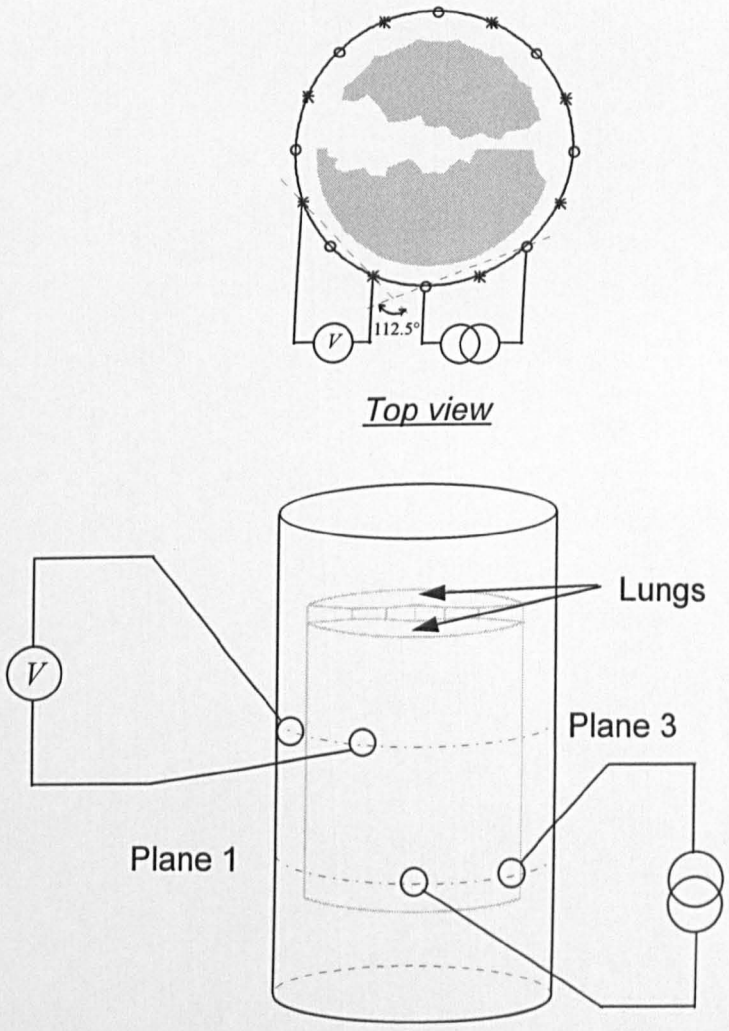

Figure 4.20 One of the 8 electrode placements having a very high value of $\Delta Z/Z$ for the theoretical data.

The following were the common features of all the 8 electrode placements.

- The drive and the receive electrode pairs were in two different and alternate horizontal electrode planes, i.e. either in plane 1 and plane 3 or in plane 2 and plane 4.
- The angle between these electrode pairs was 112.5°.

- Both, the drive and the receive electrode pairs were located on the right side of the thoracic cavity and hence, were close to the right lung.
- The distance between the drive and receive electrode pairs was the same.

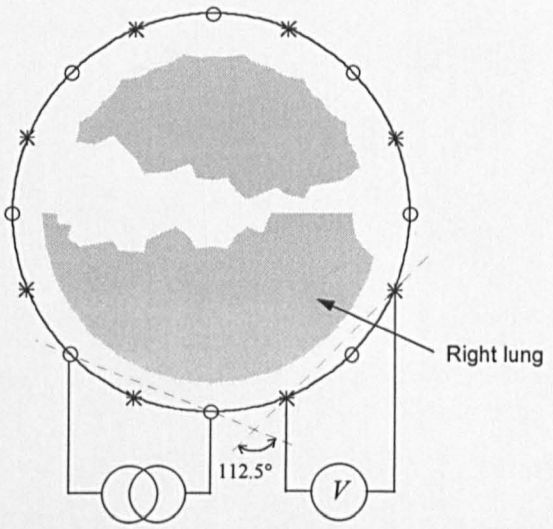

Figure 4.21 *Top view of one more electrode placements having a very high value of $\Delta Z/Z$ for the theoretical data. The drive and the receive electrode pairs were in two different and alternate horizontal planes as shown in Figure 4.20.*

It is important to note that while comparing the profiles of the boundary measurements, to examine the noise levels (Figure 4.18), it was stated that these profiles agreed reasonably well only for the adjacent electrode planes. However, the electrode placements having high theoretical $\Delta Z/Z$ had the drive and the receive electrode pairs in alternate planes. Thus, it may appear that they may have a poor SNR. However, it should be noted that the receive electrode pair shown in Figure 4.20 and Figure 4.21 is adjacent to the drive pair and hence, nearest compared to the other receive pairs in that plane. Therefore, it would be reasonable to expect sufficiently higher SNR for these electrode placements and hence, they would be suitable for use in human subjects.

The 8 electrode placements were also found to have a high value of $\Delta Z/Z$ for the experimental data. A plot of $\Delta Z/Z$ versus distance for the experimental data, shown in Figure 3.8 of the previous chapter, is shown again in Figure 4.22. All

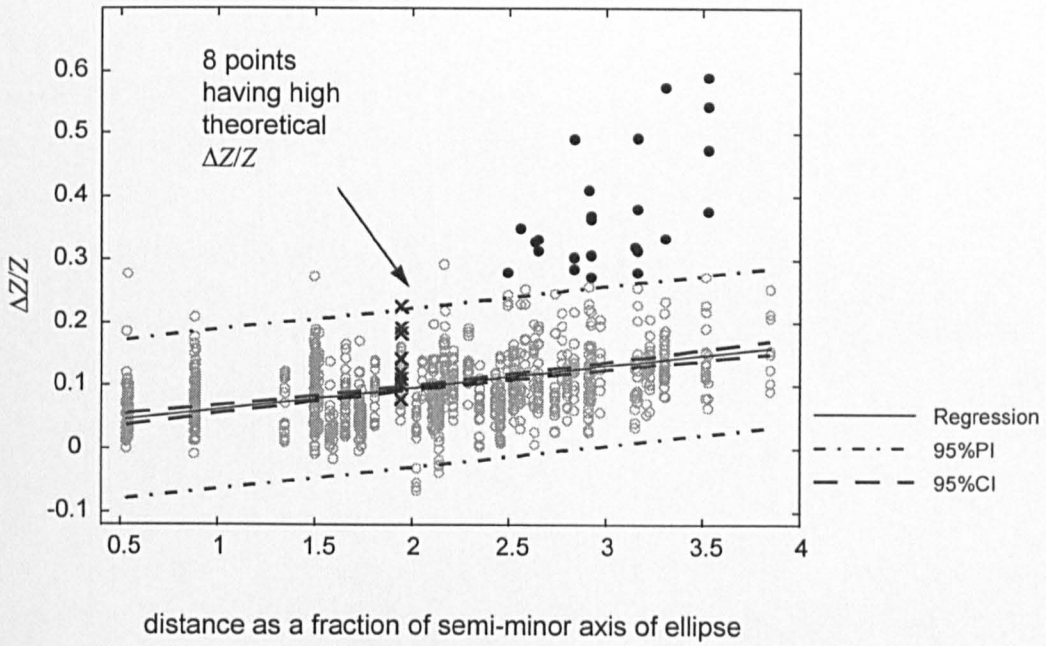

Figure 4.22 *A plot of $\Delta Z/Z$ versus distance for the experimental data showing points corresponding to high theoretical $\Delta Z/Z$. These points are marked by '×' on the plot*

the points have been plotted using 'grey circles' for clarity, along with the points corresponding to the measurements obtained from the 8 electrode placements under consideration marked by a 'cross'. Although these measurements were not the highest, their mean $\Delta Z/Z$ (0.145) was significantly higher ($p < 0.02$) than the mean $\Delta Z/Z$ (0.096) given by the regression line for the same distance value. There were points (filled circles) having much higher values of $\Delta Z/Z$ than these 8 electrode placements. However, these points also had a larger distance between the drive and the receive electrode pairs compared to the 8 electrode placements. It has been shown in the previous chapter that SNR reduces with distance (Figure 3.10). Therefore, the electrode placements having very high values of $\Delta Z/Z$ as well as the distance would be expected to have a poor SNR and hence, may not be optimum.

Thus, from the theoretical results, it was possible to identify some electrode placements that could be considered as optimum for impedance pneumography. However, it can be seen from Figure 4.20 and Figure 4.21 that the drive and the receive electrode pairs for all the 8 electrode placements were on the right side of the thoracic cavity and therefore, were close to only the right lung. Thus, the

measurements obtained from these electrode placements would be more influenced by the conductivity changes of the right lung than the left lung. To include the contribution from both the lungs, it was proposed that a second set of drive and receive electrode pairs be used with electrodes on the left of the thoracic cavity as shown in Figure 4.23.

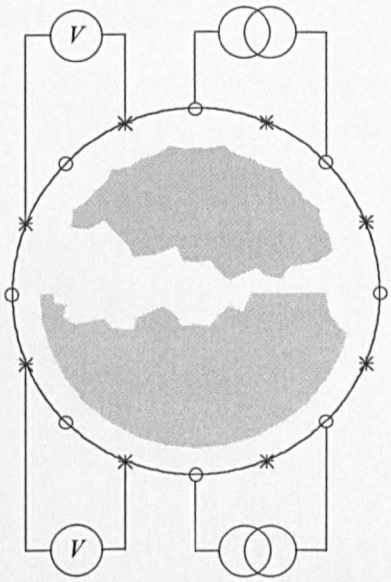

Figure 4.23 *An electrode arrangement involving two sets of drive-receive electrode pairs to maximise the contribution from both the lungs*

The next step in the theoretical study was to investigate the relationship between the electrode spacing and the impedance measurements and to understand in what way the electrode spacing affected the impedance measurements. The following is the description of this study.

4.8. Effect of electrode spacing on impedance measurements: theoretical studies

The experimental studies aimed at investigating the effect of electrode spacing on impedance measurements of the thoracic cavity were described in the previous chapter. These studies were carried out by placing an array of electrodes around the thoracic cavity of human subjects in one horizontal plane. The results of these experimental studies indicated that if a mean of all the independent measurements obtained from the electrode array was used to calculate $\Delta Z/Z$, then $\Delta Z/Z$ increased with electrode spacing. It was also observed that the absolute change in impedance during breathing (ΔZ) and hence, the SNR increased with electrode spacing. Therefore, to maximise $\Delta Z/Z$ as well as SNR, it seemed advisable to use a larger electrode spacing and to take a mean of all the independent measurements obtained from an equally spaced electrode array using the adjacent drive - adjacent receive data collection protocol

The aim of this theoretical study was to understand the underlying phenomenon behind these experimental results. The following is a description of this theoretical study.

4.8.1. Volume conductor model and electrode placements

The volume conductor model of the thoracic cavity used in this study was the same three dimensional FEM model used in the earlier study and explained in section 4.5. This model was cylindrical in shape and was assumed to have a uniform conductivity distribution. An array of 16 equally spaced electrodes was placed on the surface in one horizontal plane. This horizontal plane was located at half the height of the model as shown in Figure 4.24.

The 16-electrode array produced 104 ($N(N-3)/2;\ N=16$) independent measurements when an adjacent drive - adjacent receive data collection protocol was used. Therefore, it was necessary to generate a sensitivity matrix relating these 104 measurements to the changes in conductivity distribution of the model.

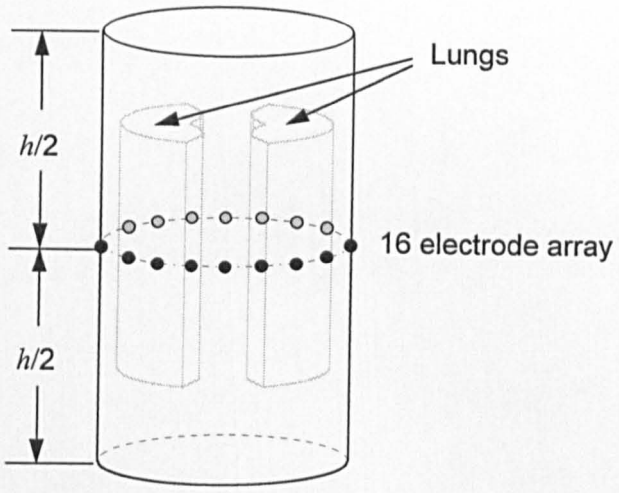

Figure 4.24 A volume conductor model with a 16 electrode array in one horizontal plane

The sensitivity matrix was generated on the lines explained in detail, in section 4.4. It was possible to make use of the cyclic symmetry in the mesh to reduce the amount of computation required for obtaining the voltage distributions as well as for calculating the sensitivity matrix.

4.8.2. Data analysis

In order to understand what factors were responsible for the experimentally observed increase in $\Delta Z/Z$ with electrode spacing, the analysis of the data was carried out in the following way.

The electrode spacing for the 16-electrode array was constant for all the electrode combinations and was equal to 1/16 times the circumference of the cylindrical model. However, for the purpose of this study, data corresponding to different values of electrode spacing was required. Therefore, the 16-electrode data was processed using superposition to generate data corresponding to electrode spacing in multiples of 1/16 times the circumference.

It was thought that, when the electrode spacing was small, the injected current remained confined to the regions in the vicinity of the drive electrodes. Thus, on this basis and on the basis of reciprocity it was expected that the measurements obtained with this electrode spacing would be more sensitive to the conductivity

changes of the regions nearer to the drive as well as the receive electrodes. On the other hand, when the spacing between the electrodes was increased, the injected current would penetrate the regions further away from the electrodes, within as well as out of the plane of the electrodes. Therefore, when the electrode spacing was increased, the measurements would be relatively more sensitive to the regions away from the electrodes.

In order to test this hypothesis, a 10% change in conductivity within a small, centrally located 'disk' shaped region, as shown in Figure 4.25a was assumed. This disk shaped region was also shifted to two off-plane locations as shown in Figure 4.25b and Figure 4.25c. The $\Delta Z/Z$ was calculated for a mean of all the independent measurements obtained using three different values of electrode spacing. In the same way, the values of $\Delta Z/Z$ were calculated assuming a 10% change in conductivity of a axially placed cylindrical region having three different heights as shown in Figure 4.26.

4.8.3. Results of the study

The mean $\Delta Z/Z$ for the three values of electrode spacing at three different vertical positions of the disk perturbation, are also plotted in Figure 4.25. The data was normalised with respect to the maximum value in each case. It can be seen from this plot that $\Delta Z/Z$ increases with electrode spacing for all the three positions of the disk perturbation. Thus, a 4-electrode configuration appears to be more sensitive to conductivity changes of the in-plane deeper regions as well as the off-plane regions.

Figure 4.26 shows the plots of mean $\Delta Z/Z$ for the three values of electrode spacing and for the three different heights of the cylindrical region. It can be seen from Figure 4.26a that the 4-electrode configuration is the least sensitive to conductivity changes of the cylindrical region of the shown height. However, for the other two heights of the cylindrical region, the 4 electrode configuration is the most sensitive. This indicates that for larger electrode spacing, the increase in $\Delta Z/Z$ is mainly due to increased contribution from the off-plane conductivity changes.

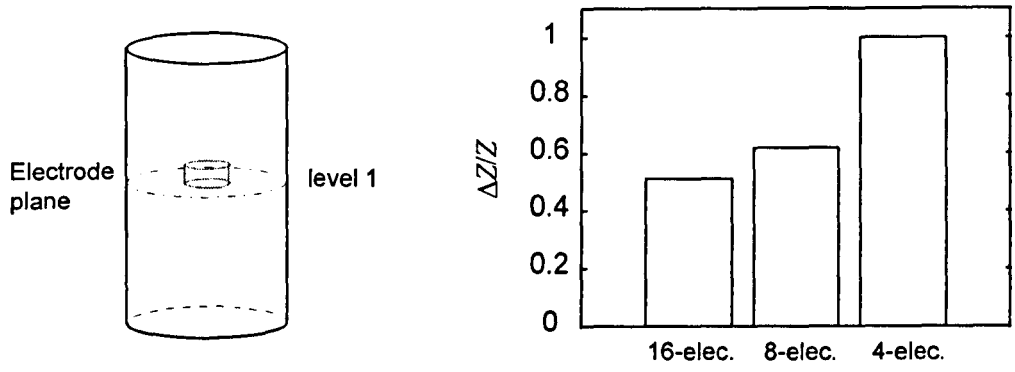

Figure 4.25a

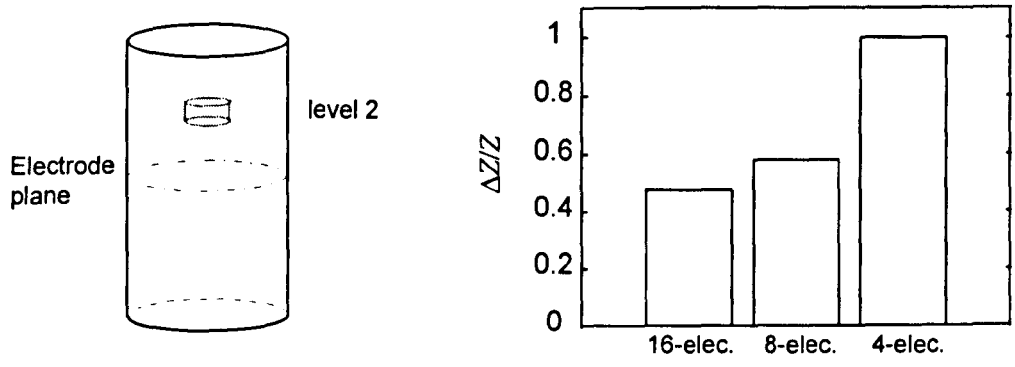

Figure 4.25b

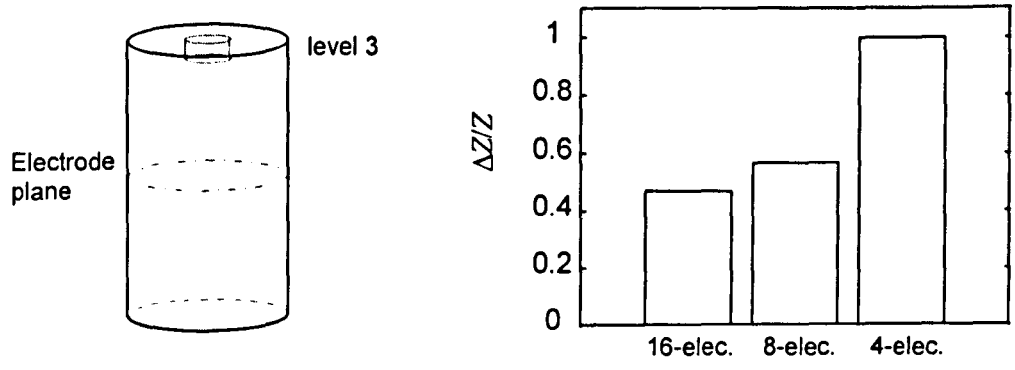

Figure 4.25c

Figure 4.25 *A plot ΔZ/Z for three different equally spaced electrode configurations for a 10% change in conductivity of an in-plane and off-plane, central 'disk' shaped region. The data is normalised by the maximum value in each case.*

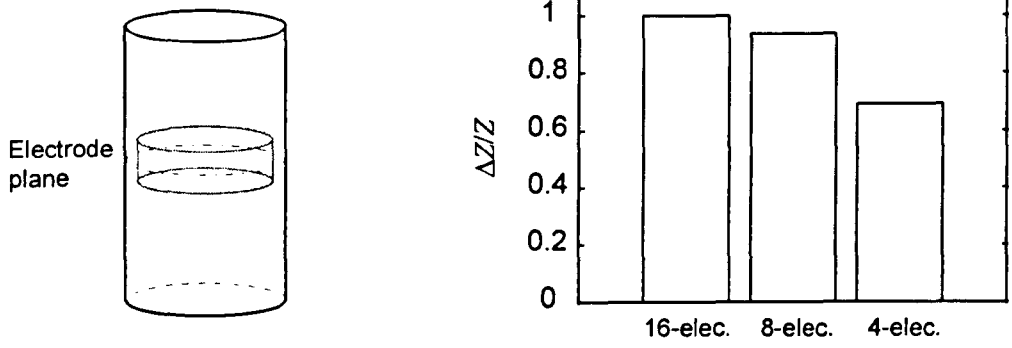

Figure 4.26a

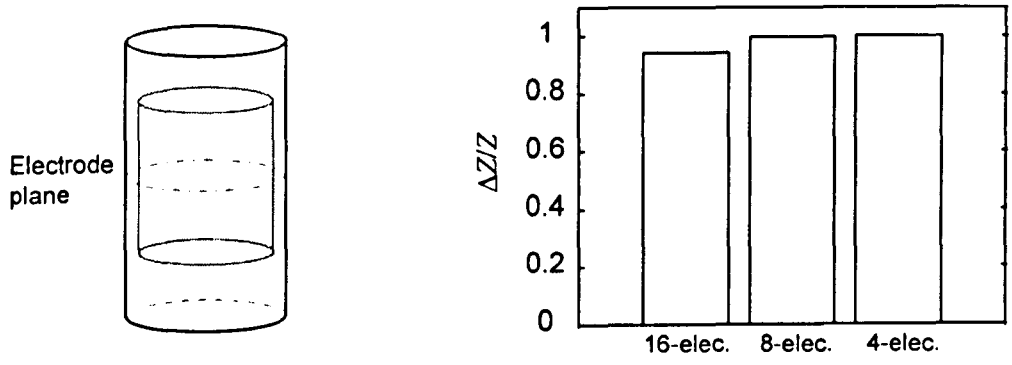

Figure 4.26b

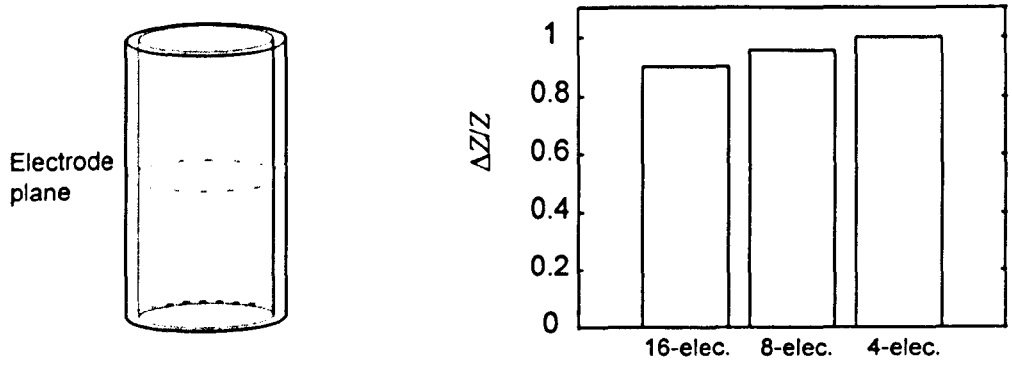

Figure 4.26c

Figure 4.26 A plot ΔZ/Z for three different equally spaced electrode configurations for a 10% change in conductivity of a axially placed cylindrical region of 3 different heights. The data is normalised by the maximum value in each case.

These results indicate that the experimentally observed increase in $\Delta Z/Z$ with electrode spacing could be due to increased contribution from the conductivity changes of the deeper lung regions as well as the regions of the lungs located out of the electrode plane.

Thus, if the above observations regarding the effect of electrode spacing on the impedance measurements are taken into consideration, then it would be possible to modify the 8-electrode configuration of Figure 4.23, which was expected to have a higher sensitivity to lung resistivity changes. Figure 4.27 shows the modified electrode placement. This electrode placement involves only 6 electrodes instead of 8 electrodes and is denoted as '6-electrode optimum configuration' in the rest of the thesis. The 3 drive electrodes (d_1, d_2 and d_3) are located in one horizontal plane and the 3 receive electrodes (r_1, r_2 and r_3) in the other horizontal plane. This 6-electrode configuration would produce 4 measurements as given in Table 4.1.

Table 4.1 The 4-measurements obtained from a 6-electrode optimum placement

Measurement	Drive electrodes	Receive electrodes
M_1	d_1, d_2	r_1, r_2
M_2	d_2, d_3	r_2, r_3
M_3	d_1, d_2	r_2, r_3
M_4	d_2, d_3	r_1, r_2

Measurements M_1 and M_2 would be sensitive to conductivity changes of the lung nearer to the electrodes, and measurements M_3 and M_4, would include contribution from the conductivity changes of both the lungs. Though it is expected that measurements M_1 and M_2 would have the maximum value of $\Delta Z/Z$ during breathing, measurements M_3 and M_4 have maximum distance between the drive and the receive electrode pairs. It has been observed in the

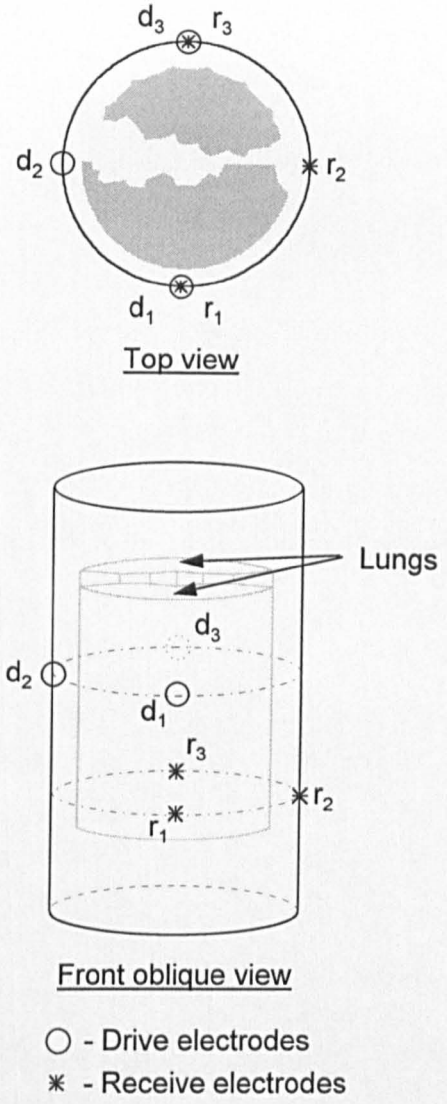

Figure 4.27 A 6-electrode optimum configuration for impedance pneumography proposed using theoretical results

experimental studies that $\Delta Z/Z$ increases with distance. Therefore, measurements M_3 and M_4 may also have higher values of $\Delta Z/Z$.

The 6-electrode 'optimum' configuration also has an advantage that it requires a fewer number of electrodes than the earlier 8-electrode configuration of Figure 4.23. In this project, it was decided as a strategy that it would be desirable to keep the number of electrodes to a minimum so that the technique would be convenient to use in a clinical environment. Therefore, any reduction in the number of electrodes was desirable.

4.9. Discussion

The relationship between electrode placements and impedance measurements was investigated theoretically as described in this chapter. The sensitivity method was used for establishing a relationship between the measured impedance and a change in conductivity within a volume conductor. The technique of FEM was used to implement this sensitivity method by developing a volume conductor model of the thoracic cavity. The model used for this study was a simplified model of the thoracic cavity in terms of its shape and conductivity distribution. The model was assumed to have a circular, rather than a more anatomically correct cross-section because it would reduce the amount of computation involved. A uniform conductivity distribution was assumed for simplicity. Two regions, having a shape similar to lungs, were defined within the cylindrical volume to represent the lungs. The 32 drive and 32 receive electrodes were placed in 4 different horizontal planes, similar to those used in the experimental studies on human subjects. A sensitivity matrix was generated, which related the 1024 boundary measurements to the changes in conductivity occurring within each element of the FEM model.

The results of the analysis of the first FEM model showed that $\Delta Z/Z$ decreased with increase in distance between the drive and the receive electrode pairs. This result was different from the experimental results, in which $\Delta Z/Z$ increased with increase in distance. The vertical distance between the adjacent horizontal electrode planes was changed to see whether it improved the agreement between the two results. The slope of the regression line of $\Delta Z/Z$ up on distance changed from negative to positive. However, this slope was close to zero and hence, did not indicate that $\Delta Z/Z$ increased with increase in distance. Therefore, the theoretical results still disagreed with the experimental results. Nonetheless, it was noticed that the vertical distance between the two horizontal electrode planes was one of the factors affecting the relationship between $\Delta Z/Z$ and distance.

A further improvement was made in the internal geometry of the FEM model so that it approximately matched the internal anatomy of the thoracic cavity. This

improvement was carried out by modifying the shape and the size of the left and right lung regions. The results of the theoretical analysis carried out on this modified FEM model showed that $\Delta Z/Z$ increased with distance. Thus, there was an agreement between the experimental and the theoretical results. Thus, this result seemed to suggest that the disagreement between the two results could be due to over simplification of the internal geometry of the earlier FEM model.

The purpose of this theoretical study was also to find an optimum electrode placement. An optimum electrode placement was the one that produced impedance measurements having high specificity to lung conductivity changes. The impedance measured using such an electrode placement would have a high value of $\Delta Z/Z$. Therefore, the theoretical data was compared with the experimental data. The correlation coefficient between the boundary data obtained theoretically and experimentally was reasonably high (r = 0.764) and significant. However, there was a scatter of points in this plot. This scatter appeared to be due to the difference between the FEM model and the thoracic cavity in terms of the shape and the internal conductivity distribution, and also due to instrumentation noise affecting the experimental measurements. It was observed that the instrumentation noise did not significantly affect the measurements when the drive and the receive electrodes were in the same or in the adjacent horizontal planes. The instrumentation noise seemed to dominate when the vertical separation between the plane containing the drive pair and the plane containing the receive pair was more than two planes. Therefore, measurements obtained from such electrode placements were discarded. A correlation coefficient was obtained between $\Delta Z/Z$ measured experimentally and $\Delta Z/Z$ calculated theoretically. This correlation coefficient was equal to 0.534 and significant. Therefore, within the limitations imposed by the simplifications regarding the shape and the internal conductivity distribution in the model, and also by the instrumentation noise, it appeared that the two data sets were comparable and the theoretical data was examined to find out an optimum electrode placement.

There were 8 electrode placements, which had a significantly higher value of $\Delta Z/Z$ compared to all the other electrode placements. These electrode placements also produced higher values of $\Delta Z/Z$ for the experimental results. In these electrode placements, the drive and the receive electrode pairs were placed in two different horizontal planes. The SNR for this electrode placements was expected to be sufficiently higher because, though the drive and the receive pairs were not located in the adjacent horizontal planes, the receive pair was located on the same side as the drive pair. Therefore, the distance between the two was not too high as it could have been for any other combination placed in alternate planes at diametrically opposite locations.

It was also observed that, for all the 8 electrode placements, the drive as well as the receive electrodes were located on the right side of the thoracic cavity model. Thus, they were located close to the right lung. As a result, the measurements obtained from these electrode placements were expected to be largely influenced by the conductivity changes of the right lung. Therefore, to maximise the contribution from both the lungs it was proposed that two sets of drive and receive electrodes should be used, one on either side of the thoracic cavity.

The theoretical studies were also aimed at investigating the underlying phenomenon behind the experimentally observed relationship of impedance measurements and electrode spacing. These studies indicated that electrode placements having a larger electrode spacing were more sensitive to conductivity changes of the in-plane deeper regions and were also more sensitive to conductivity changes of the off-plane regions. Thus, it was better to use a larger electrode spacing because the measurements in this case would be more influenced by the conductivity changes of the deeper lung regions as well as from the regions of the lungs located out of the plane of the electrodes. It is possible that the increased off-plane sensitivity may become a disadvantage because the diaphragm movements would influence the impedance measurements. Therefore, it was important to place the electrodes sufficiently away from the diaphragm when larger electrode spacing was used.

Taking into consideration the results regarding the electrode spacing a 6-electrode placement was proposed as an optimum electrode placement. This configuration involved 3 drive electrodes in one horizontal plane and on the anterior side of the thoracic cavity, and 3 receive electrodes in a second horizontal plane and on the opposite side of the thoracic cavity. The vertical distance between the two horizontal planes was the same as the alternate planes. An additional advantage of this 6-electrode placement was that it used fewer electrodes. This was preferable because using fewer electrodes would be convenient in a clinical environment.

The aim of the present project was to develop a technique of reducing movement artefacts. Therefore, it was considered important to focus further studies on the problem of movement artefacts. It was decided that the 6-electrode optimum configuration would be used to experimentally measure thoracic impedance and determine its sensitivity to lung resistivity changes as well as to movement artefacts.

The following chapter begins with a discussion on the movement artefacts. It presents a review of the literature concerning the various techniques used to reduce movement artefacts. This is followed by a description of some preliminary experimental studies carried out in this project aimed at understanding possible sources of movement artefacts and some techniques of reducing them.

Chapter 5. Movement artefacts in impedance pneumography

5.1. Introduction

The experimental and the theoretical studies described in the previous chapters were aimed at identifying an optimum electrode placement for impedance pneumography. This optimum electrode placement was characterised by maximum sensitivity to lung resistivity changes during breathing. These studies indicated that this maximum sensitivity could be obtained by placing the drive and the receive electrode pairs in two different horizontal planes, at an angle of 112.5° and on a lateral side of the thoracic cavity, i.e. close to one of the two lungs. Taking into consideration these results and keeping in mind that it would be convenient to use a minimum number of electrodes in a clinical environment, a 6-electrode placement was proposed as an optimum electrode arrangement for impedance pneumography.

The next step in this work was to study whether impedance measurements obtained from the optimum electrode placement were affected by movement artefacts. In order to develop a reliable method for monitoring breathing, it would be necessary to minimise these movement artefacts. This chapter and the following chapter describes the work carried out in this project to minimise movement artefacts in impedance pneumography.

The following section of this chapter presents a review of the work from the literature aimed at developing different methods of reducing movement artefacts. This is followed by a description of the preliminary work carried out in this project to identify a suitable electrode type and to test an electrode placement, which according to some researchers, is able to provide reduction in movement artefacts. Finally, a technique based on impedance imaging, which might help to detect breathing in the presence of movement artefacts, is described.

5.2. Techniques for movement artefact rejection: a literature review

The impedance based monitoring of breathing activity in humans was first carried out systematically by Goldensohn and Zablow in 1959. In this very first study, problems due to movement artefacts were reported and some attempts were made to reduce them. It was reported that a four-electrode configuration was purposefully used instead of a two-electrode configuration because it reduced artefacts caused by unpredictable changes in the electrode-skin contact impedance. However, artefacts due to gross body movements could not be avoided because both, the drive and the receive electrode pairs, were placed on the arms. Therefore, movement of the arms had to be restricted during recording of the data. An attempt was also made to reduce cardiac related impedance changes, which were treated as artefacts.

An 'impedance pneumograph' was developed by Geddes *et al* (1962) for monitoring breathing in space. In this case, it was necessary to allow normal movement of the arms as the space crew had to carry out their usual tasks while their breathing was being monitored. Therefore, electrodes could not be placed on the arms, but were placed bilaterally on the thoracic cavity along the midaxillary line. It was considered necessary to keep the number of electrical connections to the body to a minimum. Therefore, a two-electrode configuration was preferred although it was known to be susceptible to artefacts originating from the electrode-skin contact impedance.

It appears from the literature that a majority of subsequent studies were aimed at investigating in quantitative terms, the relationship between the thoracic impedance and the volume of the respired air (Allison *et al*, 1964; Kubicek *et al*, 1964; Hamilton *et al*, 1965; Baker *et al*, 1965,1966). Thus, even though the problem of movement artefacts was observed by the researchers, it seems that not much attention was focused on reducing it. This was probably because the experimental impedance measurements could be carried out under controlled conditions. In the studies carried out by Hamilton *et al* (1965, 1967), they designed and used a special type of 'ridged' electrodes to reduce movement

artefacts. These electrodes were placed bilaterally on the thorax along the midaxillary line with the ridge pressed into the skin. It was observed that measurements obtained from these electrodes were less affected by moderate body movements such as quiet walking. However, vigorous activity, particularly involving arm movements, introduced large artefacts.

The problem of movement artefacts was considered as a major drawback of impedance pneumography when used in a clinical environment, such as in apnoea monitors for infants. Impedance pneumography appeared to be a very suitable technique for monitoring breathing in the apnoea monitors because it was well tolerated by the infants. However, it was pointed out by many researchers that the impedance based apnoea monitors failed to detect apnoea because the absence of breathing signal during apnoea was obscured by large movement artefacts (AAMI, 1989). It was also observed that these monitors failed to detect obstructive apnoea (Warburton *et al*, 1977). In the situations in which apnoea was accompanied by bradycardia, the cardiac related impedance changes seemed to imitate breathing related impedance changes during apnoea. As a result apnoea could not be detected (Southall *et al*, 1980). Thus, a need was felt to carry out a systematic research into developing techniques for reducing movement artefacts as well as other artefacts and subsequently many studies have been carried out as reviewed below.

The studies concerned with reduction of movement artefacts can be classified into two categories. In the first category, there are studies aimed at identifying an electrode system that would have minimum movement artefacts. These studies present a comparison between different types of commercially available electrodes in terms of their ability to minimise movement artefacts. They also compare different electrode placements. In the second category, there are studies involving multi-frequency measurements for reducing movement artefacts. These studies are based on the observation that movement artefacts reduce with increase in frequency of injected current and involve developing special types of filters. The following sub-sections review these studies.

5.2.1. Electrode systems for movement artefact reduction

The researchers involved in these studies have generally defined an electrode system by three parameters, electrode type, electrode size and electrode placement. The following studies were aimed at investigating the relationship between either one or all these parameters and movement artefacts.

Sahakian *et al* (1985) carried out a study to investigate the effect of electrode size and electrode guarding on movement artefacts. The experiments were carried out on 10 normal human adults by placing two electrodes bilaterally on the midaxillary line. A two-electrode configuration was used instead of a four-electrode configuration because it was the most commonly used configuration in commercial apnoea monitors. The impedance data was recorded during normal breathing without any movement and also during breath hold while simultaneously carrying out two movement manoeuvres, which were the arm movements and running in place causing random body movements. The impedance data was also recorded during obstructed inhalation at Functional Residual Capacity to a pressure of –20 to –40 cm of water. This condition simulated the obstructive apnoea. It was observed that electrodes having a small size had large movement artefacts. When the area of these electrodes was increased from 0.8 cm^2 to 33 cm^2, the mean movement artefacts, arm movement artefacts and body movement artefacts reduced to 57%, 45% and 32% of their initial value, respectively. This reduction was attributed to a reduction in electrode-skin contact impedance due to an increase in the electrode size. It was also observed that when the large electrodes (33 cm^2) were used in a guarded configuration, the mean movement artefacts, arm movement artefacts and body movement artefacts reduced to 87%, 57% and 55%, respectively, of those observed with an unguarded configuration involving the same large electrodes. A four-electrode guarded configuration was found to be only marginally better than a two-electrode guarded electrode configuration. Therefore, it was suggested that a two-electrode guarded configuration with large electrodes was more suitable than a four-electrode guarded configuration because the former had an advantage of requiring fewer connections.

Luo *et al* (1992) carried out a detail study on the effect of electrode type, size and placement on movement artefacts. They defined a ratio called Signal-to-Artefact Ratio (*SAR*), which was a ratio of the mean amplitude of breathing signal to the mean amplitude of movement artefacts. This ratio was used to compare the performance of different types, sizes and placements of electrodes. The impedance measurements were carried out using a two-electrode configuration in human subjects. In order to decide a best electrode type for impedance pneumography, two types of electrodes, the adhesive gel electrodes and the conductive rubber electrodes, were evaluated. The electrodes were placed bilaterally along the midaxillary line at the level of the 8^{th} intercostal space. It was observed that the adhesive gel electrodes were better because they seemed to adhere reasonably well even during movements, whilst it was difficult to keep the conductive rubber electrodes in proper contact with the body due to their 'non-stick' nature. These conductive rubber electrodes, along with the stretch band used to hold them in place, had a tendency to slip during movement. Several other parameters of the electrodes such as face-to-face impedance and electrode-body impedance were also measured. In general, it was concluded that out of electrodes of twelve different make, the electrodes having a low baseline impedance, good adhesion, good physical stability, large effective (electrically conductive) area and high flexibility, provided high values of *SAR*.

These investigators also studied the effect of electrode size on movement artefacts. The aim of this study was to identify an optimum electrode size for which movement artefacts were minimum. The electrode size was increased by connecting several small electrodes rather than using one large electrode because such an arrangement reduced strain in the underlying skin and hence, seemed to provide better results. The results of this study showed that movement artefacts reduced with an increase in electrode size. However, it was difficult to find an optimum electrode size because the amplitude of the breathing signal decreased with an increase in electrode size.

Luo *et al* (1992) also carried out studies to find an electrode placement with minimum movement artefacts. The experimental set up involved placing 32

electrodes, 8 in each of the 4 horizontal planes, around the thoracic cavity. It was observed that *SAR* was minimum when one electrode was placed in the centre of the thoracic cavity on the sternum at the level of the 2nd intercostal space and the other electrode was placed in the same horizontal plane, but posteriorly over the spinal column as shown in Figure 5.1. The study also indicated that *SAR* was generally low on subjects having more subcutaneous fat.

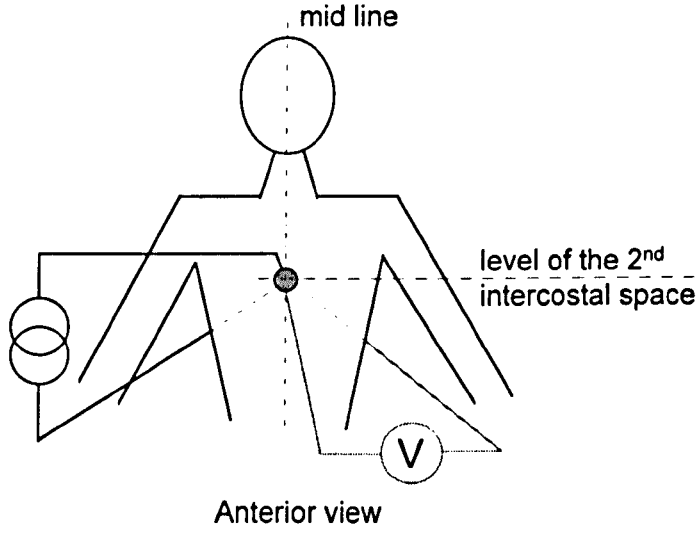

Figure 5.1 *Electrode placement having minimum movement artefacts as suggested by Luo et al (1992). The electrode placed in the anterior is seen in the figure. The second electrode was on the back at the same level. The measurements were obtained using a two-electrode configuration.*

A study was carried out by Mayotte *et al* (1994, 1996) to evaluate the suitability of ten different commercial electrodes for infant apnoea monitoring, on the basis of *SAR*. They used a two-electrode configuration with electrodes placed bilaterally along the midaxillary line at the level of the 7th intercostal space. The experiments involved adult subjects rather than infants because it was considered difficult to control breathing and movement patterns in infants. Different quantitative physical parameters such as total area, effective area, face-to-face impedance and electrode-body impedance were measured for each type of electrode and the adhesive quality of each type of electrode was rated qualitatively. The results of this study also showed that for a two-electrode configuration, movement artefacts were low when the electrodes had a good stability, strong adhesion, low

face-to-face impedance, low transthoracic-plus-electrode impedance, large effective area and large total area. It was also reported that electrode properties including gel chemistry of the hydrogel electrodes played an important role in determining their performance.

It is accepted that electrodes should adhere strongly to the body so that they do not come loose during movement. This aspect was kept in mind while choosing electrodes for the experimental work in this project.

In the studies reviewed above, it can be seen that impedance measurements have been carried out using a two-electrode configuration rather than a four-electrode configuration. This choice of electrode configuration has been based on the fact that it is the most simple configuration in terms of instrumentation and hence, used in the majority of commercial apnoea monitors. A two-electrode configuration involves fewer connections and therefore, is considered to be convenient to use in a clinical environment, especially on infants. However, when impedance measurements are made using a two-electrode configuration, the electrode-skin contact impedance is an inseparable component of the measured impedance. It is known that at least one of the components of movement artefacts originates from the unpredictable changes in this electrode-skin contact impedance. The mechanical disturbances to the electrode-skin interface during movement cause these unpredictable changes in the electrode impedance. Therefore, a first step in reducing movement artefacts would be to use a four-electrode configuration rather than a two-electrode configuration. This was the approach adopted in the present project. Thus, the results regarding reduction in movement artefacts with an increase in electrode size may not be applicable for a four-electrode configuration.

Movement artefacts were low when the electrodes were placed on the sternum and over the spinal cord. These electrode positions appear to be less disturbed physically by movements, especially that of arms, probably because the electrodes would be located at points farthest from both the arms. This was another important point noted from the study of Luo *et al* (1992). Some

preliminary experiments were carried out using a similar electrode placement in this project as described later.

The following sub-section describes studies aimed at movement artefact reduction using multi-frequency measurements.

5.2.2. Multi-frequency measurements and movement artefact reduction

The use of more than one frequency of injected current as a means of identifying movement artefacts was suggested by Rosell and Webster (1995a). They carried out experiments on nine human subjects to study the effect of frequency on movement artefacts. The electrodes were placed on the midaxillary line, 1 cm below the nipple level, and a two-electrode configuration was used in this study. It was observed that breathing related impedance changes increased by 20% with frequency in the range of 12.5 kHz to 185 kHz, but movement artefacts decreased with frequency in this range. Thus, an improvement in SAR was observed by about 30% from 12.5 kHz to 57 kHz. They explained these results by saying that the increase in breathing related impedance changes was probably due to decrease in the base impedance of the lungs at the higher frequency. This caused more current to penetrate the lungs and thus, resulted in an increase in sensitivity to resistivity changes of the lungs. The reduction in movement artefacts was assumed to be due to reduction in electrode impedance at the higher frequency. There was no correlation between frequency and amplitude for obstructive apnoea within the group. This was attributed to the variations in the level of the electrodes with respect to the diaphragm in different subjects and the differences in the way the manoeuvre of simulated obstructive apnoea was carried out by different subjects.

In a subsequent study carried out by the same research group (Rosell *et al*, 1995b), a design of an adaptive filter was proposed to reject movement artefacts using dual frequency measurements. A two electrode configuration was used in this study as well, with electrodes placed bilaterally on the midaxillary line, 1 cm below the level of the nipples. The adaptive filter was used in an adaptive noise

canceller mode. A reference signal, proportional only to movement artefacts, was derived from the impedance signals recorded at two different frequencies. A mean increase in *SAR* for arm movements was 182% and for leg movements was 133%. However, it was reported that the non-stationary nature of movement artefacts was a problem in obtaining a fast and accurate response in the adaptive filter.

Rosell and Pico, (1995c) measured impedance in 10 adults at 8 frequencies ranging from 8 kHz to 1 MHz during normal breathing and during movements. A two-electrode configuration was used in these experiments and the electrodes were placed bilaterally on the thorax on the midaxillary line at the level of the nipples. They observed that the RMS value of the real part calculated after subtracting the base impedance decreased with frequency for movement artefacts, while there was a maxima between 63 kHz and 126 kHz for the breathing related impedance changes. The decrease in real part with frequency for movement artefacts was assumed to be due to reduction in electrode impedance with frequency. They also carried out four-electrode measurements by placing one drive and one receive electrode on one side of the thorax, on either side of the midaxillary line and separated by 2 cm. The second drive and the receive electrode was placed in the same way, but on the other side of the thoracic cavity. All the electrodes were placed at the level of the nipples. They obtained Cole parameters for these measurements. The parameters for breathing related impedance changes matched well with those reported in the literature. However, they did not observe any significant differences in these parameters between breathing related impedance changes and movement artefacts.

In the studies reviewed above, a two-electrode configuration has been mainly used. Thus, the electrode-skin contact impedance is an inseparable part of the measured impedance. It is known that this impedance reduces with frequency. Therefore, the artefacts originating from the electrode-skin contact impedance would reduce with frequency. In the present project it was decided that a four-electrode configuration would be used to minimise artefacts originating from the

electrode-skin contact impedance. Therefore, the advantage of using a higher frequency of injected current is not obvious. However, it may be useful to carry out impedance measurements at more than one frequency of injected current for the following reason.

If we consider movement as a change in the geometry of the body, then it should cause an artefact which would be a constant fraction of the baseline impedance. On the other hand, the fractional impedance changes during breathing, measured by defining a region-of-interest over the lungs in an EIT image, increase with frequency (Brown *et al*, 1994). Thus, it might be possible to separate breathing related impedance changes from movement artefacts by measuring impedance at more than one frequency of injected current. This aspect was investigated in the present project and the experimental work involving multi-frequency measurements is described in the subsequent chapter.

The following sections describe preliminary studies carried out in this project to improve an understanding as to which factors are responsible for movement artefacts and thus, to decide a strategy for developing techniques to reduce them.

5.3. Selection of a suitable electrode system: a preliminary study

The aim of these preliminary studies was to identify an electrode system that would have low movement artefacts. An electrode system may be defined by three factors, electrode configuration, electrode type and electrode placement. Therefore, these studies involved deciding an electrode configuration to be used for impedance pneumography and identifying a suitable type of electrode. Thoracic impedance was recorded during breathing and movement artefacts from the common midaxillary electrode placement. These recordings were compared with those obtained from an electrode placement similar to the one shown in Figure 5.1 and for which low movement artefacts has been suggested (Luo *et al*, 1992).

For this study and in the rest of the project, it was decided that a four-electrode configuration would be used instead of a two-electrode configuration, because it was known to reduce the artefacts originating from the electrode-skin contact impedance. Thus, only the remaining two factors, the electrode type and the electrode placement required investigations. The following is a description of an empirical study carried out to identify a most suitable electrode type.

5.3.1. Selection of a suitable electrode type

The electrodes used in this study were basically different types of electrodes used for routine ECG monitoring. Electrodes of three different make were chosen. They were Medicotest (Blue sensor, R-00-S), Conmed (2045), Unitrace (Biotrace-M). Medicotest and Conmed electrodes were wet gel electrodes while Unitrace electrode were hydrogel electrodes. This study focused on a qualitative evaluation of the strength of the adhesive used in these three electrode types.

The drive electrodes were placed bilaterally along the midaxillary line at the level of xiphoid process and the receive electrodes were placed medial to the drive electrodes as shown in Figure 5.2. This midaxillary placement appeared to be getting largely affected by the arm movements and hence, represented a worst

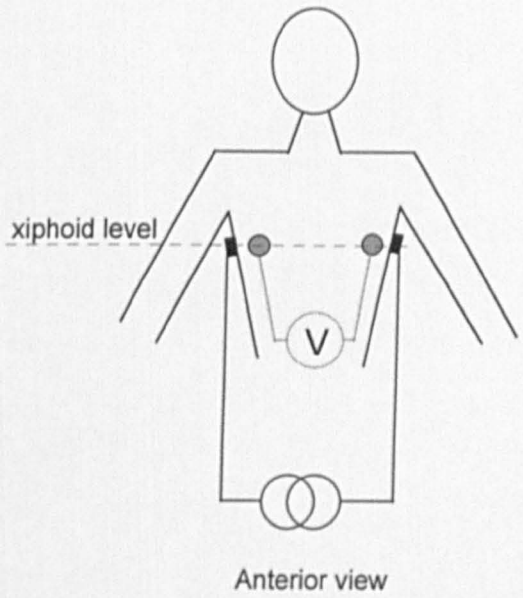

Figure 5.2 Electrode placement used for evaluating different types of electrodes

case scenario. The choice of the vertical level was based on the suggestion in the literature that for a given change in the volume of the inspired air, a maximum change in thoracic impedance for the midaxillary placement was obtained at the level of the xiphoid process (Geddes *et al*, 1962).

The impedance measurements were carried out on one subject using the three types of electrodes during normal tidal breathing in the absence of any movement and during breath hold with movements consisting of a random combination of arm and torso movements. The speed at which the movements were carried out was also varied to see whether it had any effect on the electrode adhesion. These measurements were carried out using a Sheffield Multi-frequency Tissue Impedance Meter.

The selection of a suitable electrode type was based on a qualitative analysis. It was observed that all the three types of electrodes satisfactorily recorded breathing related changes in thoracic impedance during quiet tidal breathing and in the absence of movements. Conmed 2045 electrodes appeared to have a very strong adhesion to the skin. The second best in terms of skin adhesion were Unitrace electrodes. Neither of these types of electrodes showed any signs of becoming loose even during very fast arm and torso movements. Medicotest electrodes also satisfactorily recorded data during slow movements, but seemed to come loose during fast movements. It was generally noticed that during movements the skin underneath the electrodes was stretched. Therefore, if the backing material of the electrodes was sufficiently flexible, then they would not come loose. Normally, for recording bioelectric events, the skin is cleaned using alcohol before attaching the electrodes so that the electrode-skin contact impedance is low and stable. In these experiments, it was observed that this skin preparation also improved electrode adhesion and thus, prevented them from coming loose during movements.

Thus, firstly a general conclusion drawn from this study was that Conmed electrodes were the best type of electrodes. Secondly, it was noted that before attaching the electrodes, it was important to clean the skin using a solvent such as alcohol. The following is the description of a preliminary study carried out to

compare the midaxillary electrode placement with the one suggested by Luo *et al* (1992) and shown in Figure 5.1.

5.3.2. Selection of a suitable electrode placement

The purpose of this study was to compare two different electrode placements to find out which one of the two had lower movement artefacts. A second aim of these preliminary experiments was also to find out whether there was any significant difference between the impedance-frequency relationship for breathing and movement artefacts. The following two electrode placements were compared in this experimental study.

In the first electrode placement, one of the drive and the receive electrodes was placed on the midaxillary line at the level of the xiphoid process. The second drive and the receive electrodes were placed on the opposite side of the thoracic cavity at the same horizontal level. This placement is shown in Figure 5.3 and will be referred to as electrode placement Ep_1. This electrode placement was used by many researchers in the past for monitoring breathing as described previously in this chapter and in Chapter 2.

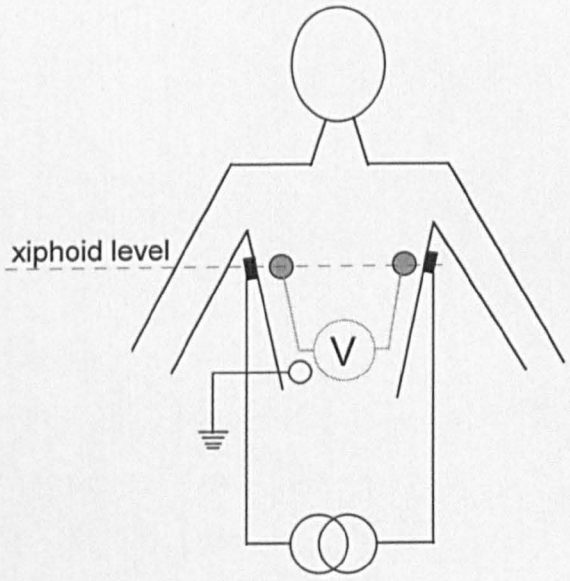

Figure 5.3 *Electrode placement Ep_1 used in the preliminary experimental study.*

In the second electrode placement, one of the drive electrodes was placed on the sternum at the level of the 2nd intercostal space and the second drive electrode was placed posteriorly over the spinal column, in the same horizontal level. The receive electrodes were placed immediately below the drive electrodes. This electrode placement is shown in Figure 5.4 and will be referred to as electrode placement Ep_2. Electrode placement Ep_2 was similar to that suggested by Luo *et al* (1992) as the one having low movement artefacts (Figure 5.1). A ground electrode was placed on the abdomen in both the placements.

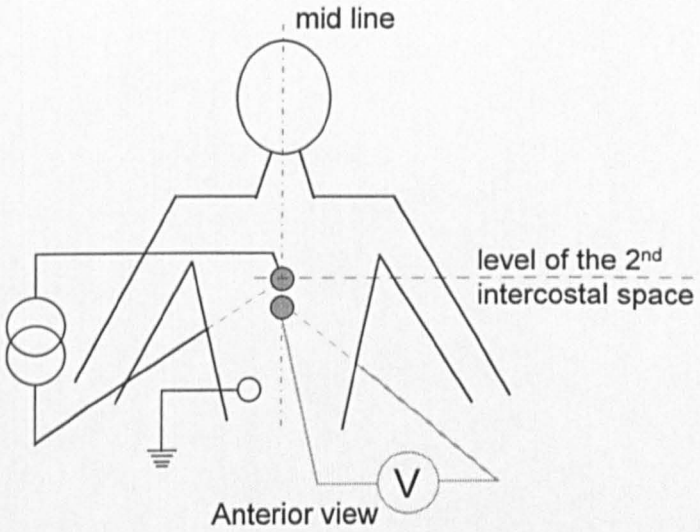

Figure 5.4 *Electrode placement Ep_2 also used in the preliminary experimental study.*

The impedance measurements were carried out using a Sheffield Multi-frequency Tissue Impedance Meter (Lu, 1995). It had one drive and one receive pair of electrodes. The impedance was measured at 7 frequencies in binary steps ranging from 9.6 kHz to 614.4 kHz. These experiments were carried out on one human subject. Each trial was of 60 s duration, consisting of a first epoch of 30 s of movements with breath hold at maximum inspiration and a subsequent epoch of 30 s of quiet tidal breathing without movements. Medicotest Blue sensor ECG electrodes (R-00-S) were used for these experiments instead of Conmed (2045) electrodes because of availability. The movement manoeuvres were carried out in an upright sitting position.

Figure 5.5 illustrates these movement manoeuvres. A typical movement manoeuvre of an arm involved starting the movement from a lower most position in an upward direction on the side until it reached the maximum vertical position by the side of the head and then downwards to its starting position. The movement manoeuvre involving both the arms, involved moving the two arms up and down alternately (Figure 5.5c) as well as simultaneously (Figure 5.5d). These movements were repeated approximately four or five times within the first 30 s of breath hold at maximum inspiration.

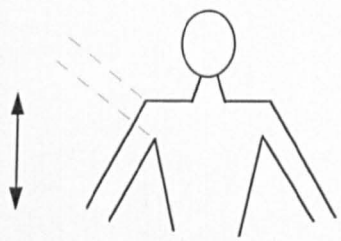

Figure 5.5a Right arm movement

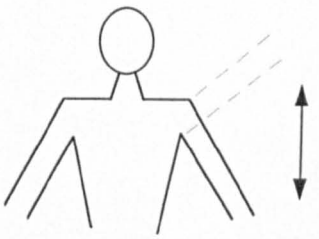

Figure 5.5b Left arm movement

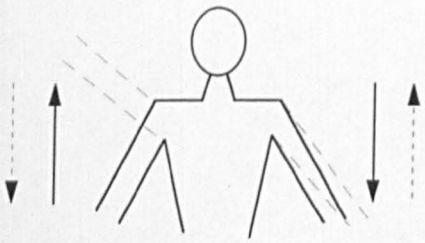

Figure 5.5c Alternate arm movement

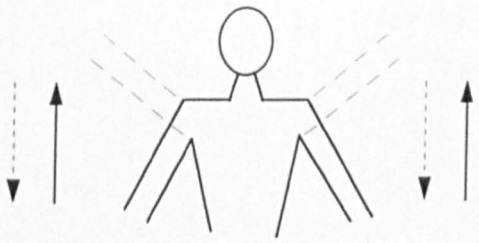

Figure 5.5d Simultaneous arm movement

Figure 5.5 Four arm movement manoeuvres used in the preliminary experiments

Figure 5.6 shows a plot of $\Delta Z/Z$ versus time of the measured thoracic impedance for the two electrode placements. The first epoch of 30 s corresponds to breath hold with right arm movement. The second epoch of 30 s corresponds to normal tidal breathing without any movement. The top trace corresponds to electrode placement Ep_1. It can be seen that for electrode placement Ep_1, the amplitude of $\Delta Z/Z$ for movement is high compared to that of the tidal breathing. The bottom trace corresponds to electrode placement Ep_2 and shows that $\Delta Z/Z$ for movement is lower than that observed for electrode placement Ep_1. It is also important to

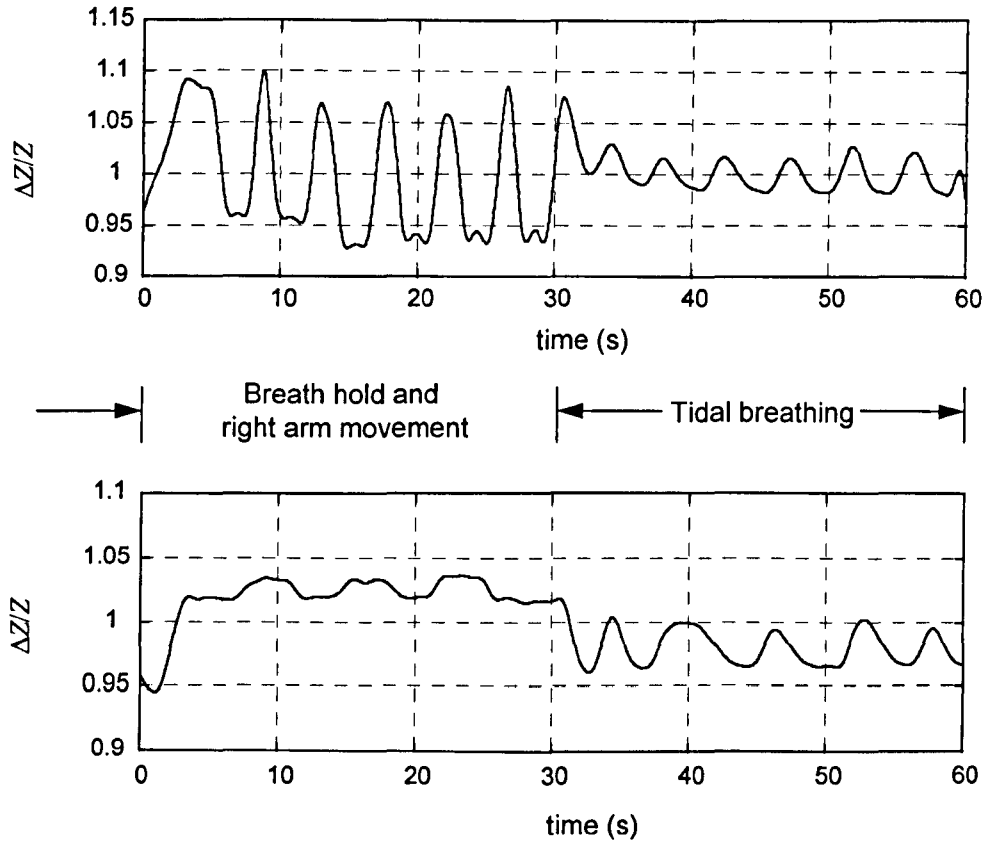

Figure 5.6 *Thoracic impedance measured at frequency 9.6 kHz during breath hold and right arm movement (0s to 30s), and tidal breathing (30s to 60s) using two different electrode placements Ep_1 (top trace) and Ep_2 (bottom trace)*

note that the amplitude of impedance change during tidal breathing is comparable in both the traces.

These results seem to suggest that the movement artefacts due to right arm movement are lower for electrode placement Ep_2. Similar results were obtained for the other three types of arm movements. These results agree with the results reported by Luo *et al* (1982) as the best electrode placement suggested by them was similar to electrode placement Ep_2. A possible explanation for these results may be that when the electrodes were placed on the sternum and on the spinal column (electrode placement Ep_2), they were located at points farthest from the arms. As a result, the electrodes would be least affected by the movement of the arms. On the other hand, when the electrodes were placed on the midaxillary line, they appeared to move up and down along with the arms and therefore,

produced large artefacts. However, it should be noted that this explanation would be valid only for arm movements. Other types of body movements, such as torso movements may still introduce large artefacts in the impedance signal measured using the electrode placement Ep_2.

It may also be noted that these preliminary experiments were carried out only on one subject because they were only meant to test the performance of the electrode placements suggested in the literature. Furthermore, neither of the two electrode placements was similar to the one found to have maximum sensitivity to lung resistivity changes in the earlier studies described in the previous chapters. Therefore, these electrode placements may not maximise the contribution of lung resistivity changes to the thoracic impedance. A detail study was carried out using the optimum 6-electrode placement and is described in the subsequent chapter. Nonetheless, a general observation made from this study is that the electrodes seemed to move along with the skin during movements and therefore, introduced artefacts in the measured impedance.

The results of this study were also examined to see whether the relationship between breathing related impedance changes and frequency was different from the relationship between movement artefacts and frequency. However, the results were not conclusive because it was observed that there was a large stray capacitance between the cables used, especially at higher frequencies (300 kHz to 600 kHz). This stray capacitance introduced additional artefacts at higher frequencies.

The next step in the present project was to develop techniques for reducing movement artefacts. As a first step, a technique based on impedance imaging was developed to detect breathing in the presence of movements. The following section describes the strategy for this development, as well as some simulation studies and experimental studies.

5.4. Detection of movements and breathing using impedance imaging

It was noted in the literature review presented at the beginning of this chapter that movement artefacts were a major drawback of impedance based apnoea monitors. The apnoea monitors failed to detect apnoea during gross body movements, because the loss of breathing signal during apnoea was obscured by large movement artefacts. It was also difficult to detect breathing and extract useful parameters such as breathing rate, during movements. Thus, a reliable apnoea monitor would be required to detect the presence or the absence of breathing in the presence of movements as well.

Ideally, any technique used for movement artefact reduction should completely reject the artefacts so that the breathing related impedance changes are not at all affected. However, it is not obvious whether this objective can be achieved in a single step. Instead, we may consider it to be achievable in successive steps. A first step can be to develop a technique for detecting the occurrence of movements. Once it is possible to detect whether the movements have occurred, a second step can be to develop a technique for detecting breathing in the presence of those movements. If these two steps can be achieved, then it would be possible to detect apnoea in the presence of movements. However, if the parameters such as breathing rate are to be measured, then it would be necessary to considerably reduce the amplitude of movement artefacts. Thus, a third step can be considered as to achieve a maximum possible reduction in the amplitude of movement artefacts.

The following is the description of a study aimed at achieving the first two steps by making use of the technique of EIT. A study was also carried out to achieve the third step and is described in the subsequent chapter.

5.4.1. Strategy for development of an EIT based breath detection technique

An EIT image of the thoracic cavity, obtained by reconstructing data measured from a 16-electrode array using an adjacent drive - adjacent receive data collection protocol, shows two distinct lung regions undergoing a change in resistivity during breathing. If both the lungs are physiologically normal, then the resistivity changes observed over the one lung region would correlate highly with those observed over the other lung region. However, during random body movements, the resistivity changes over the two lung regions would not be expected correlate. This can be seen in Figure 5.7, which shows resistivity changes measured by defining a region-of-interest (ROI) over the two lungs in an EIT image of the thoracic cavity obtained at the level of the nipples. The ROI

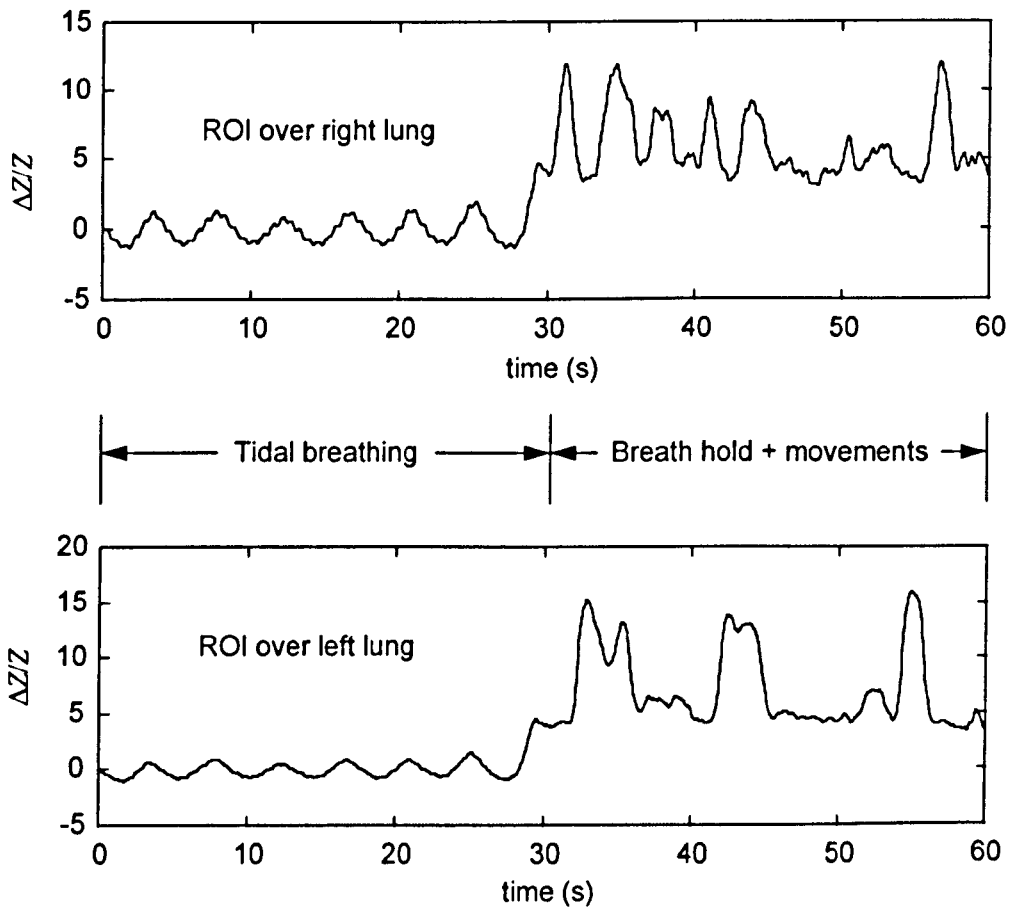

Figure 5.7a Plot of ΔZ/Z v/s time for resistivity changes observed within ROI over the right lung and the left lung in an EIT image

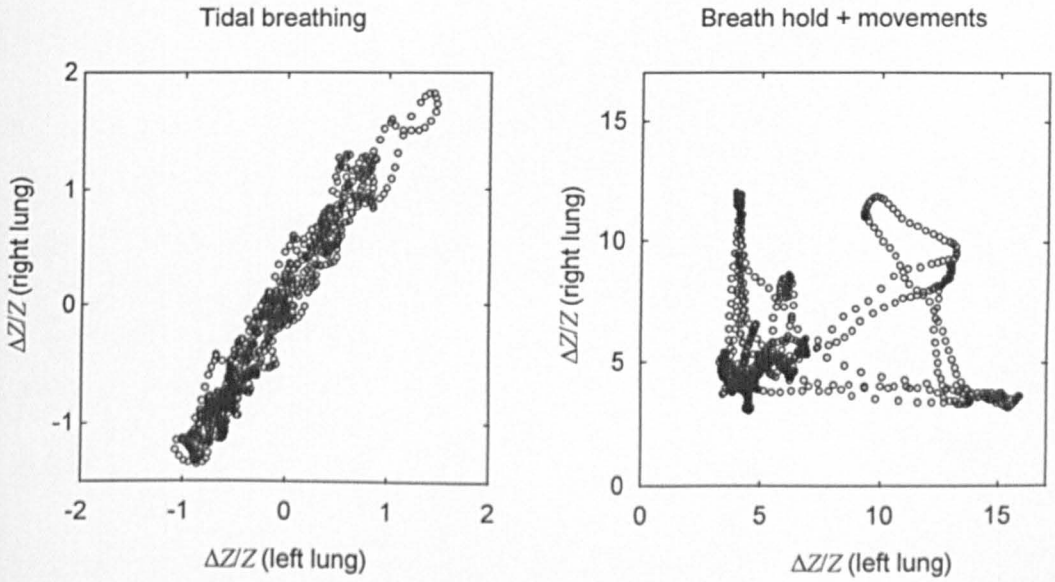

Figure 5.7b Plots of ΔZ/Z (left lung) v/s ΔZ/Z (right lung) for tidal breathing (r=0.97) and breath hold + movements (r=0.15)

over the right lung was defined by including all the pixels in the left half of the image, observed to undergo a change of 10% or more during tidal breathing. The ROI over the left lung was defined in the same way, in the right half of the image.

It can be seen from Figure 5.7a that during tidal breathing without movements (0 to 30s), the two signals correlate highly (r = 0.97) with each other. On the other hand, during movements and in the absence of breathing (30 to 60s), these two signals do not correlate (r = 0.15). This is further evident in the plots of $\Delta Z/Z$ (right lung) v/s $\Delta Z/Z$ (left lung) for tidal breathing and breath hold plus movements shown in Figure 5.7b. It may be noted that movements carried out during data collection were a random combination of arm and torso movements, rather than systematic movements, to simulate a situation similar to that in real life.

Thus, by calculating a correlation coefficient between short stretches of the two signals originating from the two lung regions, it would be possible to detect whether the movement has occurred. In this way it would be possible to achieve movement detection. Let us denote the resistivity changes observed over the right lung region by $\Delta\rho_{rt}$ and those observed over the left lung region by $\Delta\rho_{lt}$. This approach based on impedance imaging may also provide an ability to detect

breathing in the presence of movements, i.e. to achieve the second step and hence, detect apnoea.

Let us consider three different cases as stated in Table 5.1 and represented schematically in Figure 5.8. In case 1, breathing is present, but movements do not occur. Thus, the correlation coefficient between $\Delta\rho_{rr}$ and $\Delta\rho_{ll}$ will be high and close to 1.

Table 5.1 *Table describing the three cases considered in the study and the possible values of the correlation coefficient (r)*

Case no.	Breathing	Movement	Correlation coefficient (r)
1	present	absent	$r \rightarrow 1$
2	absent	present	$r \rightarrow 0$
3	present	present	$0 < r < 1$

In case 2, breathing is absent, but movements are present. Thus, the correlation coefficient (r_{mv}) between $\Delta\rho_{rr}$ and $\Delta\rho_{ll}$ will be low and close to zero. In fact, r_{mv} will never be exactly equal to zero, but will have some distribution, which would have a mean equal to zero and unknown variance. For the sake of this argument, let us assume that r_{mv} has a normal distribution with a zero mean and standard deviation s_{mv}. The value of s_{mv} would depend on the following two factors.

Firstly, the spread of the distribution of r_{mv} is expected to depend on the frequency content of the movements. If we assume that the EIT data collection system has a sampling rate of 25 samples s^{-1}, then an anti-aliasing low pass filter would be used at the input, which will have a cut-off frequency equal to or less than 12.5 Hz. Thus, the impedance signal will not have frequency components higher than 12.5 Hz. However, movement artefacts may have any frequency components up to 12.5 Hz, depending upon the speed at which the movements occur and this speed can vary from time to time. Movements can

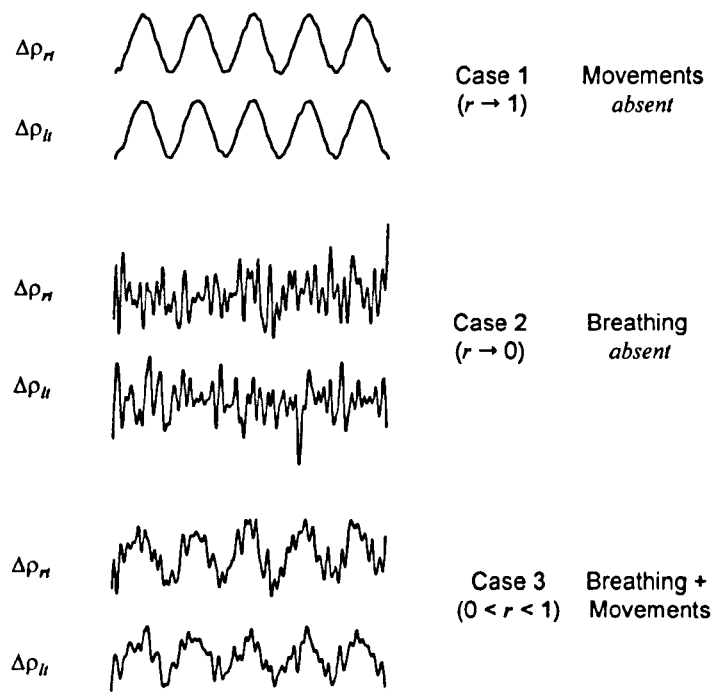

Figure 5.8 A schematic representation of the three cases under consideration

occur at any speed and thus, may not always have all the frequency components up to 12.5 Hz. For example, if the movements occur only at a slow speed, then movement artefacts would only have low frequency components. As a result, the spread of the distribution of r_{mv} would also vary. Secondly, for a given frequency content, the distribution of r_{mv} would depend on the length of the signals used to calculate r_{mv}. In case 3, breathing as well as movement artefacts are present. Therefore, the correlation coefficient between $\Delta\rho_{rr}$ and $\Delta\rho_{ll}$ will be between 0 and 1.

It can be seen from the above three cases that in the presence of movements, a high value of the correlation coefficient will indicate presence of breathing while a low value of the correlation coefficient will indicate absence of breathing. However, it may be noted that in the absence of movements, the correlation coefficient will be high and close to 1 when breathing is present, but indeterminate when it is absent. Thus, in the absence of movements, the decision regarding the presence or the absence of breathing cannot be based only on the value of the correlation coefficient. Rather, it should also be based on other features of the impedance signal such as its amplitude and periodicity. It

may be noted that the technique being considered here was supposed to be useful for detecting breathing in the presence of movements rather than in the absence of movements.

In order to understand what would happen to the value of the correlation coefficient in the presence of movements as well as breathing, let us consider case 3 in some more detail. The actual value of the correlation coefficient (r) in case 3 will depend on the ratio of the amplitude of breathing signal to the amplitude of movement artefacts. Let us call this ratio as Signal-to-Artefact Ratio (SAR) and define it in decibels as,

$$SAR = 20 \lg\left(\frac{\Delta\rho_{breathing}}{\Delta\rho_{movement}}\right) \qquad 5.1$$

The values in the numerator and in the denominator of equation 5.1 are RMS values. Let us consider the two situations in which SAR is reasonably high and very low as shown schematically in Figure 5.9.

If SAR is high, then r will be dominated by the correlated resistivity changes observed during breathing and hence, will remain close to 1, even in the presence of movements. As SAR decreases, r will also decrease because it will be more and more influenced by the uncorrelated movement artefacts. If SAR decreases to a very low value, then r will be dominated by the uncorrelated movement artefacts rather than the correlated breathing signal and hence, will be close to 0. In this situation, it is possible that r will be so low that it may lie within 99.7% confidence interval ($\pm 3s_{mv}$) of the distribution of the correlation coefficient r_{mv} of case 2, which is the correlation coefficient observed in the absence of breathing. As a result, at these very low values of SAR, it would not be possible to make a decision whether the breathing is present or absent, using the value of r. This indicates that there will be some threshold value for SAR, below which it will not be possible to detect breathing in the presence of movements using the

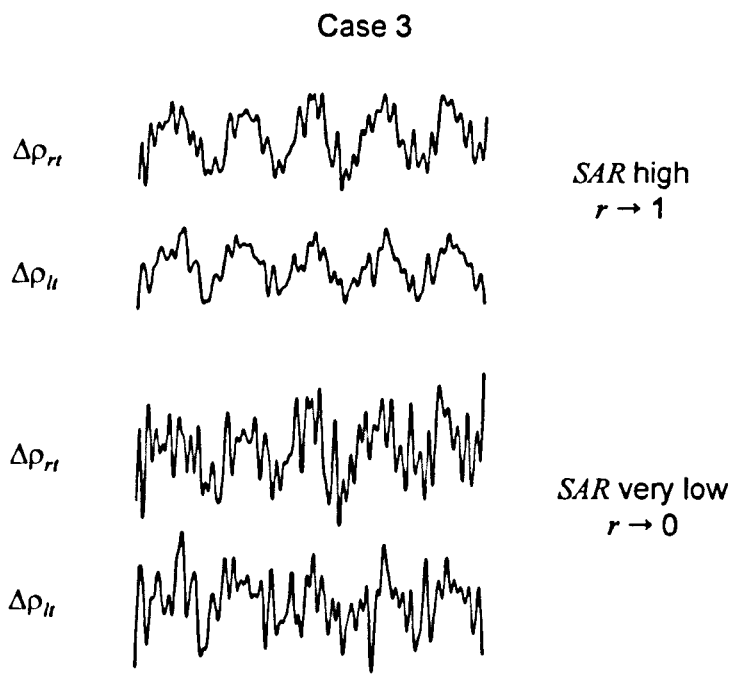

Figure 5.9 A schematic representation of the two possible situations in case 3

correlation coefficient. The purpose of the following simulation studies was to determine this threshold value of *SAR*.

5.4.2. Simulation studies: methods

The movement artefacts observed within the two lung regions of an EIT image of the thoracic cavity were simulated by two independent random signals. These two random signals were generated using a normally distributed random number generator provided in software MATLAB® (version 4.2, The Mathworks Inc., USA). A sinusoidal signal having a frequency of 0.25 Hz, which was equivalent to 15 breaths min^{-1}, was used to simulate the breathing related resistivity changes observed over both the lung regions. The sampling frequency of all the simulated signals was assumed to be equal to 25 Hz because this was the frame rate of Sheffield Mark 2 REIT system, which was used for data collection in the associated experimental studies described later in this chapter. The processing of these simulated signals was carried out by considering each of the three cases listed in Table 5.1, one by one.

Let us consider case 1. In this case, the correlation coefficient between breathing related resistivity changes observed over the two lung regions would be exactly equal to 1 because the same sinusoidal signal was used to simulate the two signals. Therefore, no further processing is required in this case.

Now, let us consider case 2. In this case, the breathing was assumed to be absent and the correlation coefficient (r_{mv}) between the two simulated movement artefact signals would have some distribution with a mean zero and unknown variance (s_{mv}). Therefore, it was necessary to find this distribution. In order to simulate movement artefacts due to movements occurring at different speeds, the simulated movement artefact signals were filtered using a low-pass filter having three different values of cut-off frequency (LPF type: Butterworth; order: 10). The distribution of r_{mv} was also obtained for three different lengths of the signals corresponding to 1/2 breath, 1 breath, and 2 breaths. In order to find the distribution of r_{mv}, 1000 values of r_{mv} were calculated by each time correlating two different stretches of data, one from each of the two simulated movement artefacts. The steps involved in this processing are summarised in Figure 5.10.

Finally, the processing in case 3 was carried out according to the steps shown in Figure 5.11. The amplitude of the two simulated movement artefacts signal was adjusted such that SAR would have a predetermined value. The sinusoidal simulated breathing signal was added to the two simulated movement artefacts and a distribution of the correlation coefficient was obtained for different values of SAR.

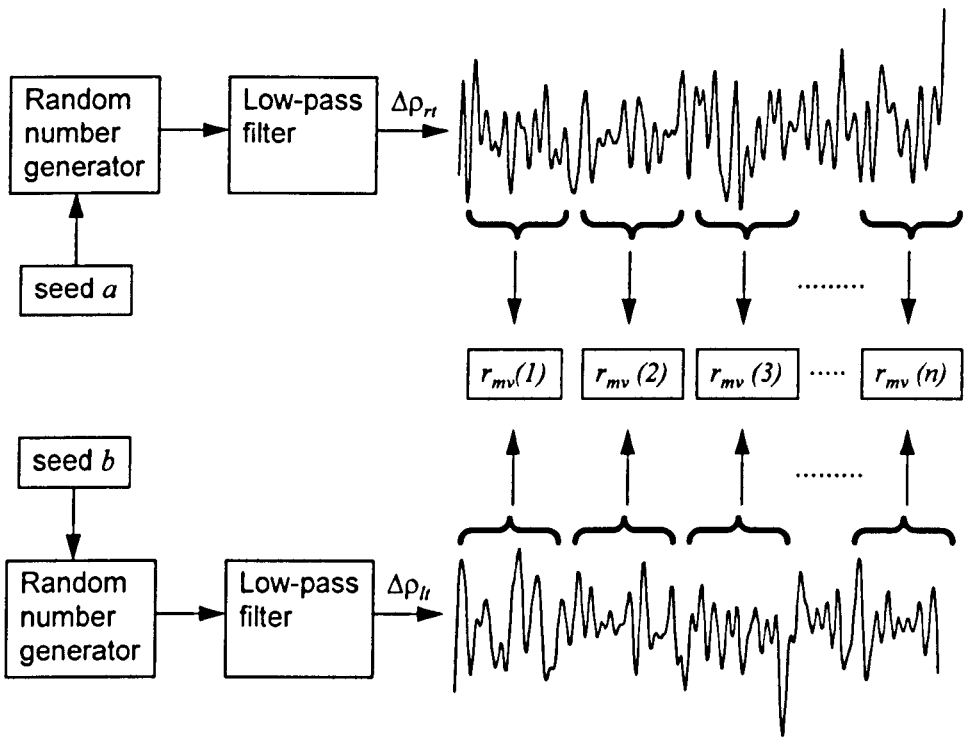

Figure 5.10 *The process for generating samples of r_{mv} in case 2 for calculating its distribution.*

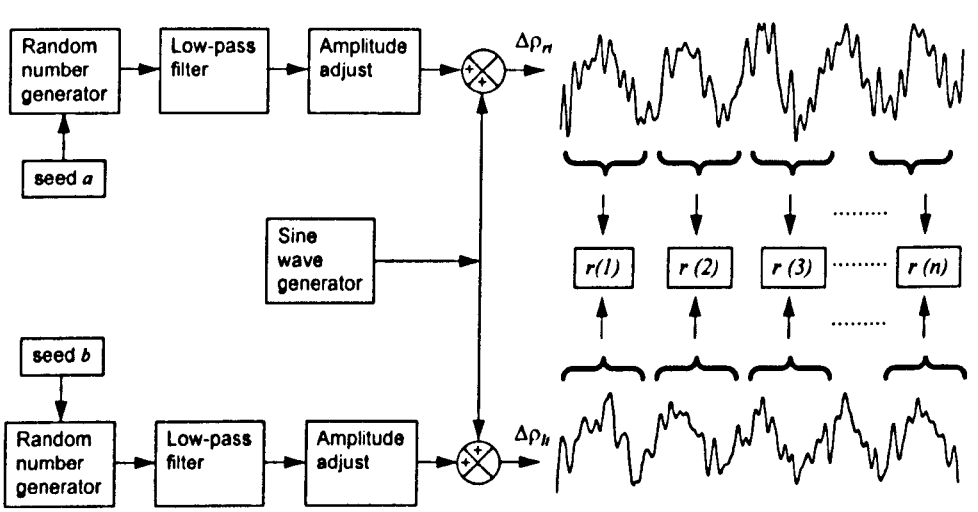

Figure 5.11 *The process for generating samples of r in case 3 for calculating its distribution.*

5.4.3. Simulation studies: results

Let us first consider the results in case 2. The first task was to find the distribution of the correlation coefficient (r_{mv}) between the two simulated movement artefacts in the absence of breathing. Figure 5.12 shows a histogram plot of 1000 values for r_{mv}. The length of the data used to calculate r_{mv} was 100 points. This was equivalent to 4 s at the assumed sampling frequency of 25 Hz, and this time period of 4 s was equivalent to 1 breathing cycle for a breathing rate of 15 breaths min^{-1}. The cut-off frequency of the digital low pass filter used to filter the two simulated movement artefacts before calculating r_{mv}, was equal to 10 Hz. It can be seen from this plot that the distribution is normal and can be represented by a curve as shown by a thick line. A test based on 68-95-99.7 rule was also carried out to confirm the normality of the observed distribution (Moore and McCabe, 1993). Furthermore, the spread of the distribution can be characterised by standard deviation (s_{mv}).

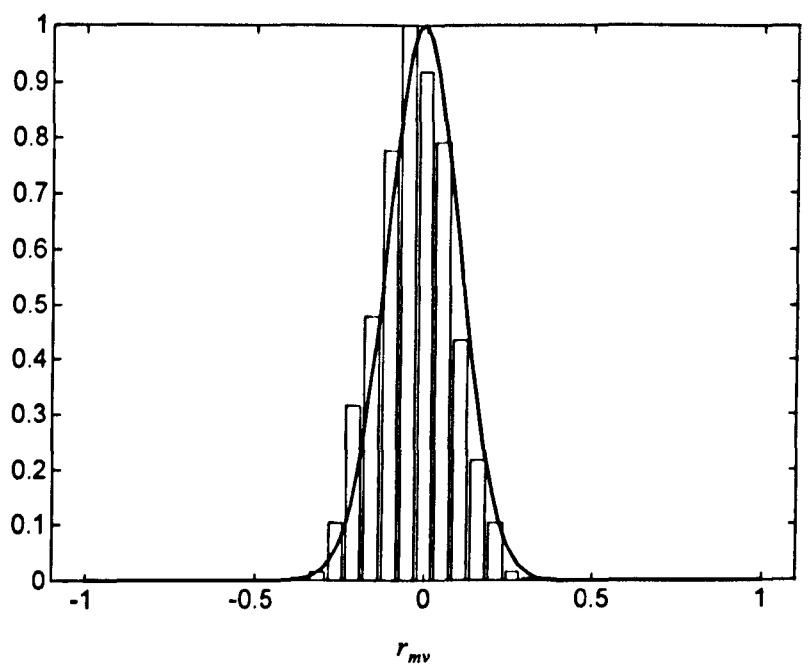

Figure 5.12 Histogram plot and normal distribution curve (thick line) for the distribution of r_{mv} (length of data = 4 s, cut-off frequency of LPF = 10 Hz)

Figure 5.13 shows the distribution curves for three different values of cut-off frequency. The length of the data used for these calculation was constant and equal to 4 s. Each curve is normalised with its maximum value. It can be seen that the spread of the distribution of r_{mv} increases as the cut-off frequency decreases.

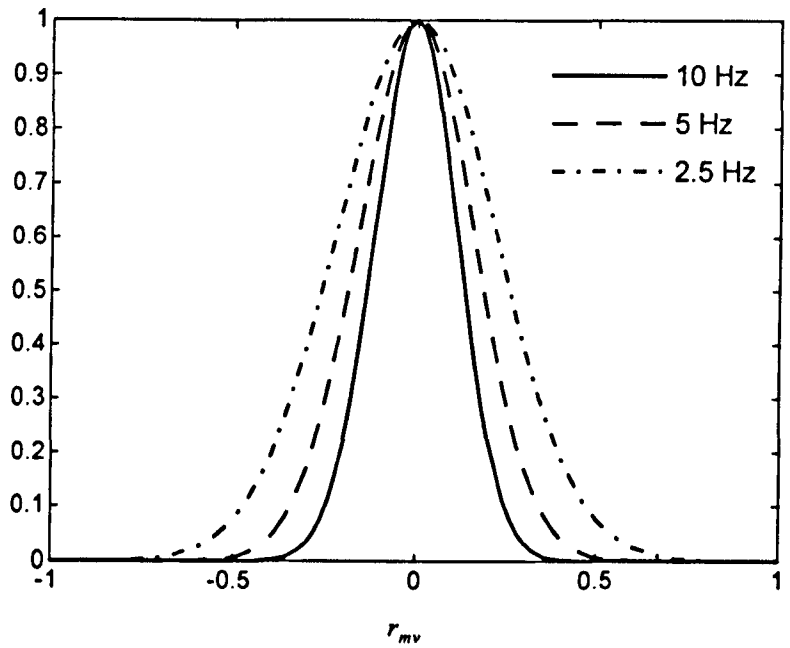

Figure 5.13 Normal distribution curves for r_{mv} for three different cut-off frequency values of the LPF used (length of data = 4 s). Each curve is normalised by its maximum value.

These distribution curves were also obtained using three different lengths of data. The cut-off frequency used for filtering the data was constant and equal to 10 Hz. Figure 5.14 shows the distribution curves for three different lengths of data. It can be seen that the spread of the distribution curve decreases as the length of the data increases.

Now, let us look at the results in case 3, i.e. when breathing as well as movements were assumed to be present. The cut-off frequency of the LPF was chosen to be 2.5 Hz because this frequency had the maximum spread for the distribution of r_{mv}. The distribution of the correlation coefficient (r) in case 3 was obtained at 6 different values of SAR. The length of data used for these

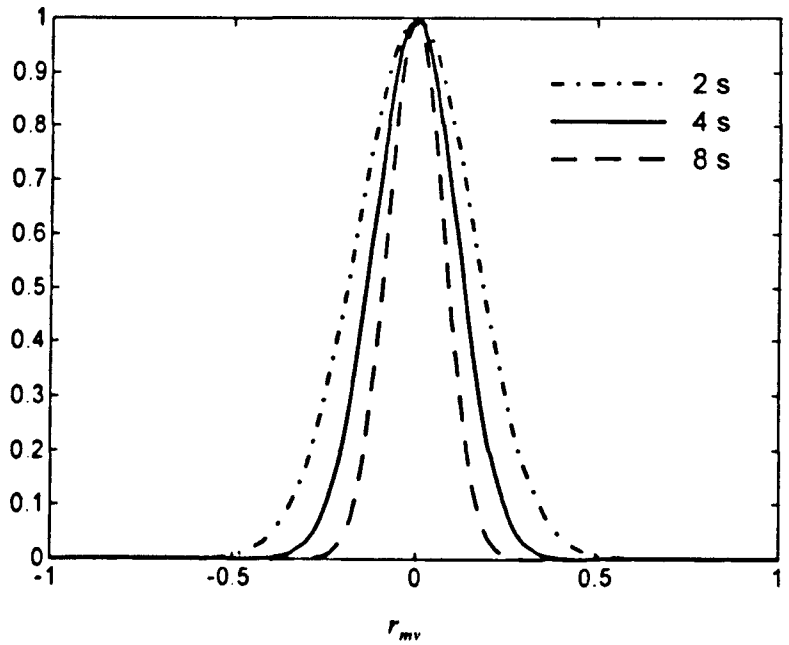

Figure 5.14 *Normal distribution curves for r_{mv} for three different lengths of data at a fixed cut-off frequency values of the LPF equal to 10 Hz. Each curve is normalised by its maximum value.*

calculations was equal to 4 s. Figure 5.15a shows the histogram plots for 1000 values of r for three different values of SAR greater than zero. This figure also shows the positive half of the distribution curve for r_{mv} of case 2.

It can be seen that when SAR is high, the values of r are distributed very close to 1. As the SAR reduces the spread of the distribution of r increases. For reasonably higher values of SAR (> 5 dB) the distribution of r and the distribution of r_{mv} do not overlap significantly. Thus, at these values of SAR it would be possible to detect breathing almost all the time even in the presence of movements. Figure 5.15b shows the histogram plots for r for SAR equal to and smaller than 0 dB. It can be seen that for these values of SAR, the histogram plots overlap considerably with the distribution curve of r_{mv}.

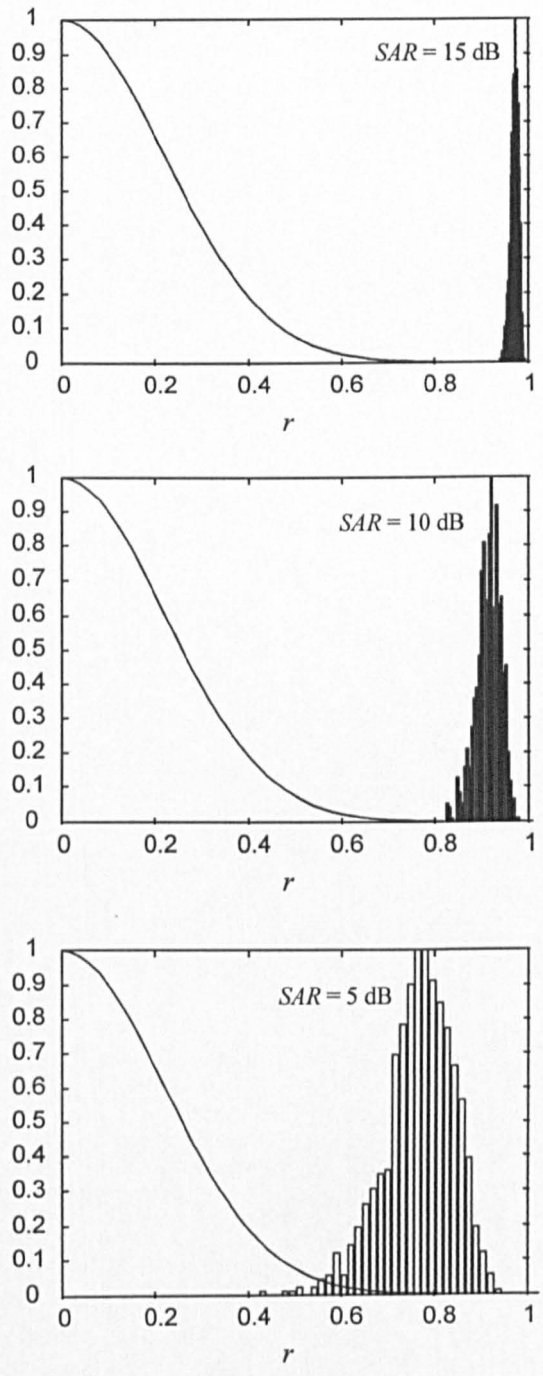

Figure 5.15a Positive half distribution plot for r_{mv} in case 2 (line) and histogram plot for r in case 3 at different SAR values

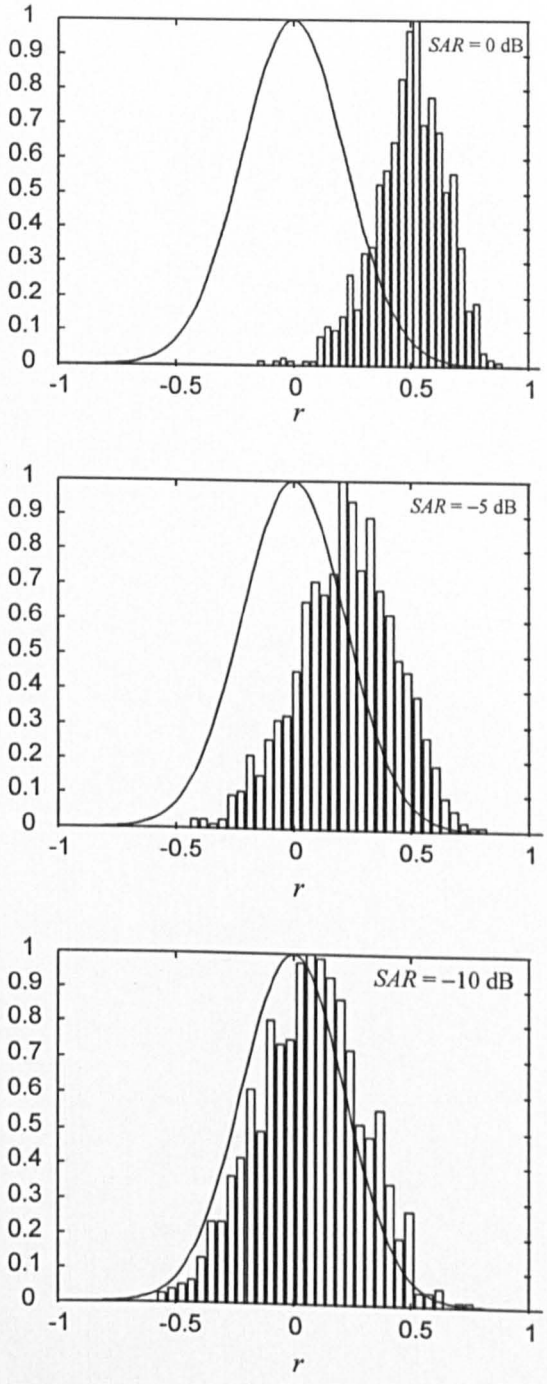

Figure 5.15b Distribution plot for r_{mv} in case 2 (line) and histogram plot for r in case 3 at different SAR values

5.4.4. Simulation studies: discussion

The purpose of these simulation studies was to find out a threshold value for SAR below which it would not be possible to detect breathing in the presence of movements using the correlation coefficient. It can be seen from Figure 5.15 that if the SAR drops below a value of 5 dB, the distributions of the correlation coefficients in the absence of breathing (r_{mv}) and in the presence of breathing (r), start to overlap. Therefore, below this value of SAR, it would not be possible to successfully detect breathing in the presence of movements. In practice, it would be desirable to have a lower threshold for SAR so that it would be possible to detect breathing even if the movement artefacts are high. This threshold can be low if the spread of the distribution of the correlation coefficient (r_{mv}) is low.

It has been observed that the spread of the distribution of r_{mv} reduces as the frequency content of the movement artefacts increases (Figure 5.12). This means that it would be easier to detect breathing if movements occur more rapidly. However, in practice, it would neither be possible to predict nor to control the speed at which movements would occur. Therefore, we may have to assume that movements would occur at a slow speed and hence, the spread of the distribution of r_{mv} would be much higher.

It has also been observed that the spread of the distribution of r_{mv} would reduce with increase in the length of the data used to calculate r_{mv} (Figure 5.13). Therefore, we may want to use longer stretches of data to calculate r_{mv}. However, if we consider the fact that it would be necessary to detect loss of breathing during apnoea as soon as possible, then we may not be able to use very long stretches of data. Apnoea is defined as absence of breathing for 20 s (AAMI, 1989). However, it would be necessary to sound an alarm much earlier than this time period. We may assume that a maximum allowed time would be not more than 4 s, which has been used as the length of the data in the present analysis. Therefore, 5 dB will have to be the threshold for SAR, below which it would not be possible to detect breathing in the presence of movements.

5.5. Breath detection using impedance imaging: experimental studies

The results of the simulation studies described in the previous section indicated that the threshold value of SAR, below which it would not be possible to reliably detect breathing using the correlation coefficient, was 5 dB. The purpose of the experimental studies was to find out the actual value of SAR by recording impedance data from human subjects.

The data plotted in Figure 5.7 was for one subject and was obtained by carrying out ROI analysis on an EIT image generated using a 16-electrode array. In this project, it was decided as a strategy that the movement artefact reduction would be achieved using a minimum number of electrodes. Therefore, the conventional EIT imaging, normally based on a 16-electrode array, was considered unsuitable. Therefore, an image reconstruction technique based on the sensitivity method and requiring only 6 electrodes was developed. This is described in the following sub-section.

5.5.1. A six-electrode sensitivity reconstruction method

A change in internal conductivity distribution of any volume conductor such as the thoracic cavity, can be related to the transfer impedance measurements made at the surface by the sensitivity method. This sensitivity method was used in the theoretical studies described in the previous chapter and a derivation of the mathematical expression of the sensitivity method has been given in that chapter. The linearised sensitivity relationship in a matrix form for a volume conductor, discretised into small elements of uniform conductivity, was given in equation 4.21 and is repeated below.

$$\Delta Z = \mathbf{S}\Delta\sigma \qquad 5.2$$

where,
ΔZ = change in boundary measurements
$\mathbf{S}$ = the Sensitivity Matrix
$\Delta\sigma$ = change in conductivity distribution

An image reconstruction involves determining the change in conductivity distribution ($\Delta\sigma$) for a given change in the measured boundary voltages (ΔZ). In mathematical terms this can be expressed as,

$$\Delta\sigma = \mathbf{S}^{-1}\Delta Z \qquad 5.3$$

where,
$\mathbf{S}^{-1}$ = inverse of the Sensitivity Matrix

It is possible to determine $\Delta\sigma$ with reasonable accuracy if $\mathbf{S}$ can be determined accurately and a stable inverse of $\mathbf{S}$ can be obtained. In order to determine $\mathbf{S}$ with a good accuracy for a particular volume conductor, it is necessary to precisely know the shape of the volume conductor and the location of the electrodes. In practice, it is difficult to measure the shape of the thoracic cavity and the location of the electrodes in human subjects, especially in a clinical environment. Therefore, it is difficult to determine $\mathbf{S}$ with the required accuracy. To overcome this problem, the fractional change in boundary measurements ($\Delta Z/Z$) can be used to reconstruct a fractional change in the conductivity distribution ($\Delta\sigma/\sigma$). The errors introduced due to difference in shape and location of the electrodes are expected to affect ΔZ and Z in the same way and hence, would tend to cancel or at least reduce in $\Delta Z/Z$. As a result the reconstruction is modified to,

$$\frac{\Delta\sigma}{\sigma} = \mathbf{F}^{-1}\frac{\Delta Z}{Z} \qquad 5.4$$

where,
$\mathbf{F}^{-1}$ = inverse of a Normalised Sensitivity Matrix

The normalised sensitivity matrix $\mathbf{F}$ can be obtained by dividing each element (S_{ij}) of the sensitivity matrix $\mathbf{S}$ corresponding to i^{th} drive-receive combination and j^{th} element, by the boundary measurement (Z_i) for the i^{th} drive-receive combination.

In the present study, a two-dimensional FEM model having a shape similar to the thoracic cavity shape was used to determine $\mathbf{S}$. The following subsection describes the steps involved in the development of this model.

5.5.2. A realistic shape FEM model of the thoracic cavity

In order to obtain the sensitivity matrix for the thoracic cavity, a model of the thoracic cavity was developed using FEM. A simplified cylindrical three dimensional model of the thoracic cavity was used in the theoretical studies carried out in the previous chapter. However, in order to make the model more realistic in terms of shape and conductivity distribution, a different FEM model, having an idealised thoracic cavity shape was developed in this study. The geometry of the internal organs was modelled on the actual shapes of the internal organs as suggested by (Coutland *et al*, 1997). The internal conductivity distribution of this FEM model was also assumed to be similar to the actual internal conductivity distribution of the thoracic cavity. However, it was thought that developing such a model in three dimensions was not a simple task. Therefore, the model used in this study was a more simple two-dimensional model.

Figure 5.16 shows the two dimensional model with four distinct regions, the two lungs, the heart and the surrounding tissues. The elements belonging to these regions were assigned different conductivity values as shown in Figure 5.16. These values were at 10 kHz and were obtained from Gabriel *et al* (1996). The conductivity of the surrounding tissues was calculated as an average of the longitudinal and the transverse conductivity values of the skeletal muscles. It was only necessary to maintain the ratio of the conductivity values of different regions rather than using the actual values. Therefore, all the values were expressed with respect to conductivity of the surrounding tissue. The conductivity of the heart region was assigned a much higher value because it was assumed to be filled with blood. The 6 electrodes (e_1 to e_6) were assumed to be equally spaced and placed at locations shown in Figure 5.16.

The model was meshed into 3642 quadrilateral elements. The potential distribution in the form of nodal voltages for each of the 6 adjacent electrode pairs was obtained by solving the FEM equations. The sensitivity coefficient (S_{ij}) for i^{th} drive-receive combination and for j^{th} element was obtained from the nodal voltages on the basis of equations 4.22 and 4.23, given Chapter 4.

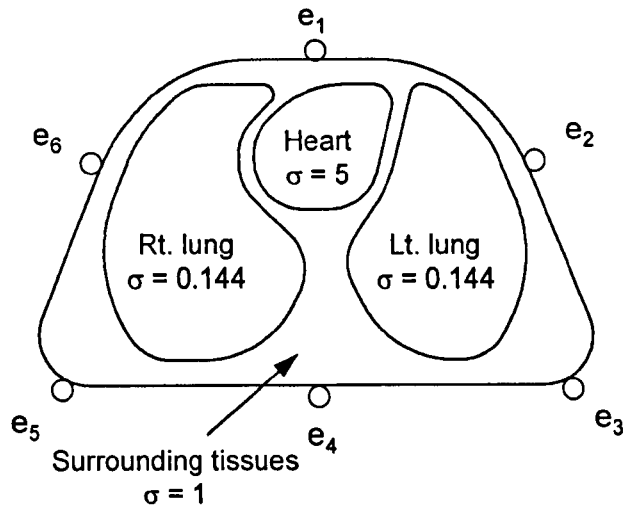

Figure 5.16 *The idealised shape FEM model with 4 regions and the corresponding conductivity values. The 6 equally spaced electrodes (e_1 to e_6) are also shown.*

The 6-electrodes produced 9 independent measurements ($N(N-3)/2$, $N = 6$) according to the adjacent drive - adjacent receive data collection protocol used in EIT. Therefore, the size of the sensitivity matrix $\mathbf{S}$ was 9 × 3642. This was a highly underdetermined case. In addition, this matrix and hence the normalised sensitivity matrix $\mathbf{F}$ was expected to be ill-conditioned (Metherall, 1998). This ill-conditioned nature of matrix $\mathbf{F}$ posed a difficulty in obtaining its stable inverse required for faithful reconstruction. In order to overcome this problem, a method suggested by Metherall (1998) was used. In this method a sensitivity coefficient for the entire region was obtained by summing the sensitivity coefficients of the elements belonging to that region. As only four regions were defined in the model, the size of $\mathbf{S}$ and hence, of $\mathbf{F}$, was reduced to 9 × 4. This was an overdetermined case and the pseudo-inverse $\mathbf{F}^{\dagger}$ for this matrix could be written as,

$$\mathbf{F}^{\dagger} = (\mathbf{F}^{t}\mathbf{F})^{-1}\mathbf{F}^{t} \qquad 5.4$$

where,
t = denotes transpose of a matrix

It was observed that the condition number of $\mathbf{F}'\mathbf{F}$ reduced from 2.26×10^3 for the underdetermined case to 106.17 for the overdetermined case. Thus, it was possible to obtain a stable inverse of a small and well conditioned matrix $\mathbf{F}'\mathbf{F}$. The reconstruction could be mathematically expressed as,

$$\left(\frac{\Delta\sigma}{\sigma}\right) = (\mathbf{F}'\mathbf{F})^{-1}\mathbf{F}'\left(\frac{\Delta Z}{Z}\right) \qquad 5.5$$

5.5.3. Data collection and processing

The impedance data was collected on 2 normal human subjects. A Sheffield Mark 2 REIT system was used for data collection (Smith *et al*, 1995). This system recorded data using an adjacent drive - adjacent receive protocol from 16 electrodes. However, for this study it was necessary to obtain data corresponding to a 6 electrode array. Therefore, superposition was used to derive the 6-electrode data from the 16-electrode data. The electrodes were placed around the thoracic cavity at the level of the nipples. The 6 electrodes of interest to this study had an equal spacing and the remaining electrodes out of total 16 electrodes were placed evenly between these 6 electrodes.

The subjects were asked to carry out tidal breathing for the first 30 s without movements in an upright sitting position. During the following 30 s, the subjects were asked to hold their breath at the level of maximum inspiration and carry out movements. The movements were performed as a random combination of arm movements and torso movements to simulate natural movements of the patients, that may occur in a typical clinical environment.

The recorded 16-electrode data was first converted to the required 6 electrode data. This data was normalised to obtain $\Delta Z/Z$ and then used to reconstruct the images of $\Delta\sigma/\sigma$. Finally, SAR was calculated using equation 5.1.

5.5.4. Results of the 6-electrode impedance imaging

Figure 5.17a shows a plot of $\Delta\sigma/\sigma$ for the four regions of the image for one subject. It can be seen that the reconstruction process is able to separate reasonably well, the breathing related conductivity changes occurring within the two lung regions from the conductivity changes occurring within the heart and the peripheral tissues. This was also true for the second subject as seen from Figure 5.17b.

The correlation coefficients were obtained between the two signals originating from the two lung regions during tidal breathing in the absence of movements (0 to 30s) as well as during breath hold and movements (30s to 60s). A 4 s second non-overlapping window was used to calculate the correlation coefficient and the 6 values of the correlation coefficients were obtained within a time period of 24 s. All these values were found to lie close to 1. On the other hand, the 6 values of the correlation coefficients obtained during the subsequent epoch of 24 s were distributed in the range of −1 to 1. The range of the correlation coefficients for each subject during only breathing and only movements is stated in Table 5.2. From this results it was possible to achieve the first step of identifying the presence of movements using the correlation coefficient.

Table 5.2 *The range of values of correlation coefficient (r) for breathing and breath hold + movements*

Subject	Tidal breathing	Breath hold + Movements
NK	$0.974 < r < 0.995$	$-0.279 < r < 0.887$
AW	$0.979 < r < 0.997$	$0.199 < r < 0.956$

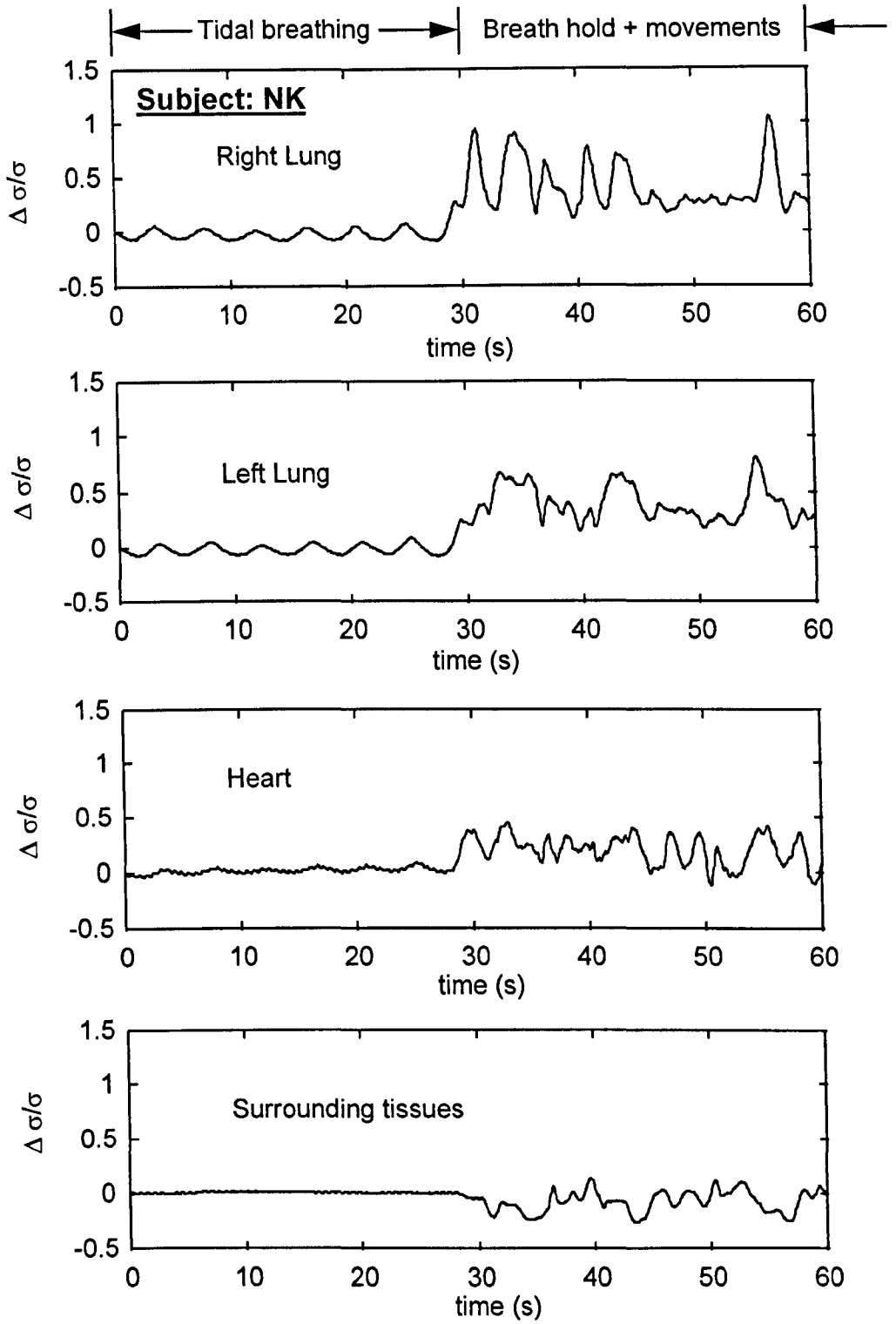

Figure 5.17a Plot of normalised conductivity changes obtained from each of the 4 regions from the image for Subject NK

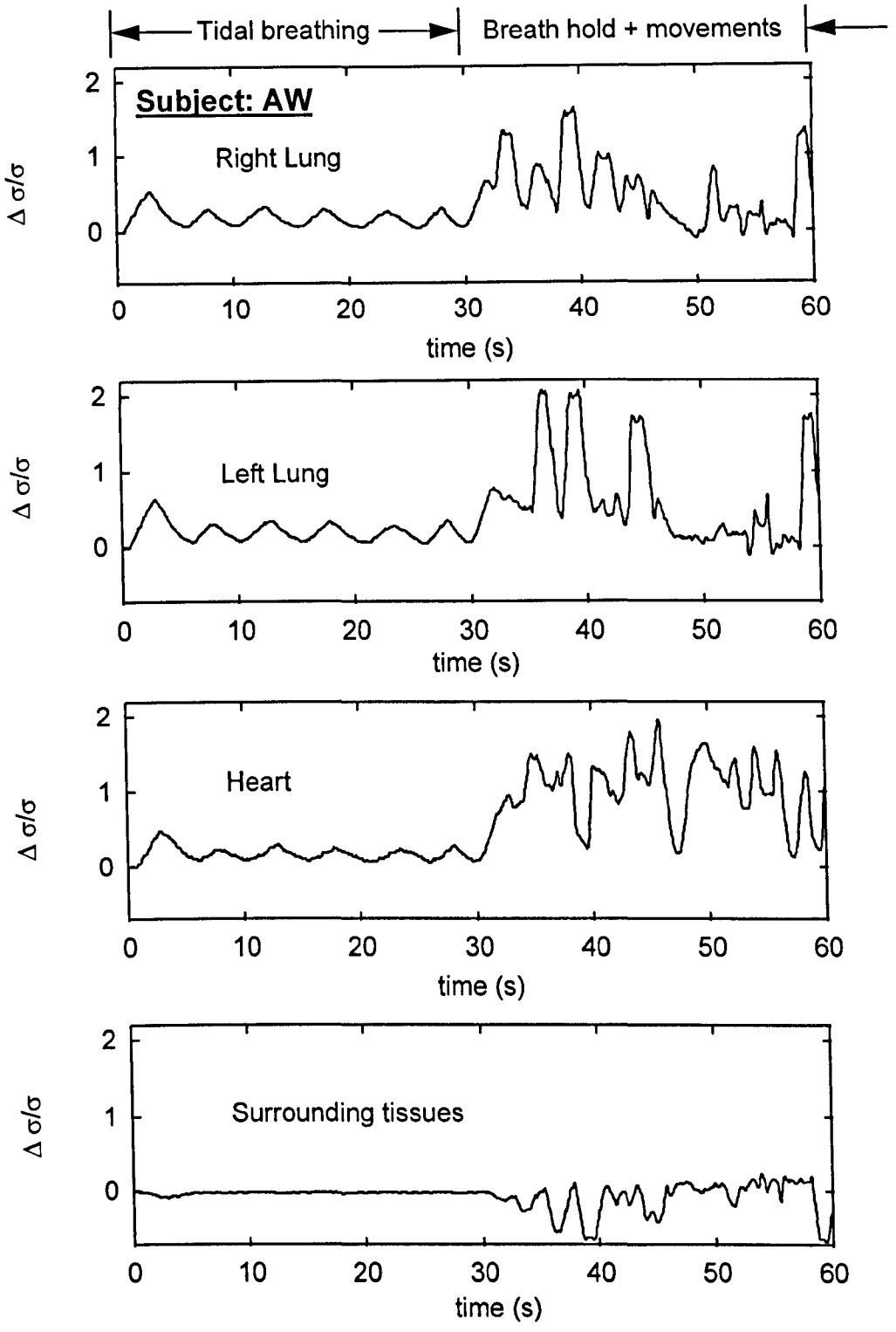

Figure 5.17b Plot of normalised conductivity changes obtained from each of the 4 regions from the image for Subject AW

The purpose of this study was also to find the values of *SAR* for the experimental data and to see whether they were below the threshold value of 5 dB so that it would be possible to detect breathing even in the presence of movements. Table 5.3 shows the *SAR* values in dB for each subject and for the left and the right lung region.

Table 5.3 *The values of SAR for the normalised changes in conductivity measured from the right and the left lung regions*

Subject	*SAR* for Right lung region (dB)	*SAR* for Left lung region (dB)
NK	−15.34	−12.62
AW	−11.27	−13.39

It can be seen that these values are much lower than the threshold value of 5 dB obtained from the simulation studies. This, indicates that it would not be possible to detect breathing in the presence of movements using this method and a significant increase in *SAR* would be required.

These low values of *SAR* obtained in both the subjects indicate two possibilities. Firstly, the sensitivity of the impedance measurements to changes in lung resistivity could be low. The electrode placement used for the 6-electrode imaging was co-planar electrode placement. It was suggested in the previous chapter that in order to obtain maximum sensitivity to lung resistivity changes, it would be necessary to place the drive and the receive electrode pairs in two different horizontal planes. Thus, one way of increasing the *SAR* would be to use the 6-electrode optimum configuration suggested in the previous chapter and develop a 3d model to generate the sensitivity matrix.

Secondly, the *SAR* could be low due to higher sensitivity of the impedance measurements to other factors such as shape changes and electrode placement. The measured impedance data was normalised to reduce the effect of difference between the model and the thoracic cavities of human subjects, in terms of

shape and electrode locations. However, this normalised data was referenced to the first frame (time = 0 s) of each data set. Thus, it can be seen from the experimental results (Figure 5.17) that during the first 30 s, i.e. when the movement was absent, the shape as well as the electrode locations remained the same as that for the first reference frame. Therefore, the reconstruction produced good results. However, during movements, the shape as well as the electrode locations seemed to change. As a result the model would become invalid causing the reconstruction to fail introducing large artefacts. This indicates that, this impedance based imaging technique of breath detection is sensitive to changes in shape and electrode locations, and unless this sensitivity is reduced it would not be possible to detect breathing in the presence of movements using this technique.

5.6. Discussion

The aim of the work described in this chapter was to understand various aspects of the problem of movement artefacts in impedance pneumography. A review of the work carried out by researchers in the past to develop different techniques of movement artefact reduction was presented at the beginning of this chapter.

In the first category, there were studies aimed at identifying an electrode configuration, type, and placement that would have low movement artefacts. The two-electrode configuration was used in a majority of the studies because it was the most simple configuration and involved fewer connections. Thus, this configuration was also used in the majority of commercial apnoea monitors. However, in a two electrode configuration, the electrode-skin contact impedance is one of the sources of movement artefacts. In this case, the electrode-skin contact impedance is an inseparable component of the measured impedance and undergoes unpredictable changes when the electrode-skin interface is mechanically disturbed during movements. These changes in the impedance manifest as artefacts in the measured signal.

It is possible to significantly reduce these artefacts by using a four-electrode configuration. In a four-electrode configuration, a constant current circuit is used

to inject current through the drive electrodes and hence, its amplitude is not affected by the variations in electrode-skin contact impedance. The voltage is measured using a separate pair of receive electrodes. If the input impedance of the voltage measuring circuit is sufficiently high, then the artefact due to electrode-skin contact impedance is considerably reduced. Therefore, even though a four-electrode configuration requires additional connections, using it would be a first step towards reducing movement artefacts.

The studies carried out to compare electrodes of different type for their ability to monitor breathing in the presence of movements, indicated that electrodes having a good adhesion to the skin were best suited for the purpose because such electrodes did not come loose during movements. The studies aimed at identifying the most suitable electrode placement indicated that when electrodes were placed on the sternum and on the back, the measurements were least affected by movement artefacts.

There have also been studies aimed at reducing movement artefacts using multi-frequency measurements. However, in a majority of these studies a two electrode configuration was used and therefore the observed reduction in movement artefacts with increasing frequency seemed to be due to reduction in electrode-skin contact impedance with frequency. Therefore, it is not obvious in what way multi-frequency measurements would help when a four-electrode configuration is used. If we assume movements as changes in geometry of the thoracic cavity, then the artefacts introduced by these movements would be a constant fraction of the base impedance. On the other hand, it has been observed in the EITS research that the fractional changes in lung impedance due to breathing increase with increase in frequency. Therefore, it might be possible to differentiate between the two using multi-frequency measurements.

This chapter also described some preliminary studies carried out to evaluate three types of electrodes for their ability to measure thoracic impedance in the presence of movements. It was observed that Conmed 2045 electrodes had the strongest adhesion to the skin and hence did not come loose even during fast movements. Therefore, these electrodes appeared to be the most suitable for

the purpose. A preliminary study was also carried out to compare the most commonly used midaxillary electrode placement with the sternum-to-back electrode placement suggested in the literature to have low movement artefacts. It was found that the amplitude of movement artefacts was much lower in the case of the sternum-to-back electrode placement. It appeared that in this electrode placement, the electrodes were located at a maximum distance from both the arms and therefore, were least affected during arm movements. On the other hand, the electrodes placed on the midaxillary line appeared to move through a considerable distance along with the skin during arm movements and this seemed to cause large artefacts.

A study was also carried out to develop a technique based on impedance imaging to detect breathing in the presence of movements. This study was based on the observation that breathing related resistivity changes observed within a region-of-interest defined over the two lungs in an EIT image correlated well, but those due to movements did not correlate. The simulation studies indicated that by calculating a correlation coefficient between the two signals it was possible to detect breathing in the presence of movements only if the Signal-to-Artefact Ratio (SAR) was higher than 5 dB.

An experimental study was carried out to find out the actual value of SAR. A sensitivity based image reconstruction algorithm was developed for this purpose. The sensitivity matrix was computed using a two dimensional FEM model having a shape and internal conductivity distribution similar to that of the thoracic cavity. It was possible to detect occurrence of movements using this method. However, SAR for the experimental data was too low and therefore, it was not possible to detect breathing in the presence of movements using the correlation coefficient. This low value of SAR suggested that the impedance measurements obtained from the 6-electrode co-planar placement were less sensitive to the lung resistivity changes and were more sensitive to changes in shape and electrode locations. Therefore, the reconstruction failed during movements introducing large artefacts. This indicated that there was a need to significantly reduce the

amplitude of movement artefacts in quantitative terms even for detecting the presence or absence of breathing using the correlation coefficient method.

The results of the studies described in this chapter seemed useful in providing some insight into the sources of movement artefacts, and also provided some hints to decide a strategy for reducing them. The movement artefacts seemed to originate from three different sources as,

1. Electrode-skin interface impedance
2. Geometrical changes of the thoracic cavity
3. Movement of electrodes along with the skin

The effect of electrode-skin contact impedance can be effectively reduced by using a four-electrode configuration instead of a two-electrode configuration. It might be possible to reduce the effect of geometrical changes by carrying out impedance measurements at more than one frequency. This aspect was investigated in the present project and the associated experimental work has been described in the following chapter. The effect of electrode movement could be reduced by placing the electrodes at locations where they might undergo least movement. This aspect was also investigated and is described in the following chapter.

The three measures noted above were mainly aimed at reducing the movement artefacts. However, it was also important to take steps to increase the amplitude of breathing related changes so that SAR would be maximised. This meant that the choice of electrode placement should be such that it would have maximum sensitivity to lung resistivity changes and minimum sensitivity to geometrical changes. Such an 'optimum' electrode placement was obtained by carrying out experimental and theoretical work in the beginning of this project as described in Chapter 3 and Chapter 4, respectively. Therefore, experimental study was carried out to measure thoracic impedance using the optimum electrode placement during breathing as well as movements to find out whether this

placement produced maximum SAR. This experimental study is described in the following chapter.

Chapter 6. Movement artefact reduction using strategic placement of electrodes

6.1. Introduction

The results of the experimental studies described in the previous chapter suggested that unless a significant quantitative reduction in the amplitude of movement artefacts was achieved, it was not possible to detect breathing in the presence of movements. In other words, it meant that it was necessary to maximise the Signal-to-Artefact Ratio (SAR), defined as a ratio of breathing related impedance changes to movement artefacts. It would be possible to maximise SAR by either maximising the breathing related impedance changes or minimising movement artefacts or both.

In Chapter 4, a 6-electrode configuration was proposed as an optimum electrode configuration. The main feature of this configuration was that it had the drive and the receive electrode pairs in different horizontal planes. This configuration was considered optimum because the measurements obtained using this configuration were expected to have a maximum fractional change in impedance during breathing. The next step in this project was to find out whether the measurements obtained from this electrode configuration also had low movement artefacts. The aim of the experimental work described in this chapter was to measure the thoracic impedance on human subjects using the 6-electrode optimum configuration and thus, experimentally determine SAR for this configuration.

It was noted in the literature review presented in the beginning of the previous chapter that it may be possible to use multi-frequency measurements for movement artefact reduction. This aspect was also investigated in the present project and is described in the later part of this chapter.

6.2. Thoracic impedance measurements using the optimum 6-electrode configuration

6.2.1. Data collection

The thoracic impedance was recorded using the optimum 6-electrode configuration shown in Figure 6.1. A Sheffield Mark 2 REIT system was used for data collection (Smith *et al*, 1995). This system recorded data from a 16 electrode array using an adjacent drive - adjacent receive protocol. However, in this study, it was necessary to measure impedance from the 6-electrode configuration. Therefore, the measurements corresponding to the 6-electrode configuration were obtained from the 16 electrode data on the basis of superposition and reciprocity.

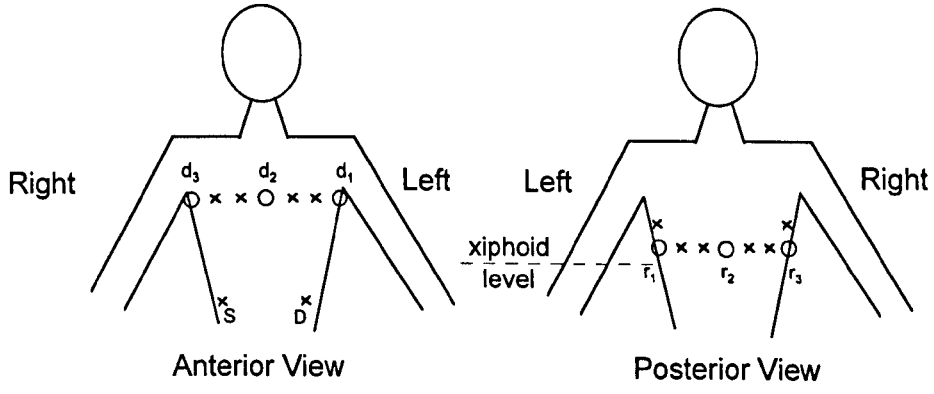

Figure 6.1 The 6-electrode optimum configuration

The placement of electrodes on the thoracic cavity is shown in Figure 6.1. The drive electrodes d_1, d_2 and d_3 were placed in a horizontal plane at the level of the axilla and the receive electrodes r_1, r_2 and r_3 were placed in a horizontal plane approximately 5 cm above the level of the xiphoid process. These two levels were corresponding to plane 4 and plane 2, respectively, of the experimental studies carried out earlier using 64 electrodes and described in Chapter 3 (see Figure 3.7). Electrode d_2, was placed over the sternum and electrodes d_1 and d_3 were placed on the midaxillary line. The receive electrodes r_1 and r_3 were also placed on the midaxillary line and electrode r_2 was placed over the spinal column. The remaining electrodes, out of the 16

electrodes, were placed in between these electrodes at locations marked by a 'cross'. The electrodes 'S' and 'D' were the sense and drive electrodes of the Common Mode Feedback system (Smith *et al*, 1995), which was used to drive the voltage on the body close to ground potential. These electrodes were placed on the abdomen as shown in Figure 6.1. The 4 measurements obtained from this electrode placement are given in Table 6.1,

Table 6.1 The 4-measurements obtained from a 6-electrode optimum placement

Measurement	Drive electrodes	Receive electrodes	Electrode locations
M_1	d_1, d_2	r_1, r_2	electrodes on the left
M_2	d_2, d_3	r_2, r_3	electrodes on the right
M_3	d_1, d_2	r_2, r_3	electrodes on both sides
M_4	d_2, d_3	r_1, r_2	electrodes on both sides

It was planned that the data would be recorded on many subjects. However, some important observations were made from the impedance data recorded on the first subject. Taking into consideration these observations, modifications were made to the electrode placement before recording the data from more subjects. First, the observations obtained on the first subject are discussed.

6.2.2. Preliminary observations on the first subject

Figure 6.2 shows a plot of measurements M_1 and M_2. The subject carried out tidal breathing without any movements during the first 30 s and then carried out a systematic arm movement while holding his breath, during the subsequent 30 s. The systematic arm movements carried out in the experimental studies in this project were described in the previous chapter (Figure 5.5). This arm movement involved moving one arm upwards, on the side, from a lower resting position until it reached a vertical position by the side of the head and then down. This movement was repeated as many times as possible within the period of 30 s.

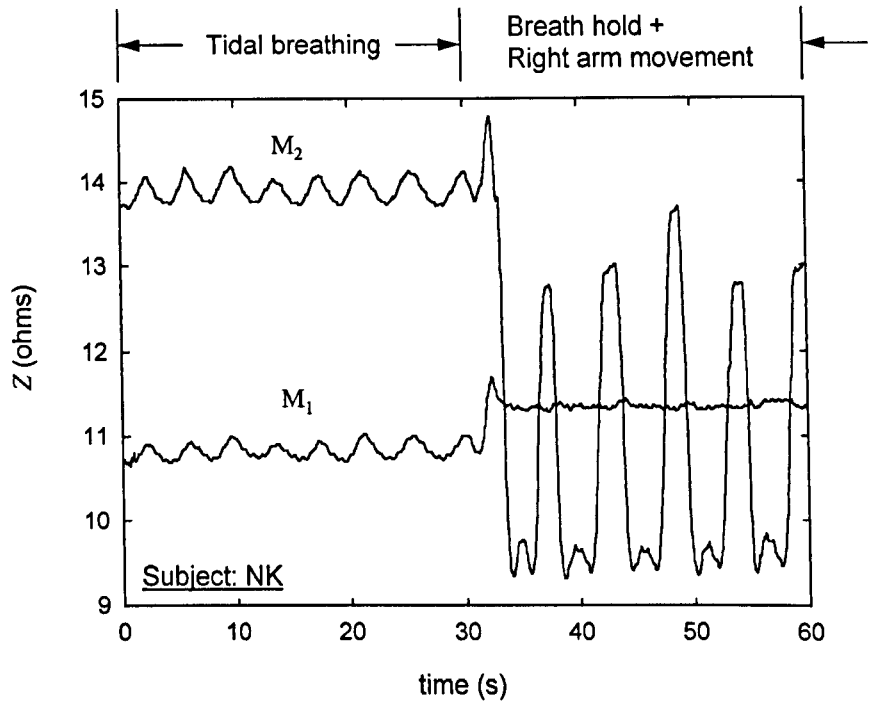

Figure 6.2a *A plot of measurements* M_1 *and* M_2 *for the first subject and obtained during right arm movement. Note that movement artefacts are absent in measurement* M_1

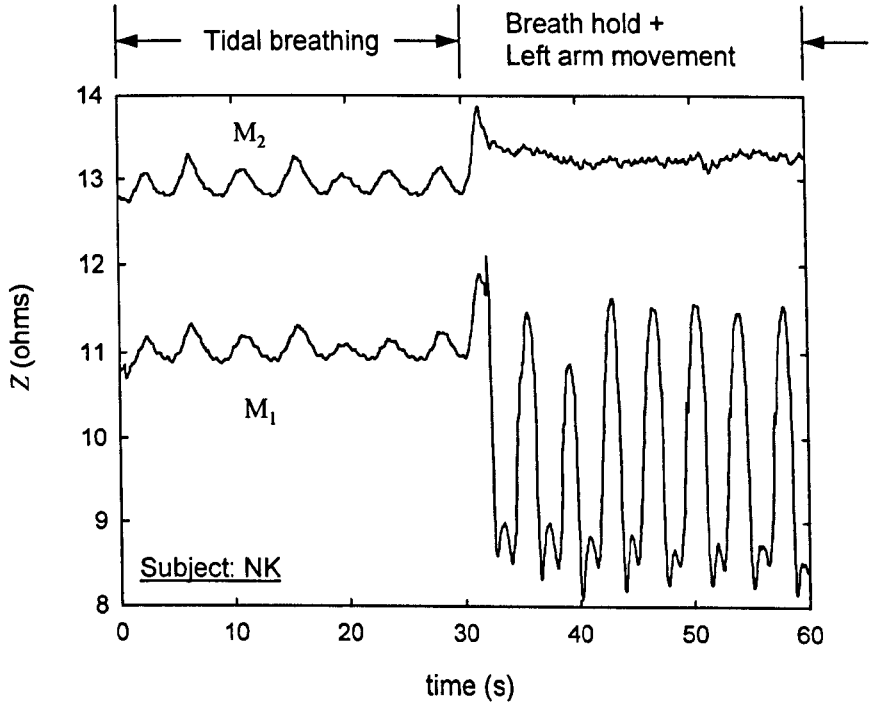

Figure 6.2b *A plot of measurements* M_1 *and* M_2 *for the first subject and obtained during left arm movement. Note that movement artefacts are absent in measurement* M_2

Figure 6.2a shows a plot of measurements M_1 and M_2 during the right arm movement. It was observed that the amplitude of movement artefacts due to movement of the right arm was much higher in measurement M_2 than in measurement M_1. In fact, measurement M_1 was not at all affected by the movement of the right arm. Figure 6.2b shows a plot of the two measurements for the left arm movement. In this case, movement artefacts were only present in measurement M_1 and were absent in measurement M_2. It can be seen from Table 6.1 and Figure 6.1 that the drive as well as the receive electrodes corresponding to measurement M_2 were on the right side of the thoracic cavity while those corresponding to measurement M_1 were on the left side of the thoracic cavity. Thus, these observations indicated that movement artefacts occurred only if the electrodes moved during movements.

A second important observation was that movement artefacts in measurements M_3 were 180° out of phase with movement artefacts in measurement M_4. On the other hand, the impedance changes due to tidal breathing were in-phase in both these measurements. This is shown in Figure 6.3a for the right arm movement and in Figure 6.3b for the left arm movement. Therefore, by simply taking a mean of the two measurements it was possible to reduce movement artefacts without affecting the amplitude of the breathing signal.

It was also observed that the value of $\Delta Z/Z$ during tidal breathing was higher in measurements M_3 and M_4 than in measurements M_1 and M_2. This is seen in Figure 6.4a and Figure 6.4b. Furthermore, the values of SAR for measurements M_3 and M_4 were also higher than those in measurements M_1 and M_2 as seen in Table 6.2. It can be also seen from Table 6.2 that SAR considerably increased when a mean of measurements M_3 and M_4 was obtained.

Thus, from these observations on the first subject, two important points were noted. Firstly, it appeared that movement artefacts were caused by movement of the electrodes along with the skin. Secondly, measurements M_3 and M_4 had a higher $\Delta Z/Z$ as well as higher SAR, and SAR could be further increased by taking a mean of these two measurements. Taking into consideration these

two points a strategy for reducing movement artefacts was decided and a simple 4-electrode configuration was proposed, which was then used to record impedance data from more subjects.

Table 6.2 *The values of SAR for the four measurements for the right and the left arm movements, and also for the mean signal* $(M_3+M_4)/2$.

Measurement	Right arm movement	Left arm movement
	SAR (dB)	*SAR* (dB)
M_1	9.47	-19.04
M_2	-21.25	7.49
M_3	-7.49	-8.31
M_4	-8.25	-7.05
$(M_3+M_4)/2$	7.49	4.39

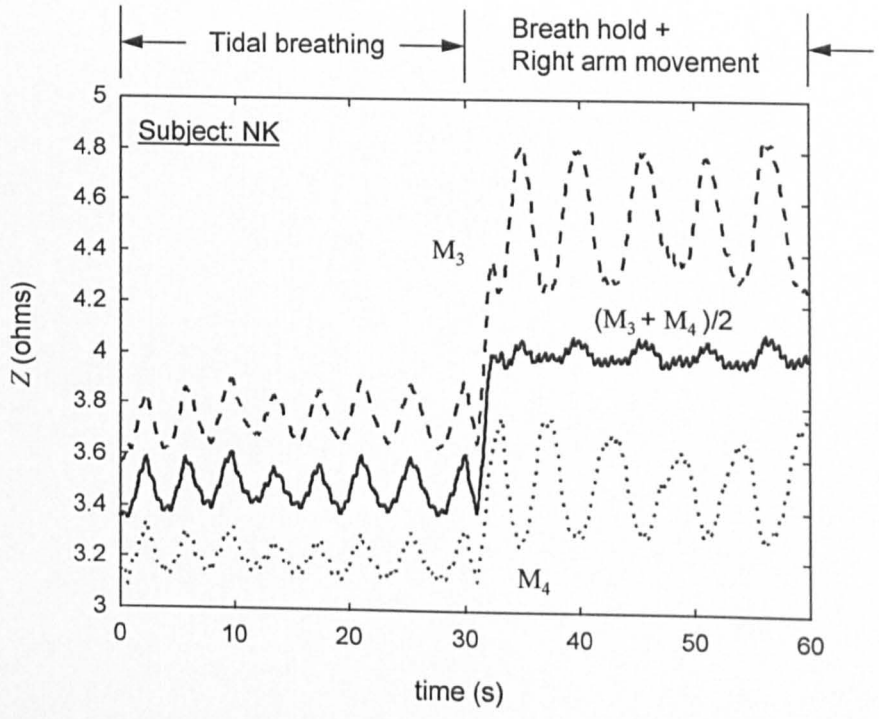

Figure 6.3a *A plot of measurements M_3 and M_4 for the first subject during right arm movement. Note the reduction in movement artefacts in the mean signal $(M_3+ M_4)/2$.*

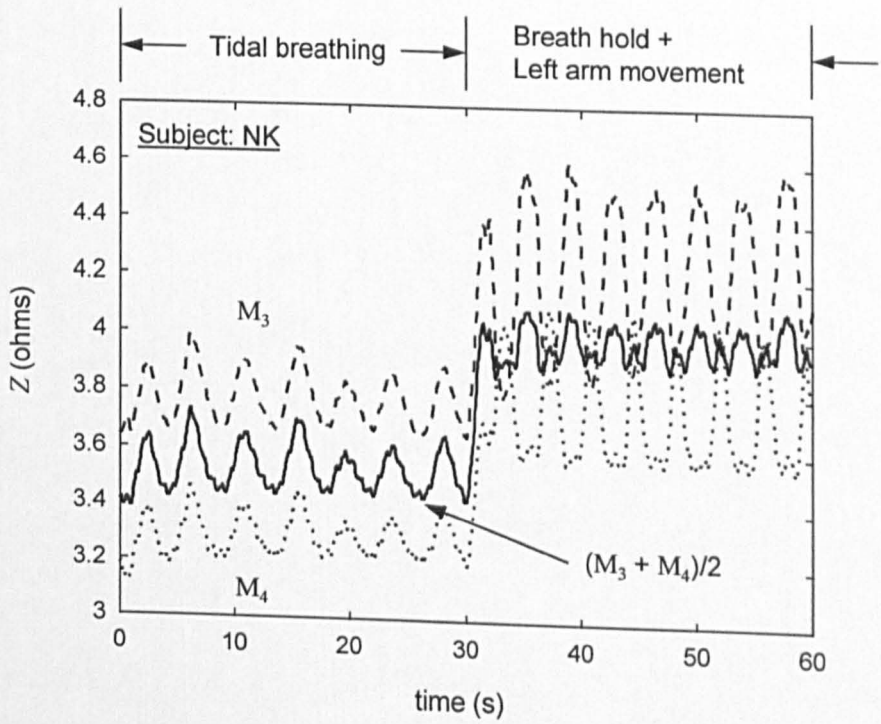

Figure 6.3b *A plot of measurements M_3 and M_4 for the first subject during right arm movement. Note the reduction in movement artefacts in the mean signal $(M_3+ M_4)/2$.*

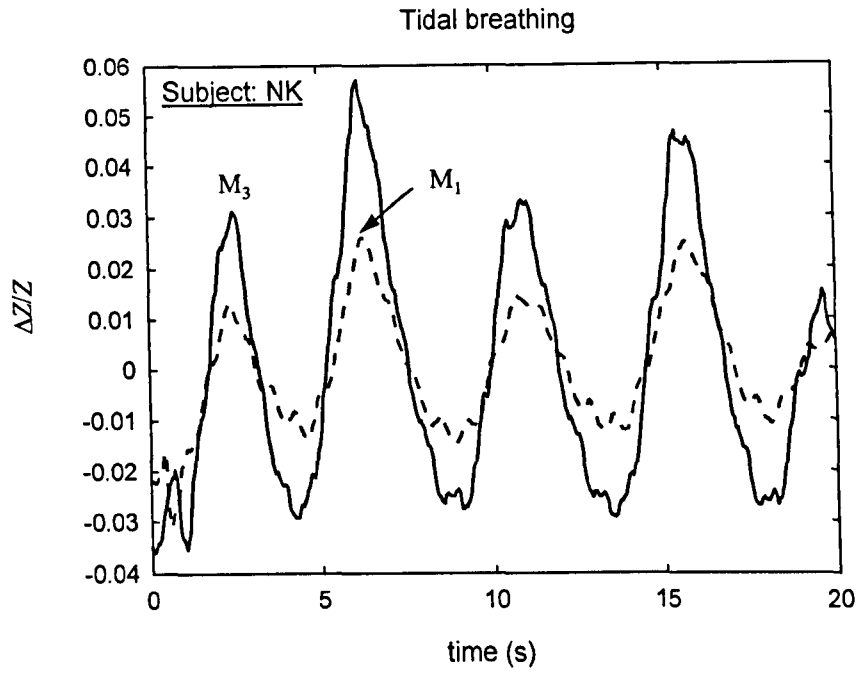

Figure 6.4a *A plot $\Delta Z/Z$ versus time for measurements M_1 and M_3 for the first subject during tidal breathing. Note that $\Delta Z/Z(M_3) > \Delta Z/Z(M_1)$.*

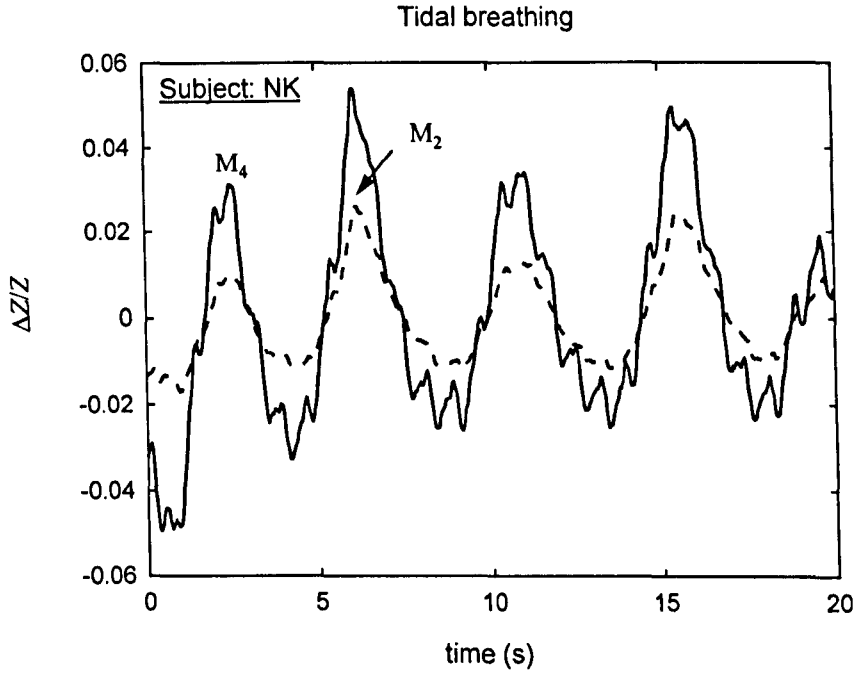

Figure 6.4b *A plot $\Delta Z/Z$ versus time for measurements M_2 and M_4 for the first subject during tidal breathing. Note that $\Delta Z/Z(M_4) > \Delta Z/Z(M_2)$.*

6.3. Movement artefact reduction using a strategic placement of 4 electrodes

The experiments carried out using the optimum 6-electrode configuration on one subject seemed to suggest that movement artefacts were caused by electrodes sliding over the thoracic cavity along with the skin. Based on this observation, a strategy was decided for placing electrodes in such a way that movement artefacts could be reduced.

It appeared that a simple 4-electrode array would be useful for reducing movement artefacts. Figure 6.5 shows a two dimensional circular conductor with four equally spaced electrodes e_1, e_2, e_3 and e_4, and the isopotential lines within this conductor due to current injection between the appropriate pair of electrodes. This arrangement produces two independent measurements A and B. Let us assume that electrodes e_1, e_2 and e_3 are not affected by the movement, but electrode e_4 shifts to a new location marked as e_4' due to movement. As a result, measurement A would increase to a, but measurement B would decrease to b. Thus, it would be possible to reduce movement artefacts by simply adding measurements A and B as they would change in opposite directions. These measurements will be referred to as 'symmetrical

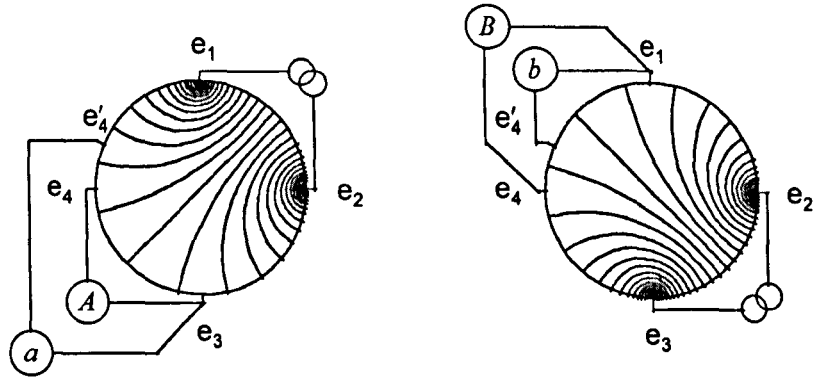

CASE 1
$a > A$
(increase in Z)

Figure 6.5a

CASE 2
$b < B$
(decrease in Z)

Figure 6.5b

Figure 6.5 A two-dimensional conductor with 4 equally spaced electrodes

measurements' and a pair of such measurements will be referred to as a 'symmetrical pair' in the rest of the thesis.

It may be noted that the symmetrical measurements were obtained across the thoracic cavity and hence, would include contribution from the resistivity changes of both the lungs. Thus, in this respect, these measurements were similar to measurements M_3 and M_4 recorded using the optimum 6-electrode configuration. However, at least 3 out of 4 electrodes used to obtain the symmetrical measurements would be in the same plane whereas the drive and the receive electrodes used to obtain measurements M_3 and M_4 were in different planes. Thus, the value of $\Delta Z/Z$ in the symmetrical measurements could be different, and perhaps lower than that observed in measurements M_3 and M_4. However, the purpose of these experimental studies was to find an electrode placement that would reduce movement artefacts rather than only maximise breathing related impedance changes. Therefore, it was considered reasonable to carry out further experiments using this 4-electrode placement because its most important feature was that it would provide reduction in movement artefacts.

6.3.1. Experimental studies using a strategic 4 electrode placement

Impedance measurements were carried out on 5 normal male volunteers (mean age: 30.1 years, range: 27-35 years) using the 4-electrode strategic placement. A Sheffield Mark 2 REIT system was used for the data collection (Smith *et al*, 1995). A circular array of 16 equally spaced electrodes was placed around the thoracic cavity. This electrode array was placed in an oblique plane instead of a horizontal plane because it was thought that such a placement would span the lungs in the vertical direction and hence, would maximise the sensitivity to lung resistivity changes in the vertical direction as well. The two independent measurements A and B were derived using superposition from the 16-electrode data.

The impedance data was recorded during a period of 60 s. The subjects were asked to carry out tidal breathing for the first 30 s and during the following 30 s, they were asked to carry out movements while holding their breath at maximum inspiration. These movements involved a random combination of arm and torso movements rather than systematic movements so that they would simulate natural movements of the patient that may occur in a clinical environment.

6.3.2. Results of the 4-electrode measurements

Figure 6.6a shows a plot of measurements A and B for one subject. It can be seen that during the second epoch of 30 s the two waveforms are out of phase. It can be also seen that a significant reduction in the amplitude of movement artefacts could be obtained by taking a mean of these two measurements. Figure 6.6b shows a plot of measurement B versus measurement A for tidal breathing and for movements with breath hold. These plots and the corresponding correlation coefficients confirm the observation that the impedance changes observed in these two measurements during tidal breathing were in-phase, but they were 180° out of phase during movements. SAR was calculated in dB for the two measurements as well as for the mean of the two measurements. Table 6.3 shows these values for the 5 subjects. The first and the second row shows the values of SAR for the individual symmetrical measurements A and B. The third row shows a mean SAR for the two measurements. The fourth row shows the value of SAR calculated from a signal obtained by taking a mean of the two symmetrical measurements. The fifth row shows an increase in SAR for each subject calculated by subtracting the value in row 3 from row 4. It can be seen that there is a significant increase in SAR of 10.79±3.97 (mean±2SE).

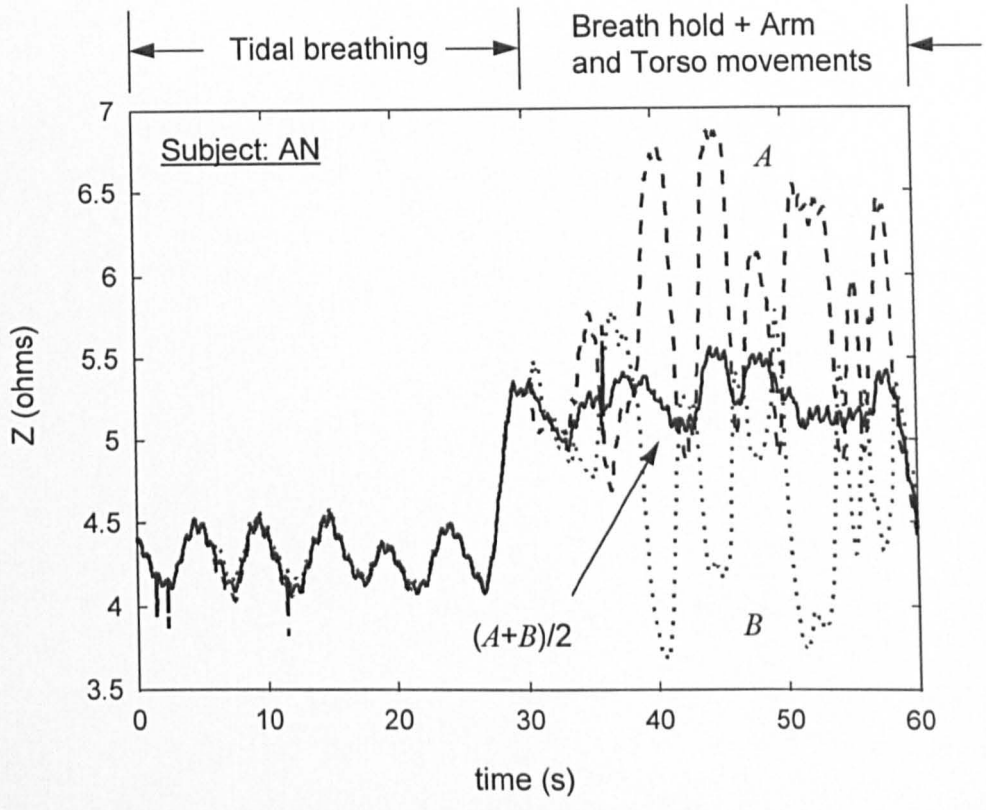

Figure 6.6a *A plot of symmetrical measurements A (dashed) and B (dotted) for one subject. Note the reduction in movement artefacts in the mean signal. Breath was held at maximum inspiration.*

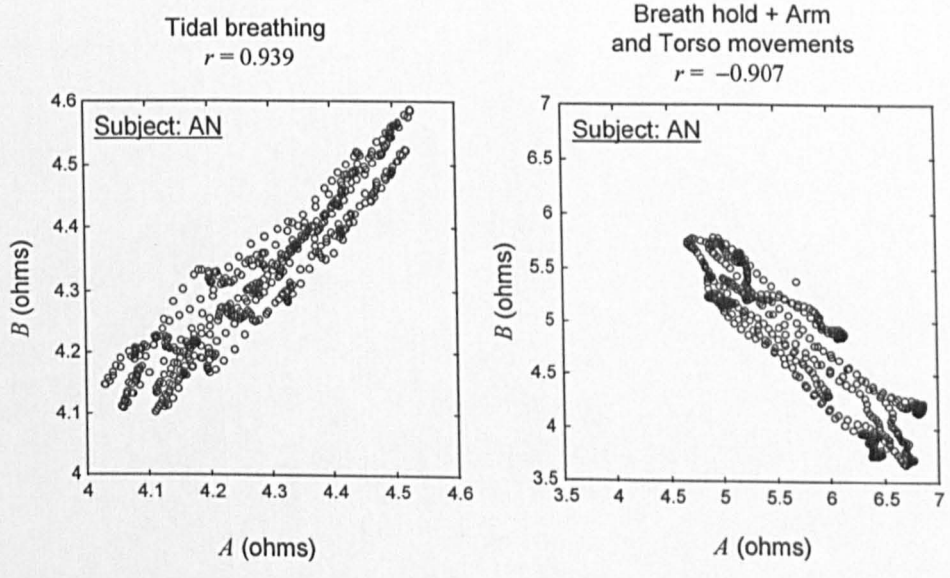

Figure 6.6b *A plot of B versus A for tidal breathing and movements with breath hold at maximum inspiration.*

Table 6.3 *Values of SAR in dB for 5 subjects for the symmetrical measurements A and B and for their mean (A+B)/2.*

	NK	AN	AK	CA	SR
SAR_A	−13.87	−8.93	−9.35	−22.73	−6.40
SAR_B	−9.07	−10.03	−9.16	−24.19	−8.56
$(SAR_A + SAR_B)/2$	−11.47	−9.48	−9.26	−23.46	−7.48
$SAR_{(A+B)/2}$	−3.59	1.98	0.21	−5.33	−0.47
(row 4−row 3)	7.88	11.46	9.47	18.13	7.01

The results of these experimental studies indicated that it was possible to reduce movement artefacts by taking a mean of the two symmetrical measurements. The thoracic cavity is a three dimensional volume conductor. Thus, it was possible to further modify the 4-electrode strategic placement to a 6-electrode strategic placement in such a way that it was possible to obtain two more symmetrical measurements in a different oblique plane. It was intuitively thought that such an electrode placement would maximise the effect of resistivity changes of the anterior and the posterior as well as of the upper and the lower parts of both the lungs, while at the same time providing movement artefact reduction. A theoretical study was carried out using a volume conductor model to investigate whether reduction in movement artefacts could be obtained using this 6-electrode strategic placement.

6.4. Movement artefact reduction using a 6-electrode strategic placement: theoretical studies

A homogeneous volume conductor model of the thoracic cavity, having an elliptical cross-section, was developed as shown in Figure 6.7. The ratio of major axis (x) to minor axis (y) was chosen to be 1.7 as suggested by Kiber (1991) and the height (h) of the model was chosen to be 1.75 times the minor axis. This model was developed using commercial FEM software ANSYS (Ansys Inc., USA, version 5.3). The model was meshed into 33600, 8 node 'brick' elements and the solution in the form of nodal voltages was obtained by solving the FEM equations for each drive configuration so that measurements A to E could be derived as shown in Table 6.4.

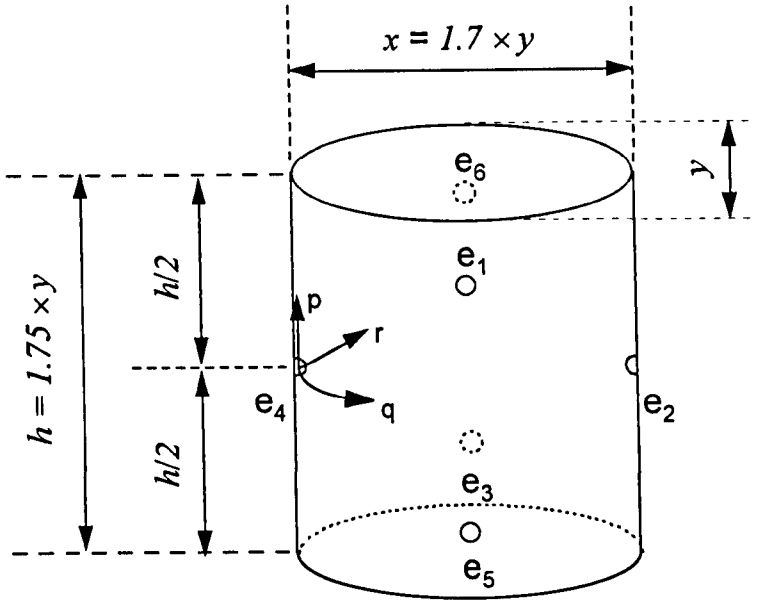

Figure 6.7 *A volume conductor model and the 6 electrodes used in the theoretical study. Electrode e_4 was assumed to shift in three directions 'p', 'q', and 'r' due to movements.*

The placement of electrodes is also shown in Figure 6.7. Electrodes e_2 and e_4 were placed on the surface at the opposite ends of the major axis and in the 'central' horizontal plane, located at half the total height of the model. Electrodes e_1 and e_6 were placed at the opposite ends of the minor axis and in a horizontal plane located at a distance equal to half the minor axis above the central plane. Electrodes e_3 and e_5 were also placed at the opposite ends of the minor axis, but in a plane located at a distance equal to half the minor axis below the central plane. Electrodes e_1, e_2, e_3 and e_4 could be configured to produce a symmetrical pair of measurements A and B, and electrodes e_6, e_2, e_5 and e_4 could be configured to produce a second symmetrical pair of measurements D and E as shown in Table 6.4. One more measurement C could also be obtained using this electrode placement.

Table 6.4 *Electrode configurations and measurements for the 6-electrode strategic placement*

Measurements	Drive electrodes	Receive electrodes
A	e_1, e_2	e_3, e_4
B	e_2, e_3	e_4, e_1
C	e_1, e_6	e_3, e_5
D	e_6, e_2	e_5, e_4
E	e_2, e_5	e_4, e_6

If we consider this 6-electrode placement on the thoracic cavity, then electrodes e_1 and e_5 would be located over the sternum, and electrodes e_3 and e_6 would be located over the spinal column. These four electrodes would be located directly over the bones of the 'rigid' rib cage. At these locations there would be less peripheral tissue underneath the electrodes, especially in normal subjects having average subcutaneous fat. Therefore, it may be reasonable to assume that these four electrodes would be less affected by movements. Moreover, they would also be less affected by movements of the arms because they would be located at a maximum distance from both the arms. On the other hand, electrodes e_2 and e_4 would be placed on the midaxillary line and would be expected to move by a great extent during movements. Therefore, this theoretical study was carried out in two steps. In the first step, movement artefacts were simulated by assuming that only electrode e_4 was affected by movements and moved in three directions, vertical, horizontal and oblique, indicated as 'p', 'q' and 'r', respectively, in Figure 6.7. All the other electrodes were assumed to remain fixed in their locations.

In the second step, it was assumed that electrodes e_2 and e_4 moved at the same time due to movements. It was assumed that first electrode e_2 shifted to a different location from its initial location and then remained at that location. The three locations to which electrode e_2 was assumed to shift are marked as e_2', e_2'' and e_2''' in Figure 6.8. Then, for each of these three locations of

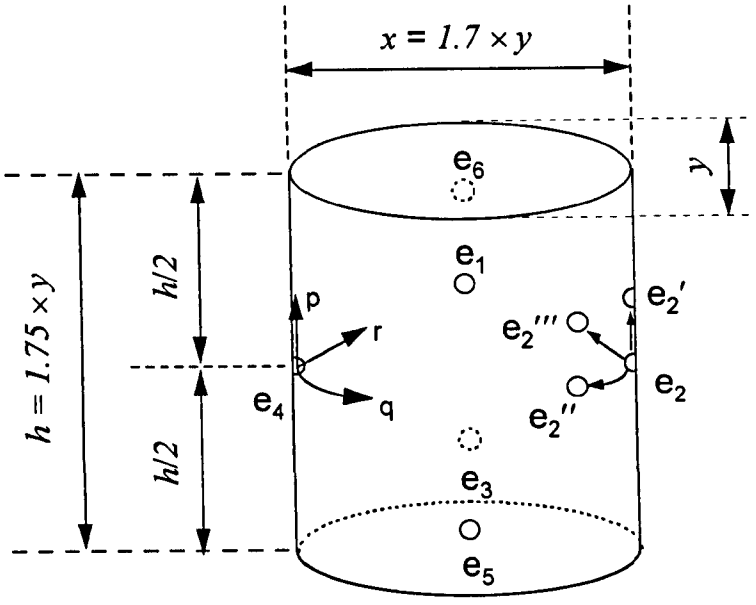

Figure 6.8 *A schematic representation of the simultaneous movement of electrodes e_2 and e_4.*

electrode e_2, it was assumed that electrode e_4 moved in three directions indicated as 'p', 'q', and 'r'.

6.4.1. Results of the theoretical study

Figure 6.9 shows the results of the analysis carried out in the first step, i.e. when it was assumed that only electrode e_4 was shifted due to movement. A plot of voltage versus distance traversed by electrode e_4 in each of the three directions is shown. It was observed that in case of movement occurring in each of the three directions, artefacts could be reduced by taking a mean of the symmetrical measurements. It may be noted that the changes observed in measurements A and D, due to movement in direction 'p', were equal in magnitude and phase, and those due to movement in direction 'q', were equal in magnitude but opposite in phase. This was due to symmetry in the electrode placement with respect to model geometry and the two directions of movement. This was also observed for measurements B and E. As a result, the plots of these measurements overlap in Figure 6.9a and Figure 6.9b. It was observed that, in case of the movement occurring in direction 'r', artefacts could be further reduced by taking a mean of all the four measurements as

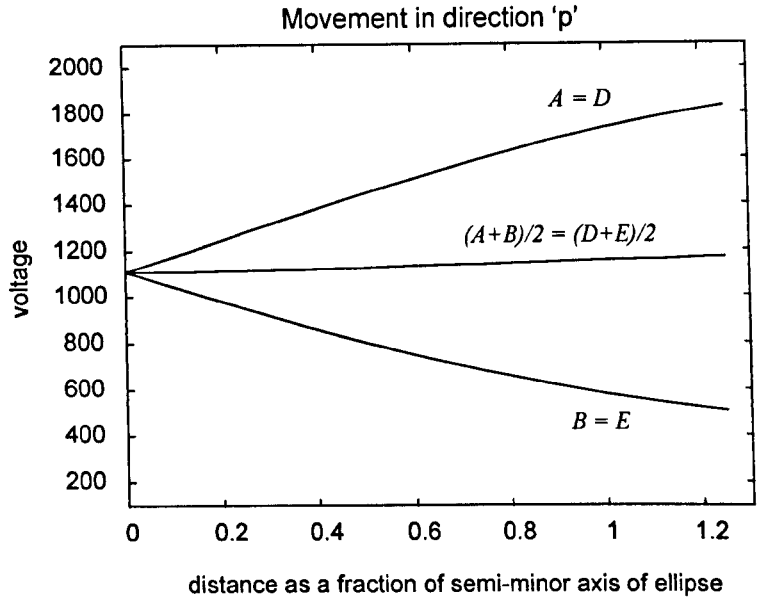

Figure 6.9a *A plot of measurements A, B, D and E for movement of electrode e_4 in direction 'p'. Note that measurements A and D, and B and E are identical due to symmetry in the model.*

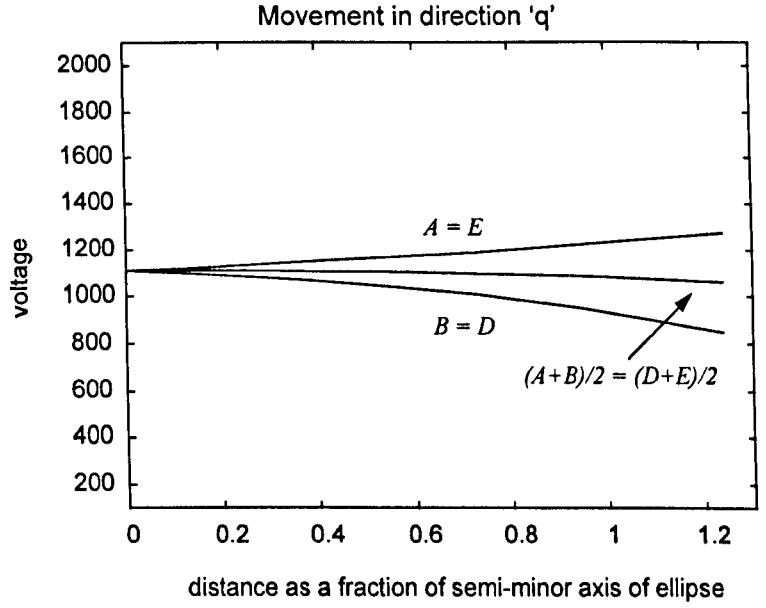

Figure 6.9b *A plot of measurements A, B, D and E for movement of electrode e_4 in direction 'q'. Note that measurements A and E, and B and D are identical due to symmetry in the model.*

shown in Figure 6.9c. This could be considered as an advantage of the 6-electrode strategic placement compared to the previous 4-electrode strategic placement.

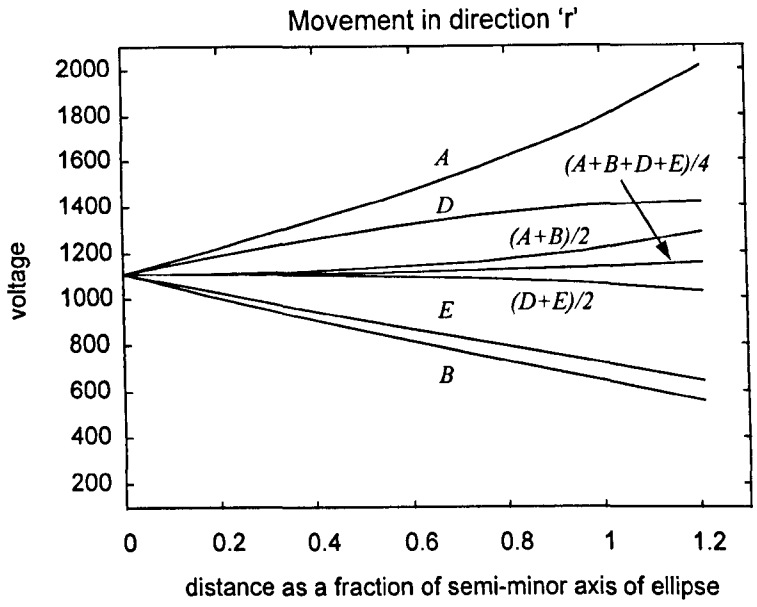

Figure 6.9c *A plot of measurements A, B, D and E for movement of electrode e_4 in direction 'r'. Note a further reduction in movement artefacts could be achieved by taking a mean of all the four measurements.*

A plot of the four symmetrical measurements for the analysis carried out in the second step, i.e. when simultaneous movement of electrodes e_2 and e_4 was assumed, is shown in Figure 6.10. These plots show voltages recorded from the symmetrical pairs when electrode e_2 was first shifted to a location denoted as e_2' in Figure 6.8, and then electrode e_4 was shifted in directions 'p', 'q' and 'r'. As seen in these plots, the symmetrical measurements changed in the opposite direction due to movement of electrode e_4. Thus, it was possible to reduce movement artefacts by taking a mean of the symmetrical measurements.

In the same way, it was possible to reduce movement artefacts when electrode e_2 was assumed to first shift to the other two locations denoted as e_2'' and e_2''', and then electrode e_4 was assumed to move in the three directions. In general, it was observed that there was no significant change in the potential distribution around electrode e_4, due to shifting of electrode e_2 to any nearby location. Therefore, movement artefacts could be reduced by taking a mean of all the symmetrical measurements as long as electrodes e_2 and e_4 moved through a short distance in any direction from their initial location.

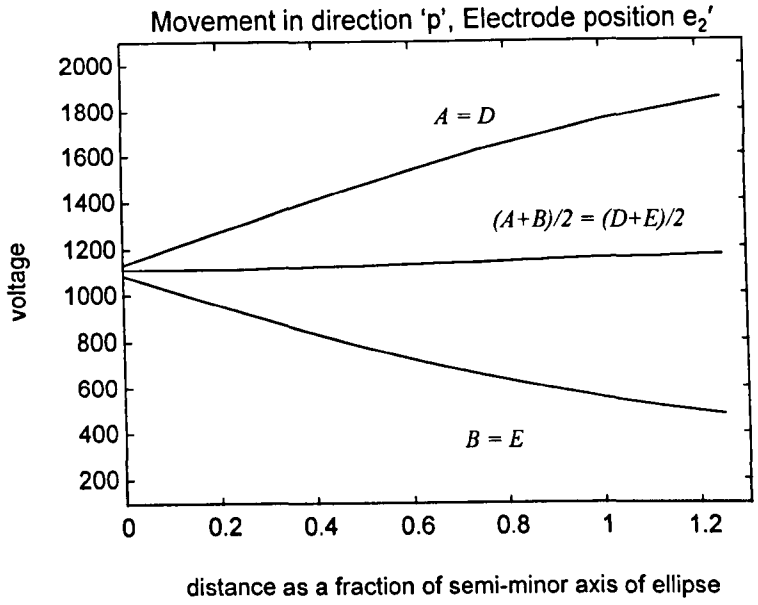

Figure 6.10a A plot of measurements A, B, D and E for movement of electrode e_4 in direction 'p' and electrode e_2 at location marked e_2' in Figure 6.8. Note that measurements A and D, and B and E are identical due to symmetry in the model.

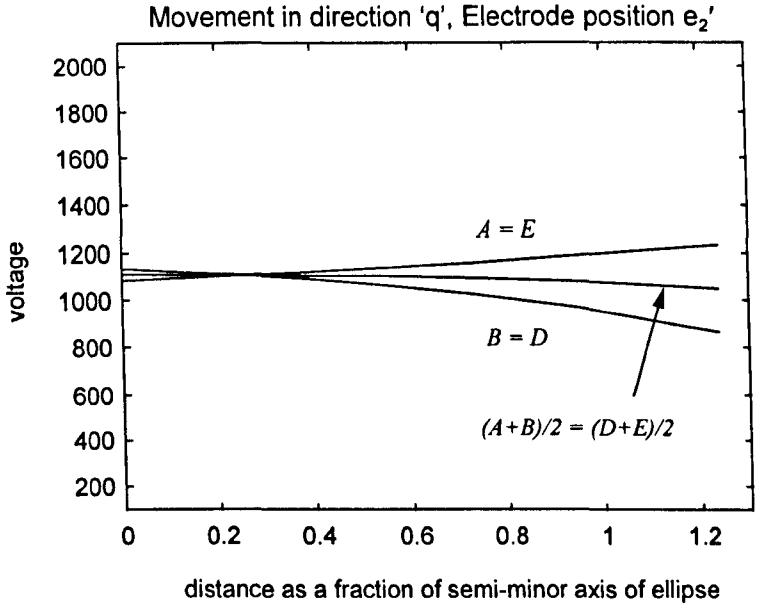

Figure 6.10b A plot of measurements A, B, D and E for movement of electrode e_4 in direction 'q' and electrode e_2 at location marked e_2' in Figure 6.8. Note that measurements A and E, and B and D are identical due to symmetry in the model.

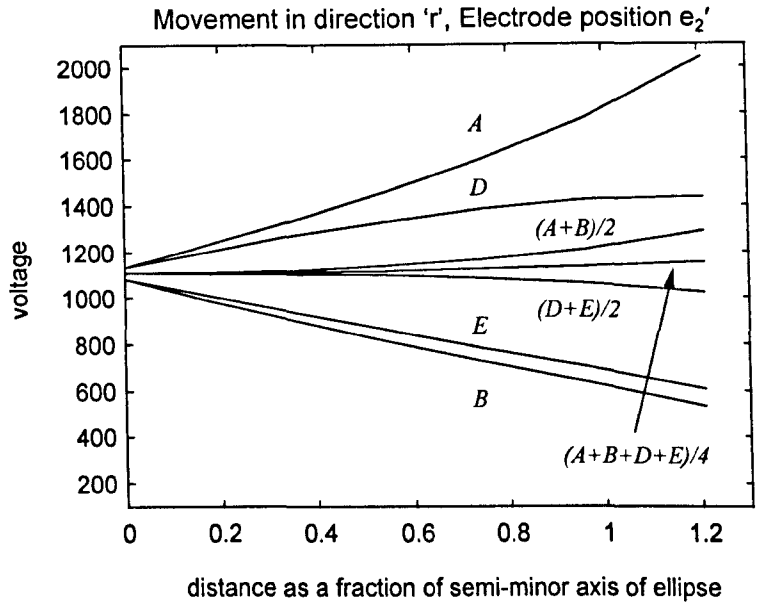

Figure 6.10c A plot of measurements A, B, D and E for movement of electrode e_4 in direction 'r' and electrode e_2 at location marked e_2' in Figure 6.8. Note a further reduction in movement artefacts could be achieved by taking a mean of all the four measurements.

The results of this theoretical study involving the 6-electrode strategic placement indicated that it would be possible to reduce movement artefacts by taking a mean of the symmetrical measurements even on a three dimensional volume conductor such as the thoracic cavity. The next step was to record data using this electrode placement on human subjects to see whether it would be possible to reduce movement artefacts in practice using the 6-electrode strategic placement.

6.5. Movement artefact reduction using a 6-electrode strategic placement: experimental studies

The purpose of these experimental studies was to record impedance data from human subjects using the 6-electrode strategic placement and thus, find out whether this electrode placement provided sufficient reduction in movement artefacts in practice. In the previous experimental studies involving the 4-electrode strategic placement, impedance data was not recorded when breathing and movements occurred at the same time. For an impedance based breathing monitor to be reliable, it should be able to detect breathing in the presence of movements as well, and preferably measure parameters such as breathing rate from the impedance signal. Therefore, in this experimental study, impedance data was recorded during breathing as well as movements. In this situation, if sufficient reduction in movement artefacts could be achieved as suggested by the theoretical studies, then the impedance signal would indicate presence of breathing. In order to verify this, the impedance signal was compared qualitatively with an artefact free breathing signal obtained from a nasal thermistor.

6.5.1. Data collection set-up

The hardware set-up of the data collection system is shown in Figure 6.11. A Sheffield Mark 2 REIT system was used to record the impedance data (Smith *et al*, 1995). The 16-electrode data recorded using this system was processed on the basis of superposition and reciprocity to extract the required 6-electrode measurements. The REIT system injected a current of 5 mA peak-to-peak at a frequency of 20 kHz and the data was captured at a frame rate of 25 frames s^{-1}. This data was stored to the hard disk of a PC denoted as DAS1.

A thermistor based breath detection circuit was developed to record an artefact free breathing signal. The thermistor was attached to a face mask worn by the subjects during data collection. The resistance value of the thermistor changed as it was heated and cooled by the expired and inspired air, respectively. A typical change in the resistance value of the glass encapsulated thermistor

attached to the face mask was observed to be from 3.5 kΩ to 4.95 kΩ. This change in resistance was converted to a voltage signal, which was suitably amplified and connected to the input of a second PC based data acquisition system (DAS2). The sampling rate of DAS2 was also set to 25 samples s^{-1}, i.e. equal to that of DAS1.

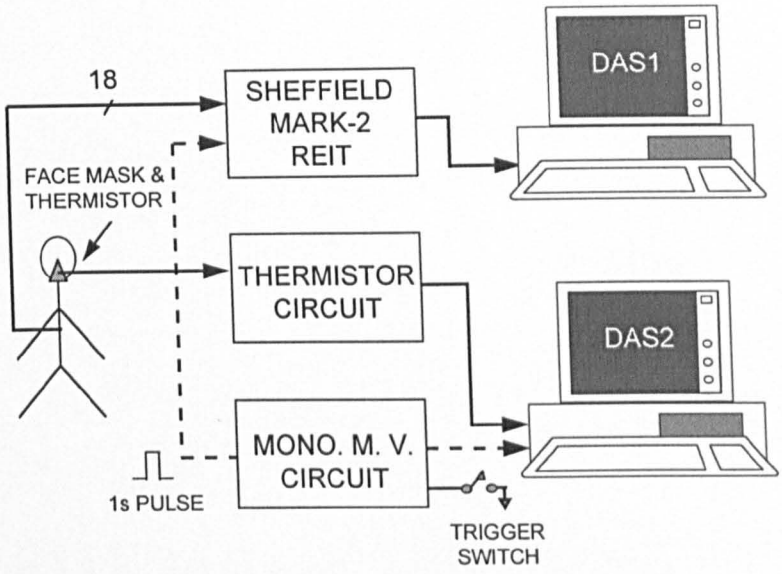

Figure 6.11 *Data collection system for the experimental studies involving a 6-electrode strategic placement*

It was necessary to synchronise in time the two data acquisition systems, DAS1 and DAS2. Therefore, a Monostable Multivibrator circuit was developed to generate a TTL compatible pulse of 1 s duration. The circuit could be triggered by pressing a switch manually. This TTL signal was connected to the 'event marker' input of REIT system and also to a second input channel of DAS2. The REIT system had a built in arrangement to mark the frames corresponding to the rising edge of the pulse. Thus, the two systems could be synchronised in time by shifting the data vectors such that the frames corresponding to the rising edge of the pulse were aligned. The same TTL pulse was also used to generate an audio signal for instructing the subjects to carry out a changeover from tidal breathing to breath hold and to start a movement manoeuvre.

6.5.2. Electrode placement on human subjects

The six electrodes under investigation were placed relative to the anatomical landmarks to minimise the inter-subject variability, and are marked by 'circles' in Figure 6.12.

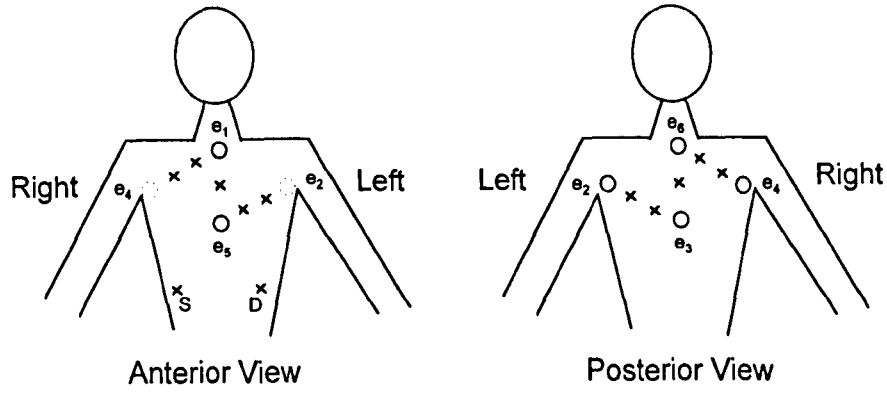

Figure 6.12 *Placement of electrodes on human subjects. The 6 electrodes marked by 'circles' were the electrodes under investigation.*

The electrodes e_5 and e_1 were attached anteriorally, one over the xiphoid process and the other over the sternum at the level of the first rib, respectively. The electrodes e_3 and e_6 were attached in the same two horizontal planes, but on the back over the spinal column. These four electrodes were those assumed to be not affected by movement in the theoretical studies. Finally, electrodes e_2 and e_4 were attached at the level of the axilla, over the Latissimus dorsi muscle on the left and on the right side, respectively. These two electrodes were expected to be affected by the movement. The placement of remaining electrodes was not critical and they were placed at locations marked by a 'cross' in Figure 6.12. The sense and the drive electrodes of the Common Mode Feedback system (Smith *et al*, 1995), marked as 'S' and 'D', respectively, were placed on the abdomen. Thus, it was possible to record measurements A to E, as given in Table 6.4, using this electrode placement. The Adult Foam 1501-025 electrodes (Conmed Corporation, USA) were used in the study because they seemed to adhere very well to the skin and did not come loose due to movements used to cause artefacts.

6.5.3. Experimental protocol and movement manoeuvres

The tidal breathing and movement artefact data were recorded from 3 normal male volunteers and 1 normal female volunteer, having a mean age of 27 years (range 24-29), in an upright sitting position. The subjects were asked to carry out four different arm movement manoeuvres; right arm moving up and down, left arm moving up and down, both arms moving up and down alternately, and both arms moving up and down together. These arm movement manoeuvres are illustrated in Figure 5.5 of the previous chapter. The data collection in each case was carried out for a duration of 120 s. During the first 60 s, the subjects were asked not to carry out any movement, but carry out tidal breathing (TB) for 20 s, followed by breath hold after maximum inspiration (BH) for 20 s and again tidal breathing for 20 s. The same sequence of breathing activity was repeated in the remaining 60 s, but a movement manoeuvre was performed simultaneously. The arm movements were not necessarily synchronised in time with the breathing activity.

6.5.4. Results and discussion for the experimental data

The impedance changes observed in the individual measurements A and B for one subject and for the right arm movements are plotted with respect to time in Figure 6.13a. The thermistor signal shows the artefact free breathing signal. The periodic impedance changes observed during the epochs 1 and 3 were due to tidal breathing and a steady base line, observed during the epoch 2, was due to breath hold. The impedance also changed due to cardiac activity, but the amplitude was relatively small. These changes, occurring at a higher cardiac frequency, are seen superimposed over the breathing related impedance changes. It was observed that the impedance changes due to movement artefacts were large and seemed to completely mask the breathing related changes during epochs 4 and 6. The steady base line, indicating breath hold, was also replaced by large artefacts during epoch 5. This indicated that it was not possible to extract any breathing related information from the individual measurements when the movement was present.

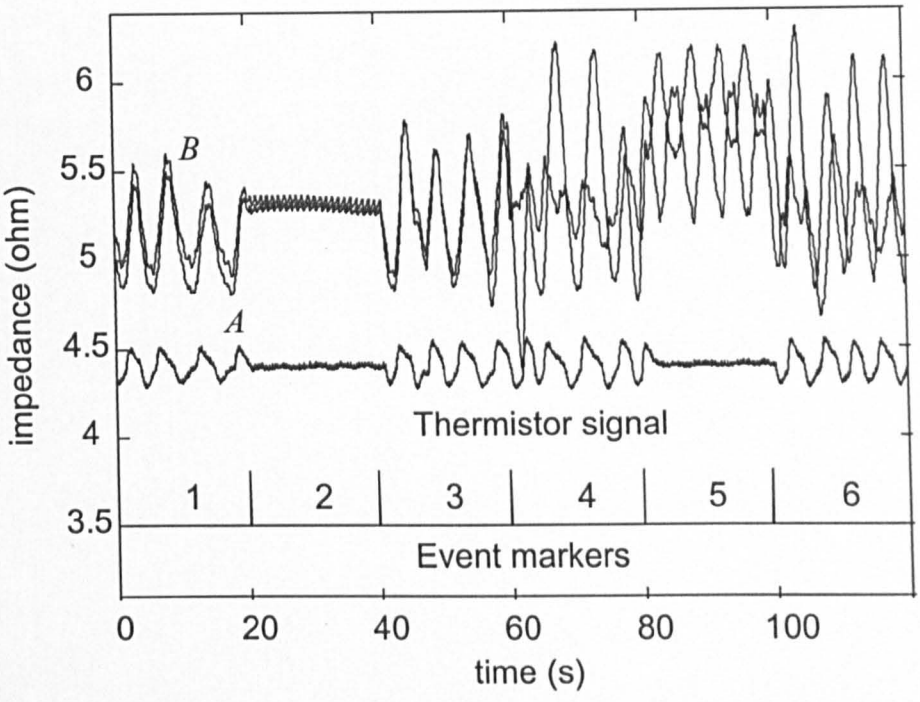

Figure 6.13a A plot of individual symmetrical measurements A and B, and the thermistor signal with time during right arm movement for subject AK. Note that movement artefacts are 180° out of phase during epoch 5.

The purpose of our experimental study was to find out whether the impedance changes due to movement, in one of the measurements belonging to a symmetrical pair were 180° out of phase with those observed in the other measurement of that pair, as predicted by the theoretical study. This was indeed observed in the case of measurements A and B and is seen during epoch 5, when the subject carried out movement by holding their breath. Similar observations were made in case of measurements D and E. Thus, it was possible to reduce the movement artefacts by taking the mean of A and B (P) and of D and E (Q), without affecting the breathing related changes as shown in Figure 6.13b. This was the first step in reducing the movement artefacts.

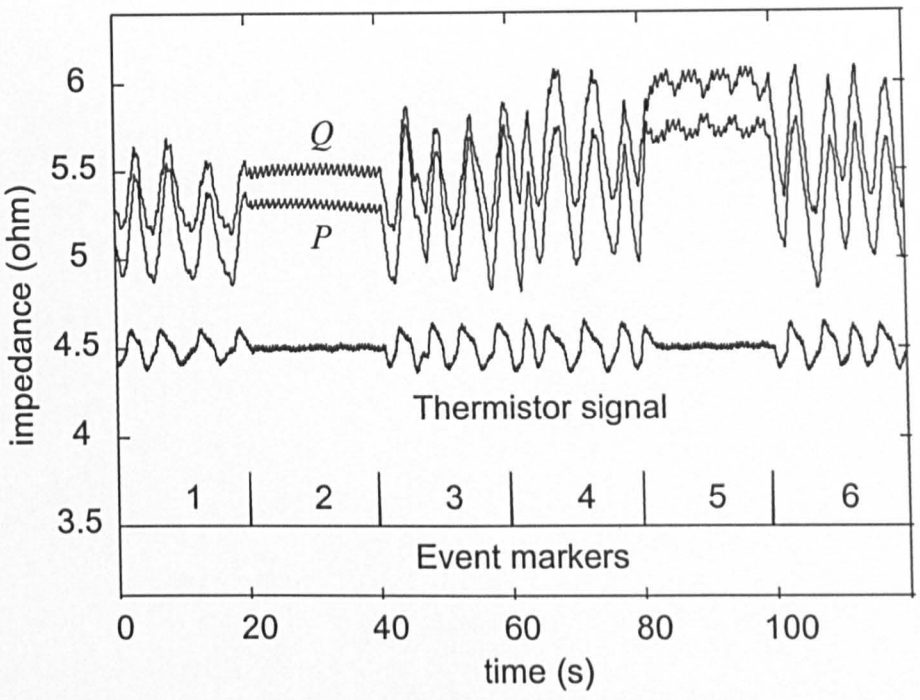

Figure 6.13b A plot of mean values of symmetrical measurements $P = (A+B)/2$ and $Q=(C+D)/2$, during right arm movement for subject AK. Note the reduction in movement artefacts during epoch 5.

It was also observed that in case of some subjects, movement artefacts in P were 180° out-of-phase with those in Q as shown in Figure 6.13b, but in the remaining subjects, they were in-phase. However, in the latter cases, the movement artefacts in P and Q were 180° out of phase with those in measurement C. In general, it was observed that the artefacts could be reduced by summing P, Q and C in case of all the subjects. The plot of the processed signal (S) is shown in Figure 6.13c. It can be seen that, even in the presence of movement during epochs 4 and 6, the instants of maximum inspiration and expiration coincide in time with those observed in the thermistor signal. The absence of breathing can also be identified during epoch 5.

The sum of P, Q and C was divided by an empirical factor equal to 4 so that the amplitude of the breathing signal in S would be in the same range as that observed in the individual measurements. This allowed a direct comparison to be made between the amplitude of movement artefacts, before and after processing the signals. It may be noted that the choice of value of 4 was only

for the sake of comparing the results of the study and has no significance as far as any clinical application of the technique is concerned.

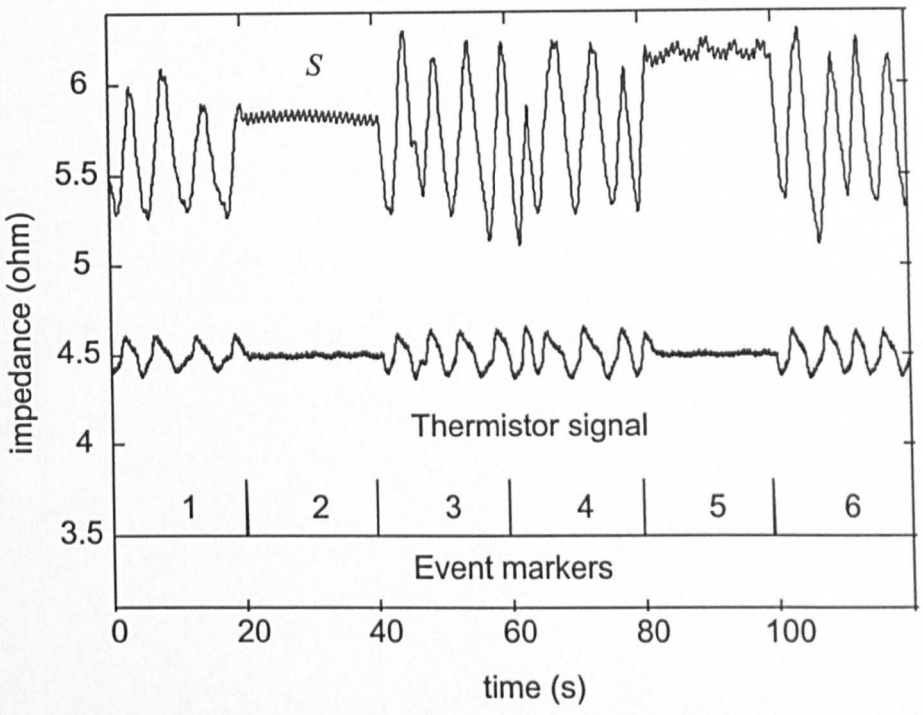

Figure 6.13c A plot of processed signal S = (P+Q+C)/4, during right arm movement for subject AK. Note a high correlation between the impedance signal and the thermistor signal.

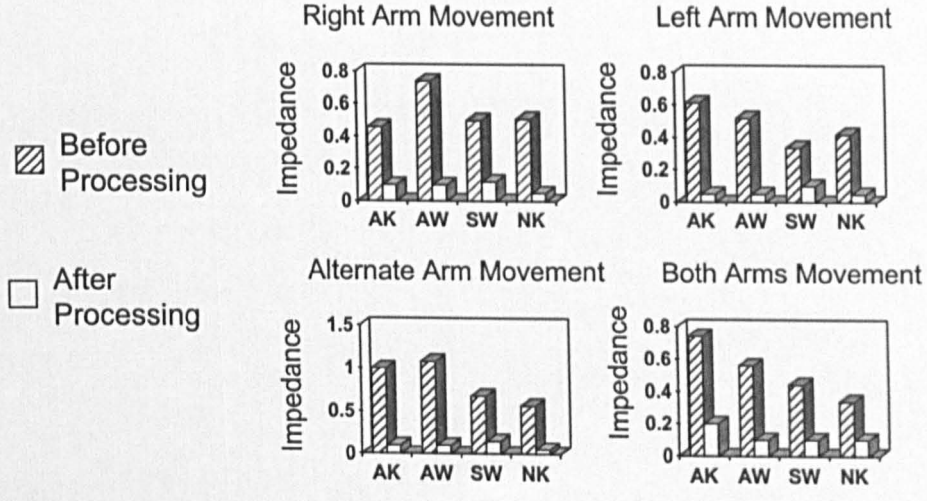

Figure 6.14 Peak-to-Peak amplitude of movement artefacts before and after processing for the four subjects and four different movement manoeuvres

The results of this experimental study are summarised in Figure 6.14. The amplitude of movement artefacts indicated as 'Before processing' was calculated by taking a mean of the peak-to-peak values of impedance changes due to movement during breath hold (epoch 5) in all the five measurements A to E. The amplitude of movement artefacts, indicated as 'After processing', is equal to the mean of peak-to-peak values of impedance changes in measurement S during the same epoch.

The thoracic cavity may be considered as a rigid volume conductor due to a relatively rigid nature of the rib cage. Then the peripheral tissues covered by the skin, can be considered as a loose outer layer that can slide over this rigid volume conductor. Thus, electrodes placed on the skin tend to slide along with the outer layer during movement and hence, move to a different isopotential line causing artefacts. The results of these experimental studies seemed to confirm this hypothesis as a significant reduction in movement artefacts was obtained by strategically placing the 6 electrodes. Thus, the sliding of electrodes along with the skin appeared to be one of the main causes of movement artefacts. In addition, the reduction in movement artefacts could be achieved in all the subjects, including one female subject. This indicated that movement artefact reduction, achieved using the 6-electrode strategic placement, was independent of the differences in shapes of the thoracic cavity of different subjects.

It is also important to note that the peripheral tissues not only slide over the rib cage during movement, but may also undergo a geometrical change, which may cause some movement artefacts. The residual artefacts seen in the final signal S may be due to these geometrical changes in the peripheral tissues. It was discussed in Chapter 5 that it might be possible to reduce movement artefacts by recording impedance at more than one frequencies. The movement artefacts introduced by the geometrical changes would be a constant fraction of the base impedance. Therefore, they may reduce at higher frequencies because the base impedance of the biological tissues reduces with increase in frequency. In order to study the effect of frequency on movement

artefacts, experimental studies involving multi-frequency measurements were carried out in this project as described in the following section.

6.6. Multi-frequency measurements using the 6-electrode strategic placement

Firstly, the purpose of these experimental studies was to investigate whether movement artefact reduction could be obtained at different frequencies of injected current using the strategic 6-electrode placement. Secondly, the aim of these studies was to find out whether movement artefacts were less at higher frequencies than at lower frequencies. Thirdly, it was also aimed at finding out whether it was possible to detect obstructive apnoea using the 6-electrode strategic placement.

In the earlier experimental studies, impedance data was only recorded during gross body movements. However, it has been reported that impedance based apnoea monitors may fail to detect obstructive apnoea (Warburton *et al*, 1977). During an episode of obstructive apnoea, the patient attempts to carry out breathing using the intercostal muscles and the diaphragm, but no movement of air can occur in and out of the lungs because the upper airway is blocked. In this situation, if the measured thoracic impedance is dominated by the geometrical changes of the thoracic cavity and the diaphragm movement, rather than the changes in lung resistivity, then the breathing related impedance variations continue to occur. As a result, the apnoea monitor fails to detect apnoea. Therefore, in these studies impedance data was also recorded from human subjects during simulated obstructive apnoea to find out whether it was possible to detect obstructive apnoea using the 6-electrode strategic placement.

6.6.1. Data collection

The impedance data was recorded from 4 normal male volunteers and 1 normal female volunteer having a mean age of 30.5 years (range 30-35). A Sheffield Mark 3a EITS system (Lu, 1995) was used for data collection. This

system injected a current of 1 mA peak-to-peak at 8 different frequencies in binary steps in the range of 9.6 kHz and 1.22 MHz. This system had 8 drive electrodes, separate from the 8 receive electrodes. The configuration of the system was such that it was possible to inject current between the adjacent drive pairs and measure voltage between the adjacent receive pairs. The placement of electrodes was carried out as shown in Figure 6.15. The locations of the 4 drive electrodes and the 4 receive electrodes, from which the symmetrical measurements were extracted, are marked by 'circles'. The electrode configurations and the corresponding symmetrical measurements are given in Table 6.5. The anatomical locations of these electrodes were the same as those explained in section 6.5.2. It was necessary to place two electrodes side by side, one as a drive electrode and one as a receive electrode, over the Latissimus dorsi muscle because the data collection system had separate drive and receive electrodes. The anatomical locations of the remaining drive and receive electrodes were not critical and they were placed at locations marked by a 'cross'. A ground electrode G was placed on the abdomen. The required symmetrical measurements were extracted from the recorded data using superposition and reciprocity.

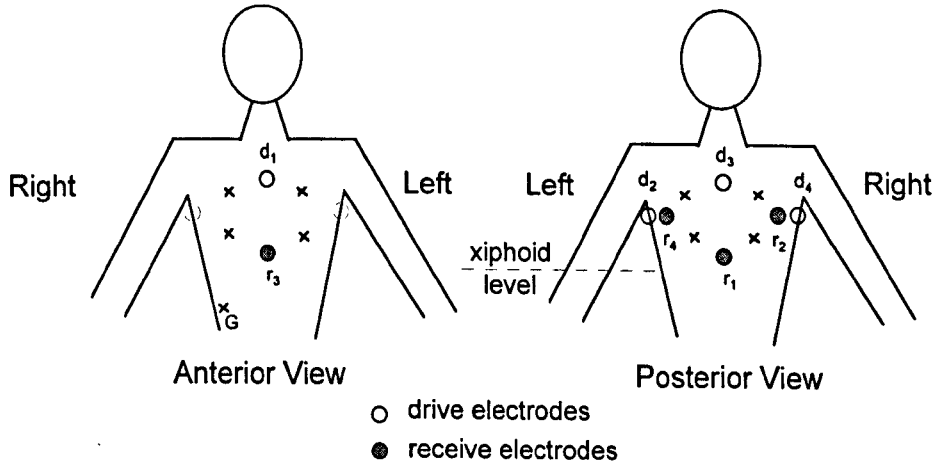

Figure 6.15 Electrode placement for multi-frequency measurements

The impedance data was recorded during tidal breathing and during movements, in the absence as well as in the presence of breathing. The movement carried out by the subjects was a random combination of the arm

Table 6.5 *Electrode configurations and measurements for the multi-frequency data*

Measurements	Drive electrodes	Receive electrodes
A	d_1, d_2	r_1, r_2
B	d_4, d_1	r_4, r_1
C	d_1, d_3	r_1, r_3
D	d_2, d_3	r_2, r_3
E	d_3, d_4	r_3, r_4

and the torso movements. In 4 out of 5 subjects, data was also recorded during simulated obstructive apnoea. In order to simulate the obstructive apnoea, subjects were asked to attempt a voluntary closure of the glottis and then try to breath using the intercostal muscles and the diaphragm. This caused the thoracic cavity to undergo geometrical changes but no movement of air could occur in or out of the lungs. A nasal thermistor was also used in this study to record an artefact free breathing signal.

6.6.2. Results and discussion for multi-frequency data

Firstly, it was observed that it was possible to reduce movement artefacts at all the frequencies by taking a mean of all the symmetrical measurements ($S=(A+B+D+E)/4$). It may be important to note that in the earlier experimental studies, an improvement in *SAR* was obtained empirically by adding measurement *C* to the final signal. It was difficult to understand the underlying explanation of this empirical result because according to the theoretical results, measurement *C* was not expected to be affected by movement artefacts. This was because the electrodes used to obtain this measurements were assumed to remain fixed during movement in the theoretical studies. Therefore, in the present study it was decided that only the 4 symmetrical measurements as suggested by the theoretical study would be used for reducing movement artefacts.

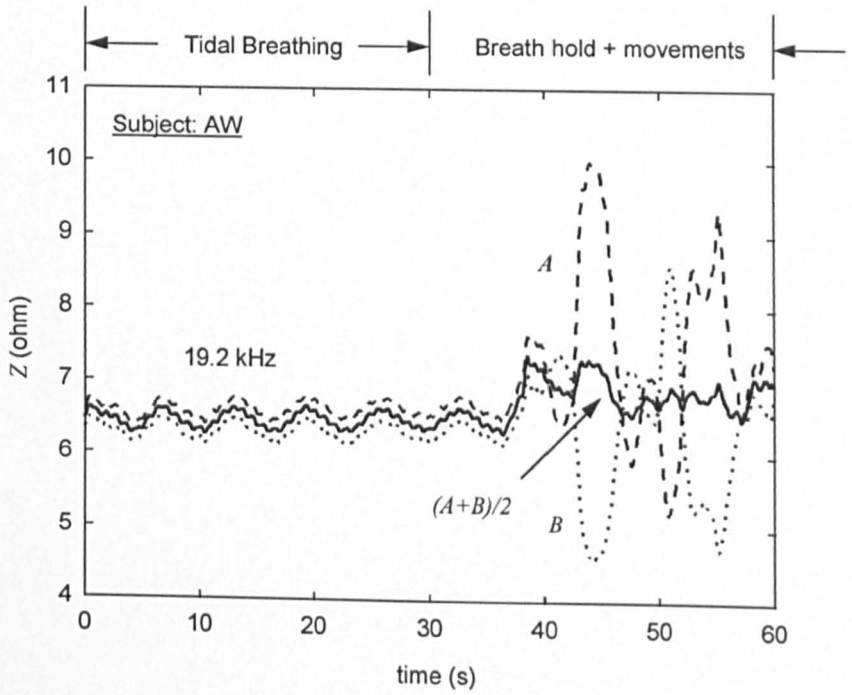

Figure 6.16a A plot of two symmetrical measurements A and B for Subject AW and their mean at a frequency of 19.2 kHz.

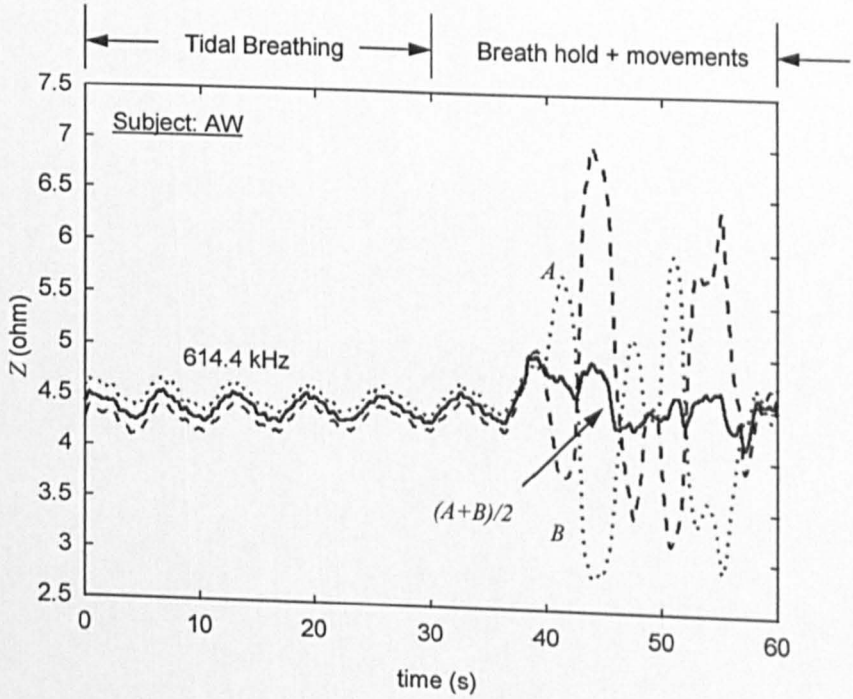

Figure 6.16b A plot of two symmetrical measurements A and B for Subject AW and their mean at a frequency of 614.4 kHz.

Table 6.6 *Values of SAR in dB for 5 subjects and for 8 frequencies*
column 1: mean value of SAR in the individual measurements $((SAR_A+SAR_B+SAR_D+SAR_E)/4)$
column 2: value of SAR in signal S $(SAR_S = SAR_{(A+B+D+E)/4})$
column 3: increase in SAR = column 2 – column 1

Subjects	AK			AW			NK			PB			SN		
freq. (kHz)	1	2	3	1	2	3	1	2	3	1	2	3	1	2	3
9.6	–8.55	6.65	15.19	–21.13	–5.63	15.50	–14.55	2.10	16.64	–13.90	–5.96	7.94	–7.81	7.54	15.34
19.2	–8.20	6.65	14.85	–20.28	–4.24	16.05	–13.82	2.36	16.18	–13.73	–5.87	7.86	–7.49	7.68	15.17
38.4	–8.14	6.29	14.43	–18.75	–2.56	16.19	–13.21	2.33	15.54	–13.47	–5.83	7.65	–7.47	7.42	14.89
76.8	–8.58	5.94	14.52	–18.87	–1.43	17.45	–13.72	1.90	15.62	–15.08	–6.21	8.87	–8.16	8.64	16.80
153.6	–9.02	5.19	14.20	–18.93	–1.46	17.47	–13.62	1.05	14.67	–14.36	–5.75	8.61	–8.47	7.76	16.23
307.2	–9.50	4.39	13.89	–19.47	–2.61	16.86	–14.57	0.15	14.71	–16.43	–6.06	10.38	–9.28	8.76	18.04
614.4	–9.51	3.19	12.71	–19.37	–5.87	13.50	–13.37	–0.25	13.12	–12.64	–3.87	8.77	–8.15	5.20	13.35
1228.8	–8.28	0.713	8.99	–19.43	–12.61	6.82	–13.81	–2.10	11.71	–14.53	–5.18	9.36	–8.66	9.31	17.97

The reduction in movement artefacts, obtained by taking a mean of the symmetrical measurements at two different frequencies, can be seen in Figure 6.16. This figure shows a plot of symmetrical measurements A and B for one subject and the mean signal for two frequencies, 19.2 kHz and 614.4 kHz. It can be seen that movement artefacts have been reduced in the mean signal at both the frequencies.

In Table 6.6, two different values of SAR are shown for each subject and at 8 frequencies. For each subject, column 1 shows a mean value of SAR for the 4 symmetrical measurements, i.e. $(SAR_A+SAR_B+SAR_D+SAR_E)/4$ and column 2 shows a value of SAR for the signal S (SAR_S). Finally, an increase in SAR for each subject is calculated by subtracting the value in column 1 from that in column 2 and is shown in column 3 of Table 6.6. In Table 6.6, it can be seen that though an increase in SAR is high for all the subjects, the absolute values of SAR_S for two subjects, AW and PB, are low and negative (see column 2 for the two subjects). Therefore, further investigations were carried out to find out whether it was possible to detect breathing related impedance changes even in

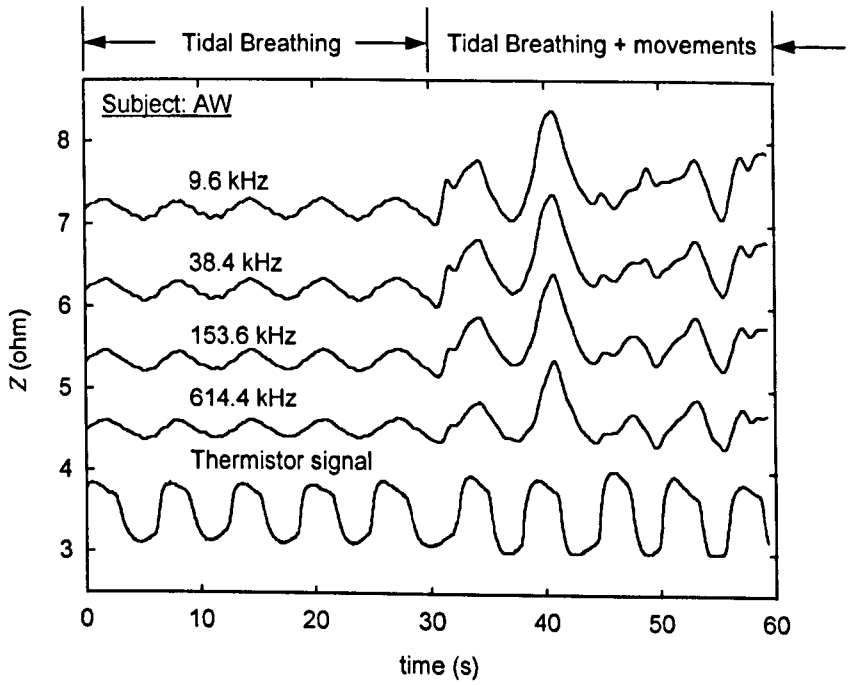

Figure 6.17 A plot of impedance waveforms at 4 frequencies for subject AW.

the presence of movements for these two subjects. Figure 6.17 shows impedance waveforms at 4 different frequencies for subject AW. During the first 30 s the subject carried out tidal breathing and during the following 30 s the subject carried out movements as well as breathing.

It can be seen that the periodic breathing signal is seen during 30 s to 60 s, i.e. even in the presence of movements. The instants of maximum inspiration and maximum expiration match reasonably well with those in the thermistor signal. However, this is only a qualitative comparison and further investigations may be required to develop techniques for further improving the amplitude of the breathing signal.

In order to see whether *SAR* increased at higher frequencies, a mean increase in *SAR* for 5 subjects was obtained at each frequency as given in Table 6.7. This table indicates that the mean increase in *SAR* decreases with frequency. This indicates that further investigations may be required to establish the relationship between frequency and movement artefacts.

Table 6.7 *A mean increase in SAR for 5 subjects at 8 frequencies. The increase in SAR was calculated in the same way as shown in Table 6.6*

frequency (kHz)	Mean ±2SE *SAR(dB)*
9.6	14.12 ±3.14
19.2	14.02 ± 3.12
38.4	13.74 ± 3.10
76.8	14.65 ± 3.05
153.6	14.24 ± 3.04
307.2	14.78 ± 2.65
614.4	12.29 ± 1.78
1228.8	10.97 ± 3.83

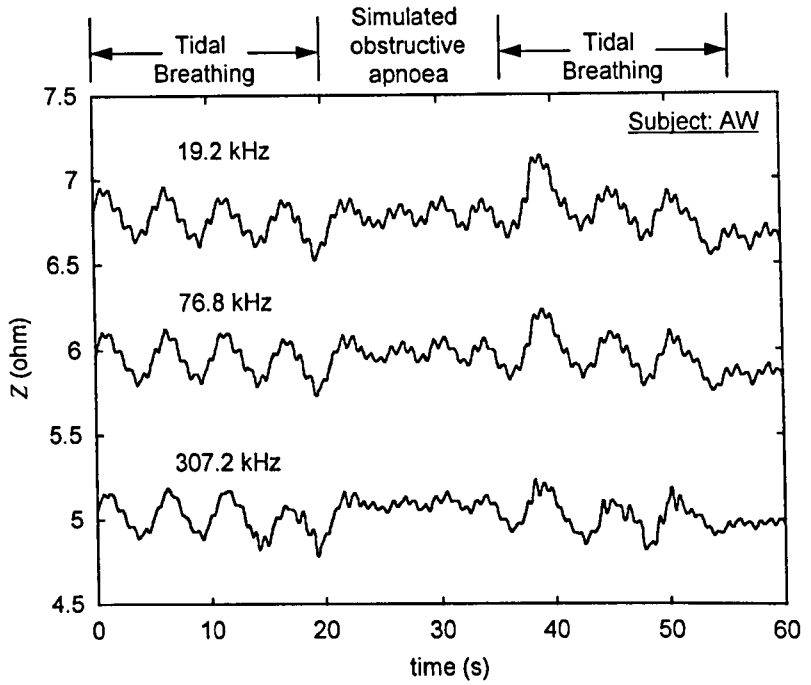

Figure 6.18 Impedance waveforms for subject AW during tidal breathing and simulated obstructive apnoea

In this study, impedance data was also recorded during simulated obstructive apnoea to see whether it was possible to detect obstructive apnoea using the 6-electrode configuration. Figure 6.18 shows a plot of impedance signal S versus time for 3 frequencies recorded during simulated obstructive apnoea in one subject. It can be seen that the amplitude of the breathing signal is much higher than that seen during the obstructive apnoea. In order to quantify this observation, a ratio of the amplitude of impedance signal during breathing to that during obstructive apnoea was calculated in dB. Table 6.8 shows a mean ratio at 8 frequencies for the 4 subjects.

A mean of this value at all the frequencies is equal to 9.8±2.9 (mean±2SE) dB. This indicates that the RMS value of the impedance changes during breathing is at least 2 times higher than that during obstructive apnoea. Thus, these results primarily indicate that it may be possible to detect obstructive apnoea using the 6-electrode optimum configuration. However, more studies would be required to confirm these results.

Table 6.8 *Amplitude ratio in dB of breathing to simulated obstructive apnoea in signal S*

frequency (kHz)	Mean ±2SE *SAR(dB)*
9.6	9.15 ±3.53
19.2	9.06 ± 3.43
38.4	8.96 ± 3.42
76.8	10.32 ± 3.27
153.6	10.01 ± 2.99
307.2	11.55 ± 2.74
614.4	8.27 ± 2.90
1228.8	11.12 ± 3.14

6.7. Discussion

The aim of the experimental work described in this chapter was to develop a method which would enable a quantitative reduction in movement artefacts. A 6-electrode optimum configuration was proposed in Chapter 4, which was expected to provide maximum sensitivity to breathing related impedance changes. Impedance data was recorded on human subjects using this configuration to find out in what way these impedance measurements were affected by movement artefacts. Some important observations were made from the data recorded on the first subject. It was observed that the transfer impedance was affected by movement artefacts only when the electrodes used to record it were physically displaced from their initial location due to movement. From this observation, it appeared that movement artefacts were mainly caused by movement of the electrodes along with the skin. It was also observed that in a pair of 'symmetrical' measurements obtained from the same electrode configuration, breathing related impedance changes were in phase, but movement artefacts were 180° out of phase. This indicated that it was possible to reduce movement artefacts by taking a mean of these measurements.

On the basis of the above observations, it was hypothesised that movement artefacts were caused by electrodes sliding over the thoracic cavity and hence,

moving to different isopotential lines. Taking into consideration this hypothesis, a strategy was decided for placing 4 electrodes in an oblique plane. Impedance data was recorded from more subjects during breathing and movements. It was observed that it was possible to reduce movement artefacts in all the subjects by taking a mean of the symmetrical measurements.

Further theoretical studies were carried out to find out whether it was possible to further reduce movement artefacts by placing electrodes in two different oblique planes. It was only necessary to use two more electrodes, i.e. total 6 electrodes, to obtain two pairs of symmetrical measurements. A three dimensional FEM model having an elliptical cross section was developed for these studies. Movement artefacts were simulated by assuming that 2 electrodes moved in three different directions while the remaining 4 electrodes were not affected by the movement. It was observed that movement artefacts reduced further when a mean of all the 4 symmetrical measurements was taken.

The 6-electrode strategic placement was also used to recorded impedance data from human subjects. It was observed that movement artefacts could be reduced in all the subjects. It was also observed empirically that a further reduction in movement artefacts could be obtained by adding a fifth measurement to the four symmetrical measurements. This fifth measurement (measurement C) was obtained from electrodes placed over the sternum and the spinal column. These electrode placements were not assumed to be affected in the theoretical study. Therefore, the underlying mechanism of the empirical observation was not clear. One possible explanation may be that the electrodes assumed to be not affected by movement in the theoretical study, may be actually getting affected by movement in practice. This may introduce additional artefacts in all the measurements, and these may reduce by adding measurement C to the 4 symmetrical measurements.

The experimental studies were also carried out to study whether it was possible to reduce movement artefacts at all the frequencies of injected current. It was also expected that movement artefacts might reduce at higher frequencies. It

was observed that movement artefacts could be reduced at all the frequencies of injected current for all the subjects using the 6-electrode strategic placement. It was also observed that movement artefacts did not reduce, i.e. the SAR did not increase, with increase in frequency.

Impedance data was also recorded during simulated obstructive apnoea. The purpose of this study was to see whether it was possible to detect obstructive apnoea using the 6-electrode strategic placement. If this electrode placement would maximise the contribution from the changes in lung resistivity, then impedance changes during obstructive apnoea would be small. Thus, it would be possible to distinguish between breathing related changes and obstructive apnoea. It was observed that the amplitude of the impedance changes during breathing was at least twice than that during obstructive apnoea, and this result was statistically significant. This, indicated that it was possible to detect obstructive apnoea using the 6-electrode strategic placement.

It was generally observed that the fractional change in impedance ($\Delta Z/Z$) obtained during tidal breathing using the 6-electrode strategic placement was in the range of 5 to 10% for different subjects. This seemed to be lower than the 14.5% obtained from the earlier 6-electrode optimum configuration from the experimental data recorded using non-planar electrode placements. However, the most important feature of the former electrode configuration was that it had significantly low movement artefacts. Moreover, from the plots of impedance waveforms it appeared that $\Delta Z/Z$ for the 6-electrode strategic placement was qualitatively higher than the instrumentation noise. Further quantitative studies may be carried out to investigate this aspect. The volume of the inspired air was not measured in the experimental studies. Therefore, further experiments may also be carried out to study in quantitative terms the relationship between the volume of inspired air and $\Delta Z/Z$.

Chapter 7. Conclusions and suggestions for future research

7.1. Introduction

Impedance pneumography is a technique for monitoring breathing by measuring impedance changes of the thoracic cavity. The main advantage of this technique is that it does not require any device to be placed within the airway, so causing a discomfort to the patient and affecting breathing. Therefore, it is well tolerated by patients. However, a major disadvantage of this technique is that large artefacts are introduced into the impedance signal due to body movements and hence, in this situation, it becomes impossible to reliably monitor breathing. This can have serious consequences, such as impedance based apnoea monitors may fail to detect apnoea when body movements are present.

Thus, the aim of the present project was to develop a technique for reducing movement artefacts in impedance pneumography. This chapter first briefly outlines the strategy adopted in the project to achieve this aim. Then it summarises the results of the work and draws some general conclusions from these results. Finally, some suggestions are given for future research.

7.2. Strategy adopted in the project

Breathing involves the movement of air in and out of the lungs. In impedance pneumography, an ultimate aim is to monitor this movement of air by measuring thoracic impedance. The thoracic impedance can change due to three factors. Firstly, the resistivity of the lung tissue is a function of its air content and hence, changes during breathing. These changes in lung resistivity cause the thoracic impedance to change. Secondly, the thoracic impedance is also a function of the thoracic geometry. The thoracic geometry and hence, the thoracic impedance changes during breathing as well as during gross body movements. Thirdly, the movement of the diaphragm also causes the thoracic impedance to undergo a

change during breathing. This change in impedance occurs due to low resistivity abdominal organs moving in and out of the measurement field.

The changes in thoracic impedance caused by the geometrical changes due to body movements do not reflect the movement of air and hence, are the 'movement artefacts'. If the changes observed in the thoracic impedance are predominantly due to geometrical changes of the thoracic cavity, then movement artefacts are large. Therefore, in order to reduce movement artefacts, it is necessary to reduce the effect of geometrical changes on the thoracic impedance. In other words this means that it is necessary to increase the contribution of lung resistivity changes to the thoracic impedance. This was the basis of the first step in the present project.

A review of the literature concerned with impedance pneumography suggested that an appropriate choice of electrode placement was required to maximise the contribution of changes in lung resistivity to thoracic impedance. Thus, a first objective of the project was defined as;

- To identify an electrode placement that maximises the contribution of lung resistivity changes to thoracic impedance

A review of the literature concerned with various techniques for reducing movement artefacts suggested that movement artefacts were related to three factors of an 'electrode system', namely the electrode configuration, electrode type and electrode placement. Therefore, a second objective of the project was defined as;

- To identify an electrode system that minimises movement artefacts by taking into consideration all the three factors, electrode configuration, electrode type and electrode placement.

Finally, studies have also been reported in the literature involving techniques for reducing movement artefacts using multi-frequency impedance measurements. Thus, the third objective of this project was defined as;

- To investigate use of multi-frequency measurements for reducing movement artefacts

The following sections summarise the findings of the work carried out in each of the three stages. Finally some general conclusions are stated.

7.3. Electrode placement and thoracic impedance measurements

A theoretical analysis was carried out to lay down criteria for an electrode placement that would maximise the contribution of the lung resistivity changes. This analysis suggested a first criterion that the required electrode placement should maximise the fractional change in thoracic impedance due to breathing ($\Delta Z/Z$). A second criteria was identified such as that the electrode placement should also maximise absolute change in impedance (ΔZ) or *SNR*. An electrode placement was considered to be an 'optimum' if it fulfilled both these criteria.

The experimental studies carried out to identify the optimum electrode placement suggested that for a co-planar electrode placement, $\Delta Z/Z$ increased with distance between the drive and the receive electrode pairs. The analysis carried out on the measurements obtained from the non-planar electrode placements, combined with those obtained from the co-planar electrode placements, also suggested that $\Delta Z/Z$ increased with distance, and this relationship was statistically significant. However, there was a large scatter of points in these plots. This scatter was mainly due to non-planar measurements. This indicated that there were some other factors affecting the relationship between $\Delta Z/Z$ and distance for the non-planar measurements. The experimental data showed that there were some non-planar electrode placements having significantly higher values of $\Delta Z/Z$. However, these electrode placements had a larger distance between the drive and the receive electrode pairs. Therefore, the measurements obtained from these electrode placements were found to have a low *SNR*. Thus, they could not be considered as optimum. These experimental studies also suggested that $\Delta Z/Z$ increased with increase in electrode spacing.

In order to further understand as to which factors were important in determining the relationship between electrode placements and impedance measurements of the thoracic cavity, theoretical studies were carried out. The sensitivity method was used to investigate the relationship between electrode placement and impedance measurements. These studies initially suggested that $\Delta Z/Z$ decreased with distance between the drive and the receive electrode pairs. This result was the opposite to that observed in the experimental results. Further modifications to the FEM model were carried out to understand the factors responsible for this disagreement. It was found that the vertical separation between the horizontal electrode plane and the internal geometry of the model was a significant factor affecting the relationship between $\Delta Z/Z$ and distance.

The purpose of the theoretical studies was also to identify the required optimum electrode placement. Therefore, the values of $\Delta Z/Z$ obtained experimentally and theoretically were correlated to compare the two data sets. The experimental measurements obtained at larger distances between the drive and the receive electrode pairs were found to be affected by the instrumentation noise and systematic errors. Therefore, these measurements were discarded before calculating the correlation coefficient between the two data sets. This correlation coefficient was low (0.534) but significant ($p < 0.001$), indicating that the two data sets were comparable. On examining the theoretical data, it was observed that there were 8 electrode placements having a very significantly higher theoretical values of $\Delta Z/Z$. These electrode placements had some features in common. Firstly, the drive electrodes and the receive electrodes were placed in two different horizontal planes, and the vertical separation between these two planes was equal to the radius of the cylindrical model. Secondly, the angle between the drive and the receive pairs for all the 8 electrode placements was 112.5°. Thirdly, the electrodes for each of the 8 electrode placements were placed on the right side of the thoracic cavity. Finally, the distance between the drive and the receive electrode pairs was the same. These theoretical studies also suggested that the increase in $\Delta Z/Z$ with increase in electrode spacing observed experimentally was due to an increase in the contribution from the deeper regions of a volume

conductor, and also from regions out of the electrode plane at higher electrode spacing.

Taking into consideration the results of these studies, an electrode placement was proposed as the optimum electrode placement. This electrode configuration involved 3 drive electrodes placed in one horizontal plane and 3 receive electrodes placed in a different horizontal plane. Thus, in this way it was possible to achieve the first objective of identifying an electrode placement having maximum sensitivity to lung resistivity changes. The next objective was to determine whether the impedance measurements obtained from this optimum electrode placement also had less movement artefacts.

7.4. Reduction of movement artefacts

At the outset of these studies it was decided that a four-electrode configuration would be suitable for impedance pneumography because this configuration minimised movement artefacts originating from the electrode-skin contact impedance. Some preliminary studies were carried out to compare, in qualitative terms, how different types of electrodes were able to record impedance in the presence of movement. It was observed that electrodes using a recessed AgCl disc (Conmed Corp., USA) had the strongest adhesion and did not come loose even during rapid movements. It was noticed that during movements, the skin underneath the electrodes became stretched and if the backing material of the electrode was not sufficiently flexible, then the electrodes had a tendency to become loose during movements. It was also observed that skin preparation further improved the adhesion of the electrodes.

Some preliminary experiments were also carried out to compare two electrode placements in terms of the amplitude of movement artefacts. It was observed that movement artefacts were lower when the electrodes were placed over the sternum and over the spinal column as compared to those obtained for the midaxillary placement commonly used in impedance pneumography. It appeared that movement artefacts were caused by movement of electrodes along with the skin. Thus, measurements obtained from the electrodes placed over the sternum

and the spinal column were less affected by movements compared to those obtained from the midaxillary placement.

A further preliminary study was carried out to develop a technique of breath detection using impedance imaging. In an EIT image of the thoracic cavity, it was observed that the resistivity changes within a ROI defined over the two lung regions correlated well during breathing, but were not correlated during random movements. As a result it was thought that breathing could be detected in the presence of movements by calculating a correlation coefficient between the two signals. Simulation studies suggested that it was possible to reliably detect breathing if the Signal-to-Artefact Ratio (SAR) in both these signals was higher than 5 dB. However, the experimental results suggested that in practice, the signal to artefact ratio was much lower than 5 dB. Therefore it was not possible to detect breathing using the correlation coefficient. From these results, it was concluded that unless a significant increase in SAR was achieved it was not possible to reliably detect breathing. Therefore, further experimental studies were carried out using the optimum 6-electrode configuration to see whether the values of SAR in the measurements obtained using this electrode placement were sufficiently high.

The impedance data recorded using the optimum 6-electrode configuration provided some important observations. It was observed that movement artefacts were only present in the transfer impedance when the electrodes used to record this transfer impedance moved along with the skin during movement. It was also observed that in a pair of measurements obtained across the thoracic cavity, the breathing related impedance changes were in phase, while those due to movement artefacts were 180° out of phase. Thus, it was possible to reduce movement artefacts by taking a mean of these two measurements.

From these observations, it appeared that movement artefacts were mainly caused by electrodes shifting along with the skin to coincide with different isopotential lines. Taking into consideration this observation a strategy was decided and a 4-electrode configuration was proposed which would reduce movement artefacts. It was possible to reduce movement artefacts in 5 subjects

by taking a mean of the two independent measurements obtained from the 4-electrode configuration. Further theoretical studies, carried out using a FEM model suggested that a 6-electrode strategic configuration could be used in three dimensions to reduce movement artefacts. This configuration was found to provide significant reduction in movement artefact in 4 subjects. It was also possible to detect breathing in the presence of movements using this configuration. These results seemed to confirm the hypothesis that movement artefacts were caused by the movement of the electrodes along with the skin to different isopotential lines. It was also observed that the amplitude of impedance changes during simulated obstructive apnoea was significantly lower than that due to breathing.

Finally, impedance measurements were carried out at more than one frequency of injected current to investigate whether it was possible to further reduce movement artefacts using the 6-electrode strategic placement. It was observed that movement artefacts were reduced by combining the symmetrical measurements at all frequencies in the range of 9.6 kHz to 1.22 MHz. However, this data did not provide any evidence that the residual movement artefacts could be reduced with frequency.

7.5. General conclusions

The results of the studies carried out in this project indicate that the main source of movement artefacts in impedance pneumography is the movement of electrodes along with the skin. The rib cage and the internal organs seem to act as a relatively rigid volume conductor. The surrounding tissues and the skin act as an outer loose layer, which is able to slide freely over the surface of this volume conductor. Thus, during movements, the electrodes move along with this outer layer to coincide with different isopotential lines and hence, record different voltage, which manifests as movement artefacts. The impedance measurements appear to be very sensitive to such movements as the artefacts are large compared to the impedance changes during breathing, even for the electrode placement that maximises the sensitivity to lung resistivity changes. Thus, only

maximising this sensitivity was not enough to achieve the aim of movement artefact reduction. Instead, some technique had to be developed to achieve a quantitative reduction in movement artefacts.

Taking into consideration the movement of electrodes as the main cause of movement artefacts, it is shown in the project that it is possible to achieve a significant reduction in movement artefacts using the 6-electrode strategic placement. Thus, it can be said that it was possible to achieve the aim of this project to a considerable extent. The significant reduction achieved in movement artefacts also indicates that it would be advisable to implement this technique in practice to develop reliable impedance based breathing monitors for clinical applications.

7.6. Suggestions for future research

Recently, a study (Pauw, 1958) was noticed, which provides a theoretical basis for the technique developed in this project. This theoretical study was aimed at measuring resistivity of an arbitrary shaped 2d homogeneous volume conductor having a uniform thickness. In this study two independent transfer impedance measurements ($R_{ab,cd}$ and $R_{bc,de}$) were made using 4 electrodes (*a*, *b*, *c* and *d*), placed on the boundary of the 2d conductor as shown in Figure 7.1. An equation was stated, which established a relationship between the two transfer impedances, the resistivity (ρ) and the thickness (d). This was given as,

$$e^{(-\pi R_{ab,cd} d/\rho)} + e^{(-\pi R_{bc,da} d/\rho)} = 1 \qquad 7.1$$

It can be seen from equation 7.1 that resistivity (ρ) in this equation is only dependent on the thickness(d) and the two transfer impedances ($R_{ab,cd}$ and $R_{bc,de}$). Thus, it is independent of the location of electrodes. This, indicates that from the two transfer impedance values and knowing the thickness of the sample, it would be possible to obtain the value of resistivity.

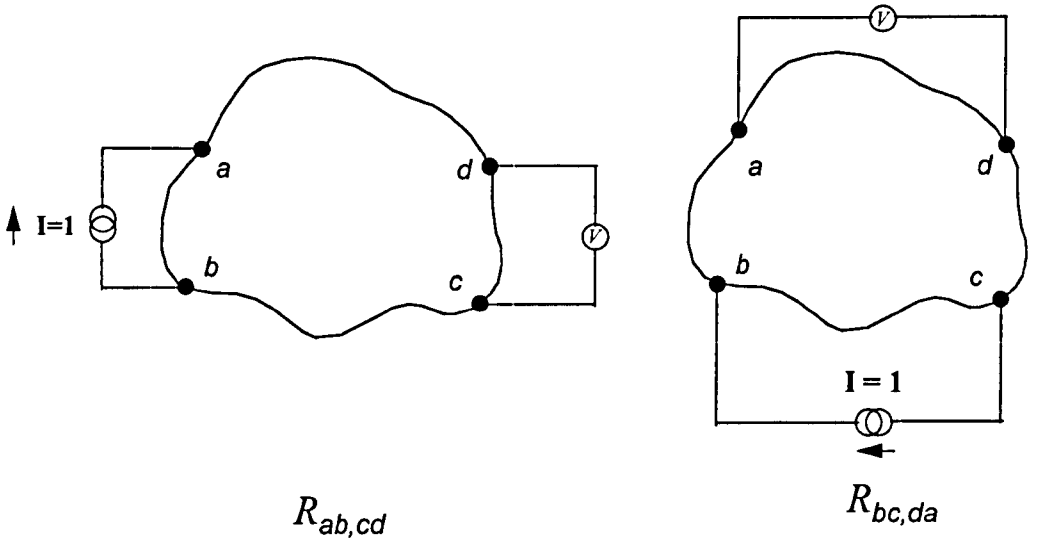

Figure 7.1 A 2d volume conductor with 4 electrodes

In the present project, it was shown that movement artefacts could be significantly reduced by taking a mean of the two 'symmetrical measurements', which were obtained in exactly the same way as suggested in this theoretical study. Thus, this mean signal appears to be only a function of the resistivity of the thoracic cavity. It was observed experimentally in this project that the main cause of movement artefacts is movement of electrodes. Since the measured quantity is proportional only to the resistivity, it would be independent of any other factors such as movement of electrodes and hence, the observed reduction. In addition, it would also be independent of shape and hence, the mean signal would be free from movement artefacts caused by the shape changes of the thoracic cavity as well.

However, it is important to note that the above theory has been shown to be valid for a 2d conductor whereas the thorax is a 3d volume conductor. In this project it has been shown that the movement artefacts can be reduced using this technique in 3d as well, on a FEM model as well as in the experimental studies. It might be possible to derive an equation similar to equation 7.1, for a 3d volume conductor. If so, then there may exist a better combination of the measured transfer impedances, which would reduce movement artefacts even further than achieved in this project.

It is also important to note that the theoretical study described above has been carried out for a homogeneous volume conductor whereas the thoracic cavity is a nonhomogeneous volume conductor. In this context, the use of an appropriate frequency of injected current becomes important. The resistivity of biological tissues depends on the frequency of injected current. At very high frequencies (approximately > 1 M Hz) the current penetrates through the cell membrane. Thus, the measured resistivity starts to become independent of the tissue structure at and beyond these frequencies. As a result, the thoracic cavity would appear to be more homogeneous at high frequencies.

There may be one more advantage of using higher frequency of injected current. It is known that the muscle tissues are anisotropic (Duck, 1990). They have a low resistivity in the direction of the fibres while the resistivity across the fibres is high. If we take into consideration the orientation of the muscles around the thoracic cavity, then it can be seen that a larger fraction of injected current would flow around the thoracic cavity through a low resistivity path provided by the muscle fibres. Thus, a relatively smaller fraction of the injected current would penetrate the deeper tissues of the thoracic cavity such as lungs. As a result, the measured impedance would more sensitive to the impedance changes of the surrounding muscle tissues than the deeper lung tissues. The impedance changes of the surrounding muscle tissues can occur due to geometrical changes during movements. However, the anisotropy of the muscle tissues is also a function of frequency and is known to reduce with increase in frequency (Epstein and Foster, 1983). Thus, more current would penetrate into the deeper lung tissues at higher frequencies causing a decrease in the sensitivity of the measured impedance to muscle tissues. Some residual movement artefacts have been observed in the mean of the two symmetrical measurements. If these artefacts are due to geometrical changes of the peripheral muscle tissues, then they might reduce at higher frequencies. Some multi-frequency measurements were carried out in the present project. However, no significant reduction in the residual movement artefacts was obtained at higher frequencies compared to lower frequencies. Thus, a more systematic study may be required to investigate changes in movement artefacts with frequency. It is important to note that at

higher frequencies improvement in the hardware performance will also be required.

In addition, clinical studies can be carried out to find out whether it is possible to obtain significant reduction in movement artefacts in neonates using the 6-electrode strategic placement. If so, then it would lead to a more reliable impedance based technique for monitoring apnoea.

In this context, it is important to note that in neonates, if the apnoea is accompanied by bradycardia, then there is a possibility that the apnoea may go undetected because the cardiac related impedance changes mimic the breathing related changes (Southall, 1980). This happens because, firstly the breathing rate is high in neonates, and hence an overlap may occur in the cardiac rate and the breathing rate during bradycardia. Secondly, in order to maintain a constant cardiac output at these lower heart rates, the stroke volume increases. As a result, large changes in blood volume occur within the thoracic cavity causing the amplitude of the cardiac artefacts to become comparable to that of observed during shallow breathing. It would be possible to reduce this artefact by simultaneously recording an ECG signal. This ECG signal can be used as a reference input to an Adaptive Filter operating in an Adaptive Noise Canceller, which then would be expected to cancel the cardiac artefacts in the main input signal. Thus, a significant improvement in the reliability of impedance based apnoea monitors can be obtained by achieving movement artefacts as well as cardiac artefact reduction.

Another clinical application that may be considered is that of monitoring lung water. The resistivity of the lung tissue reduces due to accumulation of fluids in some clinical conditions such as heart failure. The theoretical study described above suggests that the mean signal would be only a function of the resistivity of the thoracic cavity. If it can be shown that this is also valid for a 3d volume conductor, then it would be possible to measure the drop in resistivity of the lungs due to lung water. Experimental studies will have to be carried out to establish the ranges for the normal lungs and after fluid accumulation.

The studies carried out in this project only involved subjects having a normal size of the thoracic cavity. A study can be carried out to find out whether it is possible to reduce movement artefacts in subjects having different levels of subcutaneous fat on their thoracic cavity. A study can also be carried out to study whether the proposed 6-electrode placement is able to reduce artefacts originating during activities such as walking and jogging. If so, then it would be possible to use this placement combined with suitable instrumentation for ambulatory monitoring purposes.

The volume of inspired air was not measured in the present project. It would be possible to establish a relationship between the volume of inspired air and the impedance changes. This relationship normally depends on the size and shape of the thoracic cavity and hence, changes from subject to subject. However, if we assume that the 6-electrode strategic placement reduces the effect of shape and the size, then the relationship may become independent of these factors. Further improvement may be obtained by relating the fractional changes in impedance ($\Delta Z/Z$) rather than absolute changes (ΔZ).

References

AAMI. (1989) Apnea monitoring by means of thoracic impedance pneumography. *Technical Information Report*, 4, 243.

Albisser, A. M. and Carmichael, A. B. (1974) Factors in impedance pneumography. *Med. Biol. Engng.*, 12(5), 599-605.

Allison, R. D., Homes, E. L. and Nyboer, J. (1964) Volumetric dynamics of respiration as measured by electrical impedance plethysmography. *J. Appl. Physiol.*, 19, 166-173.

Avis, N. J. (1993) *Image Reconstruction in Electrical Impedance Tomography.* Ph.D. Thesis. University of Sheffield.

Baker, L. E. (1979) Electrical Impedance Pneumography. *In*: P. Rolfe (ed.) *Non-Invasive Physiol. Meas.*, Vol. 1. London, Academic Press. p 65-91.

Baker, L. E., Geddes, L. A. and Hoff, H. E. (1965) Quantitative evaluation of impedance spirometry in man. *Am. J. Med. Electron.*, 4, 73-77.

Baker, L. E., Geddes, L. A. and Hoff, H. E. (1966) A comparison of linear and non-linear charecterizations of impedance spirometry data. *Med. Biol. Engng*, 4, 371-379.

Baker, L. E., Geddes, L. A., Hoff, H. E. and Chaput, C. J. (1966) Physiological factors underlying transthoracic impedance variations in respiration. *J. Appl. Physiol.*, 21(5), 1491-1499.

BBC. (1999) Sudden Death: The search for the truth about Cot Death, *Horizon*, February 25, 9.30 p.m. BBC 2.

Bhat, S. (1990) Clinical Applications. *In*: J. G. Webster (ed.) *Electrical Impedance Tomography.* New York, Adam Hilger.

Bhattacharya, G. K. and Johnson, R. A. (1977) *Statistical Concepts and Methods.* New York, John Wiley and Sons.

Boone K., Barber, D. C., and Brown, B. H. (1997) Imaging with electricity: Report of the European Concerted Action on Impedance Tomography. *J. of Med. Engng. and Tech.*, 21(6), 201-232

Brown, B. H. and Seager, A. D. (1987) The Sheffield data collection system. *Clin. Phys. Physiol. Meas.*, 8 (Suppl. A), 91-98.

Brown, B. H., Barber, D. C., Wang, W., Lu, I., Leathard, A. D., Smallwood, R. H., Hampshire, A. R., MacKay, R. and Hatzigalanis, K. (1994) Multi-frequency imaging and modelling of respiratory related electrical impedance changes. *Physiol. Meas.*, 15, 1-11.

Brown, B. H., Leatherd, A. D., Lu, L., Wang, W. and Hampshire, A. (1995) Measured and expected Cole parameters from electrical impedance tomographic spectroscopy images of the human thorax. *Physiol. Meas.* 16 (Suppl. A), A57-A67.

Brown, B. H., Tidy, J. A., Boston, K., Blackett, A. D., Smallwood, R. H., Sharp, F. (2000) The relationship between tissue structure and imposed electrical current flow in cervical neoplasia. *Lancet*, 355, 892-895.

Bruce, I. and Sohrab, A. (1980) *Techniques of Finite Elements*. Chinchester, Ellis Harwood.

Carter, B. L., Morehead, J., Wolpert, S. M., Hammerschlag, S. B., Griffiths H. J. and Kahn, P. C. (1977) *Cross-sectional Anatomy: Computed Tomography and Ultrasound Correlation*. New York, Appleton-Century-Crofts.

Consensus Statement (1987) National Institutes of Health Consensus: Development Conference on Infantile Apnea and Home Monitoring. Sept. 29 to Oct. 1, 1986. *Paediatrics*, 79(2), 292-299.

Cooley, W. L. and Logini, R. L. (1968) A new design for impedance pneumograph. *J. Appl. Physiol*, 25(4), 429-432.

Coutand, F., Garnero, L. and Fonroget, J. (1997) Anatomical Data Fusion for Quantitative Reconstruction in Myocardial Tomoscintigraphy Using a Spline Model of Thoracic Organs. *IEEE Trans. Biomed. Engng.*, 44(7), 575-584.

Dijkstra A M, Brown, B. H., Leatherd, A. D., Harris, N. D., Barber, D. C. and Edbrooke, D. L. (1993) Clinical applications of electrical impedance tomography. *J. Med. Eng. Tech.* 17(3), 89-98.

Duck, F. A. (1990) *Physical Properties of Tissue: A Comprehensive Reference Book*. London, Academic Press.

Epstein, B. R. and Foster, K. R. (1983) Anisotropy in the dielectric properties of skeletal muscle. *Med. Bio. Engng. Comput.*, 21, 51-55.

Faes, T. J. C., Van der Meij, De Munck, J. C. and Heethar, R. M. (1999) The electric resistivity of human tissues (100Hz - 10MHz): a meta-analysis of review studies. *Physiol. Meas.*, 20, R1-R10.

Farman, J. V. and Juett, D. A. (1967) Impedance spirometry in clinical monitoring. *Br. Med. J.*, 4, 27-29.

Fenning, C. (1936-1937) A new method for recording. I. Recording respiration in small animals. *J. Lab. Clin. Med.*, 22, 1279-1280.

Gabriel, C., Gabriel, S. and Corthout, E. (1996) The dielectric properties of biological tissues: I- Literature survey. *Phys. Med. Biol.*, 41, 2231-2249.

Gabriel, S., Lau, R. W. and Gabriel, C. (1996) The dielectric properties of biological tissues: II. Measurements in the frequency range 10 Hz to 20 Ghz. *Phys. Med. Biol.*, 41, 2251-2269.

Gabriel, S., Lau, R. W. and Gabriel, C. (1996) The dielectric properties of biological tissues: III. Parametric models for the dielectric spectrum of tissues. *Phys. Med. Biol.*, 41, 2271-2293.

Geddes, L. A. and Baker, L. E. (1967) The specific resistance of biological material - a compendium of data for the biomedical engineer and physiologist. *Med. Biol. Engng.*, 5, 271-293.

Geddes, L. A. and Baker, L. E. (1989) Principles of Applied Biomedical Instrumentation. 3rd edition. New York, Wiley Publications. p 566-576.

Geddes, L. A., Hoff, H. E., Hickman, D. M. and Moore, A. G. (1962) The impedance pneumograph. *Aerospace Med.*, 33, 28-33.

Geselowitz, B. D. (1971) An application of electrocardiographic lead theory to impedance plethysmography. *IEEE Trans. Biomed. Engng.*, 18, 38-41.

Goldensohn, R. A. and Zablow, L. (1959) An electrical spirometer. *J. Appl. Physiol*, 14, 463-464.

Gonzalez-Correa, C. A., Brown, B. H., Smallwood, R. H., Kalia, N., Stoddard, C. J., Stephenson, T. J., Haggie, S. J., Slater, D. N. and Bardhan, K. D. (1999) Virtual Biopsies in Barrett's Esophagus Using an Impedance Probe. *In*: P. J. Riu, J. Rosell, R. Bragos and O. Casas (eds.) Electrical Bioimpedance Methods. *Annals of the New York Academy of Sciences*, 873, 313-321.

Graham, M. (1965) Guard ring use in physiological measurement. *IEEE Trans. Biomed. Engng.*, 12 (3), 197-198.

Hamilton, L. H., Beard, J. D. and Kory, R. C. (1965) Impedance measurement of tidal volume and ventilation. *J. Appl. Physiol*, 20, 565-568.

Hamilton, L. H., Beard, J. D., Carmean, R. E. and Kory, R. C. (1967) An Electrical Impedance Ventilometer to Quantitate Tidal Volume and Ventilation. *Medical Research Engineering*, 11-16.

Hampshire, A. R., Smallwood, R. H., Brown, B. H. and Primhak, R. A. (1995) Multi-frequency and parametric EIT images of neonatal lungs. *Physiol. Meas.*, 16 (Supplement 3A), A175-A190.

Harris, N. D., Suggett, A. J., Barber, D. C. and Brown, B. H. (1988) Applied potential tomography: a new technique for monitoring pulmonary function. *Clin. Phys. Physiol. Meas.*, 9 (Suppl. A), 79-85.

Harris, N. D., Suggett, A. J., Barber, D. C. and Brown, B. H. (1987) Applications of applied potential tomography (APT) in respiratory medicine. *Clin. Phys. Physiol. Meas.*, 8 (Suppl. A), 155-165.

Henderson, R. P. and Webster, J. G. (1978) An impedance camera for spatially specific measurements of the thorax. *IEEE Transactions on Biomed. Engng.*, 25, 250-254.

Hill, D. W. (1979) The Role of Electrical Impedance Methods for the Monitoring of Central and Peripheral Blood Flow Changes. *In*: P. Rolfe (ed.) *Non-Invasive Physiol. Meas.* Vol. 1. London, Academic Press. p 95-110.

Jossinet, J. and Kardous, G. (1987) Physical study of the sensitivity distribution in multi-electrode systems. *Clin. Phys. Physiol. Meas.*, 8 (Suppl A), 33-37.

Kawakami, K., Kira, S., Ito, A., Hukushima, Y. and Kanno, R. (1973) Associated change of transthoracic electrical impedance with regional ventilation of the lung. *Med. Biol. Engng.*, 11(4), 469-479.

Kawakami, K., Watanbe, A., Ikeda, K., Kanno, R. and Kira, S. (1974) An analysis of the relationship between transthoracic impedance variations and thoracic diameter changes. *Med. Biol. Engng.*, 12(4), 446-453.

Khalafalla, A. S., Stackhouse, S. P. and Schmitt, O. H. (1970) Thoracic Impedance Gradient with Respect to Breathing. IEEE, *Trans. Biomed. Engng.*, 17(3), 191-198.

Kiber, A. (1991) *Determination of object boundary shape for electrical impedance tomography.* PhD Thesis, University of Sheffield.

Kjellmer, I., Olsson, T. and Victorin, L. (1970) Transthoracic Impedance: II. Experimental evaluation of the method in the cat. *In:* T. Olsson and L. Victorin (eds.) Transthoracic Impedance with Special Reference to Newborn Infants and the Ratio Air-to-Fluid in the Lungs. *Acta. Paedia. Scand.*, Supplement 207, 15-28.

Kreyszig, E. (1993) *Advanced Engineering Mathematics* (7th edition). New York, John Wiley and Sons Inc.

Kubicek, W. G., Kinnen, E. and Edin, A. (1964) Calibration of an impedance pneumograph. *J. Appl. Physiol.*, 19, 557-560.

Lehr, J. (1972) A vector derivation useful in impedance plethysmographic field calculations. *IEEE Trans. Biomed. Engng*, 19(2), 156-157.

Logic, J. L., Maksud, M. G. and Hamilton, L. H. (1967) Factors affecting transthoracic impedance signals used to measure breathing. *J. Appl. Physiol.*, 22(2), 251-254.

Lorrain, P. and Corson, D. (1962) *Electromagnetic Fields and Waves.* (2nd edition). San Fransisco, W. H. Freeman and Company.

Lu, L. (1995) *Aspects of an Electrical Impedance Tomography Spectroscopy (EITS) System.* Ph.D. Thesis. University of Sheffield.

Luo, S., Alfonso, V. X., Webster, J. G. and Tompkins, W. J. (1992) The electrode system in impedance based ventilation measurement. *IEEE Trans. Biomed. Engng.*, 39, 1130-1141.

Mayotte, M. J., Webster, J. G. and Tompkins, W. J. (1994) A comparison of electrodes for potential use in paediatric/infant apnoea monitoring. *Physiol. Meas.*, 15, 459-467.

Mayotte, M. J., Webster, J. G. and Tompkins, W. J. (1996) Reduction of motion artefacts during paediatric/infant apnoea monitoring. *Med. Biol. Engng. Comput.*, 34, 93-96.

McAdams, E. T. and Jossinet, J. (1995) Tissue Impedance: a historical overview. *Physiol. Meas.*, 16 (Supplement 3A), A1-A14.

Metherall, P. (1998) *Three- dimensional electrical impedance tomography of the human thorax*. Ph.D. thesis, University of Sheffield, UK.

Metherall, P., Barber, D. C., Smallwood, R. H. and Brown, B. H. (1996) Three-dimensional electrical impedance tomography. *Nature*, 380(6574), 509-512.

Moore, D. S. and McCabe, G. P. (1993) *Introduction to the Practice of Statistics*. (2nd edition). New York, W. H. Freeman and Company.

National Institute of Health Consensus (1987) Development Conference on Infantile Apnea and Home Monitoring. *Pediatrics*, 79 (2), 292-299.

Nopp, P., Harris, N. D., Zhao, T. X. and Brown, B. H. (1997) Model for the dielectric properties of human lung tissue against frequency of air content. *Med. Bio. Engng. Comput.*, 35, 695-702.

Nopp, P., Rapp, E., Pfutzner, H., Nakesch, H. and Ruhsam, Ch. (1993) Dielectric properties of lung tissue as a function of air content. *Phys. Med. Biol.*, 38, 699-716.

Olsson, T., Daily, W. and Victorin, L. (1970) Transthoracic Impedance: I. Theoretical considerations and technical approach. *In:* T. Olsson and L. Victorin (eds.) Transthoracic Impedance with Special Reference to Newborn Infants and the Ratio Air-to-Fluid in the Lungs. *Acta Paed. Scand.*, Supplement 207, 15-28.

Pacela, A. (1966) Impedance Pneumography --- a survey of instrumentation techniques. *Med. Bio. Engng.*, 4,1-15.

Pallett, J. E. and Scopes, J. W. (1965) Recording aspirations in newborn babies by measuring impedance of the chest. *Med. Electron. Biol. Engng.*, 3, 161-168.

Pasquali, E. (1967) Problems in Impedance Pneumography: Electrical Characteristics of Skin and Lung Tissue. *Med. and Biol. Engng.*, 5, 249-258.

Pauw Van der, L. J. (1958) A Method Of Measuring Specific Resistivity And Hall Effect Of Discs Of Arbitrary Shape. *Philips Research Reports*, 13(1), 1-9.

Pethig, R. (1987) Dielectric properties of body tissues. *Clin. Phys. Meas.*, 8 (Suppl. A), 5-12.

Plonsey, R. and Collin, R. (1977) Electrode guarding in electrical impedance measurements of physiological systems - a critique. *Med. Biol. Engng. Comput.*, 15(5), 519-527.

Rabbani, K. S., Sarker, M., Akond, M. H. R. and Akhter, T. (1999) Focused Impedance Measurement (FIM): A New Technique with Improved Zone Localization. *In*: P. J. Riu, J. Rosell, R. Bragos and O. Casas (eds.) Electrical Bioimpedance Methods. *Ann. N. Y. Acad. Scs.*, 873, 408-420.

Rigaud, B., Hamzaoui, L., Chauveau, N., Granie, M., Scotto Di Rinaldi, J-P. and Morucci, J-P. (1994) Tissue charecterisation by impedance: a multi-frequency approach. *Physiol. Meas.*, 15, A13-A20.

Rigaud, B., Morucci, J-P. and Chauveau, N. (1996) Biomedical Impedance Techniques in Medicine. Part I: Bioimpedance Measurement. Second Section: Impedance Spectrometry. *In:* J. R. Bourne (ed.) *Crit. Rev. Biomed. Engng.*, 24(4-6), 257-351.

Rosell, J. and Webster, J. G. (1995a) Signal-to-motion artifact ratio versus frequency for impedance pneumography. *IEEE Trans. Biomed. Engng.,* 42, 321-323.

Rosell, J., Kohen, K. P. and Webster, J. G. (1995b) Reduction of motion artifacts using a two-frequency impedance plethysmography and adaptive filtering. *IEEE Trans. Biomed. Engng.,* 42, 1044-1048.

Sahakian, A. V., Tompkins, W. J. and Webster, J. G. (1985) Electrode motion artifacts in electrical impedance pneumography. *IEEE Trans. Biomed. Engng.*, 32, 448-451.

Sahalos, J. N., Nicolaidis, A. and Gotsis, N. (1986) The electrical impedance of the human thorax as a guide in evaluation of intrathoracic fluid volume. *Phys. Med. Biol.*, 31(4), 425-439.

Seagar, A. D., Barber, D. C. and Brown, B. H. (1987) Theoretical limits to sensitivity and resolution in impedance imaging. *Clin. Phys. Physiol. Meas.*, 8 (Suppl. A), 13-31.

Seager, A. D. and Brown, B. H. (1987) Limitations in hardware design in impedance imaging. *Clin. Phys. Physiol. Meas.*, 8 (Suppl. A), 85-90.

Seager, A. D., Barber, D. C. and Brown, B. H. (1987) Theoretical limits to sensitivity and resolution in impedance imaging. *Clin. Phys. Physiol. Meas.*, 8 (Suppl. A), 13-31.

Severinghaus, J. W., Catron, C. and Noble, W. (1972) A focusing electrode bridge for unilateral lung resistance. *J. Appl. Physiol.*, 32(4), 526-530.

Smith, R. W. M., Brown, B. H., Freeston, I. L. and McArdle, F. J. (1990) Real-time impedance tomography. *In*: T. Hames (ed.) *Proceedings of the Copenhagen Meeting on Electrical Impedance Tomography*. Sheffield, Sheffield University Press.

Smith, R. W. M., Freeston, I. L. and Brown, B. H. (1995) A Real - Time Electrical Impedance Tomography System for Clinical Use - Design and Preliminary Results. *IEEE Trans. Biomed. Engng.*, 42(2), 133-140.

Southall, D. P. *et al* (1980) An explanation for the failure of impedance apnea alarm systems. *Arch. Dis. Child.*, 55, 63-65.

Steinschneider, A. (1972) Prolonged apnea and the sudden infant death syndrome: clinical and laboratory observations. *Paediatrics*, 50, 646-654.

Stroud, K. A. (1972) *Engineering Mathematics*. (2nd edition). London, MacMillan publishers limited.

Toratora, G. J. and Grabowski, S. R. (1993) *Principles of Anatomy and Physiology.* (7th edition). New York, Harper Collins College publishers.

Valentinuzzi, M. E., Geddes, L. A. and Baker, L. E. (1971) The law of impedance pneumography. *Med. Biol. Engng*, 9, 157-163.

Valentinuzzi, M. E., Morucci, J-P. and Felice, C. J. (1996) Bioelectrical Impedance Techniques in Medicine. Part II: Monitoring of Physiological Events by Impedance. *In*: J. R. Bourne (ed.) *Crit. Rev. Biomed. Engng.*, 24(4-6), 353-466.

Wade, O. L. (1954) Movements of the Thoracic Cage and Diaphragm in Respiration. *J. Physiol.*, 124, 193-212.

Warburton, D., Stark, A. R. and Tacusch, H. W. (1977) Apnea monitor failure in infants with upper airway obstruction. *Paediatrics*, 60, 742-744.

Wilson, A. J., Franks, C. I. and Freeston, I. L. (1982) Algorithms for the detection of breaths from respiratory waveform recordings of infants. *Med. and Biol. Eng. and Comput.*, 20, 286-292.

Witsoe, D. A. and Kinnen, E. (1967) Electrical resistivity of lung at 100 kHz. *Med. Biol. Engng.*, 5, 239-247.

Appendix A

The scientific papers published in journals are as follows.

Khambete, N., Metherall, P., Brown, B., Smallwood, R. and Hose, R. (1999) Can We Optimise Electrode Placement for Impedance Pneumography? *In*: P. J. Riu, J. Rosell, R. Bragos and O. Casas (eds) Electrical Bioimpedance Methods. *Annals of the New York Academy of Sciences*, 873, 535-542.

Khambete, N. D., Brown, B. H. and Smallwood, R. H. (2000) Movement artefact rejection in impedance pneumography using six strategically placed electrodes. *Physiol. Meas.*, 21, 79-88.

Can We Optimize Electrode Placement for Impedance Pneumography?

N. KHAMBETE, P. METHERALL, B. BROWN, R. SMALLWOOD, AND R. HOSE

Department of Medical Physics and Clinical Engineering, University of Sheffield, Royal Hallamshire Hospital, Sheffield S10 2JF, United Kingdom

ABSTRACT: In this paper, we discuss issues involved in defining an optimum placement of four electrodes for impedance pneumography. We observed a general trend where the change in impedance (ΔZ) decreased while the sensitivity ($\Delta Z/Z$) increased with distance between the drive and receive electrode pairs. However, the theoretical study indicated that $\Delta Z/Z$ should decrease with distance. The scatter of points in the plots indicated that sensitivity was influenced by factors other than distance. The correlation coefficient between the theoretical and measured $\Delta Z/Z$ was low, but significant. This suggested that the best electrode configuration can be derived from the theoretical data. High $\Delta Z/Z$ was obtained when the drive and receive electrode pairs were placed close to the lungs and in different horizontal planes.

INTRODUCTION

Impedance pneumography is a technique of monitoring respiration by measuring changes in the electrical impedance of the thoracic cavity. The impedance of the thoracic cavity increases with an increase in lung air volume during inspiration and decreases during expiration. This measurement is achieved by injecting a high-frequency, low-amplitude alternating current into the body using a pair of surface electrodes and measuring the resultant changes in voltage by the same or a different pair of electrodes placed at an appropriate location. There exists a good correlation between the volume of inspired air and the impedance of the thoracic cavity.[1]

The impedance of the thoracic cavity has two components. The base impedance (Z) depends upon the impedance of all the tissues within the cavity, while the time-varying component of impedance (ΔZ) depends upon changes occurring due to breathing. The impedance also changes due to the cardiac activity, but these changes are small compared to those caused by breathing. The sensitivity of an electrode configuration to pulmonary changes can be expressed as the ratio $\Delta Z/Z$. This sensitivity is a function of electrode placement for a given subject.[2,3]

In this paper, we have reported results of our work aimed at finding an optimum electrode placement for impedance pneumography. We studied the relationship between ΔZ and $\Delta Z/Z$, and the distance between the drive and receive electrode pairs. Impedance data were recorded from normal human subjects by placing 32 drive and 32 receive electrode pairs around the thoracic cavity. We also studied this relationship theoretically using the sensitivity method of Geselowitz.[4]

METHODS

Experimental Studies

Impedance changes from the thoracic cavity were recorded during spontaneous tidal breathing from eight normal human subjects with a mean age of 27.9 years (range, 22–56) using the Sheffield Mark 3b data collection system.[5] The system consisted of 32 drive and 32 receive electrode pairs separated in 4 horizontal planes, with each plane having 16 equally spaced electrodes forming 8 drive and 8 receive interleaved pairs. This arrangement produced 1024 electrode configurations. The anatomical locations of the planes are shown in FIGURE 1. The current (2 mA peak-to-peak) was injected between one pair of drive electrodes, and the voltage from all the 32 receive electrode pairs was recorded. This was repeated for all the 32 drive pairs, resulting in a set of 1024 measurements. The system was designed to inject current at 8 frequencies in the range of 9.6 kHz to 1.22 MHz in binary steps. We chose measurements at a single frequency (76.8 kHz) for our analysis. The frame rate achieved by the system was 16.7 Hz. Volunteers were asked to relax in an upright sitting position and to perform normal tidal breathing. The data were collected for a duration of approximately 1 minute from each subject.

The data obtained from each electrode configuration were first low-pass filtered (Butterworth filter of order 10, cutoff frequency of 0.8 Hz) to reduce noise and the impedance changes occurring due to the cardiac activity. The mean impedance change with time for breathing was obtained by taking the mean of all the 1024 measurements. This waveform was processed using a peak detection algorithm to determine the frames corresponding to

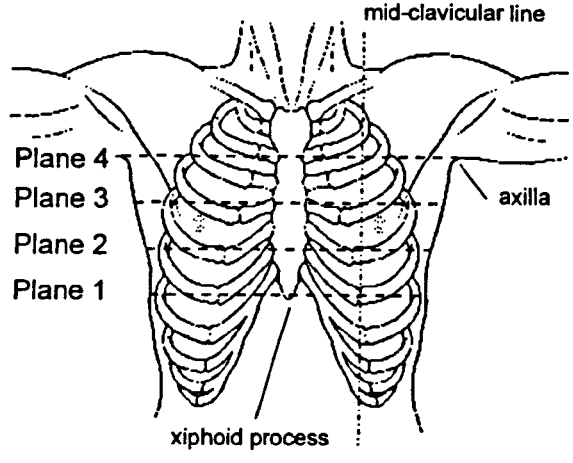

FIGURE 1. Electrode placement in 4 planes. Sixteen electrodes were placed around the thorax in each plane.

instants of maximum inspiration and expiration. The change in impedance (ΔZ) for each of the 1024 measurements was calculated by subtracting the mean value of impedance for the expiration frames from the mean value of impedance for the inspiration frames. The base impedance (Z) was calculated as the mean impedance for the entire time duration. The sensitivity was given by the ratio $\Delta Z/Z$.

The distance between the midpoint of each drive and receive pair was calculated geometrically. The thoracic cavity was assumed to have an elliptical cross section with a ratio of major to minor axis of 1.7.[6] The vertical separation between the electrode planes was assumed to be equal to half the minor axis.

Theoretical Studies

The purpose of our theoretical studies was to determine the same relationships using the sensitivity method of Geselowitz.[4] A simplified model was developed for the thoracic cavity, assuming it to be a homogeneous cylindrical volume conductor consisting of two regions to represent the two lungs as shown in FIGURE 2. It was necessary to generate a sensitivity matrix that could relate impedance changes occurring within these two regions to the voltages recorded by the 32 receive electrodes when a unit current was injected between each of the 32 drive pairs. The finite element modeling (FEM) technique was used for this purpose.

The cylindrical model was meshed into 37,632 "brick" elements, each having 8 nodes, using Ansys software (Ansys Inc., version 5.3.). The node voltages were obtained by solving the finite element model for the 32 drive and 32 receive pairs. The elemental voltage

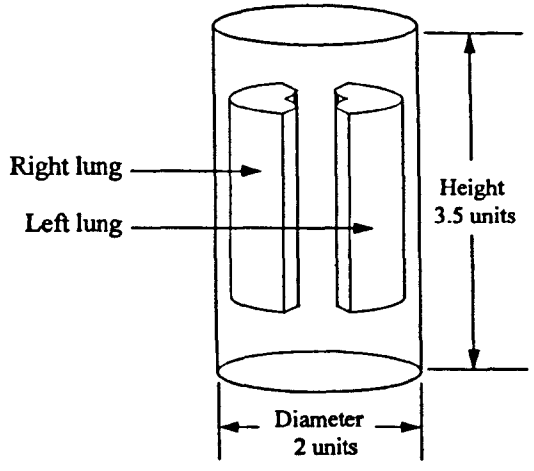

FIGURE 2. Cylindrical volume conductor model for the thoracic cavity showing location of the lungs.

gradient for the j-th element for a particular drive or receive electrode pair was calculated from the node voltages using equation 1:

$$\nabla\Phi = \nabla N \cdot V_{jn} \tag{1}$$

where

$\nabla\Phi$ = voltage gradient for the j-th element,
N = shape function of the brick element with 8 nodes,[7]
V_{jn} = node voltages for $n = 8$ nodes of the j-th element.

The sensitivity coefficient corresponding to the j-th element and i-th drive-receive configuration was given by the scalar product of the elemental voltage gradients $\nabla\Phi_i$ (drive pair) and $\nabla\Psi_i$ (receive pair) as shown in equation 2:[8]

$$S_{ij} = -\int_{j\text{-th element}} \nabla\Phi_i \cdot \nabla\Psi_i dv. \tag{2}$$

The integration is over the volume of the j-th element.

The base impedance (Z) for the 1024 configurations was evaluated by premultiplying the resistivity vector (c) by the sensitivity matrix (S) as in equation 3:

$$Z = S \cdot c. \tag{3}$$

The resistivity value of all the elements in c was set to 1 for evaluating Z. The breathing-related impedance changes were simulated by specifying a 10% change from the uniform resistivity value of the elements belonging to the two lung regions. It was assumed that this perturbation of 10% did not affect the isopotential surfaces, and the linearized sensitivity matrix S could be used to generate a new set of 1024 boundary voltage measurements ($Z_{10\%}$) using equation 3. Finally, the ΔZ and $\Delta Z/Z$ were given by

$$\Delta Z = Z - Z_{10\%} \tag{4}$$

$$\Delta Z/Z = (Z - Z_{10\%})/Z. \tag{5}$$

The distance between the drive and receive electrode pair was also calculated geometrically from the electrode coordinates extracted from the FEM model. Thus, this calculation was based on the circular cross section and not on the elliptical cross section, as in the case of experimental data.

RESULTS

Measured Data

FIGURES 3a and 3b plot ΔZ and $\Delta Z/Z$ versus distance for the measured data, respectively. The solid line indicates the regression line of y-axis values on x-axis values. The dashed line indicates the 95% confidence interval and the dash-dot line indicates the 95% prediction interval. The ΔZ and $\Delta Z/Z$ values are the mean of the eight subjects and the distance is expressed as the fraction of the minor axis of the ellipse used to calculate the distance. The plot of ΔZ versus distance, shown in FIGURE 3a, indicates a decreasing trend with distance (slope = –0.157, $p < 0.005$). FIGURE 3b shows the plot of $\Delta Z/Z$ versus dis-

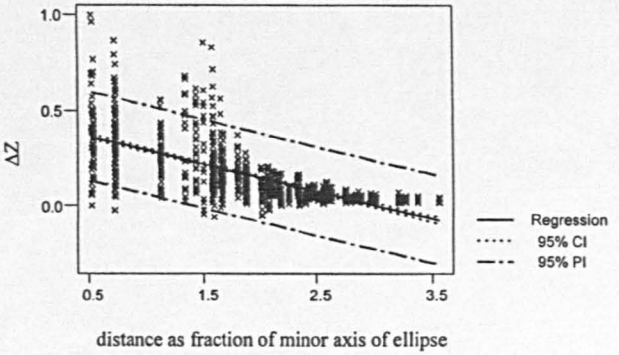

FIGURE 3a. Plot of ΔZ versus distance for measured data.

tance and has an increasing trend (slope = 0.053, $p < 0.005$). The data sets were normalized to their respective maximum values to make them comparable to the theoretical data.

Theoretical Data

FIGURES 4a and 4b show similar plots for the theoretical data. The distance in this case is expressed as the fraction of the cylinder radius. The relationship of ΔZ versus distance shown in FIGURE 4a has a decreasing trend (slope = –0.146, $p < 0.005$) similar to that

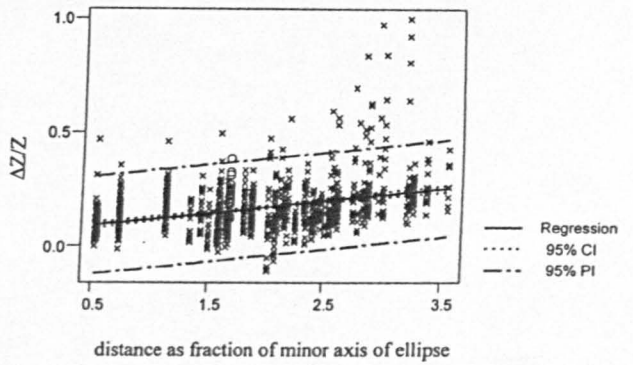

FIGURE 3b. Plot of ΔZ/Z versus distance for measured data. The 16 electrode configurations that gave the highest theoretical sensitivity are marked by open circles in the vicinity of distance 1.5.

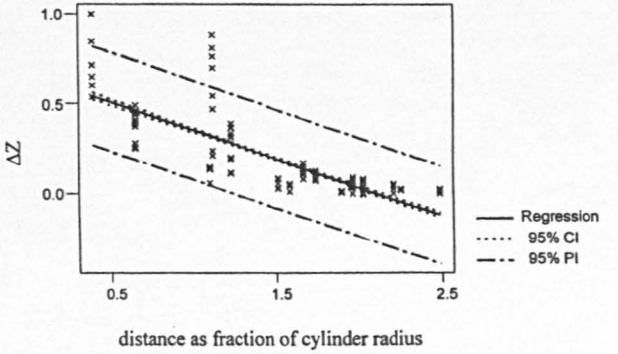

FIGURE 4a. Plot of ΔZ versus distance for theoretical data.

observed in the case of measured data. The plot of ΔZ/Z versus distance is shown in FIGURE 4b and has a decreasing trend (slope = –0.186, $p < 0.005$). This result is opposite to that obtained for the measured data. The scale limits of this plot are adjusted to make it comparable with the plot shown in FIGURE 3b. As a result, certain ΔZ/Z values for some electrode combinations corresponding to distance values in the vicinity of 2 units are not seen on the plot. These values were very high and negative and were due to very small magnitude and negative values of Z for the particular electrode combinations.

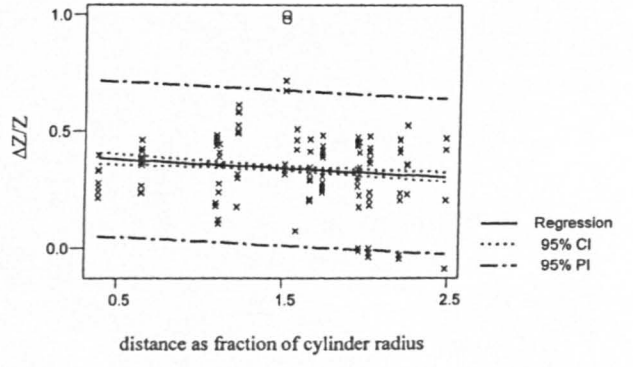

FIGURE 4b. Plot of ΔZ/Z versus distance for theoretical data. The 16 electrode configurations that gave the highest sensitivity are marked by open circles. Each point has 8 overlapping points.

DISCUSSION

The relationship between ΔZ and $\Delta Z/Z$ and the distance between the drive and receive electrode pair is statistically significant, but there is a large scatter of points in the plots. This indicates that the sensitivity is influenced by factors other than distance.

The purpose of our study was to determine the electrode configurations with high sensitivity. The correlation coefficient between the measured and theoretical values of $\Delta Z/Z$ was obtained in order to find out whether the two results were comparable. The value of the correlation coefficient was low ($r = 0.34$), but significant ($p < 0.005$). We believe that the low value of the correlation coefficient was because a cylindrical cross section was assumed for the FEM model, whereas the thoracic cavity is more elliptical in shape. This also might be the reason for the opposite sign of gradients of the best-fit line describing the relationship between $\Delta Z/Z$ and distance for measured and theoretical data. The significance of the correlation coefficient suggested that it would be possible to find out the electrode combination having high sensitivity by examining the theoretical data. The theoretical data would also be independent of the variations in the shape of the thoracic cavity of different subjects. We observed that there were 16 different electrode configurations that gave high sensitivity. These points are marked in FIGURE 4b by an open circle. Each of the two points has 8 overlapping points. The corresponding points for the measured data are marked also by an open circle and are seen in the vicinity of a distance value of 1.5 in FIGURE 3b. These points also have sensitivity higher than the mean sensitivity. However, these are not the points having the highest sensitivity. The points having the highest sensitivity correspond to electrode configurations separated by larger distances. At these distances, the value of Z is very small in magnitude and is prone to measurement errors due to a poor signal-to-noise ratio.[8] Hence, these highest sensitivity values are not reliable.

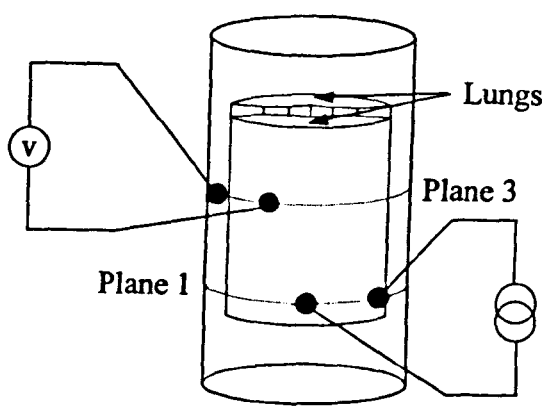

FIGURE 5. Placement of the drive and receive electrode pairs having high sensitivity.

The electrode placement for one of the 16 configurations having the highest theoretical sensitivity is shown in FIGURE 5. The drive and receive electrode pairs for this configuration were located close to one of the lungs. They were placed in two different horizontal planes separated by a vertical distance equal to the radius of the cylinder and displaced by an angle of 67.5°. The high sensitivity for this configuration is because the region of sensitivity in three dimensions for the particular placement of the electrodes has maximum overlap with the region occupied by the lung that is close to the electrodes. The remaining high sensitivity combinations also had a similar placement with respect to the lung proximity. This was due to the symmetry in the model.

CONCLUSIONS

In this paper, we have described our experimental and theoretical studies aimed at defining an optimum placement of 4 electrodes for impedance pneumography. The sensitivity of an electrode configuration depends not only on the distance between the drive and receive electrode pair, but also on the anatomical location of the lungs with respect to placement of the electrode. The maximum sensitivity was obtained when the drive and receive electrode pairs were placed over the same lung, but in different horizontal planes. High sensitivity was obtained in this case because the sensitivity region in three dimensions had maximum overlap with the lung close to the electrodes. Movement artifacts also contribute to the noise and their contribution will also depend on the placement of the electrodes. We are now planning to study the relationship between movement artifacts and electrode placements. These studies will help us to identify the best electrode placement for impedance pneumography.

ACKNOWLEDGMENTS

N. Khambete would like to thank the Association of Commonwealth Universities, United Kingdom, for the financial support provided in the form of a Commonwealth Scholarship. We also wish to thank Action Research and the EPSRC for providing the funds required in the development of the data collection system used in this study. We thank the volunteers who participated in the study.

REFERENCES

1. BAKER, L. E., L. A. GEDDES & H. E. HOFF. 1965. Quantitative evaluation of impedance spirometry in man. Am. J. Med. Electron. **April–June:** 73–77.
2. KHALAFALLA, A. S., S. P. STACKHOUSE & O. H. SCHMITT. 1970. Thoracic impedance gradient with respect to breathing. IEEE Trans. Biomed. Eng. **17:** 191–198.
3. SHEN, L., V. X. AFONSO, J. G. WEBSTER & W. J. TOMPKINS. 1992. The electrode system in impedance-based ventilation measurement. IEEE Trans. Biomed. Eng. **39:** 1130–1141.
4. GESELOWITZ, D. B. 1971. An application of electrocardiographic lead theory to impedance plethysmography. IEEE Trans. Biomed. Eng. **18:** 38–41.
5. METHERALL, P., D. C. BARBER, R. H. SMALLWOOD & B. H. BROWN. 1996. Three-dimensional electrical impedance tomography. Nature **380:** 509–512.
6. KIBER, A. 1991. Determination of object boundary shape for electrical impedance tomography. Ph.D. thesis, University of Sheffield, United Kingdom.

7. BRUCE, I. & A. SOHRAB. 1980. Techniques of Finite Elements. Ellis Horwood. Chichester, United Kingdom.
8. METHERALL, P. 1998. Three-dimensional electrical impedance tomography of the human thorax. Ph.D. thesis, University of Sheffield, United Kingdom.

Physiol. Meas. 21 (2000) 79–88. Printed in the UK PII: S0967-3334(00)09892-0

Movement artefact rejection in impedance pneumography using six strategically placed electrodes

N D Khambete†‡, B H Brown† and R H Smallwood†

† Department of Medical Physics and Clinical Engineering, The University of Sheffield, Royal Hallamshire Hospital, Glossop Road, Sheffield S10 2JF, UK

‡ Sree Chitra Tirunal Institute for Medical Sciences and Technology, Biomedical Technology Wing, Poojapura, Thiruvananthapuram 695 012, India

Received 16 July 1999

Abstract. In this paper, we have proposed a technique for reducing movement artefacts in impedance pneumography by placing six electrodes at appropriate locations and suitably combining the measurements obtained. The strategy for electrode placement was based on the observation that the electrodes appeared to slide over the rib cage along with the skin, during movement. A volume conductor model of the thoracic cavity was developed and movement artefacts were simulated by shifting the electrodes to a different location on the surface. The impedance changes due to movement in one of the measurements of a 'symmetrical pair' were 180° out of phase with respect to those observed in the other measurement of that pair. However, the impedance changes due to breathing were in phase in both these measurements. Thus, it was possible to reduce movement artefacts by taking a mean of these measurements without affecting the breathing related changes. The six electrodes could be configured into two such symmetrical pairs. The same observation was made in experimental data recorded from human subjects. This indicated that movement artefacts were caused by sliding of electrodes along with the skin and could be reduced by using the six-electrode configuration.

Keywords: movement artefacts, electrode placement, impedance pneumography

1. Introduction

Impedance pneumography is a non-invasive technique for monitoring respiration and involves measuring changes in the electrical impedance of the thoracic cavity. The resistivity of lung tissue increases due to increase in air volume during inspiration and decreases due to decrease in air volume during expiration. These changes in resistivity combined with diaphragm movements and changes in chest circumference affect the overall impedance of the thoracic cavity during breathing (Baker *et al* 1966). There exists a good correlation between the volume of inspired air and impedance of the thoracic cavity (Baker *et al* 1965). These impedance changes are measured by injecting a low-amplitude, high-frequency, constant current using a pair of 'drive' electrodes and recording the resultant voltage changes either from the same pair of electrodes as in a two-electrode (bi-polar) configuration or from a different pair of 'receive' electrodes placed at an appropriate location as in a four-electrode (tetra-polar) configuration (Pacela 1966).

Impedance pneumography is well tolerated by patients because it does not involve placing any device within the airway that may cause discomfort to the patient. Therefore, it is the most widely used technique for the purpose of long-term monitoring and home monitoring

(AAMI 1989). An additional advantage of impedance pneumography is that the same electrodes can be used for recording the ECG signal (Geddes *et al* 1962).

A major disadvantage of impedance pneumography is that the breathing related impedance changes are masked by large artefacts due to movement of the patient. Under such circumstances, it is impossible to extract any useful information from the impedance signal such as respiration rate, or to detect absence of respiration.

Various techniques have been suggested in the literature for reducing movement artefacts. The tetra-polar or guarded bi-polar electrode configuration with electrodes having large effective area has been preferred to the bi-polar configuration (Sahakian *et al* 1985). The tetra-polar configuration performs better because it is not affected by the artefacts originating from the disturbances occurring to the electrode–skin interface during movement. Mayotte *et al* (1994, 1996) have suggested that it is necessary to use electrodes having good stability, strong adhesion, low face-to-face impedance, low transthoracic-plus-electrode impedance, large effective area and large total area. The amplitude of movement artefacts also depends on the electrode placement. The best 'signal-to-artefact' ratio for a bi-polar configuration was obtained by Luo *et al* (1992), by placing one electrode on the sternum at the level of the second intercostal space and another electrode at the same horizontal level on the back. The use of multi-frequency measurements for movement artefact rejection has been proposed by Rosell *et al* (1995a, b). They reported that it was possible to extract an impedance signal proportional only to the movement by processing the impedance signals recorded at two different frequencies. This signal was used as a reference input to an adaptive noise canceller for movement artefact rejection.

This study was aimed at finding an appropriate placement of electrodes for reducing movement artefacts. A theoretical study was carried out by developing a volume conductor model of the thoracic cavity and simulating movement artefacts by shifting the electrodes to a different location. A six-electrode configuration was used in this study and the measurements were suitably combined to reduce the movement artefacts. The impedance measurements were also carried out on normal human subjects during breathing, breath hold and arm movements, by using the same six-electrode configuration. The movement artefacts could be reduced by combining the appropriate measurements in case of all the four subjects and for the four types of arm movement.

2. Theoretical studies

2.1. Electrode placement strategy

While carrying out some preliminary experiments, it was observed that the electrodes seemed to slide over the rib cage along with the skin during movement. The artefact signals were probably due to the electrodes shifting to different iso-potential lines as a result of this sliding movement. Therefore, it appeared that a simple four-electrode arrangement would be useful in reducing the movement artefacts. Figure 1 shows a two-dimensional circular conductor with four equally spaced electrodes 1, 2, 3 and 4. This arrangement will produce two independent measurements A and B. The electrodes 1, 2 and 3 were assumed to be not affected by movement, and the electrode 4 was assumed to be shifted to a new location (4′), due to movement. As a result of this shift, measurement A would increase to a, but measurement B would decrease to b. Thus, it would be possible to reduce movement artefacts by adding A and B, as they changed in opposite directions. A pair of such measurements will be referred to as a 'symmetrical pair' in the rest of the paper. A volume conductor model of the thoracic cavity was developed using finite element methods (FEMs) to obtain quantitative results.

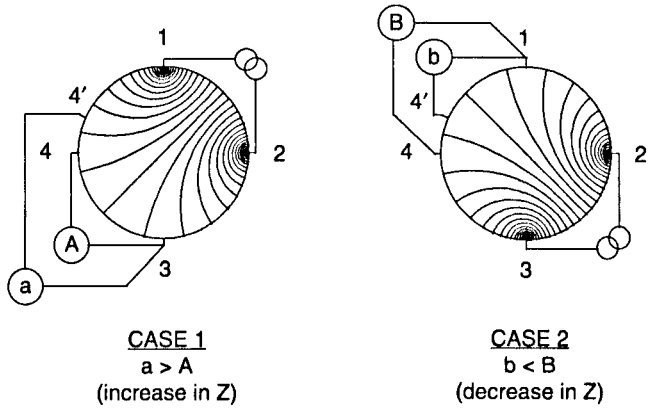

Figure 1. Two-dimensional conductor model with four equally spaced electrodes.

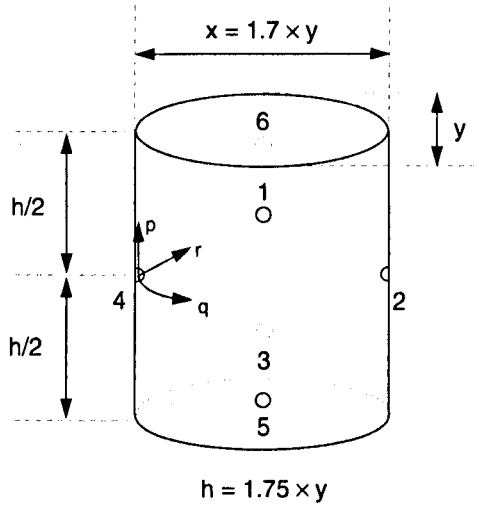

Figure 2. Elliptical volume conductor model of the thoracic cavity with six electrodes.

2.2. Volume conductor model of thorax

A homogeneous volume conductor model of the thoracic cavity, having an elliptical cross-section, was developed as shown in figure 2. The ratio of major axis (x) to minor axis (y) was chosen to be 1.7 as suggested by Kiber (1991) and the height (h) of the model was chosen to be 1.75 times the minor axis. The electrodes 2 and 4 were placed on the surface at the opposite ends of the major axis and in the 'central' horizontal plane, located at half the total height of the model. The electrodes 1 and 6 were placed at the opposite ends of the minor axis and in a horizontal plane located at a distance equal to half the minor axis above the central plane. The electrodes 3 and 5 were also placed at the opposite ends of the minor axis, but in a plane located at a distance equal to half the minor axis below the central plane. The electrodes 1, 2, 3 and 4 were configured to produce a symmetrical pair of measurements A and B, and the electrodes 6, 2, 5 and 4 were configured to produce a second symmetrical pair of measurements D and E as shown in table 1. The measurement C could also be obtained using this electrode placement.

Table 1. Electrode configurations and measurements under investigation.

Measurement	Drive electrodes	Receive electrodes
A	1–2	3–4
B	2–3	4–1
C	1–6	3–5
D	6–2	5-4
E	2–5	4–6

The movement artefacts were simulated by assuming that electrode 4 moved in three directions, vertical, horizontal and oblique, indicated in figure 2 as p, q and r, respectively. All the other electrodes were assumed to be not affected by movement. The volume conductor was meshed into 33 600, eight-node 'brick' elements using commercial software Ansys (Ansys Inc., USA, version 5.3). The solution in the form of nodal voltages was obtained by solving the FEM equations for each drive configuration so that measurements A to E could be derived.

2.3. Results of the theoretical study

The plot of voltage versus distance traversed by electrode 4 in each of the three directions is shown in figure 3. It was observed that in the case of movement occurring in each of the three directions, artefacts could be reduced by taking the mean of the measurements belonging to each symmetrical pair. In case of the movement occurring in direction r, artefacts could be further reduced by taking a mean of all the four measurements.

The impedance changes in measurements A and D due to movement in direction p were equal in magnitude and phase, and those due to movement in direction q, were equal in magnitude but opposite in phase. This was due to symmetry in the electrode placement with respect to model geometry and the two directions of movement. This was also observed for measurements B and E. Therefore, the plots of these measurements overlap in figure 3(a) and figure 3(b). The results of this theoretical study indicated that it was possible to reduce movement artefacts by using the six-electrode configuration.

3. Experimental studies

3.1. Data collection system

The hardware set-up of the data collection system is shown in figure 4. The Sheffield mark 2 real-time electrical impedance tomography (REIT) system was used to collect impedance data during breathing, breath hold and movements (Smith *et al* 1995), and a thermistor based breath detection circuit was developed to record an artefact free breathing signal.

In this study, a six-electrode adjacent measurement system would have been suitable. However, the available 16-electrode system could be used by placing the extra electrodes, equally spaced, between each pair of electrodes under investigation. The required six-electrode measurements were derived by appropriately combining the 16-electrode measurements on the basis of superposition. The REIT system recorded one frame of data by injecting current of 5 mA peak to peak at 20 kHz between each pair of adjacent electrodes and measuring voltage from all the remaining pairs of adjacent electrodes. The data were captured at a frame rate of 25 frames s^{-1} and stored to the hard disk of a PC denoted as DAS1.

The thermistor, used to record an artefact free breathing signal, was attached to a face mask worn by the subjects during data collection. The resistance value of the thermistor changed

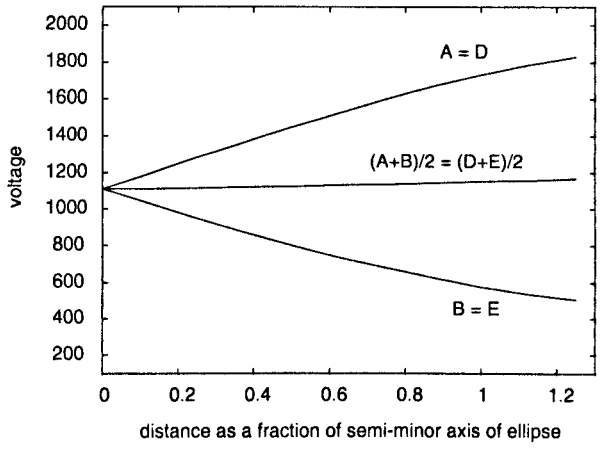

(a)

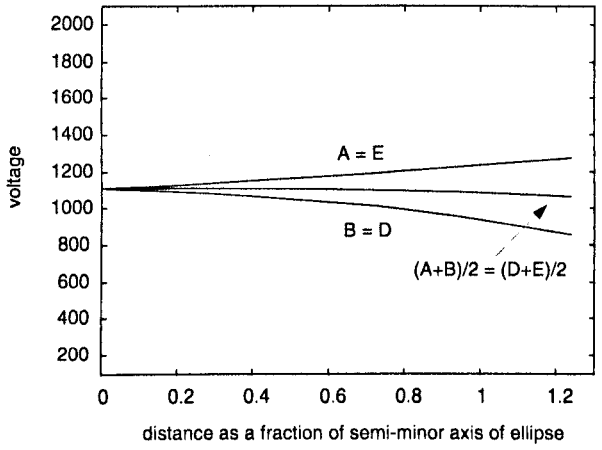

(b)

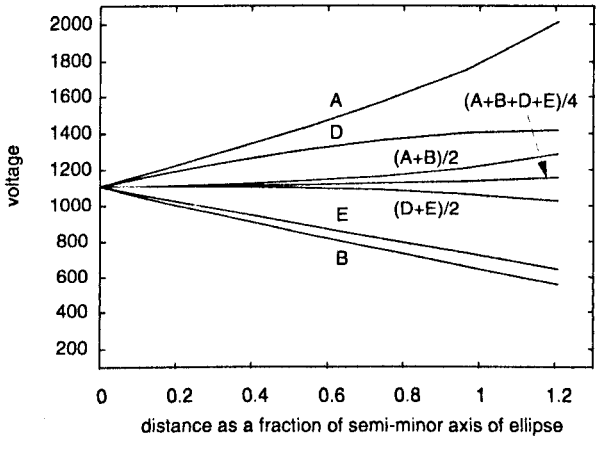

(c)

Figure 3. (a) Plot of measurements A, B, D and E for movement in direction 'p'. Note that the measurements A and D, and B and E are identical. (b) Plot of measurements A, B, D and E for movement in direction 'q'. Note that the measurements A and E, and B and D are identical. (c) Plot of measurements A, B, D and E for movement in direction 'r'. Note the reduction in artefact achieved by taking the mean of all the four signals.

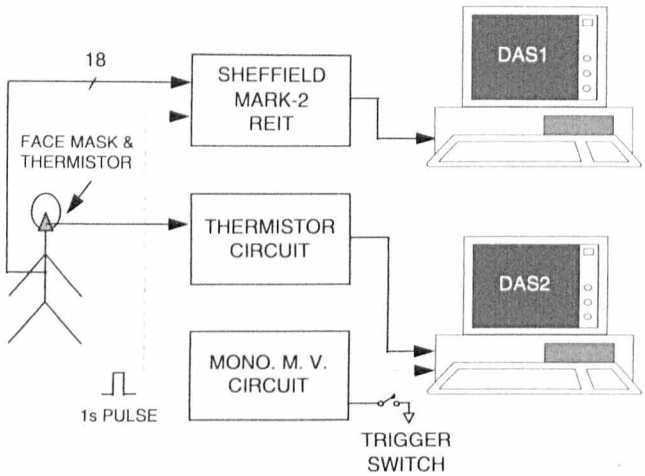

Figure 4. Hardware set-up of the data collection system.

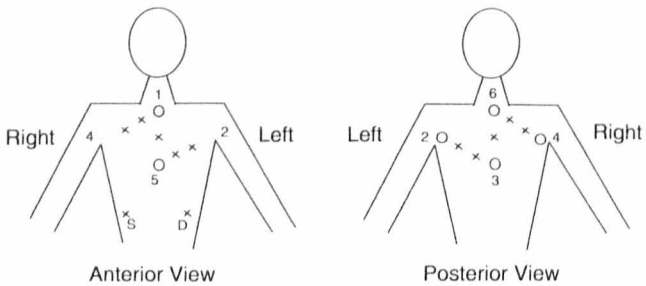

Figure 5. Placement of electrodes on human subjects. The six electrodes indicated by the circles are the electrodes under investigation.

as it was heated and cooled by the expired and inspired air, respectively. This change in resistance was converted to a voltage signal and was connected as an input to the first channel of a second PC based data acquisition system (DAS2). The sampling rate of DAS2 was also set to 25 samples s^{-1}, equal to that of DAS1. However, it was necessary to synchronize the two systems in time. Therefore, a monostable multivibrator circuit was developed to generate a TTL compatible pulse of 1 s duration. The circuit could be triggered by pressing a switch manually. This TTL signal was connected to the 'event marker' input of the REIT system and to a second channel of DAS2. The REIT system had a built-in arrangement to mark the frames corresponding to the rising edge of the pulse. Thus, the two systems could be synchronized in time by shifting the data vectors such that the frames corresponding to the rising edge of the pulse were aligned. The same pulse was also used to generate an audio signal for instructing the subjects to carry out a changeover from tidal breathing to breath hold and to start the movement manoeuvre.

3.2. Electrode placement on human subjects

The six electrodes under investigation were placed relative to the anatomical landmarks to minimize the inter-subject variability, and are marked by circles in figure 5. The electrodes 5 and 1 were attached anteriorally, one over the xiphoid process and the other over the sternum

at the level of the first rib, respectively. The electrodes 3 and 6 were attached in the same two horizontal planes, but on the back over the spinal column. These four electrodes were those assumed to be not affected by movement in the theoretical studies. They seemed to be least affected by arm movements because they were placed directly over the bones, which formed the rigid structure of the rib cage, and were also located at the farthest possible points from both the arms. These positions were also similar to the best electrode locations suggested by Luo *et al* (1992) as reported in the introduction. Finally, electrodes 2 and 4 were attached at the level of the axilla, over the Latissimus dorsi muscle on the left and the right side, respectively. These two electrodes were expected to be affected by the movement. The placement of remaining electrodes was not very critical and they were placed at the locations marked by crosses in figure 5. The two ground electrodes, marked as 'S' and 'D', were placed on the abdomen. Thus, it was possible to record measurements A to E, as given in table 1, using this electrode placement. The Adult Foam 1501-025 electrodes (Conmed Corporation, USA) were used in the study because they seemed to adhere very well to the skin and did not come loose due to movements used to cause artefacts.

3.3. Experimental protocol and movement manoeuvres

The tidal breathing and movement artefact data were recorded from four normal human subjects having a mean age of 27 years (range 24–29), in an upright sitting position. The subjects were asked to perform four different arm movement manoeuvres; right arm moving up and down, left arm moving up and down, both arms moving up and down alternately, and both arms moving up and down together. The data collection in each case was carried out for a duration of 120 s. During the first 60 s, subjects were asked not to perform any movement and carry out tidal breathing (TB) for 20 s, followed by breath hold after maximum inspiration (BH) for 20 s and again tidal breathing for 20 s. The same sequence of breathing activity was repeated in the remaining 60 s, but a movement manoeuvre was performed simultaneously. The arm movements were not necessarily synchronized in time with the breathing activity.

4. Results

The impedance changes observed in the individual measurements A and B for one subject and right arm movement manoeuvre are plotted with respect to time in figure 6(a). The thermistor signal shows the breathing activity not affected by movement as expected. The periodic impedance changes observed during the epochs 1 and 3 were due to tidal breathing and a steady base line, observed during the epoch 2, was due to breath hold. The impedance also changed due to cardiac activity, but the amplitude was relatively small. These changes, occurring at a higher cardiac frequency, are seen superimposed over the breathing related impedance changes. It was observed that the impedance changes due to movement artefacts were large and seemed to completely mask the breathing related changes during epochs 4 and 6. The steady base line, indicating breath hold, was also replaced by large artefacts during epoch 5. This indicated that it was not possible to extract any breathing related information from the individual measurements when the movement was present.

The purpose of our experimental study was to find out whether the impedance changes due to movement, in one of the measurements belonging to a symmetrical pair, were 180° out of phase with respect to those observed in the other measurement of that pair, as predicted by the theoretical study. This was indeed observed in the case of measurements A and B and is seen during epoch 5, when the subjects carried out movement when holding their breath. Similar observations were made in the case of measurements D and E. Thus, it was possible

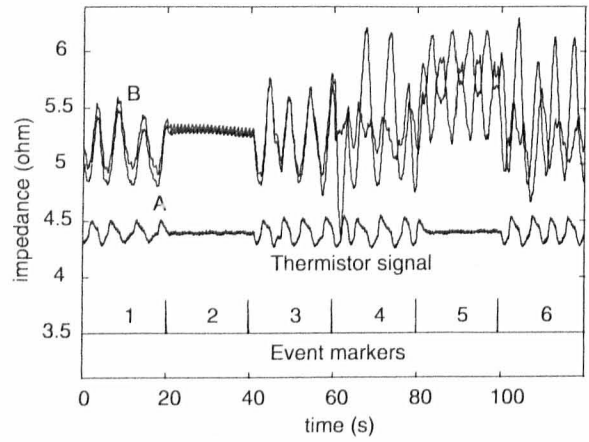

(a)

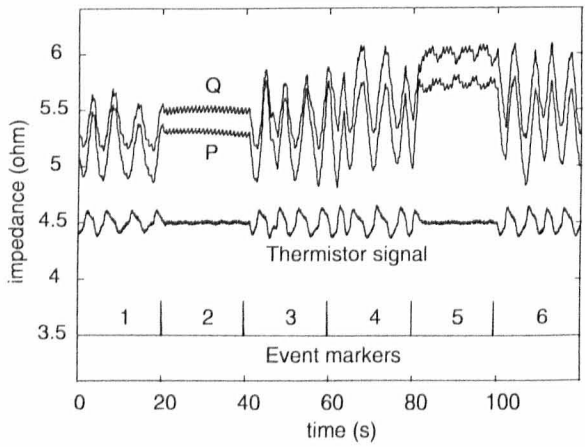

(b)

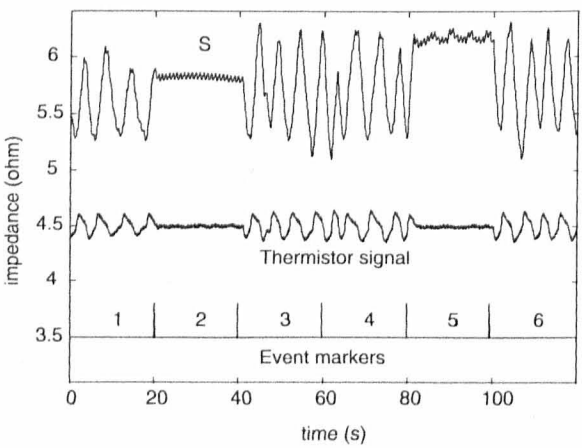

(c)

Figure 6. (a) Plot of individual measurements A and B, and the thermistor signal with time, during right arm movement for subject AK. Note that the movement artefacts are 180° out of phase during epoch 5. (b) Plot of the mean values of the symmetrical pairs; $P = (A+B)/2$ and $Q = (C+D)/2$, during right arm movement for subject AK. Note the reduction in movement artefacts during epoch 5. (c) Plot of the processed signal $S = (P+Q+C)/4$, during right arm movement for subject AK. High correlation is seen between the impedance signal and the thermistor signal.

to reduce the movement artefacts by taking the mean of A and B (P) and of D and E (Q), without affecting the breathing related changes as shown in figure 6(b). This was the first step in reducing the movement artefacts.

It was also observed that the movement artefacts in P were 180° out of phase with respect to those in Q in the case of some subjects as in figure 6(b), but were in phase in case of the remaining subjects. However, in the latter cases, the movement artefacts in P and Q were 180° out of phase with respect to those in measurement C. In general, it was observed that the artefacts could be reduced by summing P, Q and C in all the subjects. The plot of the processed signal (S) is shown in figure 6(c). It can be seen that, even in the presence of movement during epochs 4 and 6, the instants of maximum inspiration and expiration coincide in time with those observed in the thermistor signal. The absence of breathing can also be identified during epoch 5.

The sum of P, Q and C was divided by an empirical factor equal to 4 so that the amplitude of the breathing signal in S would be in the same range as that observed in the individual measurements. This allowed a direct comparison to be made between the amplitude of movement artefacts, before and after processing the signals. It may be noted that the choice of value of 4 was only for the sake of comparing the results of the study and has no significance as far as any clinical application of the technique is concerned.

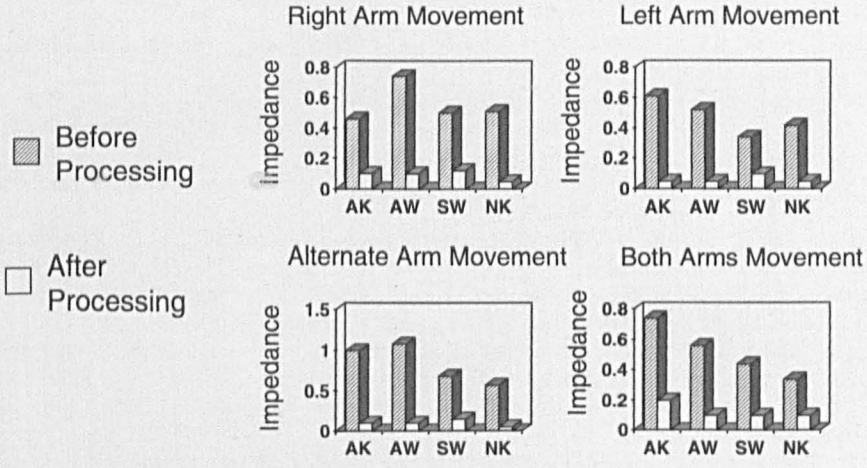

Figure 7. Peak-to-peak amplitude of the movement artefacts before and after processing for the four subjects and four arm movement manoeuvres.

The results are summarized in figure 7. The amplitude of movement artefacts indicated as 'before processing' was calculated by taking a mean of the peak-to-peak values of impedance changes due to movement during breath hold (epoch 5) in all the five measurements A to E. The amplitude of movement artefacts, indicated as 'after processing', is equal to the mean of peak-to-peak values of impedance changes in measurement S during the same epoch.

5. Conclusion

The aim of this study was to find an electrode placement for impedance pneumography that would have minimum movement artefact. The theoretical study suggested that movement artefacts could be reduced by using a six-electrode configuration and by adding the measurements obtained from the 'symmetrical pairs' of electrodes. The experimental results

agreed with theoretical results and the movement artefacts could be reduced in all the four subjects and for the four types of arm movement. The variations between subjects seemed to be due to the variations in shape and size of the thoracic cavity, and due to small errors in placing the electrodes relative to the anatomical landmarks.

This study indicated that arm movements caused the electrodes to slide along with the skin over the rib cage. This resulted in a relative movement between the drive and receive electrodes. Therefore, the receive electrodes moved to different iso-potential lines and recorded different voltages, manifested as artefacts in the recorded signal.

Acknowledgments

Niranjan Khambete would like to thank the Association of Commonwealth Universities, UK for providing funds in the form of Commonwealth Scholarship to carry out this project. We also thank the volunteers participating in the study.

References

AAMI 1989 Apnea monitoring by means of thoracic impedance pneumography *Technical Information Report* 4 p 243

Baker L E, Geddes L A and Hoff H E 1965 Quantitative evaluation of impedance spirometry in man *Am. J. Med. Electron.* **4** 73–7

Baker L E, Geddes L A, Hoff H E and Chaput C J 1966 Physiological factors underlying transthoracic impedance variations in respiration *J. Appl. Phys.* **21** 1491–9

Geddes L A, Hoff H E, Hickman D M and Moore A G 1962 The impedance pneumograph *Aerospace Med.* **33** 28–33

Kiber A 1991 Determination of object boundary shape for electrical impedance tomography *PhD Thesis* University of Sheffield

Luo S, Afonso V X, Webster J G and Tompkins W J 1992 The electrode system in impedance based ventilation measurement *IEEE Trans. Biomed. Eng.* **39** 1130–41

Mayotte M J, Webster J G and Tompkins W J 1994 A comparison of electrodes for potential use in paediatric/infant apnoea monitoring *Physiol. Meas.* **15** 459–67

——1996 Reduction of motion artefacts during paediatric/infant apnoea monitoring *Med. Biol. Eng. Comput.* **34** 93–6

Pacela A F 1966 Impedance pneumography—a survey of instrumentation techniques *Med. Biol. Eng.* **4** 1–15

Rosell J, Cohen K P and Webster J G 1995b Reduction of motion artifacts using a two-frequency impedance plethysmography and adaptive filtering *IEEE Trans. Biomed. Eng.* **42** 1044–8

Rosell J and Webster J G 1995a Signal-to-motion artifact ratio versus frequency for impedance pneumography *IEEE Trans. Biomed. Eng.* **42** 321–3

Sahakian A V, Tompkins W J and Webster J G 1985 Electrode motion artifacts in electrical impedance pneumography *IEEE Trans. Biomed. Eng.* **32** 448–51

Smith R W M, Freeston I L and Brown B H 1995 A real-time electrical impedance tomography system for clinical use-design and preliminary results *IEEE Trans. Biomed. Eng.* **42** 133–40